THE DYNAMIC BEHAVIOR OF A FLOATING, CABLE-MOORED PLATFORM CONTINUOUSLY IMPACTED BY ICE FLOES

by

M. Matsuishi and R. Ettema

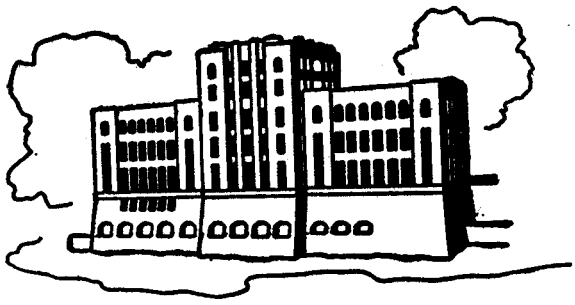

IIHR Report No. 294

Iowa Institute of Hydraulic Research
The University of Iowa
Iowa City, Iowa 52242

November 1985

THE DYNAMIC BEHAVIOR OF A FLOATING, CABLE-MOORED PLATFORM CONTINUOUSLY IMPACTED BY ICE FLOES

by

M. Matsuishi and R. Ettema

IIHR Report No. 294

Iowa Institute of Hydraulic Research
The University of Iowa
Iowa City, Iowa 52242

November 1985

ABSTRACT

The dynamic behavior of a floating, moored platform undergoing continuous impact with a field of ice floes was investigated using the ice towing tank of the Iowa Institute of Hydraulic Research (IIHR). In particular, the study was directed to investigate the influences of ice-floe diameter and speed on the ice-related forces and motions experienced by a moored platform of conical hull form.

A 1.5-meter-diameter (at the load waterline) test platform was connected to a linear-spring mooring harness which simulated the system of cables used to moor a floating, conical platform. For a parallel series of experiments, the test platform was fixed so that it was restrained from moving. Comparison of results from the moored and fixed conditions enabled the effects of platform motions on ice-related forces to be established. The experimental results are compared with the design requirements of an existing conical platform, "Kulluk", which the test platform simulated at a scale of 1:45.

The experiments showed that, for both the moored and the fixed conditions of platform support, the maximum and average values of mooring and restraining (ice-related) forces due to ice-floe impact increased with increasing diameter of ice floe; the value asymptotically approached that associated with the impact of a floe of annual ice much larger than the platform. This increase is attributed primarily to the added resistance required to flexurally break an ice floe impacting against the platform.

The average and maximum values of mooring forces experienced by the moored platform increased with increasing speed of ice-floe impact. When impacted by ice floes, the moored platform experienced larger fluctuations of surge displacements for relatively slow speeds (0.01 to 0.02 m/s, test speed) of ice-floe movement. This result can be ascribed to a resonance condition that was set up between the platform's oscillation and the dominant frequency of ice breaking. Commensurately, the fluctuation of mooring force experienced by the platform was greater at lower speeds of ice-floe impact, because the mooring force was proportional to the displacement of the linear harness.

The average and maximum values of vertical, restraining forces experienced by the platform in the fixed condition decreased with increasing speed of ice-floe impact.

The maximum mooring forces experienced by the test platform and the design value of mooring force for the platform "Kulluk" were found to be in very good agreement. Also in good agreement were the magnitude of the horizontal ice force calculated using Ralston's (1980) formulation and that measured during the slow impact of ice with the test platform fixed from moving.

ACKNOWLEDGEMENTS

This study was conducted as part of a cooperative research agreement between Hitachi Zosen Corporation of Japan, and The University of Iowa, Institute of Hydraulic Research (IIHR), USA.

The authors wish to thank Messrs. S. Iwata, R. Hamer and J. Cramer for technical support provided during the experiments. Additionally, the authors would like to thank Dr. J.F. Kennedy, IIHR Director, for useful advice offered in the course of the study.

TABLE OF CONTENTS

LIST OF FIGURES

LIST OF TABLES

THE DYNAMIC BEHAVIOR OF A FLOATING, CABLE-MOORED PLATFORM CONTINUOUSLY IMPACTED BY ICE FLOES

I. INTRODUCTION

A floating, cable-moored platform of conical hull shape is a means for providing a stable platform from which drilling activities can be conducted through relatively deep, ice-covered waters. One such platform, "Kulluk," is already in service (see, e.g., Hnatiuk and Wright 1984) in the Beaufort Sea. The hull form and mooring configuration of a floating, conical platform of similar design to "Kulluk" are shown in figure 1.

A major concern for the designers and operators of a floating platform is its dynamic response or the magnitudes of forces as well as accelerations and displacements, that the platform is likely to encounter when impacted by a field of ice floes.

A. Scope of Study. The principal objectives of the study were to determine the influences of floe diameter and speed on the ice-related loadings and motions (accelerations as well as displacements) that a conical platform would encounter while being continuously impacted by a field of annual-ice floes. Additionally, because a floating, moored platform can surge, pitch and heave when impacted by ice, a further objective of the study was to evaluate the influences of platform motions on the ice loadings encountered by the platform.

To meet these objectives, model tests were conducted, at the IIHR ice towing tank, using a 1.5-meter diameter (at the load waterline) test platform. The test platform, which is illustrated in figure 2, was approximately a 1:45-scale replica of the hull of the existing platform "Kulluk."

So that the influences of platform motions on ice loadings would be clearly discernable, a parallel series of tests were conducted with the platform fixed, or restrained from surging and heaving, and partially restrained from pitching.

The ice floes were prepared from sheets of urea ice which were cut into regular arrays of square slabs. From a different view-point, the cut sheets of ice can be considered as sheets with certain spatial concentrations of long, linear fractures.

The results forthcoming from the model tests are compared with ice loadings predicted using Ralston's (1980) formulation for quasi-static ice-floe impact with a fixed, conical structure. Ralston's formulation is presently the only readily accessible analytical model for predicting ice loadings against a conical structure.

The results of the model tests are also compared with the performance criterion for the cable-mooring system of the platform "Kulluk." By linking the model tests to a "prototype" platform such as "Kulluk" it is intended that the results of this study be of direct and immediate interest to designers and operators of floating platforms for use on ice-covered waters.

B. Drilling Platforms for Ice-Covered Waters. A variety of design concepts have been proposed for platforms from which oil-related drilling activities can be conducted through ice-covered waters. A major factor influencing the selection of a particular platform concept is the depth of water at potential drilling sites. Other factors include the ice and wave conditions at drill sites, and, if required, the mobility or portability of a platform. The importance of these and other factors are ultimately reflected by the cost of fabricating and operating a platform.

At present, a cable-moored conical hull such as the one depicted in figure 1 appears to be an economically viable and practicable means for creating a relatively stable platform for conducting drilling operations through relatively deep, ice-covered waters--i.e., water depths in the range of about 20 to 60 meters. The symmetry of the conical hull form makes it more stable than the conventional form of a ship hull which may be prone to problematical loading conditions resulting from lateral impact with ice.

Design constraints such as strength limitations of mooring systems, together with weight and cost limitations, dictate the ice conditions

that a floating moored platform can operate in. For example, "Kulluk," when moored is designed (according to Gaida et al. 1983) to withstand impact by floes of annual ice 1 to 1.5-m thick. When floes of thicker ice, especially floes of thick, multiyear ice, and large ice ridges approach "Kulluk," it is designed to be towed from the drill site where it is operating. For this purpose, and for general ice management around "Kulluk," ice-breaking ships are required to regularly attend and escort it (Hnatiuk and Wright 1984, Loh and Stamberg 1984). Typically, therefore, a moored platform such as "Kulluk" encounters fields of ice floes and ice rubble rather than large monolithic sheets of ice, floes of multiyear ice, or large ice ridges.

For relatively shallow, ice-covered waters, a convenient and a comparatively cheap method of creating a drilling platform has been to fashion an artificial island from gravel, sand or both. Outlines of the design criteria used for island platforms can be found in a variety of sources; e.g., Exxon (1979). For deeper waters, gravel/sand islands become less attractive fiscally because excessively large amounts of fill material are required, and, not unrelatedly, unacceptably long construction periods are needed. A caisson-retained, artificial island has been found to be an appropriate platform concept for water depths between about 20 to 30 meters. The main advantages of a caisson-retained island is that it entails less fill material, and can be constructed so as to be portable. An outer shell, or caisson, can be used to retain an inner core of sand or gravel. The caisson itself can be fabricated so that it can be refloated and reassembled at other drill sites.

A fairly detailed summary of concepts for drilling platforms in ice-covered waters is offered by Frederking (1984). His summary indicates the broad range of designs that have been conceived for arctic rilling platforms.

The foregoing background sets the scene for the present study. Before embarking on the full presentation and discussion of the results of the study, a brief review of literature related to ice loading of inclined surfaces and conical structures is offered in Section II.

II. LITERATURE REVIEW

The literature on the dynamics of floating conical platforms in ice-covered waters is not extensive. However, it is beginning to grow since the recent awakening of interest in the potential recovery of oil from deeper waters of the Arctic. The following brief review, which primarily deals with studies related to ice loading of conical structures, begins with a short discussion of ice forces against an inclined plane.

A. Ice Forces Against an Inclined Plane. Possibly the simplest ice-structure interaction occurs when a level ice sheet impacts an inclined plane (figure 3). Quite a large number of experiments and theoretical studies of ice forces on an inclined plane structure have been carried out (e.g., Sorensen 1975, Tryde 1977, Frederking 1980, Croasdale 1980, Ralston 1978, Abdelnour 1979, Timco 1984, Frederking and Timco 1985).

A recent study was conducted by Frederking and Timco (1985) who conducted experiments to determine ice-force components as well as to formulate and verify an analytical model for predicting ice forces against inclined planes. They found that the flexural failure of an ice sheet against a flat plane of finite width was characterized by the formation of radial cracks emanating from the plane, and a circumferential crack, as depicted in figure 3. Frederking and Timco attribute the ice forces associated with the flexural failure of an ice sheet pressed against an inclined plane to three components: breaking of the ice sheet, rotation of ice slabs and sliding of broken ice slabs. These components are further divided as follows: horizontal force (y is taken as the horizontal axis, and x as the vertical axis in this report),

$$F_y = F_b + F_r + F_s + F_p; \tag{1}$$

and vertical force

$$F_x = F_y \frac{(\sin \alpha + \mu \cos \alpha)}{(\cos \alpha - \mu \sin \alpha)} . \tag{2}$$

In (1), F_b = horizontal component of the maximum force associated with the development of either radial or circumferential cracks (see figure 3), which do not form simultaneously through an ice sheet. Frederking and Timco suggest that the larger value of F_b associated with the formation of either radial or circumferential cracks be used for estimating ice forces against an inclined plane. Also in (1), F_r = horizontal component of the force associated with the rotation of ice slabs until they become parallel to the inclined plane; F_s = the force generated by ice slabs sliding up the inclined plane; while F_p = the horizontal component of force attributable to the pressure exerted against the inclined plane by the impinging ice sheet as it thrusts ice slabs up the plane. In (2), α = the angle of plane (figure 3); and μ = coefficient of friction between ice slabs and the inclined plane.

The analytical model proposed by Frederking and Timco is useful for conducting parametive studies on ice forces exerted against inclined planes. They do note, however, that the predicted values of total ice load were about 20% larger than the ice loads that they measured during model-scale experiments.

B. Ice Forces Against Conical Structures. Frederking and Schwarz (1982) conducted a series of model tests with the purpose of investigating the ice-breaking performance of a downward-breaking cone which was restrained from moving (see figure 4). In the course of their experiments, they examined the influences of cone angle, which they varied from 15 to 60 degrees, and relative speed between ice and structure, which they varied from 0.01 to 0.5 m/s. The effects of thickness and flexural strength of ice were also investigated. Some of the results from their study are shown in figures 5 through 8. They observed that horizontal forces increased with increasing speed of ice impact (figure 5). Ice thickness was observed to have a more pronounced influence on the vertical forces than on the horizontal forces (figure 7). Vertical and horizontal forces, both, decreased with decreasing flexural strength (figure 8).

Frederking and Schwarz also conducted tests with a vertically and horizontally oscillating cone which had a cone angle of 45-degrees. They

found that, for the oscillating cone, the horizontal force component of the ice force was two-thirds of that measured for the cone restrained from moving.

Ralston (1978, 1980) formulated a relationship for determining the ice forces imposed against upward- and downward-breaking conical structures impacted by ice sheets. In his formulation, he assumed that an elasto-plastic foundation response could be used to describe the submerged reaction (involving the submerged weight of ice) for downward-breaking cone and the emerged reaction for upward-breaking cone (involving the weight of ice). Two plastic-limit failure criteria were used to evaluate breaking of an ice sheet. Ralston's formulation does not take into account the dynamic, or inertial, effects resulting from the interactions between platform, ice and water.

The following relationships were proposed by Ralston for estimating horizontal and vertical components, F_y and F_x, of the ice force exerted by an ice sheet impacting against an upward-breaking conical structure (for downward-breaking cones, $\rho_w g$ should be replaced by $\rho_w g/9$ in all of the expressions):

$$F_y = \frac{\tan\alpha}{1-\mu\, g(\alpha,\mu)} \{2M_o \left[\frac{\rho}{\rho-1}\right] + 2M_o \left[\frac{1-\rho + \rho \ell n \rho}{\rho-1}\right]$$

$$+ (3.422\, M_o + 1.422\, M_o) \frac{\rho\, \ell n\, \rho}{\rho-1} + 0.9\, \rho_w g\, t\, D^2(\rho^2 + \rho - 2)/12$$

$$+ \frac{0.9\, \rho_w g\, t_R\, (D^2 - D_T^2)}{4} \left[\frac{1}{\cos\alpha} + \frac{\mu E(\sin\alpha)}{\sin\alpha} - \mu\, \frac{f(\alpha,\mu)\, g(\alpha,\mu)}{\tan\alpha}\right]\} \quad (3)$$

and vertical force

$$F_x = R_H \left[\frac{h(\alpha,\mu)}{\frac{\pi}{4}\sin\alpha + \frac{\mu\alpha}{\tan\alpha}}\right]$$

$$+ \frac{0.9\, \rho_w g\, t_R\, (D^2 - D_T^2)}{4} \left[\frac{\pi}{2}\cos\alpha - \mu\alpha - \frac{f(\alpha,\mu)\, h(\alpha,\mu)}{\frac{\pi}{4}\sin\alpha + \frac{\mu\alpha}{\tan\alpha}}\right] \quad (4)$$

in which F,E = the complete elliptic integral of the first and second kinds, respectively; D = waterline diameter of the cone; D_T = top (or bottom) diameter of cone; M_o = bending moment capacity of ice sheet; t_R = ride-up (accumulation) thickness of ice ; ρ = a non-dimensional parameter which defines the size of the deforming ice region in fron of the cone; and

$$f(\alpha,\mu) = \sin\alpha + \mu \cos\alpha \, F(\sin\alpha) \; ;$$

$$g(\alpha,\mu) = \left(\frac{1}{2} + \frac{\alpha}{\sin 2\alpha}\right)\Big/\left(\frac{\pi}{4}\sin\alpha + \frac{\mu\alpha\cos\alpha}{\sin\alpha}\right) \; ;$$

$$h(\alpha,\mu) = \cos\alpha - \frac{\mu}{\cos\alpha}\left[E(\sin\alpha) - \cos^2\alpha \, F(\sin\alpha)\right] .$$

Equation (3) corresponds to the Johansen yield criterion. The corresponding forms of (3) and (4) for the Tresca yield criterion are virtually the same, except that the term 1.422 M_o is deleted.

A sample calculation by Ralston showed that a downward-breaking cone offers some advantages over an upward-breaking cone. In particular, a downward-breaking cone produces lower values of horizontal loads compared to those associated with an upward-breaking cone. This load reduction occurs because lesser forces are needed to submerge broken ice pieces than are needed to push them up and over the surface of an upward-breaking cone. However, Ralston pointed out that additional factors, such as the contribution of the vertical force to the over-turning moment and the potential jamming of ice ridges against a downward-breaking cone in shallow-water, should also be considered when downward-breaking geometries were of interest. Equations (3) and (4) are used, in section V.H, to compare Ralston's formulation with ice forces measured from the test platform.

Milano (1975) formulated a model for predicting the resistance likely to be encountered by ship and other hull forms in level ice. His formulation is based on the principle of conservation of energy applied to a hull in the continuous mode of icebreaking. Milano's formulation holds that, if the ice is relatively thick, the total amount of energy lost during a typical cycle of ice-breaking can be written as

$$E_T = E_1 + E_{21} + E_3 + E_4 + E_5 \tag{5}$$

in which

E_1 = energy lost due to hull motion through floating broken ice;

E_{21} = energy lost due to impact of the hull's bow with cuspate ice wedges, causing local crushing of ice;

E_3 = energy lost when the hull's bow slides onto the ice until sufficient force is generated to cause ice failure;

E_4 = energy lost as the hull's bow slides downwards after ice failure;

E_5 = energy lost due to submerging broken ice beneath the hull;

If the ice is relatively thin, it can be flexurally failed to form cuspate wedges before total impact energy is absorbed. In this case the total energy loss is

$$E_T = E_1 + E_{22} + E_f + E_b + E_4 + E_5 \tag{6}$$

in which

E_{22} = energy lost due to ice crushing, the strain energy of deflection of cusp wedges and due to ice impact with the hull's bow;

E_f = frictional energy loss at bow and side cusps during hull motion onto the ice field;

E_b = frictional energy involved in deformation of ice wedge at the bow;

If the ice is very thin, impact will cause both bow and cusp wedges to fail due to bending before total available impact energy can be absorbed. The total energy loss in this case is

$$E_T = E_1 + E_{23} + E_f + E_4 + E_5 \qquad (7)$$

in which

E_{23} = energy lost due to strain energy of deflection of cusp wedges, bending and crushing for all cusps.

In each of the above summations, total resistance to hull motion, F_T, may be taken as the total energy lost, E_T, divided by the distance x' over which the cycle of ice-breaking takes place; i.e.,

$$F_T = E_T/x' \ . \qquad (8)$$

Although the above expression is seemingly general, its applicability is largely limited to the hull forms of conventional icebreaker ships. Because extrapolation of Milano's model to commercial hulls, for which the pattern of icebreaking is unknown, is often difficult, Milano (1980) extended his model so that it could be applied to hull forms of large commercial bulk carriers configured for effective movement through ice. Milano (1982) applied the extended version of his model so as to predict ice forces exerted against a conical, floating structure. The results of his calculations are shown in figures 9 and 10.

Wessels (1984) reported the results of an extensive program of model tests that were conducted for the purpose of documenting the influences of an array of parameters on the ice forces exerted against conical structures. He varied cone angle, platform diameter at the waterline, ice-breaking mode (upward- and downward-flexure), friction coefficient between ice and cone surface, speed of ice, and ice thickness.

Wessels conducted most of his tests with cones rigidly fixed to an underwater carriage, which was pushed by a motorized carriage. For testing the behavior of moored conical structures impacted by ice sheets, Wessels attached a test cone via a single steel cable to the underwater carriage. In this experimental harness, the cone was free to pitch, heave and surge about the single, centerline mooring point. Some of the results from Wessels tests are shown in figures 9 and 10.

Milano (1982) used some of Wessels data to compare with loading predictions obtained from his extended formulation. The predicted and test values were in reasonable agreement (see, for example, figures 9 and 10). As was also shown by Ralston (1980), Wessel's data confirmed that, compared to the loads experienced by an upward-breaking fixed cone, a very large decrease in horizontal and vertical forces occurred for a downward-breaking cone. This result was found for both the fixed and floating conditions of cone support.

III. EXPERIMENTS

A. Experimental Facilities.

1. The IIHR ice towing tank. The experiments were conducted using the IIHR ice towing tank which is 20-m long, 5-m wide, and 1.3-m deep. A schematic layout of the tank and the cold room, in which the ice tank is housed, and its cooling system is given in figure 11. The cooling system is composed of two compressors which provide coolant to the two cooler units situated at each end of the cold room. The compressors are in turn cooled by water pumped from a 200 m^3 sump. If the sump exceeds a certain limiting temperature, a cooling tower situated out-doors is operated to cool the sump water.

Fans inside the four cooler units draw air from the cold room and, after the heat exchange has occurred, discharge it into eight ducts which extend the whole length of the cold room. The chilled air is forced through an array of 20-mm diameter holes along the base of each duct, thereby producing a flow of chilled air over the towing tank. The four

ducts are alternately arrayed so as to provide an even distribution of cold air. Every two hours, one pair of cooler units is defrosted by electrical heating. Depending on the ambient air temperature outside the cold room, the total cooling capacity of the system varies between 15 and 20 kW, which enables an ice sheet to grow at a rate of 1.5 to 2.0 mm per hour.

The 5-m-wide, 2.4-m-long motorized carriage, depicted in figure 12, was used to push ice floes against the model platform. The carriage runs along rails on the tank's walls. The level of each rail was adjusted to a tolerance of ± 1.5 mm along its length. An angle beam on one side of the basin gives the lateral guidance to the carriage and carries the rack of the rack-and-pinion drive mechanism. The D.C. motor on the carriage has a maximum torque of 31 Nm and a speed range of 58 to 1750 RPM. A 1:15 gear box increases the torque to 465 Nm and gives a reduced speed range of 3.9 to 117 RPM. The effective radius of the pinion is 0.06 m; consequently the carriage has a maximum driving force of 7750N and a velocity range of 0.024 m/sec to 0.74 m/sec. Higher velocities, up to 2.2 m/sec, can be achieved if a 1:5 gear box is coupled to the D.C. motor.

In order to measure the velocity of the carriage, a wheel carrying a circular array of holes is mounted on the drive shaft of the D.C. motor. The passage of each hole, as the shaft rotates, is sensed by a photo detector which emits a light through the hole. The number of pulses counted during a time interval is proportional to the velocity of the carriage. The length of the time interval is 0.371 seconds so that 1000 pulses correspond to a velocity of 0.333 m/sec. After each interval of 0.371 sec, the number of pulses is latched to a display and to a digital-analog converter which holds the voltage during the following interval until the next measurement is available. The mean velocity of the preceding interval is therefore, displayed and can be sampled.

2. The test platform. The test platform was similar in form to the existing floating, cable-moored platform "Kulluk." For modelling purposes, a scale of 1:45 can be used to relate geometrically the test model to "Kulluk." The principal dimensions of the test platform and

"Kulluk" are listed in table 1. The test platform was shaped as an inverted cone which flared down to a circular cylinder as is shown in figure 13.

A floating, cable-moored platform is secured by mooring-cable tensions and supported by the foundation reaction of the water upon which it floats. The reaction is equal to the weight of water displaced. The mooring cables and restoring forces can be related to the platform's displacement by treating these forces as linear spring systems. The equivalent spring stiffnesses of the floating, moored test platform were

a) spring stiffness of mooring cables

$$k_s = 1.7 \text{ kN/m} \tag{9}$$

b) spring stiffnesses of the foundation reaction

$$k_h = 17.3 \text{ kN/m, for heave} \tag{10}$$

and

$$k_p = 35.1 \text{kNm/degree, for pitch.} \tag{11}$$

The ratio of water depth, where floating platforms are typically designed to operate, to the length of mooring cable is typically in the range of 0.02 to 0.05 (Gaida et al. 1983). Consequently, the vertical component of the mooring forces is much smaller than the horizontal component. Moreover, as the spring stiffness of mooring cables, (9), is an order of magnitude smaller than that of the foundation, (10), the contribution of mooring cables to restraining surge and pitch motions can be disregarded. It is therefore possible to idealize the cable mooring system as a linear horizontal spring.

Although a system of mooring cables for use in shallow waters can respond non-linearly to applied mooring forces, the mooring system for a floating, drilling platform can be treated as being linear for the following reasons:

a. the stiffness of the mooring system is increased by initial tensioning of cables, such that the relationship between cable tension and platform displacement becomes virtually linear; and,

b. the maximum drift, or surge displacement, of a platform is restricted to a value less than 5% of water depth, in order that the drill pipe is not subjected to excessive, and dynamic, loadings. For this relatively small value the relationship between mooring force and platform displacement can be taken as being linear.

A fuller discussion of cable-mooring for floating platforms is given in Appendix 2, following Appendix 1 which contains the time histories of measured quantities.

3. Instrumentation. The test platform was connected to an instrument beam by way of a linear mooring harness and a load cell, as shown in figures 14 and 2. The mooring harness was comprised of a pair of elastic leaf springs which exerted a horizontal (surge) restoring force, a spline bearing, stroke bearings and universal bearings, as indicated in figures 14 and 16. The harness facilitated the accurate simulation of the motion of a floating, moored platform. Horizontal mooring force and surge displacement were measured using a 490-newton NISHO DENKI LMC-3502-50 load cell which connected the instrument harness to the instrument beam. Yawing and swaying of the moored platform were restricted by two vertical rods located at the fore and aft of the platform, as shown in figure 15. The 10-mm diameter rods were constrained to slide in 10.5-mm wide slots as shown in figure 16. The floating, moored platform had three-degrees of freedom for motion: surge, heave and pitch.

The heave and pitch motions of the moored platform were measured by recording, with two linear voltage displacement transducers (LVDT's), the vertical motion of the platform at two positions. The LVDT's were excited using 12 volts, which corresponded to a full stroke movement

range of 0.15 m. The outputs of the potentiometers were transmitted by means of two voltage followers.

Vertical and horizontal accelerations of the moored platform were measured with three, 2g (19.6 m/s^2) KYOWA ASQ-2BL accelerometers.

In order to examine the performance of the platform when restrained from moving, and compare it with the platform's performance when it was moored, the test platform was directly connected to a load cell which was bolted to the instrument beam. Figure 17 depicts this test arrangement which was used to simulate the impact of ice floes with a fixed, downward-breaking cone.

The horizontal and vertical restraining forces and pitching moment experienced by the fixed platform were measured using a 196-newton and 98-newton-meter NISHO DENKI LMC-4107-20 load cell.

The locations of the measuring sensors and the positive directions of recorded data are shown in figure 18.

The output voltages from the load cells, LVDT's, accelerometers and the carriage velocimeter were scanned using a digital voltmeter. The digitized data were serially transmitted through a telephone link to the IIHR HP-1000E computer system, and were there stored on disk. The bandwidth of the data acquisition link was 120 Hz, although each channel was sampled at a rate of 4, 5 or 10 Hz.

4. Calibration of transducers. For each of the data-logging transducers (force, displacement, acceleration, velocity) the zero level and sensitivity of the transducer were determined before each test.

Each output voltage of the load cells and accelerometers V was measured for a calibration strain ε_c created by an amplifier. The sensitivity, S, of each transducer was evaluated as

$$S = (V/\varepsilon_c)\, C \qquad (12)$$

in which C is a predetermined ratio of strain to force or acceleration experienced by transducer.

The sensitivity of LVDT's, were evaluated by measuring the voltage change for a given displacement of the transducer rod, and were determined to be 13.03 mm/volt and 12.92 mm/volt.

The sensitivity of the circuit for the carriage velocity was determined by correlating its output voltage with the mean velocity of the carriage (determined by use of a stop watch and a length scale). Then, the analogue setting of the carriage speed control was calibrated against the voltage output.

B. The Platform's Natural Periods of Oscillation. Free-oscillation tests were carried out to determine the natural periods and logarithmic decrements of surge and pitch oscillations of the test platform. The recorded data are shown in table 4. The platform's natural period of heave was estimated as

$$T = 2\pi/\omega = 2\pi / \sqrt{\rho_w g A_w/(M+m)} \qquad (13)$$

for which

A_w = water plane area of the platform $= \pi D_{LW}^2/4$; D_{LW} = the load waterline diameter of the platform; M = mass of the platform; m = added mass assumed to be 1.2 M (from Faltinsen 1975, Van Oortmersen 1976); and $\rho_w g$ = specific weight of water.

C. Openwater Tests. Openwater tests were conducted to examine if the push-blade attached to the carriage caused additional hydrodynamic forces to be exerted against either the moored or the fixed platform. It was found that the additional hydrodynamic forces exerted against the platform in open-water were negligibly small for the velocity range tested.

D. Ice Floes

1. Model ice. Ice sheets were grown from a 0.7-percent, by weight, urea solution according to the following procedure: With the cooler system operating at full capacity, the urea solution was cooled to a temperature of about 0.1°C above the solution's freezing temperature

(-0.30°C) and the air in the room was chilled to about -12°C. A water circulation system provided the necessary mixing of the solution to prevent the formation of an unwanted ice cover. Before being wet-seeded, the surface of the urea solution was screened to remove any ice which may have formed during the solution cooling process. Then, the water circulation and the blowers of the cooling units were shut off and the cold room was fogged with a fine spray of water droplets. The spray was produced using a pressurized air spray gun and a pressurized tank. The water droplets froze in the air and settled onto the surface of the water which had by then reached the freezing temperature of the solution (-0.30°C). This wet-seeding process prevented the unwanted formation of relatively large ice crystals and enabled a multitude of small crystals to grow simultaneously over the surface of the urea solution.

Each ice sheet was grown to about 85-percent of its final thickness 30 mm (1.35 m prototype thickness). The room temperature was then raised so that the air temperature at an elevation of about 10 mm above the ice sheet was about 2 to 4°C, and the ice sheet was warmed and weakened.

The flexural strength, σ_f, and the flexural modulus of elasticity, E_f, were monitored until σ_f attained a prescribed value of about 20 kPa. The load F to fail a cantilever beam of length ℓ, thickness h, and width b, in downwards flexure, was used to estimate σ_f;

$$\sigma_f = \frac{6F\ell}{bh^2} \tag{14}$$

Four to six cantilever beams were tested at several locations around the ice sheet in order to obtain a representative mean value of σ_f at regular periods before the test.

The flexural elastic modulus E_f was determined by measuring the increment δ of the vertical deflection of the ice sheet due to small increments of a point load ΔP, which was applied at the center-point of the ice sheet. Thereby,

$$E_f = 0.188 \frac{(1-\nu^2)}{\rho_w g h^3} \left(\frac{\Delta P}{\delta}\right)^2 \tag{15}$$

in which ν = Poisson ratio for ice, which was taken as 0.3; ρ_w = density of water; and, g = gravity acceleration.

The principal dimensions of the ice sheets are listed in table 2. The data associated with each ice sheet are listed in table 3.

2. Preparation of ice floes. The ice sheet grown prior to each test was cut into square ice floes having uniform width or nominal diameter, D_i, in the range of 0.075 to 5 m (3 to 225 m in prototype).

E. Test Procedure. A total of 15 tests were conducted; eight using the cable-moored, floating platform and seven using the fixed platform as shown in figure 19. For each test series, ice floes were pushed with a constant speed in the range of 0.01 to 0.12 m/s (0.13 to 1.6 kts in approximate prototype scale for "Kulluk") against the test platform. The relationships between model and prototype values of ice-floe speeds are given in figure 20, while the relationships between forces and moments of model platform and those of prototype are shown in figure 21.

For some ice sheets, two tests were conducted: an initial test with smaller ice floes, a second test with a sheet of level ice corresponding to an ice-floe diameter of 5 m (225 m in prototype).

IV. PRESENTATION OF RESULTS

The time-histories of horizontal (surge) mooring forces, vertical displacement (heave) and pitching angle during full contact between the moored platform and floes of level ice were analyzed to yield values of the temporal mean, standard deviation about the temporal mean, together with the maximum and the minimum values for each transduced signal. The resulting values are presented in table 5. Appendix 1 contains records of the time histories.

The effects of ice-floe diameter on mooring force, heave displacement and maximum pitch angle due to ice-floe impact are plotted in figures 22, 23 and 24, respectively. The effect of ice-floe speed on the horizontal component of mooring force, vertical displacement (heave) and pitch angle can be seen in figures 25, 26 and 27.

The time-histories of restraining forces (heave and surge) and moment (pitch) during full contact between fixed platform and floes of level ice were analyzed to yield the temporal mean, standard deviation about the temporal mean, and the maximum and the minimum for each record. The resulting values are given in figures 22 through 27 and are listed in table 6.

The effects of ice-floe diameter on the restraining forces and moments experienced by the fixed platform are plotted in figures 28, 29 and 30. The effects of ice-floe impact speed on restraining forces and moments are shown in figures 31, 32 and 33.

V. DISCUSSION OF RESULTS

It was found that the test platform's facility to surge, heave and pitch significantly affected the ice-related forces that it experienced. The following discussion documents the influences of platform motions on ice-related forces and describes the effects of ice-floe diameter and speed on both the ice-related forces and motions that were experienced by the test platform.

A. Observations of Ice-Floe Impact with the Test Platform.

When the field of ice floes impacted the test platform, ice was deflected downwards and flexurally failed to produce cusp-shaped ice rubble. The impact of ice floes, together with the vertical force required to break the ice floes, caused horizontal and vertical forces to be exerted against the platform. Together, these forces exerted a pitching moment about the platform's center of gravity. Pieces of ice rubble were rotated until they were parallel to the surface of the platform, then were slid down and along the platform. Some ice rubble accumulated in front of the platform and some were pushed beneath it. Usually a layer of about two-pieces thick accumulated in front of the platform, while a single layer of ice rubble became lodged beneath the platform.

The foregoing description of ice-floe impact with the platform is schematically depicted in figure 34. The series photographs shown in figure 35 illustrate ice-floe impact for the four sizes of ice floes that were used for the study.

The flexural failure of the ice floes, together with the submergence, sliding and accumulation of broken ice pieces, and friction between ice and platform, all exerted forces against the platform. These forces caused the moored platform to respond dynamically, by heaving, surging and pitching. For the test platform fixed or restrained from moving the ice forces invoked restraining forces acting through the multi-axial load cell.

Because the ice forces acted intermittently for varying periods of time and over different areas of the platform's hull, the test platform experienced unsteady ice loadings. For this reason, the mean values and the standard deviations of the ice forces and platform displacements are plotted in figures 21 through 33.

The smaller ice-floes (ratio of ice-floe diameter to waterline diameter of the platform, $D_i/D_{LW} \leq 0.1$) when impacting the platform did not fail by bending because they were of similar size, or smaller than the ice rubble produced by the flexural failure of the large floes. As the smaller ice floes advanced toward and impacted the platform, they were pushed down without flexural failure, they were then rotated until becoming parallel to the surface of the platform and finally slid along the surface of the platform's hull. The smaller ice floes moved in a similar manner around the platform as did ice rubble broken from larger ice floes ($D_i/D_{LW} \geq 0.5$). The movement of the smaller ice floes around the platform did not involve the flexural failure of ice, therefore the ice forces generated by smaller ice floes were smaller than those produced by bigger ice floes which had to be broken flexurally, so that they could pass around the platform.

The simulated field of ice floes did not become laterally unstable and did not buckle during the tests.

B. The Effect of Ice-Floe Diameter on Ice Loads. The maximum values of measured mooring and ice forces are here taken to be the temporal average value plus two times the standard deviation of the values recorded during full contact between ice floes and the platform. For estimating the maximum values of measured forces, moment, etc., the limited length of the time histories of the recorded data, and the possible variation of mechanical properties of ice over the test floes, a 97.7% confidence limit would be statistically more reliable than the measured maximum value.

For the test platform when either moored or fixed, the maximum and temporal mean values of mooring or restraining forces due to ice-floe impact increased with increasing ice-floe diameter (see figures 22 and 28). The forces asymptotically approached that associated with impact of the platform with an ice floe much larger than the platform. This increase is attributable primarily to the added resistance associated with the flexural failure of ice floes, which becomes increasingly significant when ice-floe diameter approaches either platform diameter (for "circumferential", or lateral, dimension of the ice rubble) of the characteristic length (see figures 3 and 4) of the ice floe (for radial dimension of the resulting ice rubble).

The maximum and average values of moored platform's motions (surge, heave and pitch) due to ice-floe impact increased with increasing ice-floe diameter (see figures 23 and 24). These increases can be explained in terms of the additional ice load resulting from the flexural failure of ice. The effect of ice-floe diameter on the platform's surge displacement can be seen in figure 22; surge force $k_s y$ was proportional to the platform's surge displacement.

As is suggested in section I, because the test ice sheet was cut into regular arrays of rectangular slabs, the effect of floe diameter--slab size--can, perhaps, be also viewed as the effect on ice loads of fracture/crack density in an ice sheet. From this view-point it is apparent that lesser ice loads are generated when fracture/crack density is large, or floe size is small.

C. The Effect of Ice-Floe Speed on Ice Loads. The average values of the horizontal component of the mooring forces experienced by the moored platform increased linearly with increasing speed of ice-floe impact, as is shown in figure 25. From figures 26 and 27 it can be seen that the average values of heave and pitch motions that the moored platform underwent increased slightly with increasing speed of ice-floe impact. The maximum values of the mooring force, and the heave and pitch motions increased generally with increasing speed of ice-floe impact, as is indicated in figures 25, 26 and 27.

A marked difference occurred in the surge motion of the moored platform for relatively low speeds (0.01 to 0.02 m/s in model scale, 0.13 to 0.21 kts in prototype scale) compared to the larger speeds (see figure 25). When continuously impacted by ice floes, the moored test platform experienced its largest fluctuation of surge motion for relatively slow speeds of impact (see figure 25). This result can be attributed to a resonance condition that was set up between the oscillation of the platform and the dominant forcing frequency associated with ice breaking. For this reason, the fluctuations of mooring force experienced by the moored platform were greatest at lower speeds because the mooring force was proportional to the displacement of the linear mooring harness.

The average values of horizontal restraining force experienced by the fixed platform were not influenced by the speed of ice-floe impact (see figure 31). However, the maximum values of horizontal restraining force did increase linearly with increasing speed of ice-floe impact. Conversely, the average and maximum values of the vertical restraining forces experienced by the fixed platform decreased with increasing speed of ice-floe impact (see figure 32).

D. Inertia Forces and Moments Experienced by the Moored Platform. The equations of motion for a floating, moored platform can be written in tensor form as:

$$\underset{(i)}{(m_{ij} + \mu_{ij})}\ddot{x}_j + \underset{(ii)}{c_{ij}\dot{x}_j} + \underset{(iii)}{k_{ij}x_j} = \underset{(iv)}{F_i} \qquad (16)$$

in which terms (i) relate to platform inertia; terms (ii), (iii) and (iv) relate to damping, mooring and water-reaction restoring force/moment, and ice force/moment, respectively; m_{ij} = mass matrix components; μ_{ij} and c_{ij} = added-mass and damping coefficients, respectively; per convention, x = is a displacement for j = 1,2,3 and a rotation for j = 4,5,6; k_{ij} = stiffness matrix components; F_i = force matrix components.

Note that in this report the following nomenclature is used:

$y = x_1$, displacement in the surge direction;
$x = x_3$, displacement in the heave direction
$z = x_2$, displacement in the sway direction;
$\theta_p = x_3$, pitch rotation;
$k_s = k_{11}$, stiffness in surge direction;
$k_h = k_{33}$, stiffness in heave direction;
$k_p = k_{55}$, stiffness in pitch rotation;
$M_s = (m_{11} + \mu_{11})$ = virtual mass for surge;
$M_n = (m_{33} + \mu_{33})$ = virtual mass for heave;
$I_p = (m_{55} + \mu_{55})$ = virtual mass moment of inertia for pitch;
$F_1 = F_y$, ice force in surge direction;
$F_3 = F_x$, ice force in heave direction;
$F_5 = M_z$, pitch moment induced by ice forces F_1 and F_3;
$c_{11}, c_{33}, c_{55} = c_s$, c_h and c_p, respectively. The parameters M_s, M_h, I_p, k_s, k_h and k_p are properties of platform geometry and structure, and were estimated in accordance with their openwater values. The damping coefficients c_s, c_h and c_p for ice were not determined.

The magnitudes of inertia forces and moments, terms (i), were determined by multiplying measured acceleration and angular acceleration with the corresponding factors given in (16). Values of the restoring forces and restoring moment, terms (iii), were obtained by multiplying recorded surge and heave displacements and pitch angle with the corresponding spring stiffnesses given in (9) through (11).

Time histories of the force and moment components experienced by the floating, moored platform are shown in figures 36 through 39. Temporal records of the instantaneous ratio of inertia forces (for surge, heave

and pitch) to mooring forces during the period of full contact between ice floes and the platform are shown in figure 40.

The mean value of inertia force plus two times the standard deviation of the inertia force, which corresponds to a 97.7% confidence limit, were calculated from the measured record. The ratios of the 97.7% confidence limit of inertia force to that of mooring force for the period of full contact between ice floes and the platform are given in table 7.

During Exp. No. 5-2 (ice-floe diameter 5 m and ice-floe impact speed 0.08 m/s), the platform experienced large peak values of inertia force associated with surging (see figure 36). This occurred because Exp. No. 5-2 was the first experiment and no low-pass filter was used to filter noise from the transduced acceleration signals. For subsequent experiments (e.g., see figure 37) low-pass filters with a cut-off frequency 10 Hz were used to eliminate frequencies greater than 10 Hz from the accelerometer signals.

It can be concluded from figures 36 through 40 that the maximum value of the instantaneous ratio of inertia forces to mooring forces had a value of approximately 0.5. However, due to phase differences between inertia forces and mooring forces, the maximum inertia force, which corresponds to a 97.7% confidence limit, was approximately one third of the maximum mooring force as shown in table 7. The value of this ratio decreased with decreasing speed of ice impact.

E. The Dominant Period of Platform Motion During Ice Impact. The variance spectral densities of the dynamic behavior (forces and motions) of the floating, moored platform were analyzed using a Fast Fourier Transformation technique. The densities are plotted in figures 41 through 44. The periods corresponding to the 1st through 4th peaks in the spectra were evaluated and are presented in table 8.

For better resolution of the variance spectral density, longer time histories with higher sampling frequencies are needed. For the present study, the results were obtained using relatively short time histories due to the size limitation of computer memory that was available for the present study. (Considerably greater computer memory capacity will be available for future tests.)

Two distinct periods can be identified in the records of mooring force ($k_s y$); i.e., shorter and longer periods. The shorter period was approximately equal to the natural period for surge motion of the floating platform (see table 4). The longer period can be attributed to the occurrence of beating during platform motions.

The equation of surge motion, ((16) with i,j, = 1), can be rewritten and used to explain the occurrence of beating. In order to simplify the analysis, let the damping force in (16), $c_s \dot{y}$, be neglected and the pitch moment be uncoupled. Also assume that the ice force F_y is given as

$$F_y = F_{yo} \sin \omega t \ . \tag{17}$$

in which F_{yo} = the maximum value of an ice-force cycle with a frequency of ω. For an initial condition,

$$y = \dot{y} = 0, \text{ at } t = 0, \tag{18}$$

(16) can be solved (assuming motions to be uncoupled) to yield

$$y = \frac{q}{p^2 - \omega^2} \left(\sin \omega t - \frac{\omega}{p} \sin pt\right), \tag{19}$$

in which

$$p = \sqrt{k_S/M_S}$$

and

$$q = F_{yo}/M_S .$$

If the frequency, ω, of the ice force approaches the natural frequency of the mooring system, p, the following relation holds

$$p - \omega = 2\Delta \tag{20}$$

in which Δ is infinitesimally small. For this condition, the moored platform moves as if it were undergoing a beating oscillation, and the surge motion of the platform is given as

$$y = -\frac{q}{2\omega\Delta} \sin \Delta t \quad \cos \omega t. \qquad (21)$$

The term $\sin\Delta t$ in (21) represents the longer-period oscillation, while $\cos \omega t$ is the shorter-period oscillation.

When the moored platform was impacted by ice floes moving relatively slowly (0.01 to 0.02 m/s), the platform's surge motion was in resonance with the frequency of ice breaking and the platform experienced its largest surge motion.

The dominant periods of the mooring force during Exp. No. 10-2 (ice-floe diameter 5 m, ice impact speed 0.02 m/s) were longer than the natural period of surge motion. The component of the natural period of surge can be observed in the time histories given in figure of 39(a). Its amplitude was not dominant.

The dominant periods of pitch motion were approximately equal to the natural period of pitch motion as given in table 4. The dominant periods of heave motion were longer than the natural period of heave.

F. The Effect of Platform Motion on Ice Loads. In order to examine the effect of platform motion on ice-related forces, the restoring forces and moments experienced by the moored test platform were compared with restraining forces and moments experienced by the platform fixed so that it could not move. Values of the mooring and restoring forces ($k_s y$ and $k_s x$) and moments ($k_p \theta_p$) were determined by multiplying displacements and pitching angles with the corresponding values given in (9), (10) and (11). The ratios of the restraining forces to the restoring forces are shown in Table 9.

It is evident that, for slow impacts, the horizontal and vertical restoring forces experienced by the moored platform were of similar magnitude to the restraining forces experienced by the fixed platform. However, for the larger speed, the mooring force, $k_s y$, experienced by the moored platform was significantly less than the horizontal restraining force, F_x, experienced by the fixed platform.

The ratio of the restraining pitch moment, M_z, experienced by the fixed platform to the pitch moment, $k_p \theta_p$, experienced by the moored test platform was in the range of 0.41 to 0.67. This occurred because the lever arm of the pitching moment was bigger than the diameter of the load cell which was used to fix the platform. In other words, the twisting stiffness of the load cell was insufficient to fully restrain the platform from pitching. The pitching moment applied to the fixed platform was counteracted by both the load cell and water pressure which was equal to the product of the spring stiffness, (11), and pitching angle.

G. Comparison with the Performance Criterion for "Kulluk." The platform "Kulluk" is designed to be moored by twelve cables of diameter 85 mm, length 1150 m and breaking strength per cable, P_u, of 5.1 MN (from Gaida et al. 1983). The layout of cables in shown in figure 45. Because the ratio of water depth to cable length is as low as 0.02 to 0.05, the equilibrium of forces in the horizontal (surge) direction need only be considered.

The total mooring force associated with ice-floe impact, F_p, can be stated as

$$\sum_{n=1}^{N} F_n = F_p \qquad (22)$$

in which F_n = increment of mooring tension of n-th cable in the direction of ice movement; and, N = number of cables. The increment of mooring tension acting through each cable due to ice-flow impact is

$$F_n = k_n \delta \cos^2 \beta_n \qquad (23)$$

in which k_n = the equivalent spring stiffness of the n-th cable; β_n = angle of n-th cable with respect to the direction of ice movement; and, δ = displacement of moored platform, as is indicated in figure 45.

The platform experiences a maximum mooring force when tension in cable 1 reaches one-third of its breaking strength (Det Norske Veritas 1984). Commensurately, each cable exerts the following tension increments (figure 45):

$$F_1 = P_u/3 - F_t$$

$$F_2 = F_{12} \doteq F_1 \cos^2 \beta_2$$

$$F_3 = F_{11} = \doteq F_1 \cos^2 \beta_3$$

$$F_4 = F_{10} \doteq F_1 \cos^2 \beta_4 = 0$$

$$F_5 = F_9 = (F_t - F_{5R}) \cos^2 \beta_5$$

$$F_7 = F_t - F_{7R} \qquad (24)$$

in which F_t = initial cable tension; suffix R = residual tension of each cable when the platform experiences a maximum mooring force. If it is assumed that the residual tensions are negligibly small and that each cable is sized using a safety factor of 3 (Det Norske Veritas 1984), (22), (23) and (24) determine that F_p = 5.1 MN.

Using the Froude-number similarity criterion for scale-testing of vessels or structures in water, the maximum mooring force experienced by the model platform can be compared with the design value of mooring load for the cables of "Kulluk." The corresponding magnitude of F_p at a geometric model scale of 1:45 is

$$F_m = (1/45)^3 F_p = 56 \text{ N} \qquad (25)$$

The maximum mooring force that was experienced by the test platform occurred for the 5-m diameter test floe moving with the largest test speed (see table 2). the maximum measured mooring force was 56.0N, although the mean force plus two times its standard deviation was 50.9N. Both values are in remarkably good agreement with the design value estimated for "Kulluk."

H. Comparison with Ice Forces Predicted Using Ralston's Formulation. Measured values of ice forces are compared in figures 46

and 47 with values of ice forces that were calculated using (3) and (4), as proposed by Ralston (1980). It should be noted that Ralston's formulation does not take into account the dynamic effects associated with the relative motion of ice and platform. For this reason, the predicted values are compared with the test values obtained from the the platform fixed, so that it did not move, and for the slowest speed of ice-floe impact; 0.04 m/s and the largest diameter of ice floes; D_i = 5 m (Exp. No. 4-2). The measured value of horizontal ice force which the fixed platform experienced was in quite good agreement with the values calculated by Ralston's plastic limit formulation (figure 46). However, Ralston's formulation predicts a larger vertical ice force than was measured during the test (figure 47).

Parametric studies were conducted using (3) and (4) to investigate the effects of ice-sheet properties and platform geometry on the ice forces likely to be experienced by conical platforms. The parameters varied were flexural strength and thickness of ice sheets, ice accumulation around a concial platform, cone angle of platform, and frictional coefficient between ice and platform. The results are shown in figures 48 through 52.

Ralston's formulation of F_y and F_x indicates that F_y is linearly proportional to the flexural strength of an impacting ice floe (figure 48), and is proportional to 2.4 powers of ice-floe thickness (figure 49). His formulation also indicates that both F_y and F_x are linearly proportional to the amount of ice accumulated against a conical hull (figure 50), and that F_y is affected by both cone angle of the hull (figure 51) and friction coefficient between hull and ice (figure 52). However, his formulation suggests that vertical force, F_x, is not influenced significantly by either cone angle or coefficient of friction.

VI. CONCLUSIONS

The following principal conclusions were drawn from the study:

1. When the test platform was either moored or fixed, the mooring or

restraining forces, respectively, increased with increasing diameter of impacting ice-floes (figures 22 and 28). The forces asymptotically approached values that are associated with the impact of the platform with an ice floe that is much larger than the platform. This trend is attributed primarily to the fact that more ice breaking occurred when a field of larger ice floes impacted and was pushed around the platform.

2. Commensurately with item 1, the moored platform experienced larger displacements and accelerations when it was impacted by larger ice floes (figures 23 and 24).

3. The mooring forces experienced by the test platform increased with increasing speed of ice-floe impact (figure 25).

4. When continuously impacted by ice floes, the moored test platform experienced its largest fluctuation of surge motion for relatively low speeds of impact (0.01 to 0.02 m/s in model scale, 0.13 to 0.26 kts in prototype scale). This result can be attributed to a resonance condition set up between the oscillation of the platform and the dominant frequency of ice breaking. Relatively, the fluctuation of mooring force of the platform was greater for lower speeds, because mooring force was proportional to the displacement of the linear mooring harness.

5. The average values of the horizontal restraining force experienced by the fixed platform were independent of the speed of ice-floe impact (figure 31). However, the maximum values of horizontal (surge) restraining force increased linearly with increasing speed of ice-floe impact. Average and maximum values of vertical (heave) restraining force, on the contrary, decreased with increasing speed of ice-floe impact (figure 32).

6. The maximum inertia force, determined for the 97.7% confidence limit, was approximately one third of the maximum mooring force. The value of this ratio decreased with decreasing speed of ice-floe impact.

7. For very slow impact with ice floes, the restoring forces experienced by the moored test platform were almost equal to the restraining forces experienced by the platform when it was fixed. However, with increasing impact speed, the moored test platform experienced lesser forces than did the fixed platform. The restraining pitching moment of the fixed platform was smaller than the restoring moment of the floating platform. This was due to the smaller twisting stiffness of the load cell which was used for fixing the platform.

8. There were two, distinct periods in the temporal records mooring forces experienced by the moored test platform. One period was approximately equal to the natural period of the surge motion. The other, and longer, period is attributed to the set-up of beating in platform motion. When the platform experienced the large surge motion at relatively low speed (0.01 to 0.02 m/s) due to a resonance condition set up between the oscillation of the platform and the dominant frequency of ice breaking, the dominant periods of the mooring forces was longer than the natural frequency of the surge motion. The dominant periods of pitch motion were close to the natural period of pitch. The dominant periods of heave motion were longer than the natural period of heave.

9. The measured value of the maximum mooring force experienced by the model test platform and the design value for the prototype platform "Kulluk" were in remarkably good agreement.

10. For the slowest speed of ice-floe impact (0.04 m/s), the measured value of the horizontal ice force exerted against the platform when fixed from moving was in quite good agreement with the values calculated using Ralston's (1980) formulation. However, Ralston's formulation predicts a larger vertical force than was measured during the model tests.

11. It was found through parametric studies that the horizontal ice forces experienced by a conical platform fixed from moving are linearly dependent on the flexural strength of ice, the thickness of ice accumulation around the platform and frictional coefficient between ice and platform, and on 2.4 powers of ice thickness, and cone angle. Vertical ice forces are linearly dependent on flexural strength of ice and ice accumulation thickness, and on 2.4 powers of ice thickness. Frictional coefficient and cone angle do not signficantly effect vertical ice forces.

REFERENCES

Abdelnour, R. (1979), "Model Tests of an Icebreaking Inclined Plane", Arctec Canada Limited, FR 289C-2.

Croasdale, K. (1980), "Ice Forces on Fixed, Rigid Structures", CRREL, Spec. Rept. 80-26, p. 34-106.

Det Norske Veritas, 1984, "Rules for Classification of Mobile Offshore Units," Part 6, Chapter 2, pp. 3-4, Hovik, Norway.

Exxon Company, USA (1979), "Technical Seminar on Alaskan Beaufort Sea Gravel Island Design", Anchorage, Alaska (October 15) and Houston, Texas (October 19).

Faltinsen, O.M. (1975), "Motion of Large Structure in Waves at Zero Froude Number", Int. Symp. on Dynamics of Marine Vehicles and Structures in Waves, p. 99-114.

Frederking, R. (1984), "Exploration and Production Concepts and Projects for Arctic Offshore", Proc. IAHR Symposium on Ice, Hamburg, W. Germany, Vol. 4, p. 387-411.

Frederking, R. and Timco, G. (1985), "Quantitative Analysis of Ice Sheet Failure Against an Inclined Plane", Offshore Mechanics and Arctic Engineering Conference, Dallas, p. 160-169.

Frederking, R. and Schwarz, J. (1982), "Model Test of Ice Forces on Fixed and Oscillating Cones", Cold Regions Science and Technology, Vol. 6, p. 61-72.

Frederking, R. (1980), "Dynamic Ice Forces on an Inclined Structure", Physics and Mech. of Ice, P. Tryde (Ed.), IUTAM Symp., Copenhagen, p. 104-116.

Gaida, K.P., Barnes, J.R. and Wright, B.D. (1983), "Kulluk - An Arctic Exploratory Drilling Unit", OTC4481, OTC, p. 337-346.

Hnatiuk, J. and Wright, B.D. (1984), "Ice Management to support the Kulluk Drilling Vessel," Proc. 35th Annual Technical Meeting of Petroleum Society of CIM, Calgary, Paper No. 84-94, pp. 333-65.

Loh, J.K.S. and Stamberg, J.C. (1984), "New Generation Arctic Drilling System: Overview of First Year's Performance", Proc. 16th Offshore Technology Conference, Houston, Paper No. 4797.

Milano, V. (1975), "Ship Resistance to Continuous Motion in Ice", Trans. SNAME, Vol. 81, p. 274-306.

Milano, V. (1980), "A Reanalysis of Ship Resistance when in Continuous Motion through Solid Ice", INTER MARITEC 80, Hamburg.

Milano, V. (1982), "Correlation of Analytical Prediction of Ship Resistance in Ice with Model and Full Scale Test Results", Intermaritec '82, Hamburg, p. 350-372.

Ralston, T. (1978), "Ice Force Design Considerations for Conical Off-Shore Structures", POAC, p. 741-752.

Ralston, T. (1980), "Plastic Limit Analysis of Sheet Ice Loads on Conical Structures", Physics and Mechanics of Ice, Per Tryde (Ed.), IUTAM Symp., Copenhagen, p. 289-308.

Sorensen, C. (1978), "Interaction Between Ice Sheets and Sloping Structures", Inst. of Hydrodynamics and Hydraulic Eng., Tech. Univ. of Denmark, Series Paper No. 19.

Timco, G. (1984), "Model Tests of Ice Forces on a Wide Inclined Structure", IAHR Symposium on Ice, Vol. 2, p. 87-96.

Tryde, P. (1977), "Intermittent Ice Forces Acting on Inclined Wedges", CRREL, Report 77-26.

Van Oortmerssen G. (1976), "The Motion of a Ship in Shallow Water", Ocean Engineering, Vol. 3, p. 221-255.

Wessels, E. (1984), "Model Test Investigation of Ice Forces on Fixed and Floating Conical Structures", IAHR Symposium on Ice, Hamburg, Vol. 3, p. 203-220.

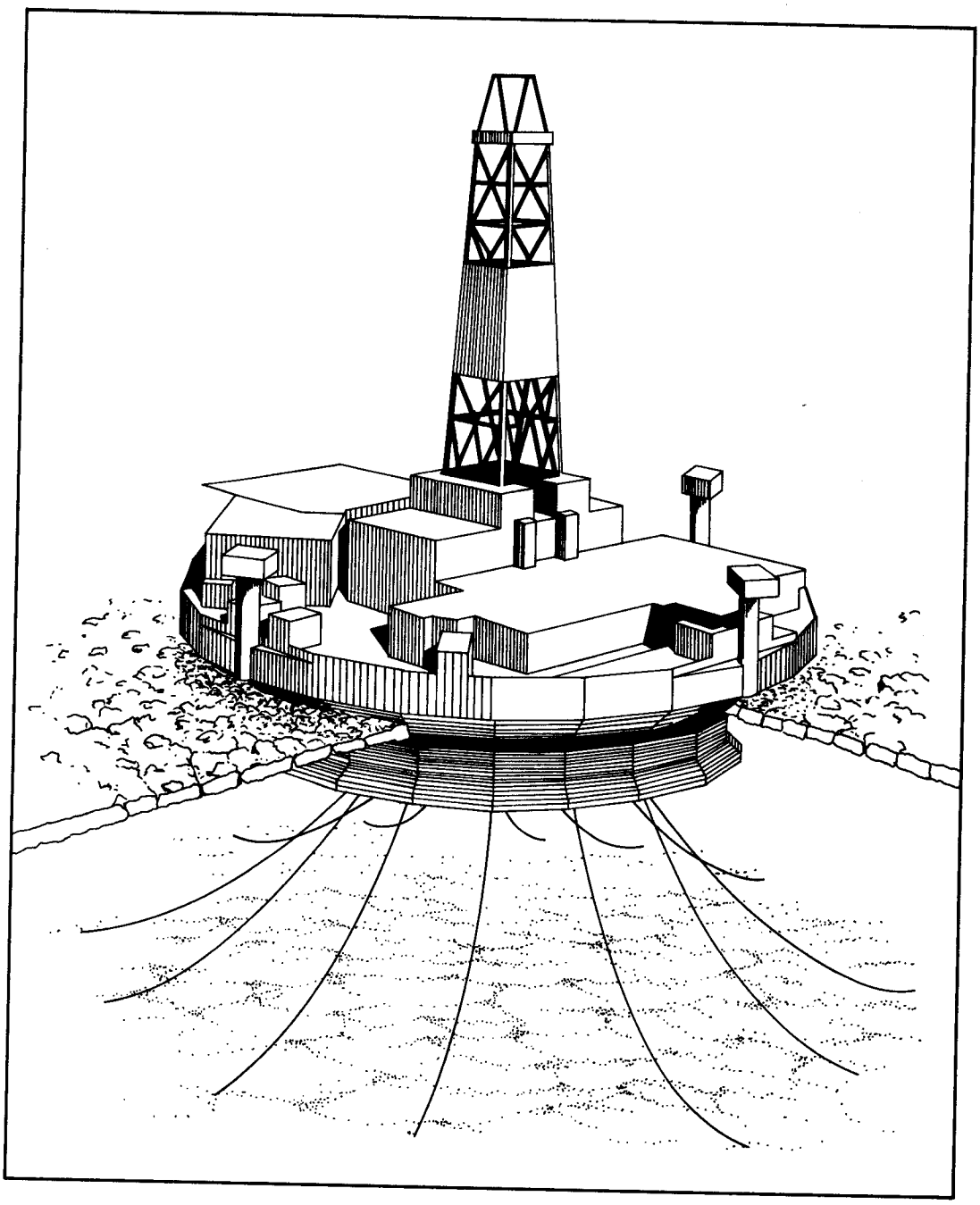

Figure 1. Layout of a floating, moored platform in ice-covered waters.

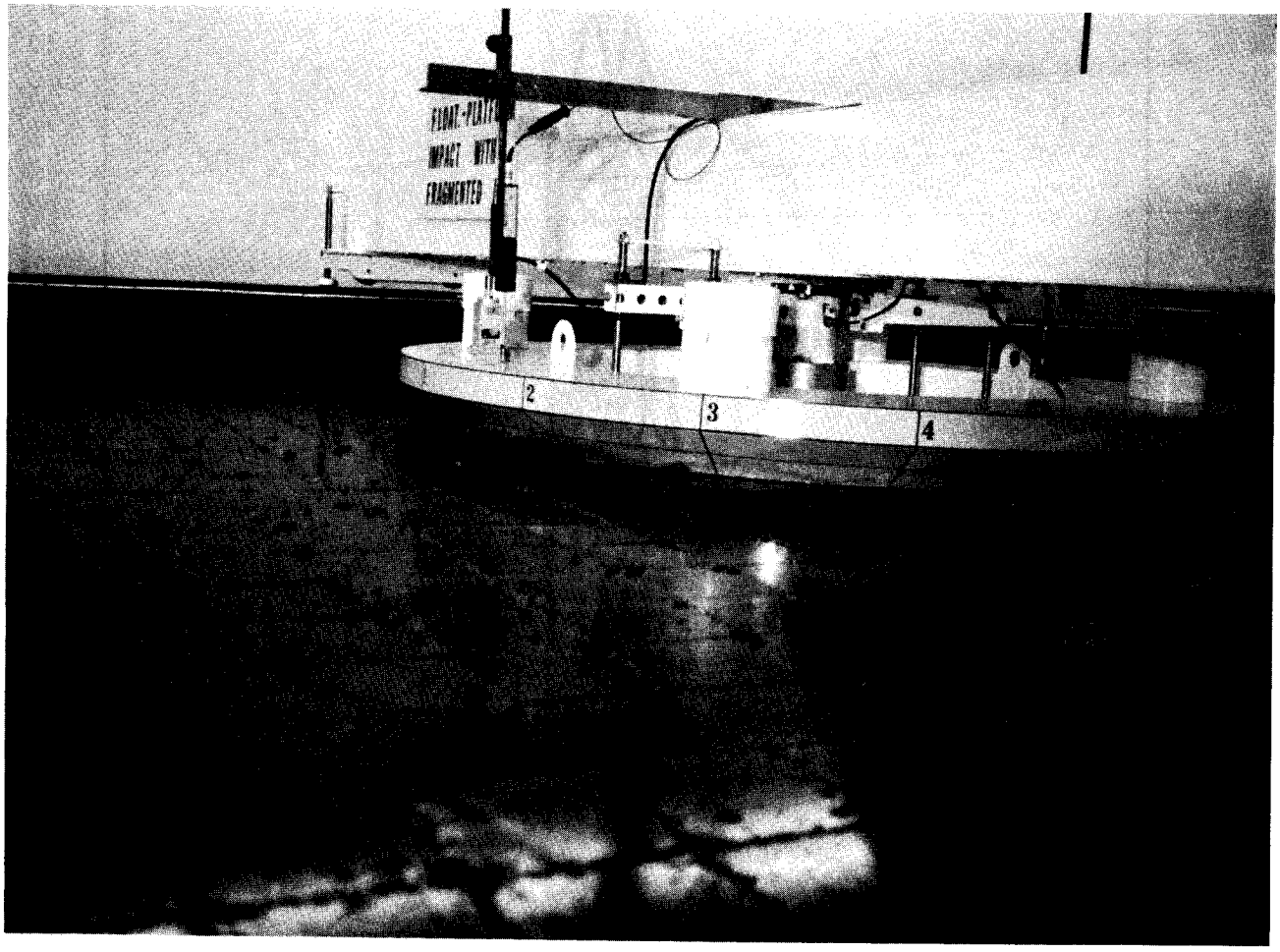

Figure 2. The test platform undergoing impact with ice floes.

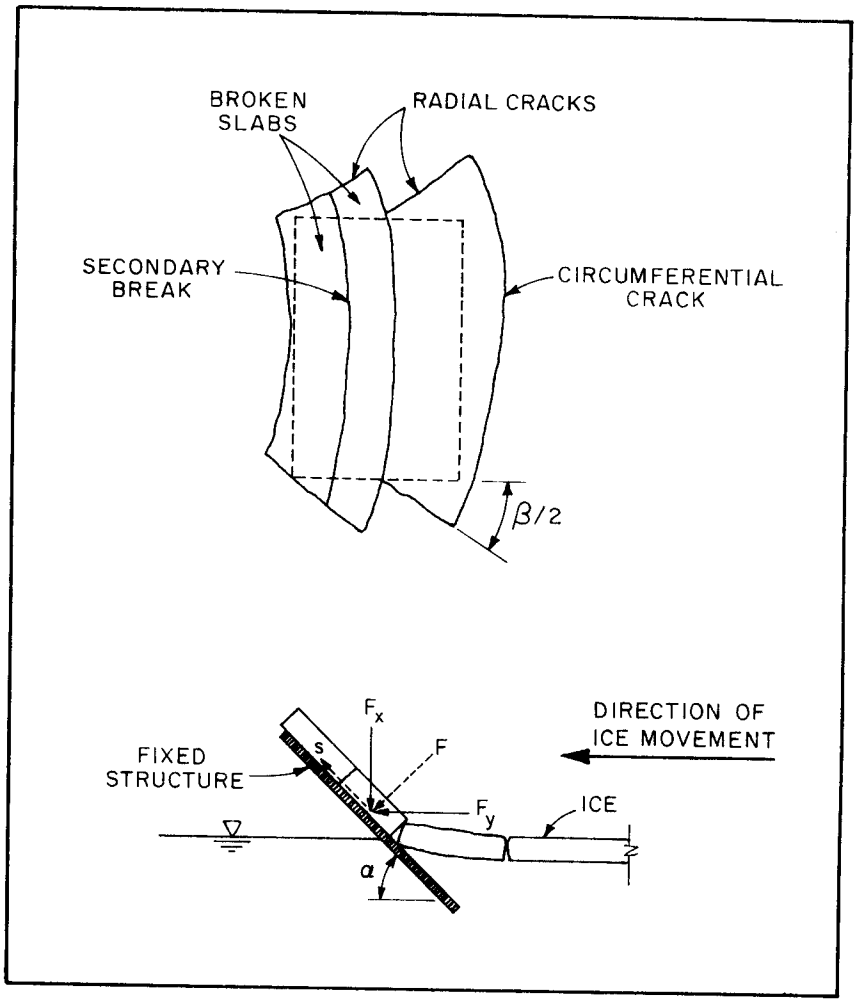

Figure 3. Schematic of ice-sheet impact against an inclined plane structure.

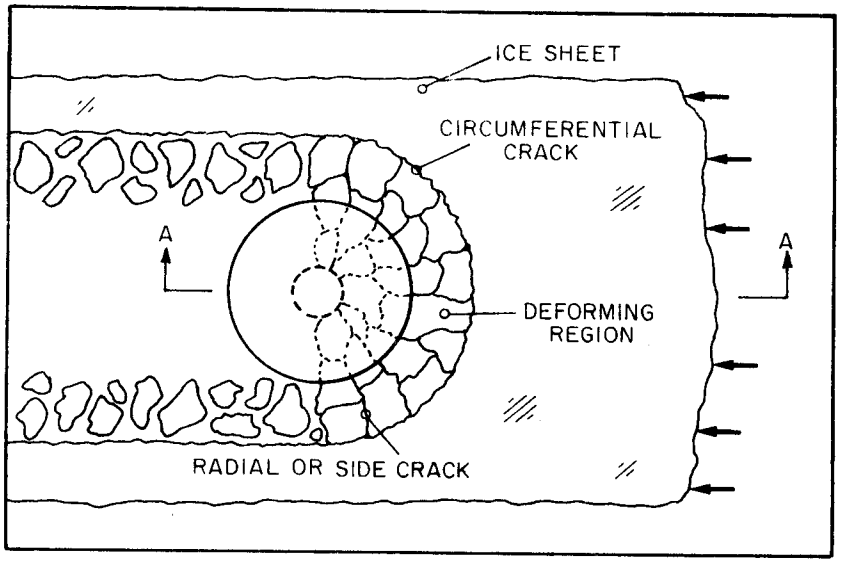

PLAN VIEW

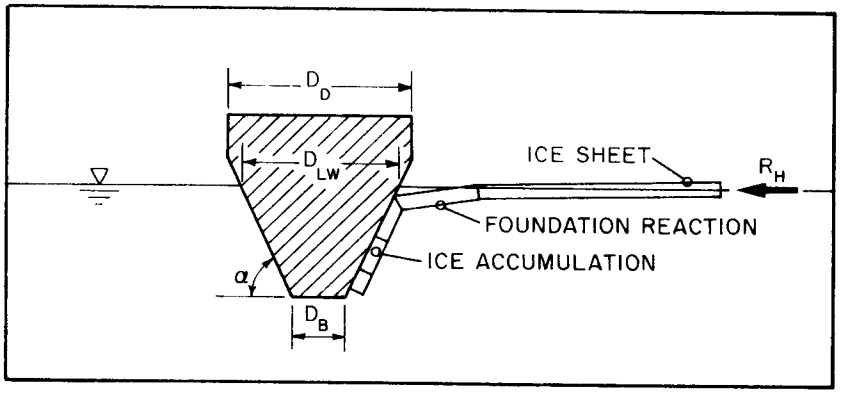

SECTION A-A

Figure 4. Sheet ice-sheet impact against a conical structure.

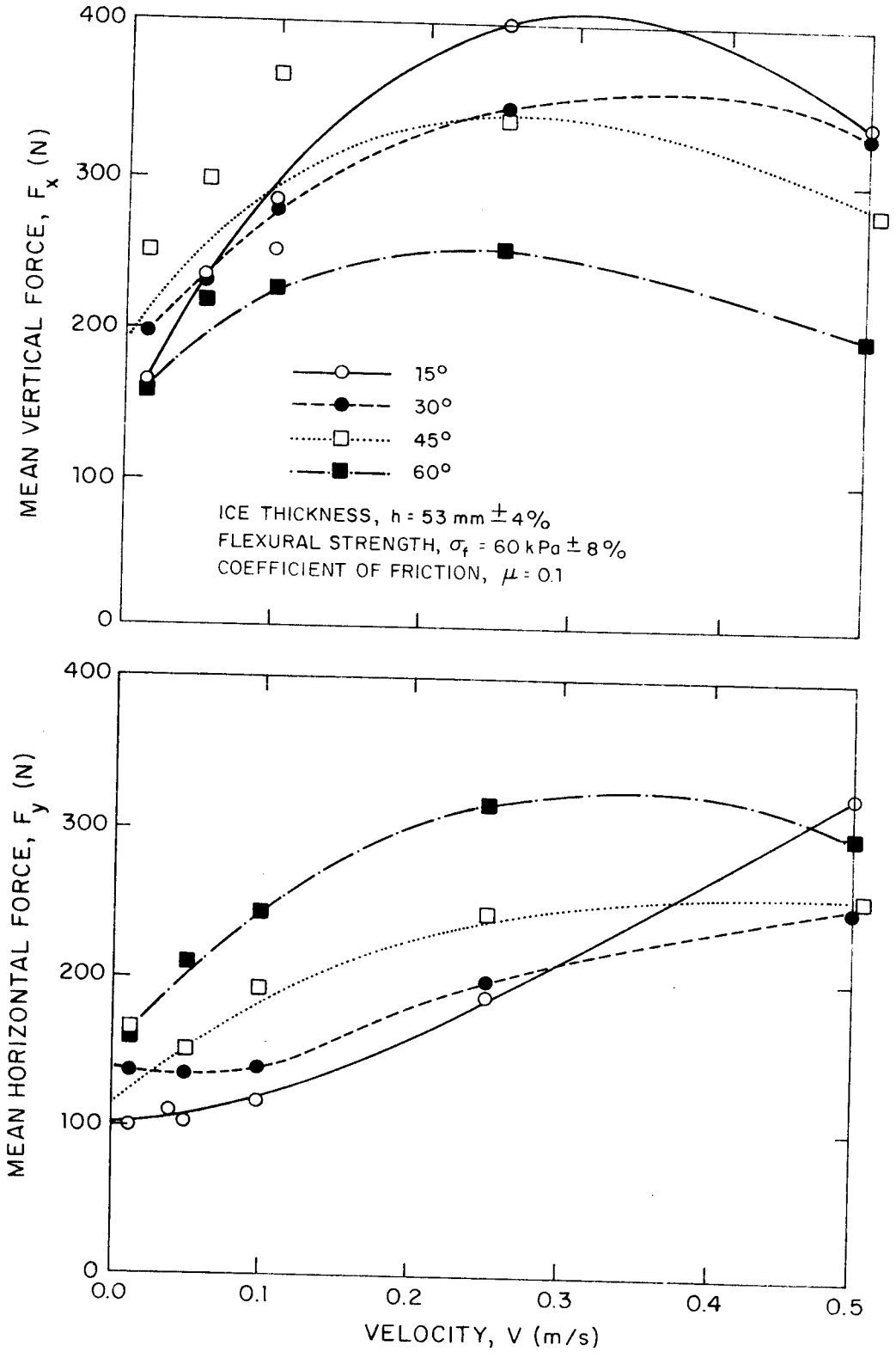

Figure 5. Mean values of vertical and horizontal ice forces against a cone (Frederking and Schwarz 1982).

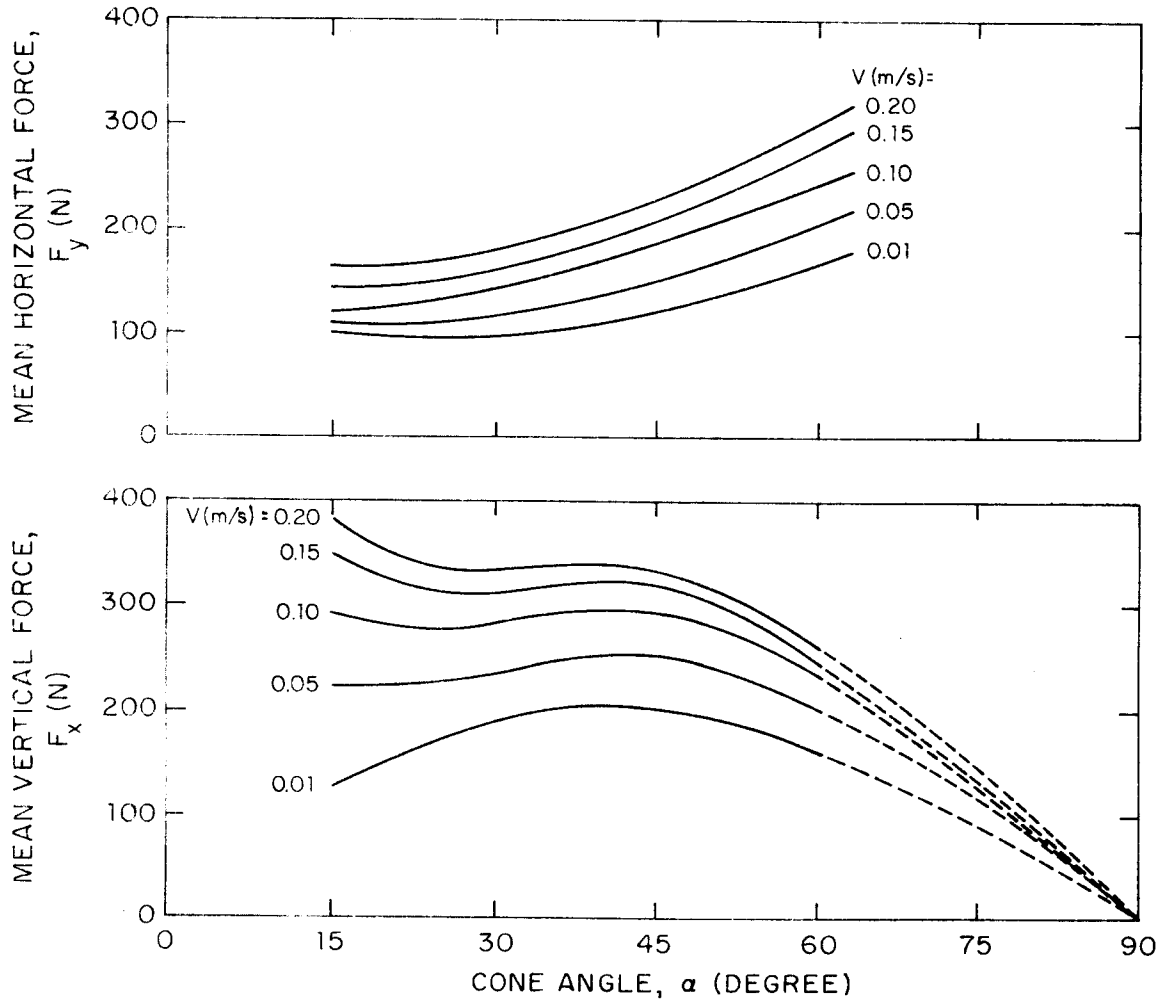

Figure 6. Influence of cone angle on ice forces (Frederking and Schwarz 1982).

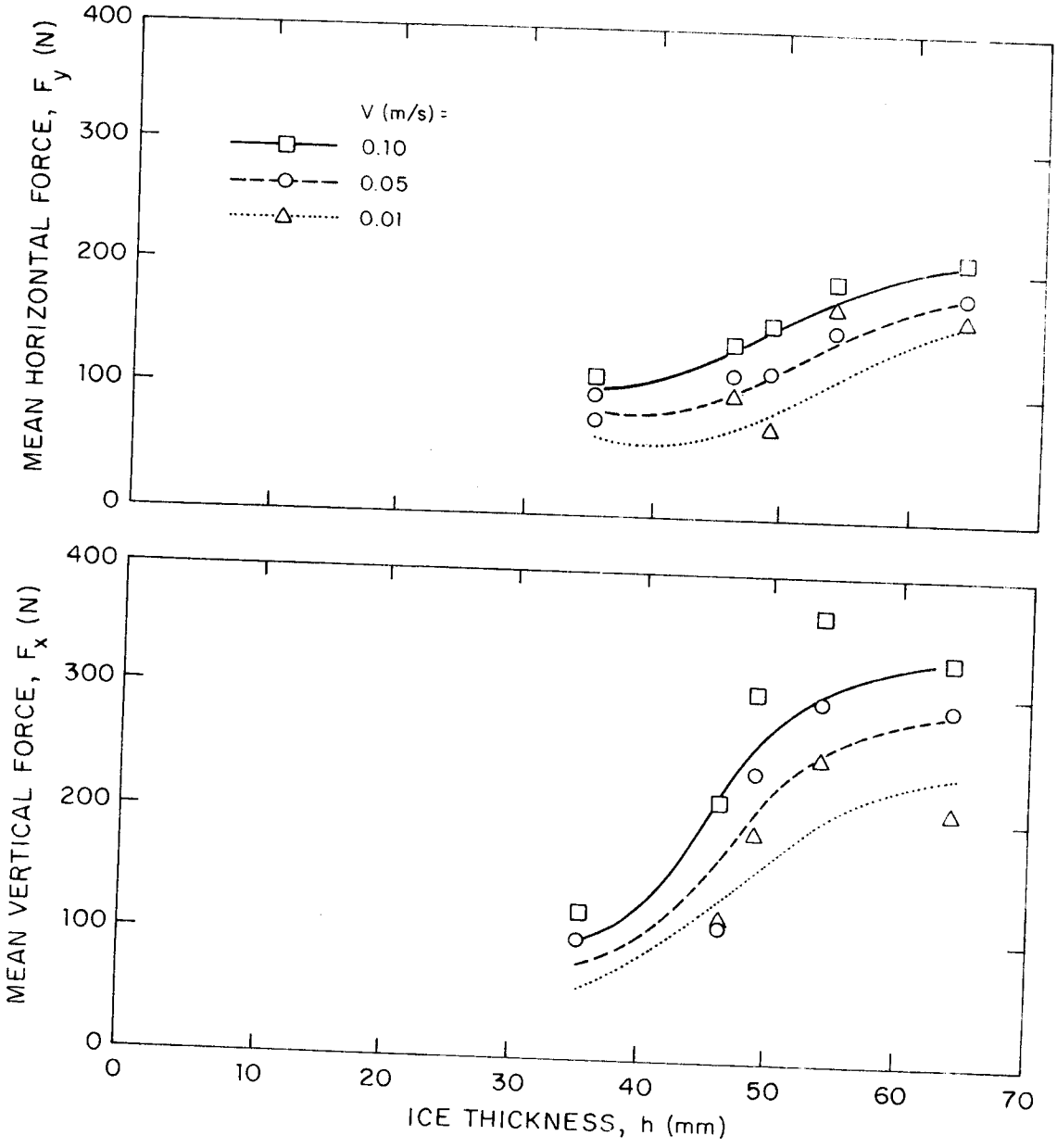

Figure 7. Vertical and horizontal ice-forces versus ice-sheet thickness (Frederking and Schwarz 1982)

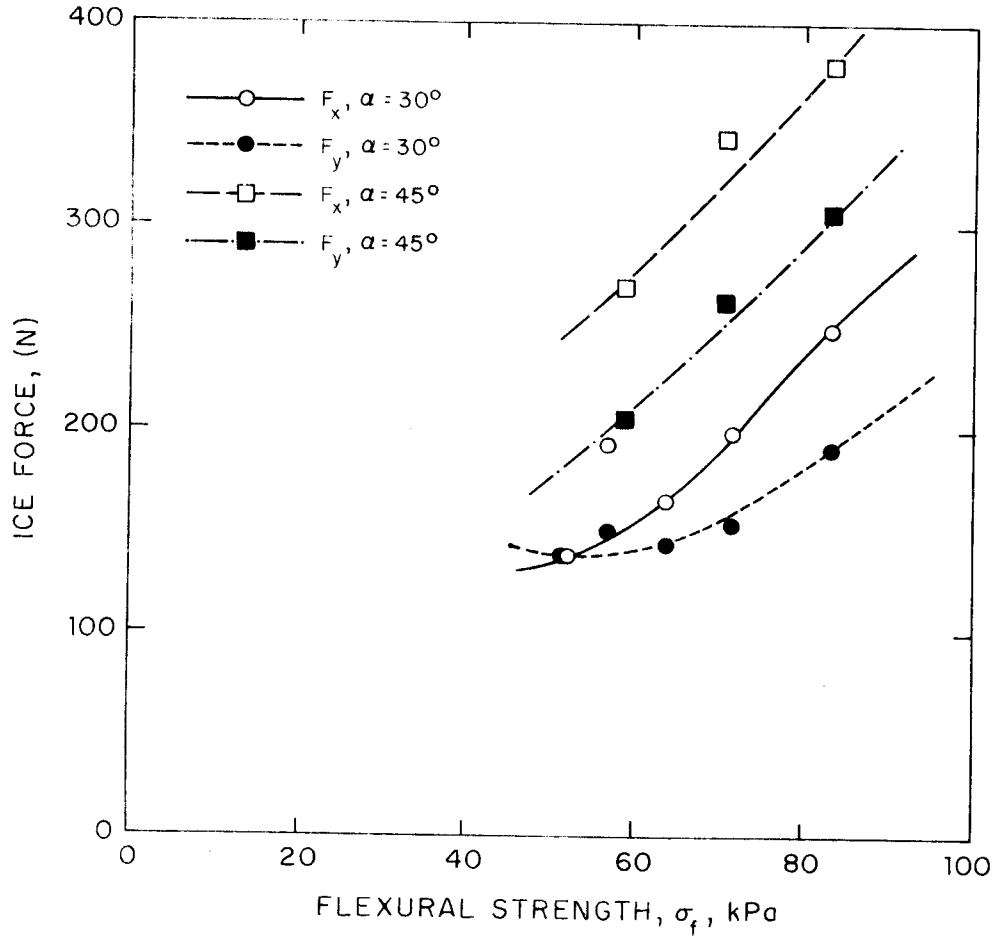

Figure 8. Influence of flexural strength on vertical and horizontal ice forces (Frederking and Schwarz 1982).

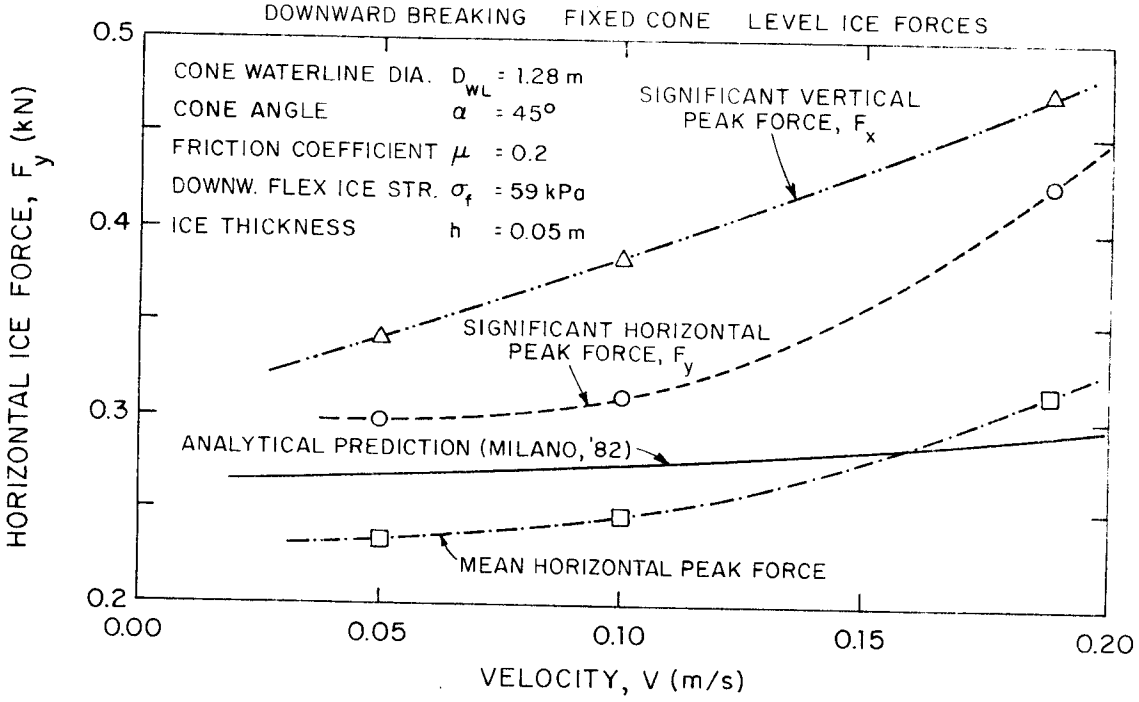

Figure 9. Measured and calculated ice forces versus velocity (Wessels 1984).

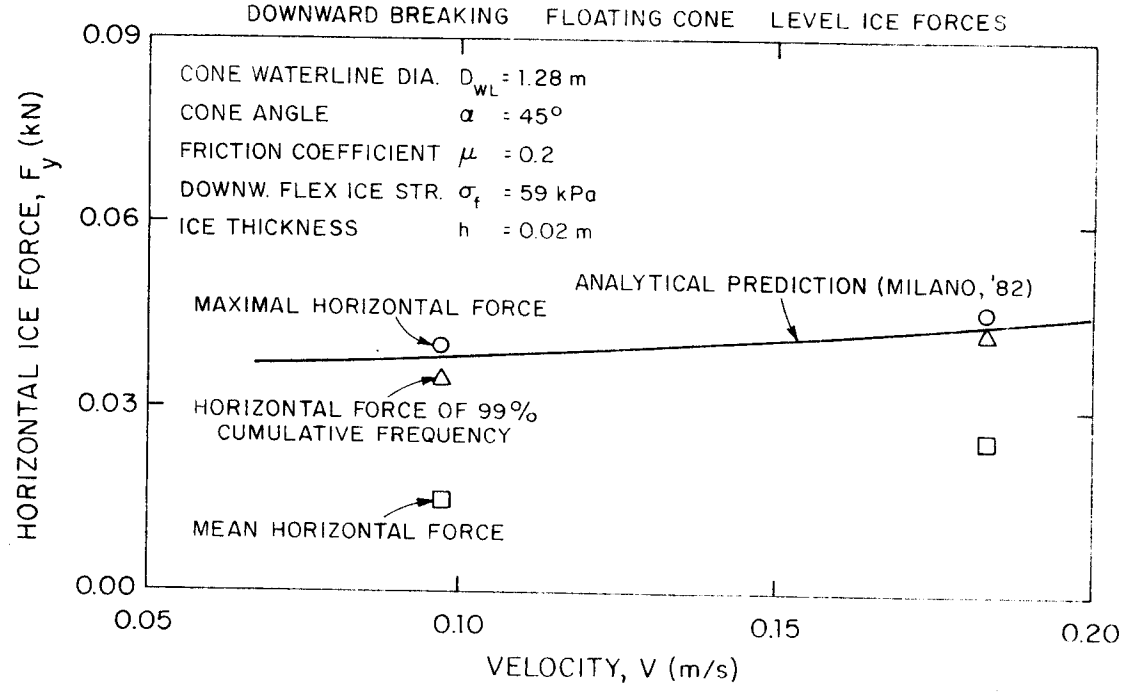

Figure 10. Measured and calculated ice forces versus velocity (Wessels 1984).

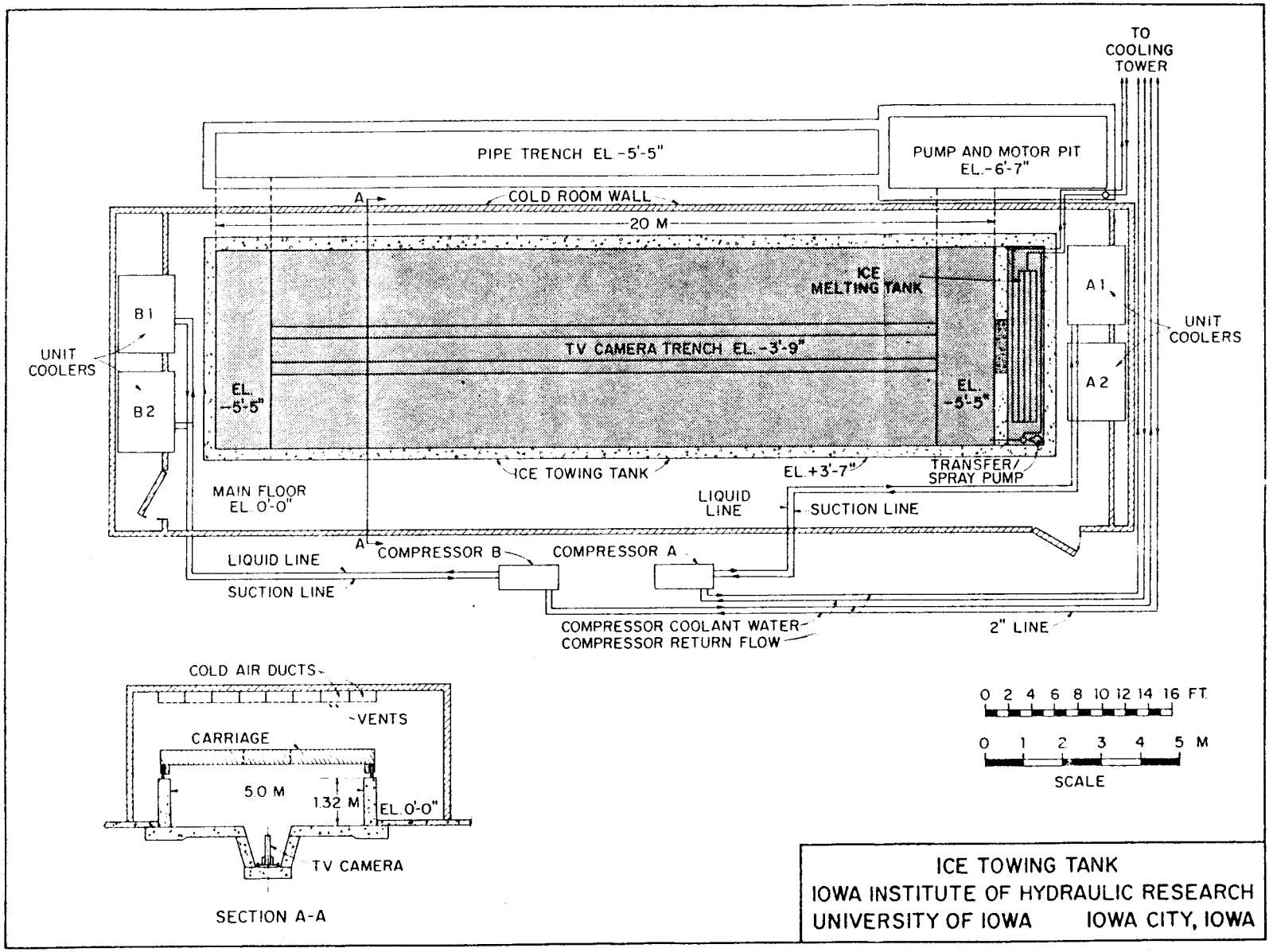

Figure 11. IIHR's ice towing tank.

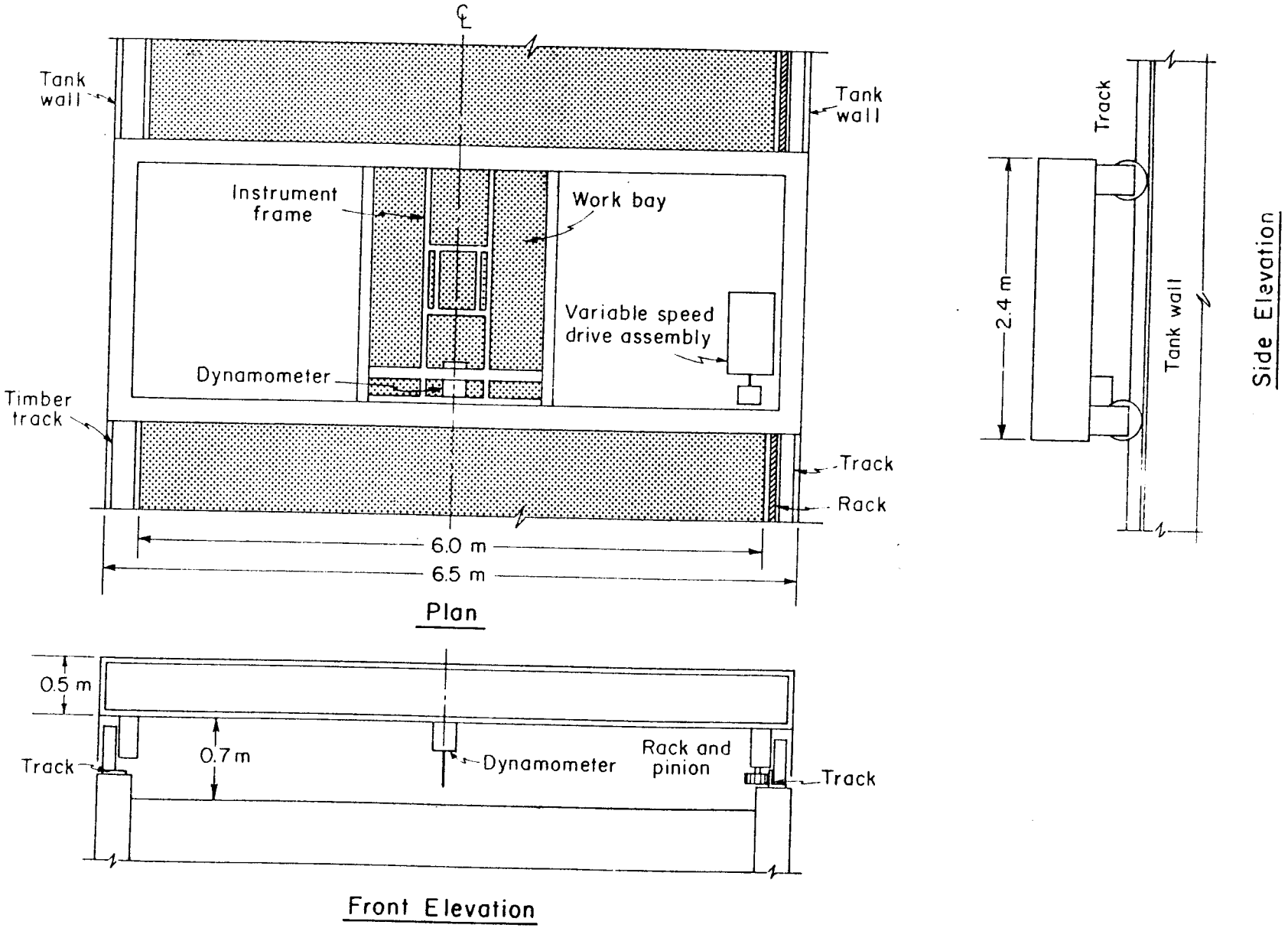

Figure 12. The towing carriage.

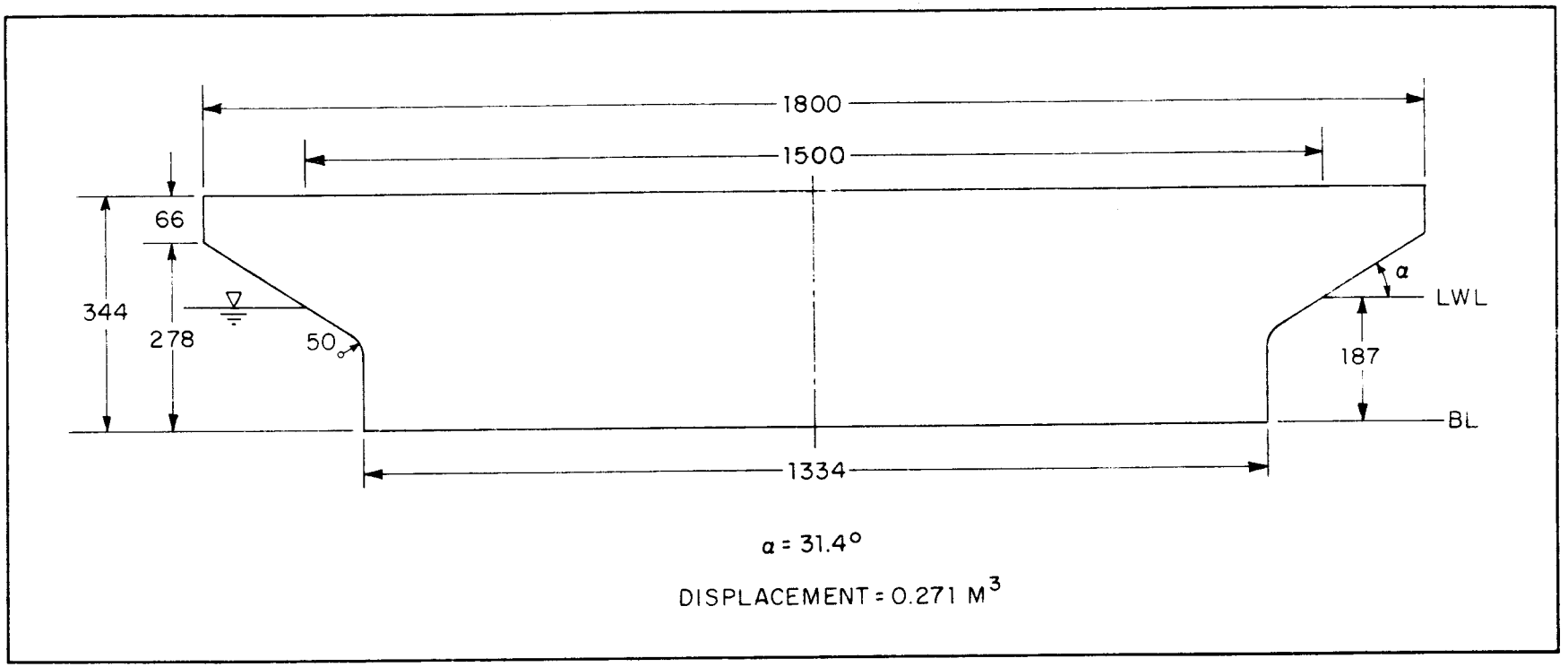

Figure 13. Form and principal dimensions of the test platform.

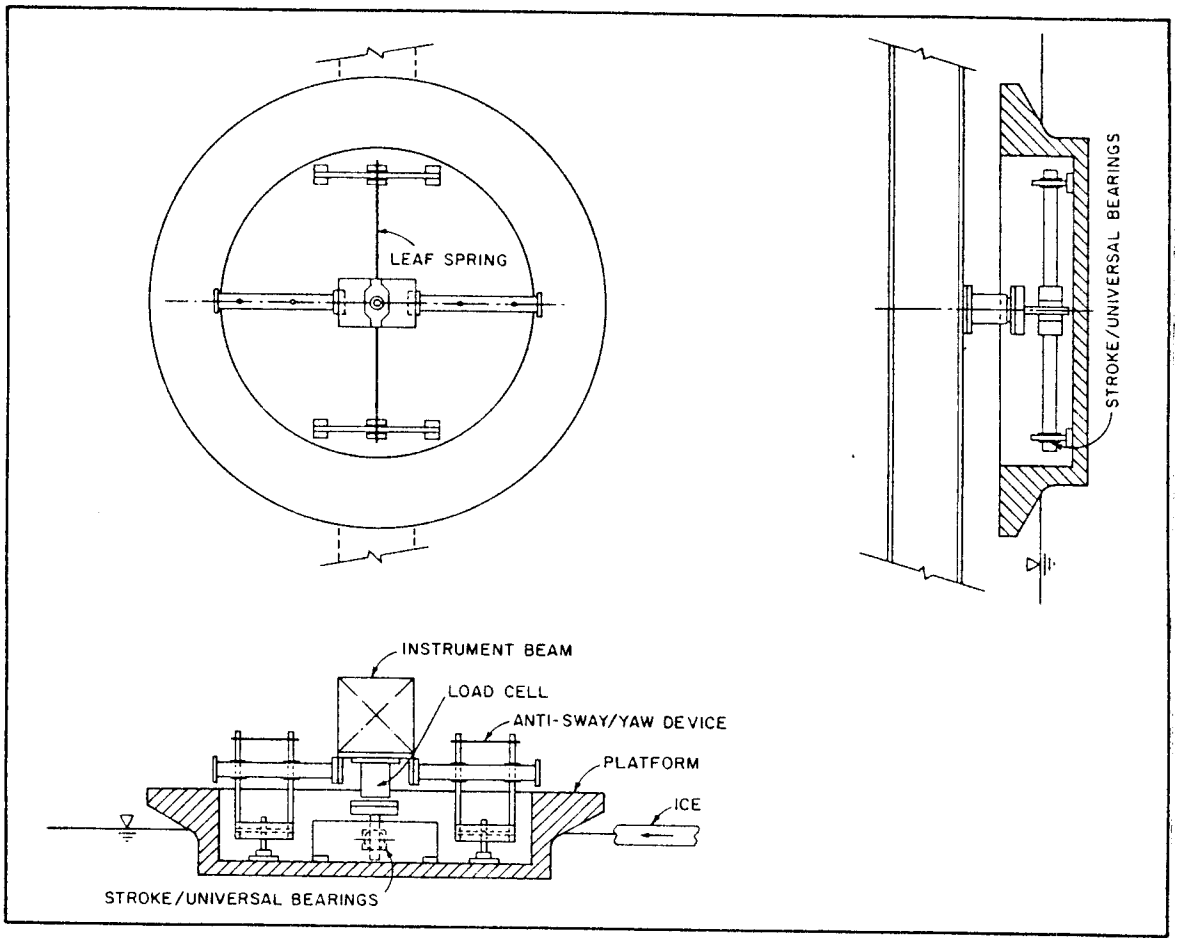

Figure 14. Instrumentation of moored platform.

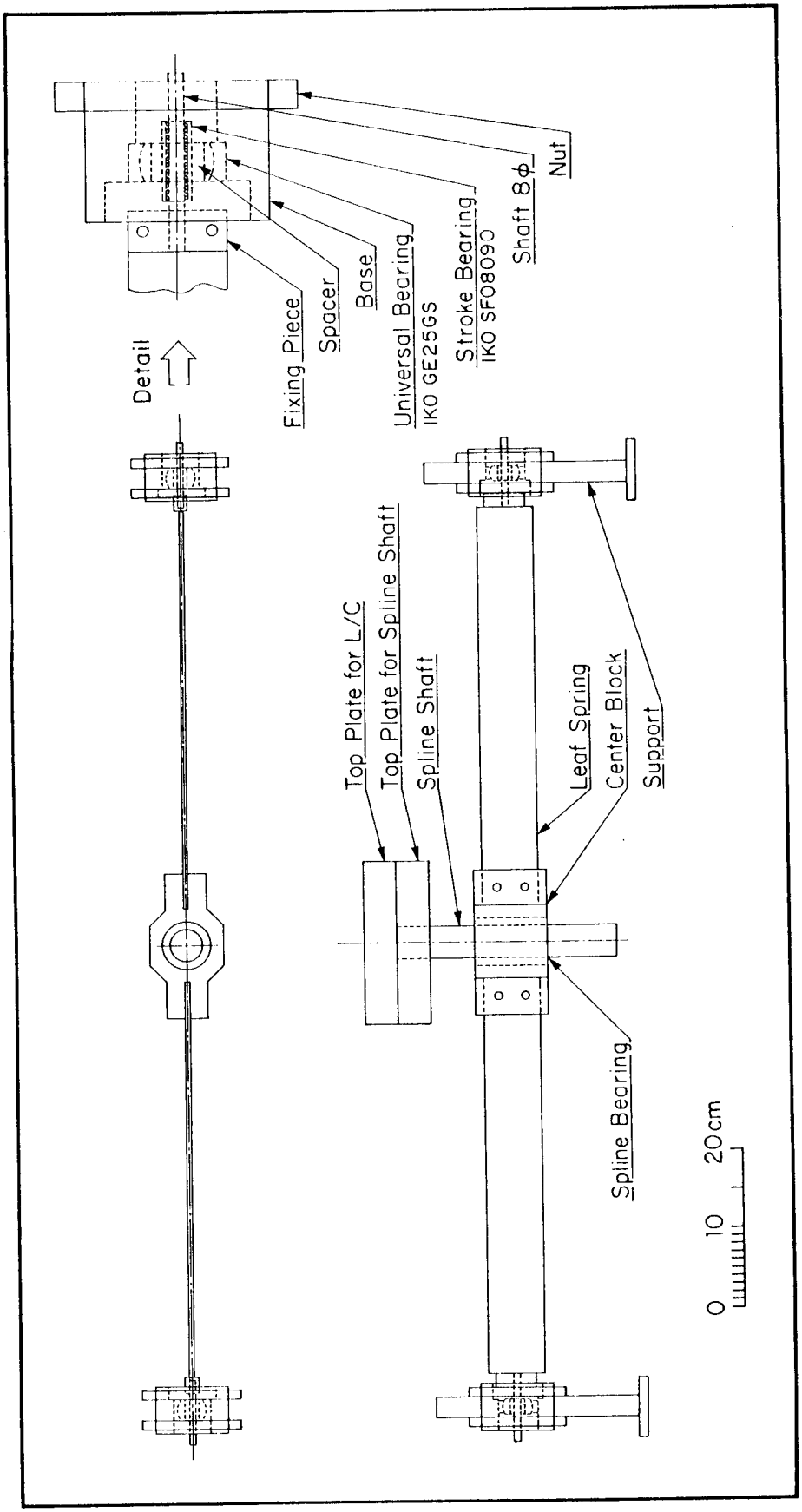

Figure 15. Details of mooring harness.

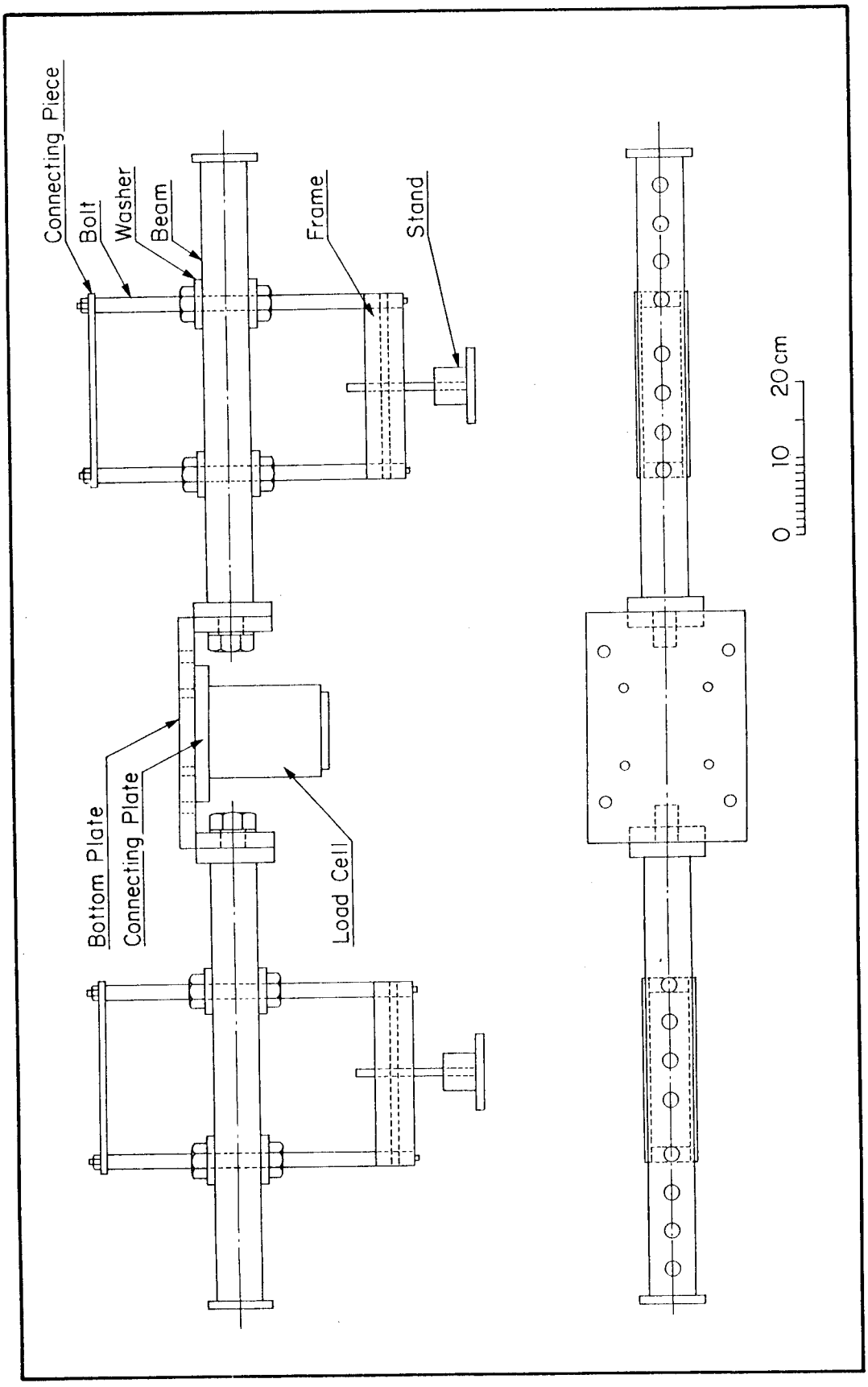

Figure 16. Details of the sway and yaw restraining device.

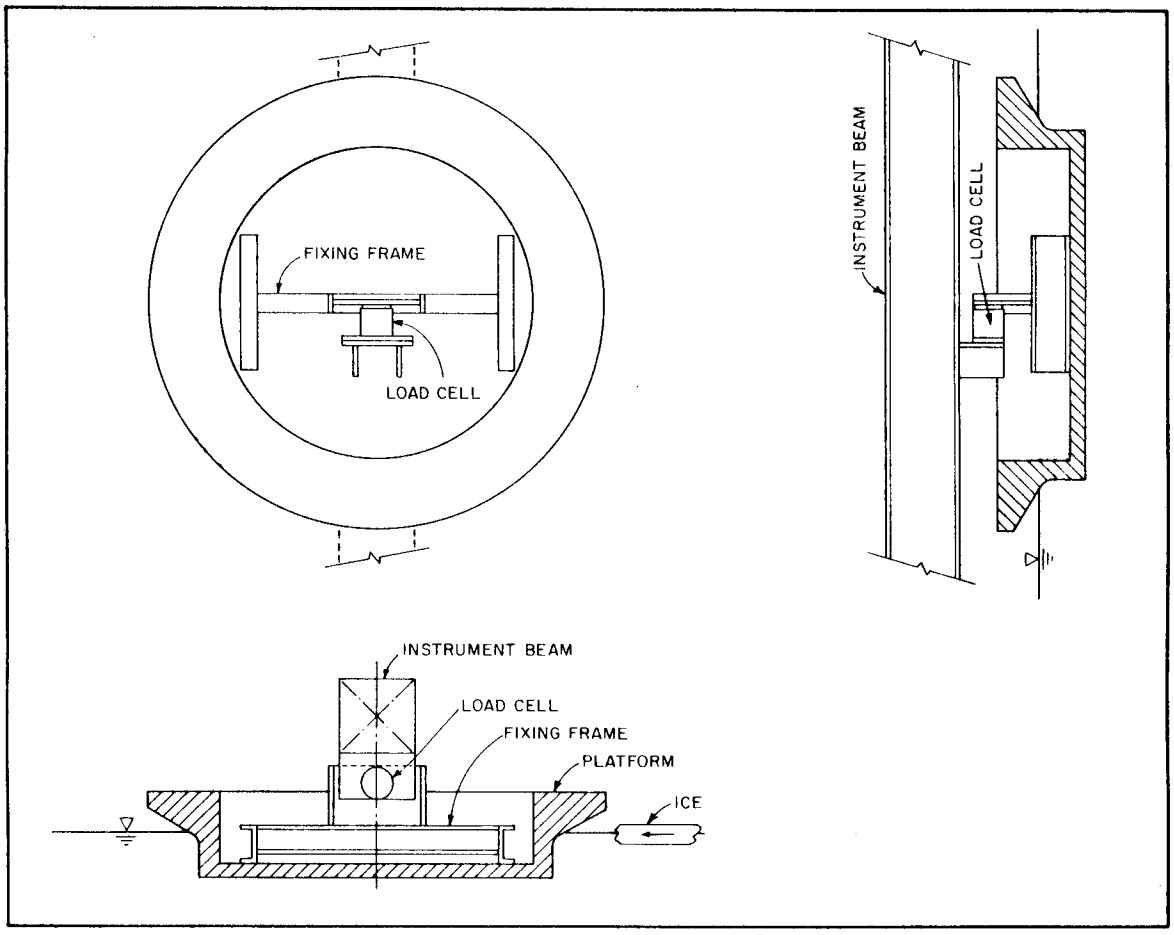

Figure 17. Instrumentation of fixed platform.

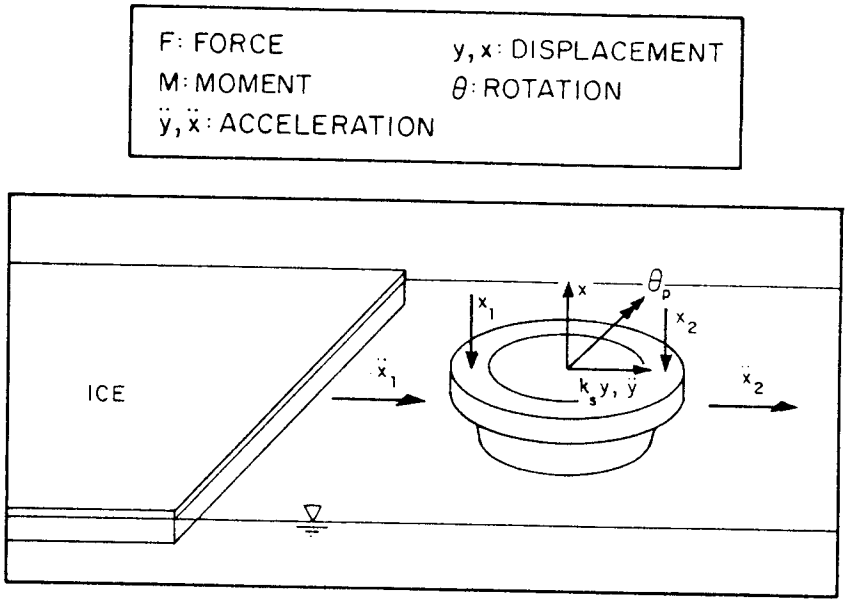

(a) MOORED PLATFORM

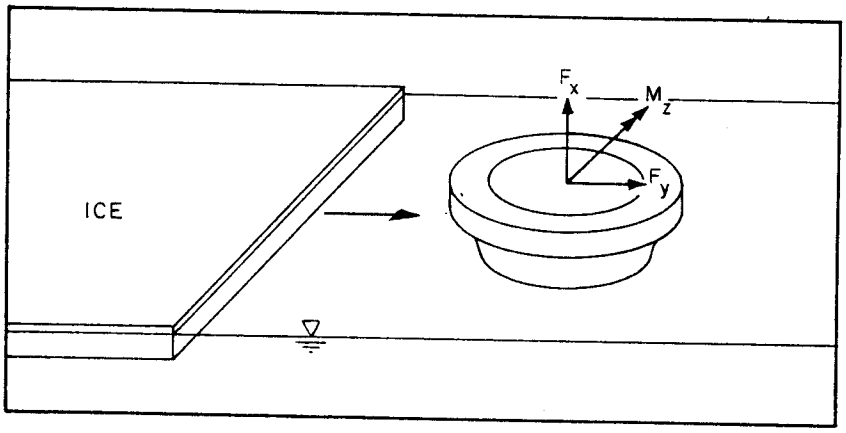

(b) FIXED PLATFORM

Figure 18. Locations of measurements and positive directions.

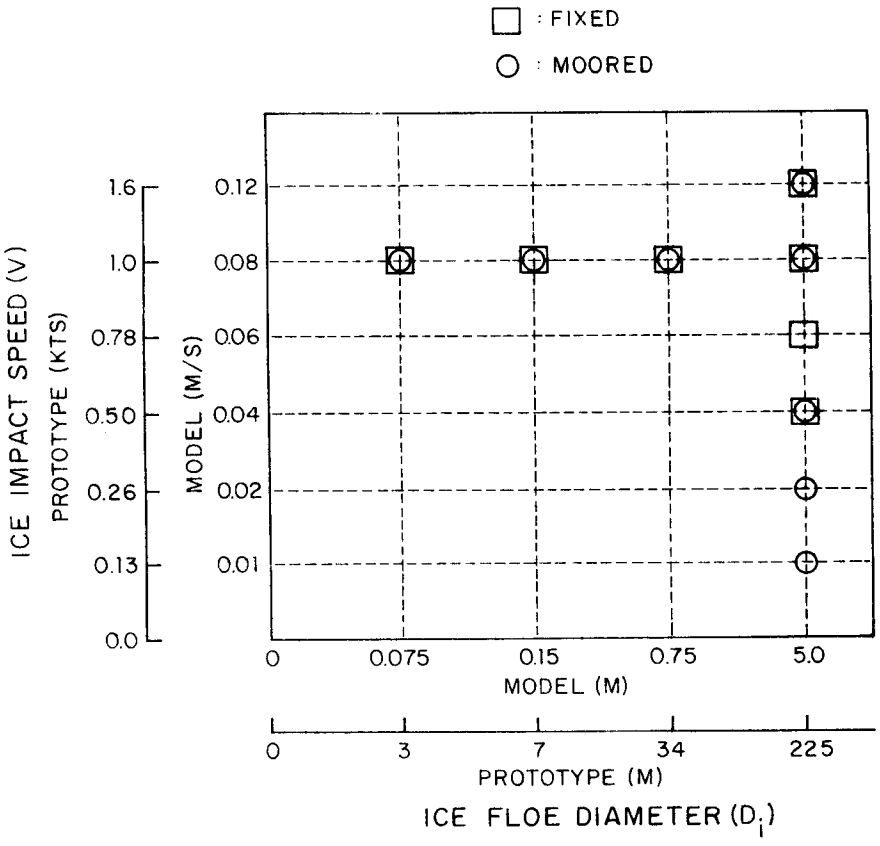

Figure 19. Program of experiments.

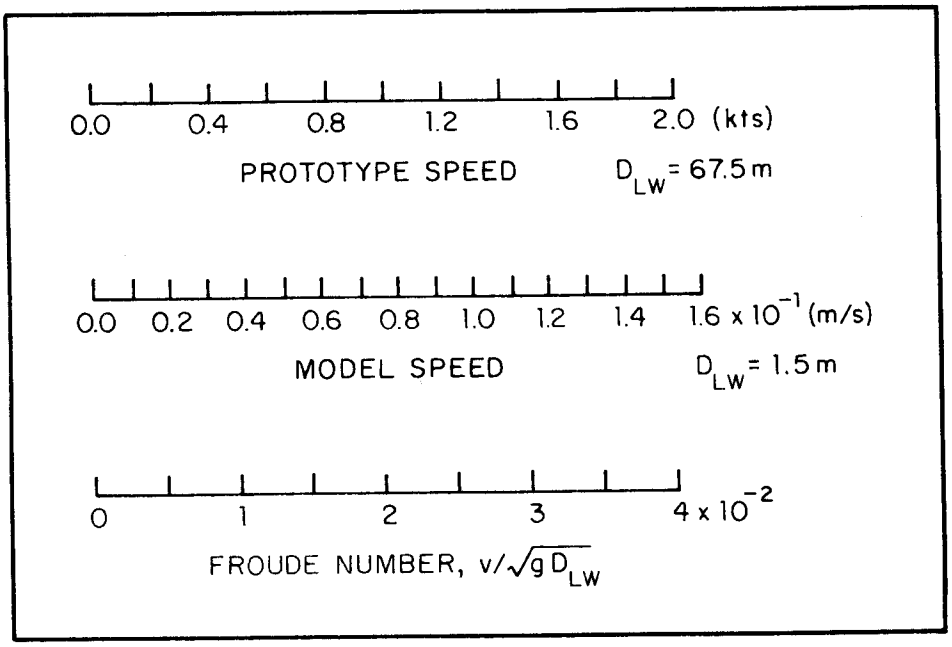

Figure 20. Relationships between model and prototype ice impact speed.

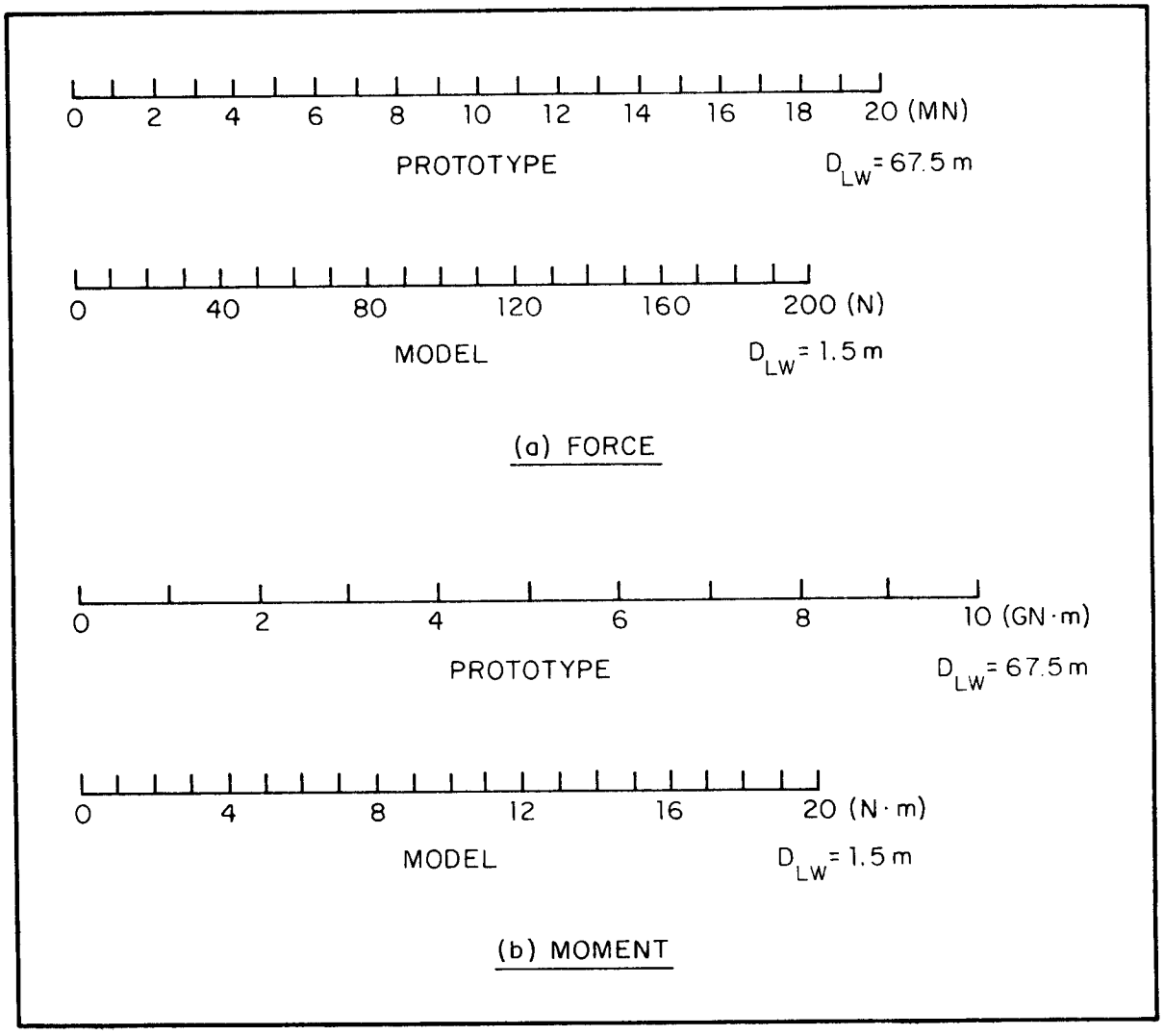

Figure 21. Relationships between model and prototype forces.

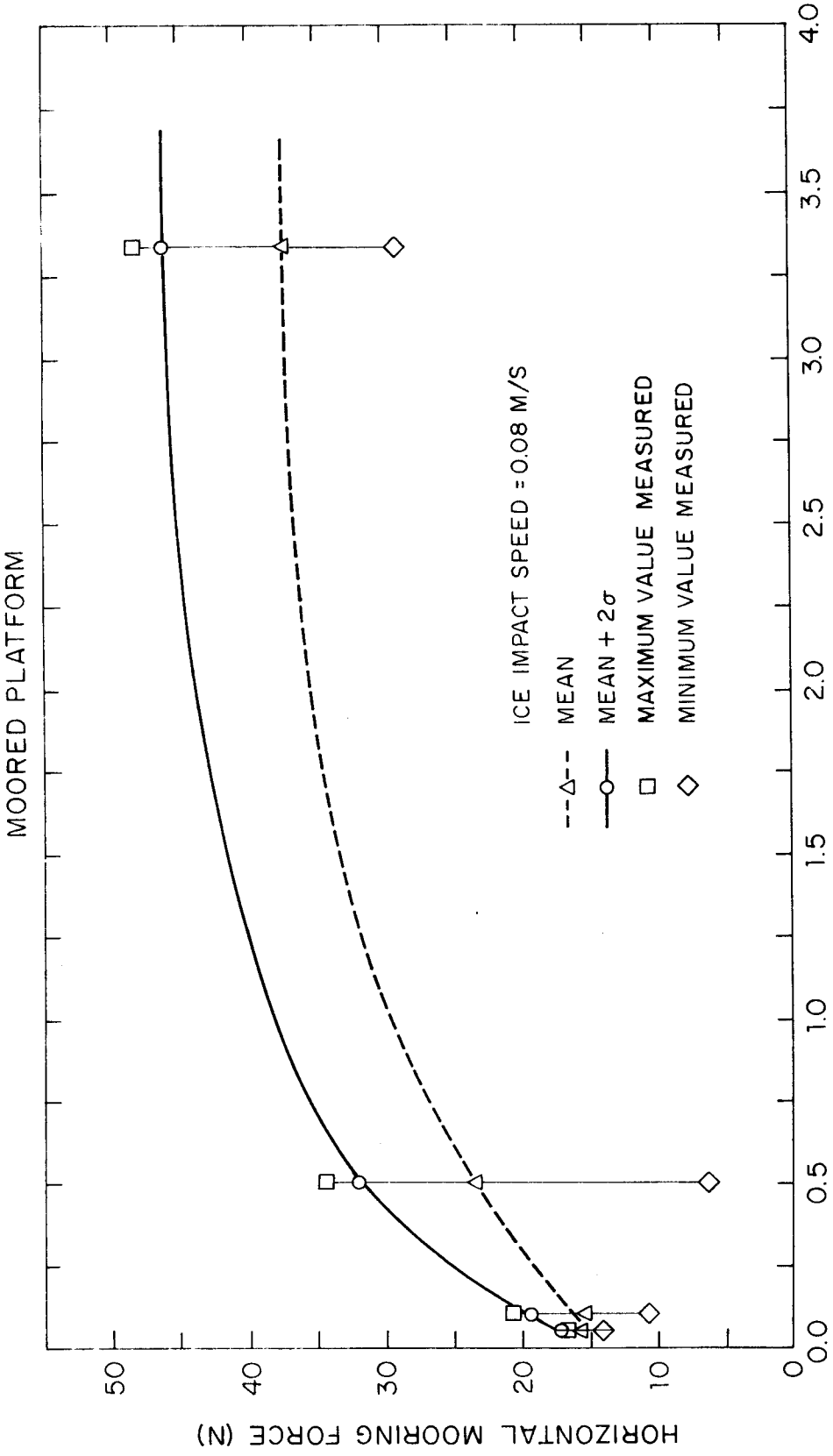

Figure 22. The effect of ice-floe diameter on mooring force.

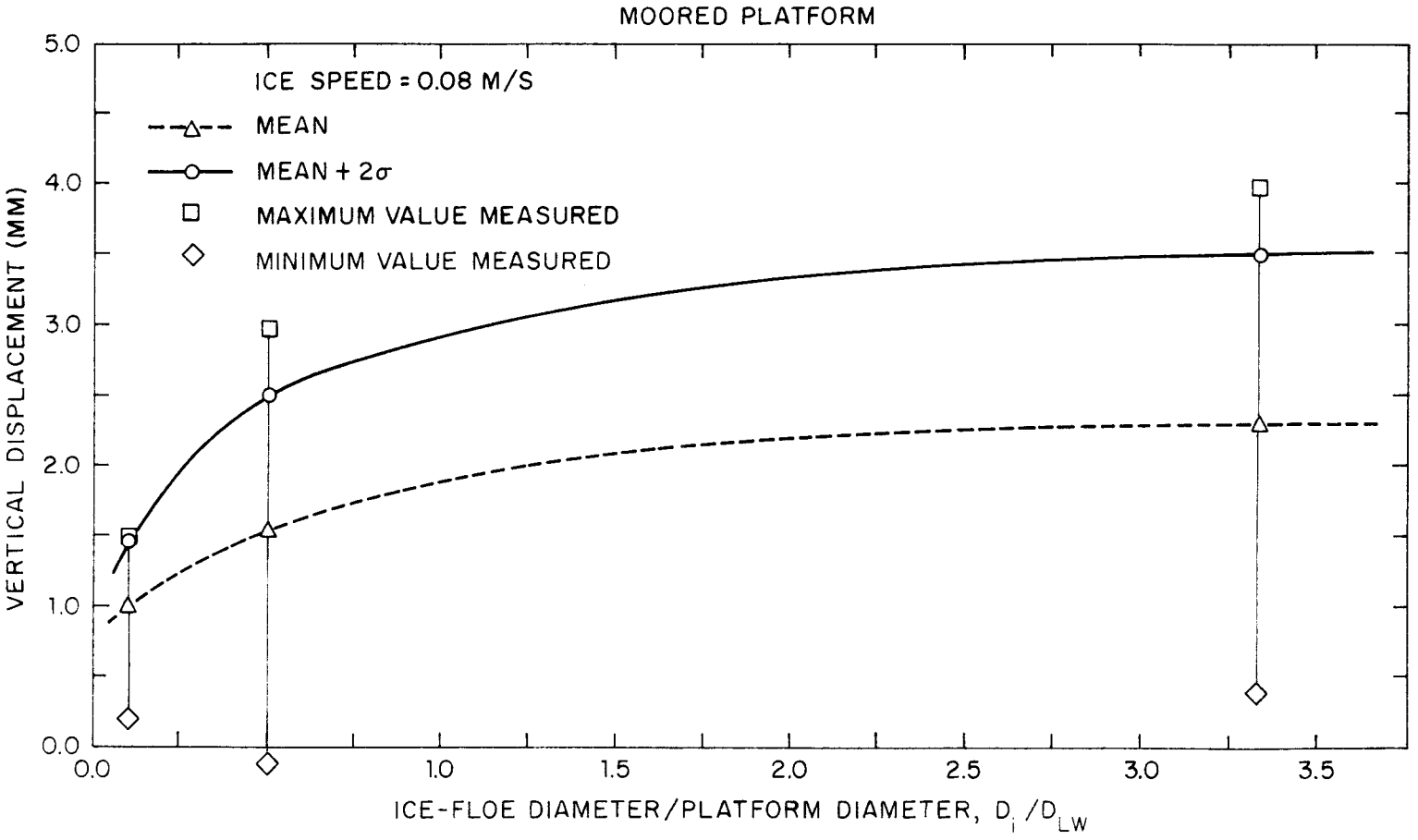

Figure 23. The effect of ice-floe diameter on vertical displacement.

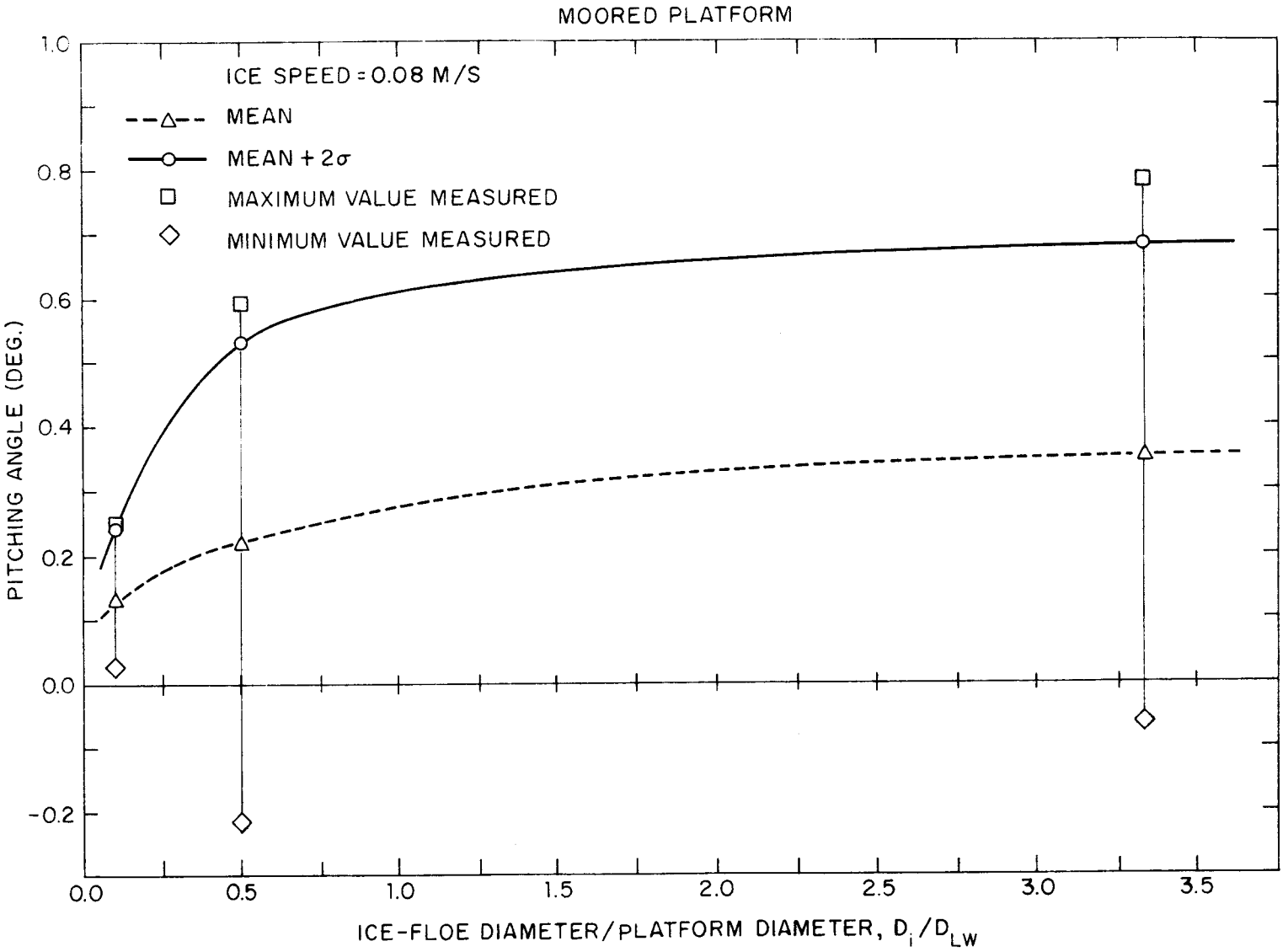

Figure 24. The effect of ice-floe diameter on pitching angle.

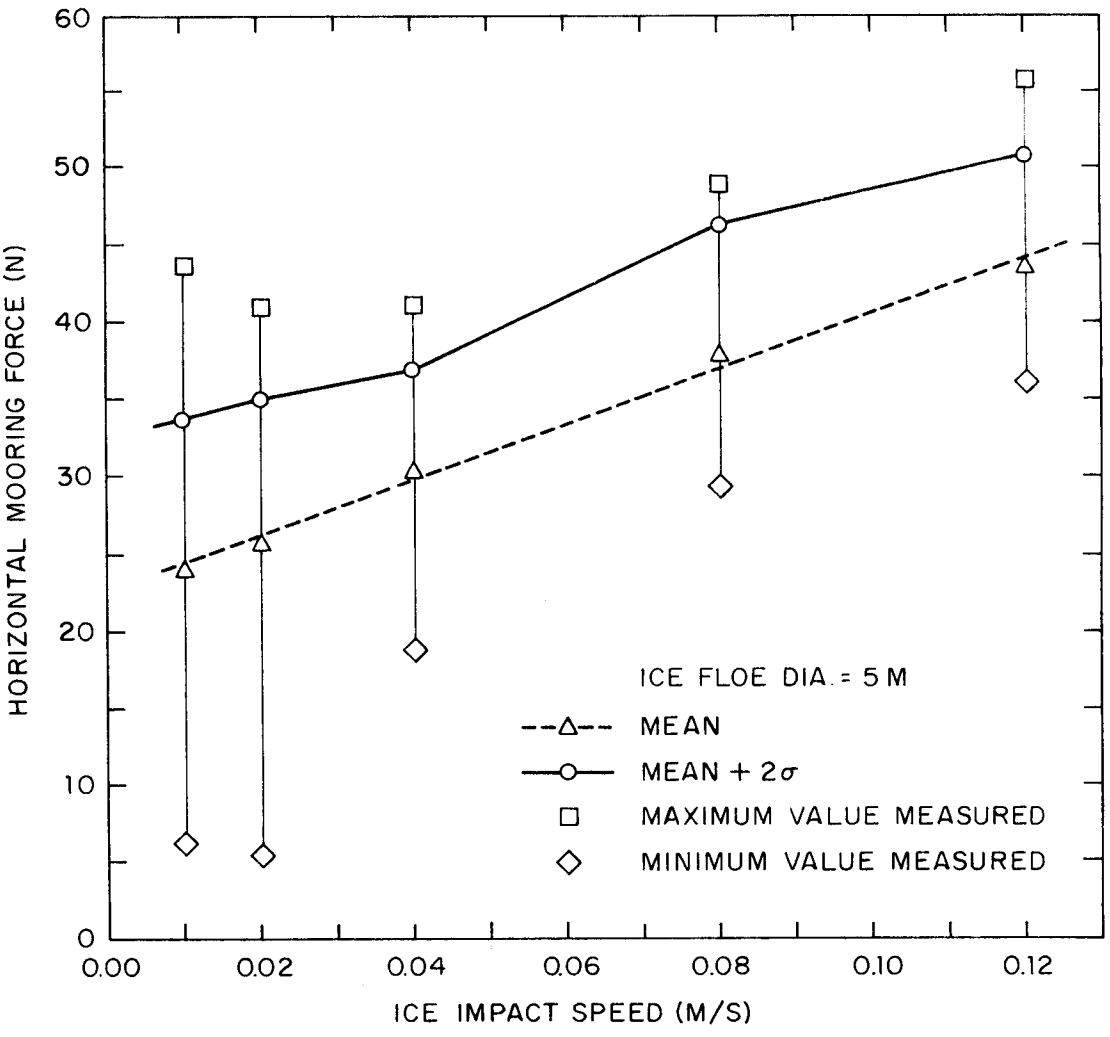

Figure 25. The effect of ice speed on mooring force.

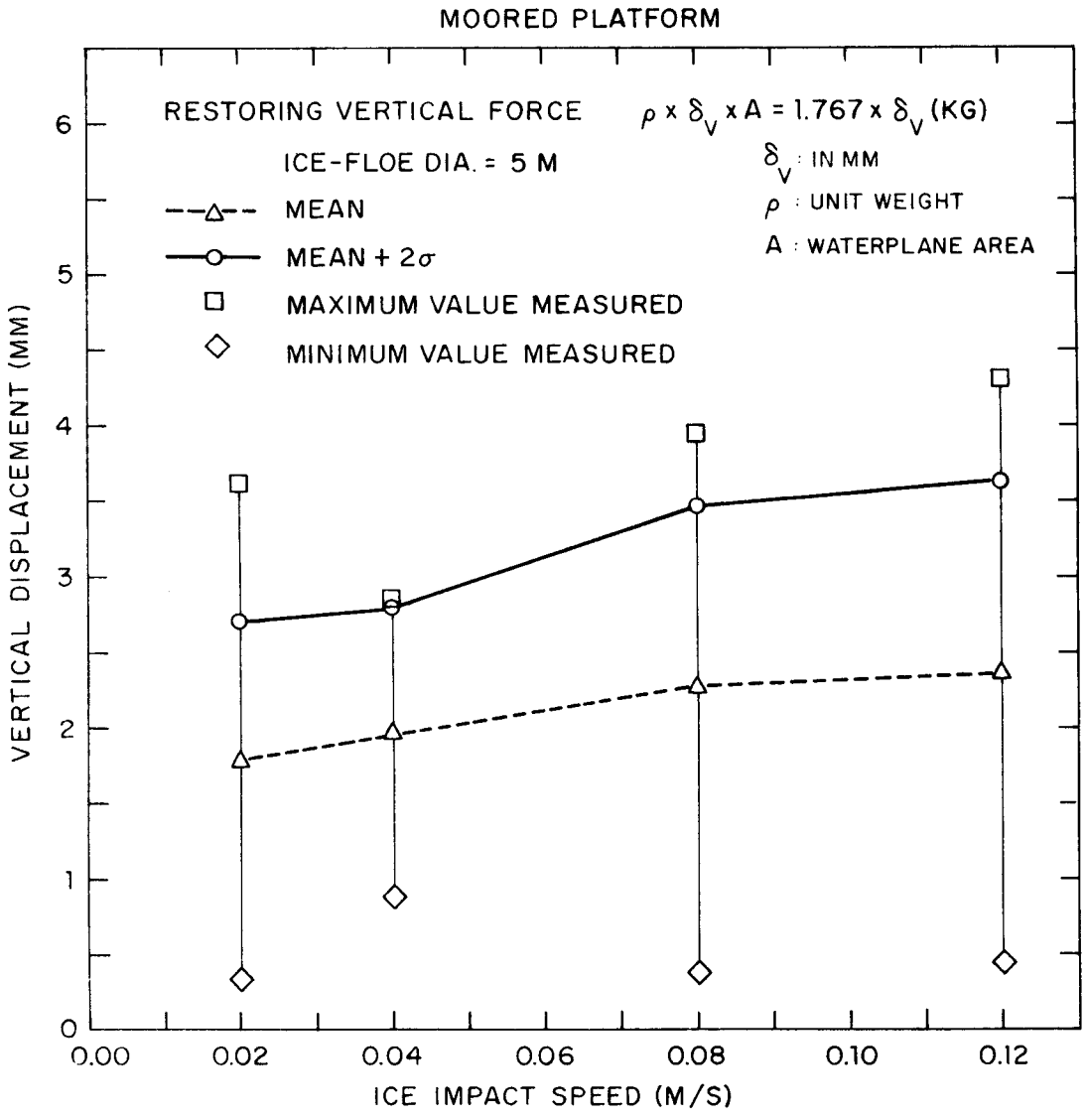

Figure 26. The effect of ice speed on vertical (heave) displacement.

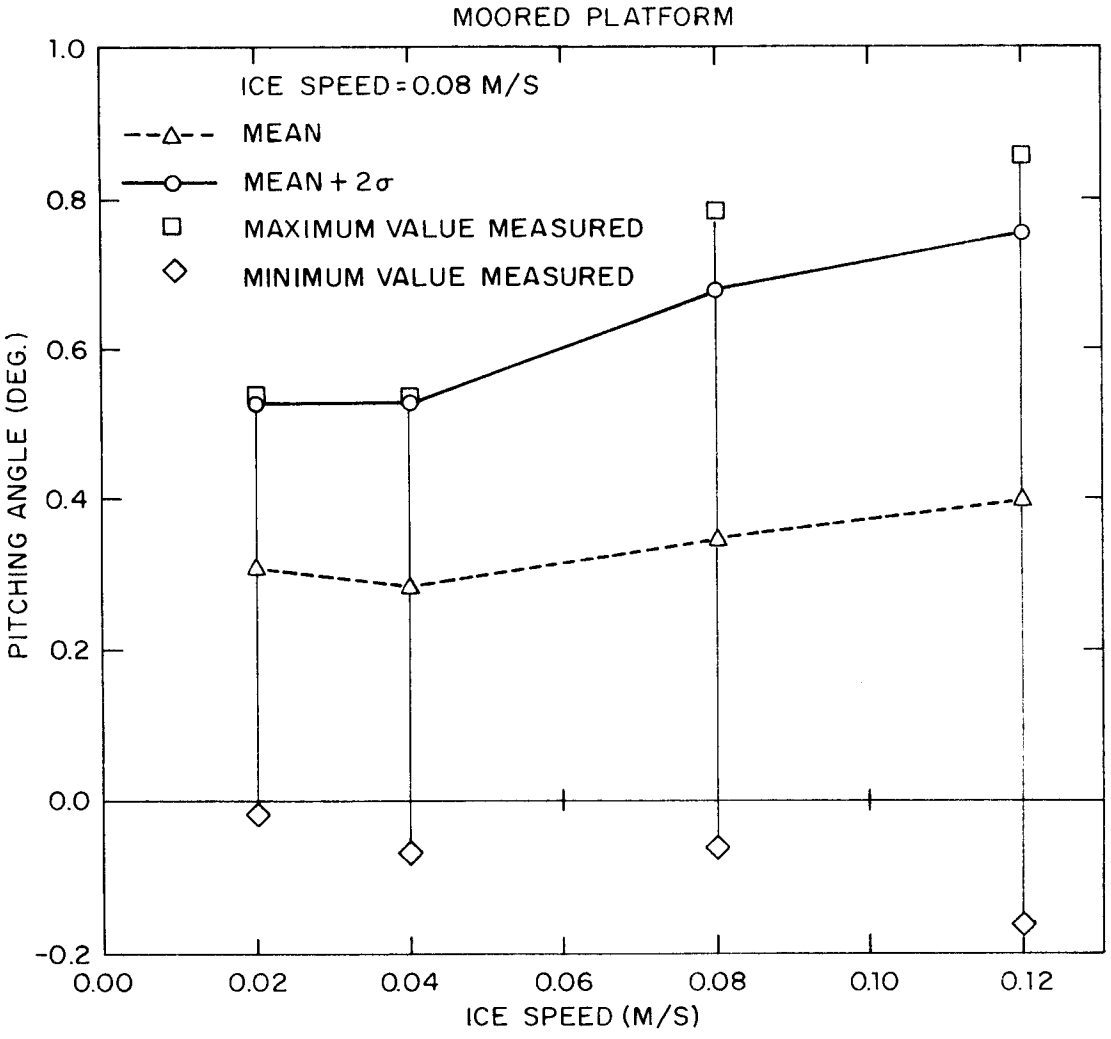

Figure 27. The effect of ice speed on pitching angle.

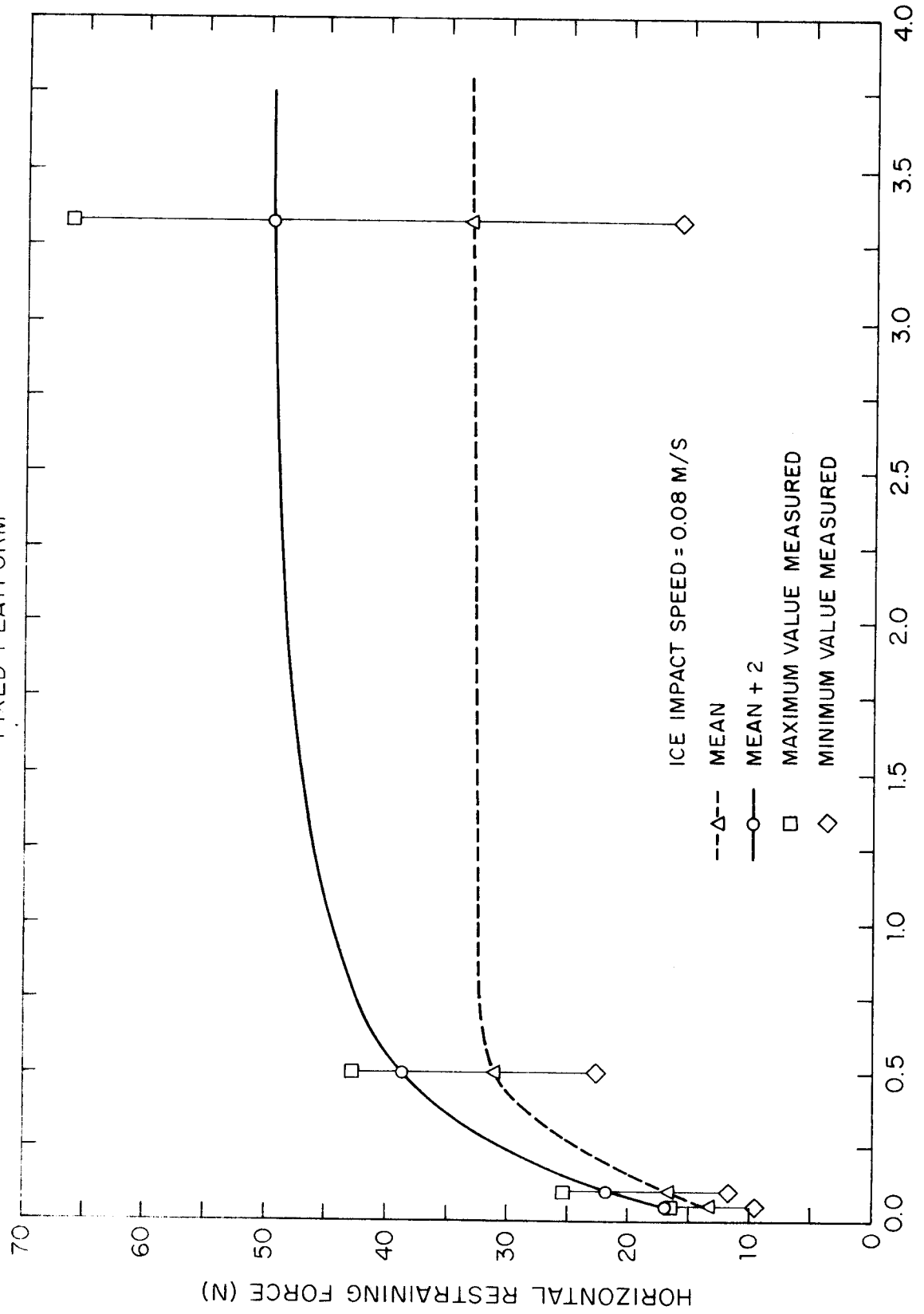

Figure 28. The effect of ice-floe diameter on horizontal (surge) restraining force.

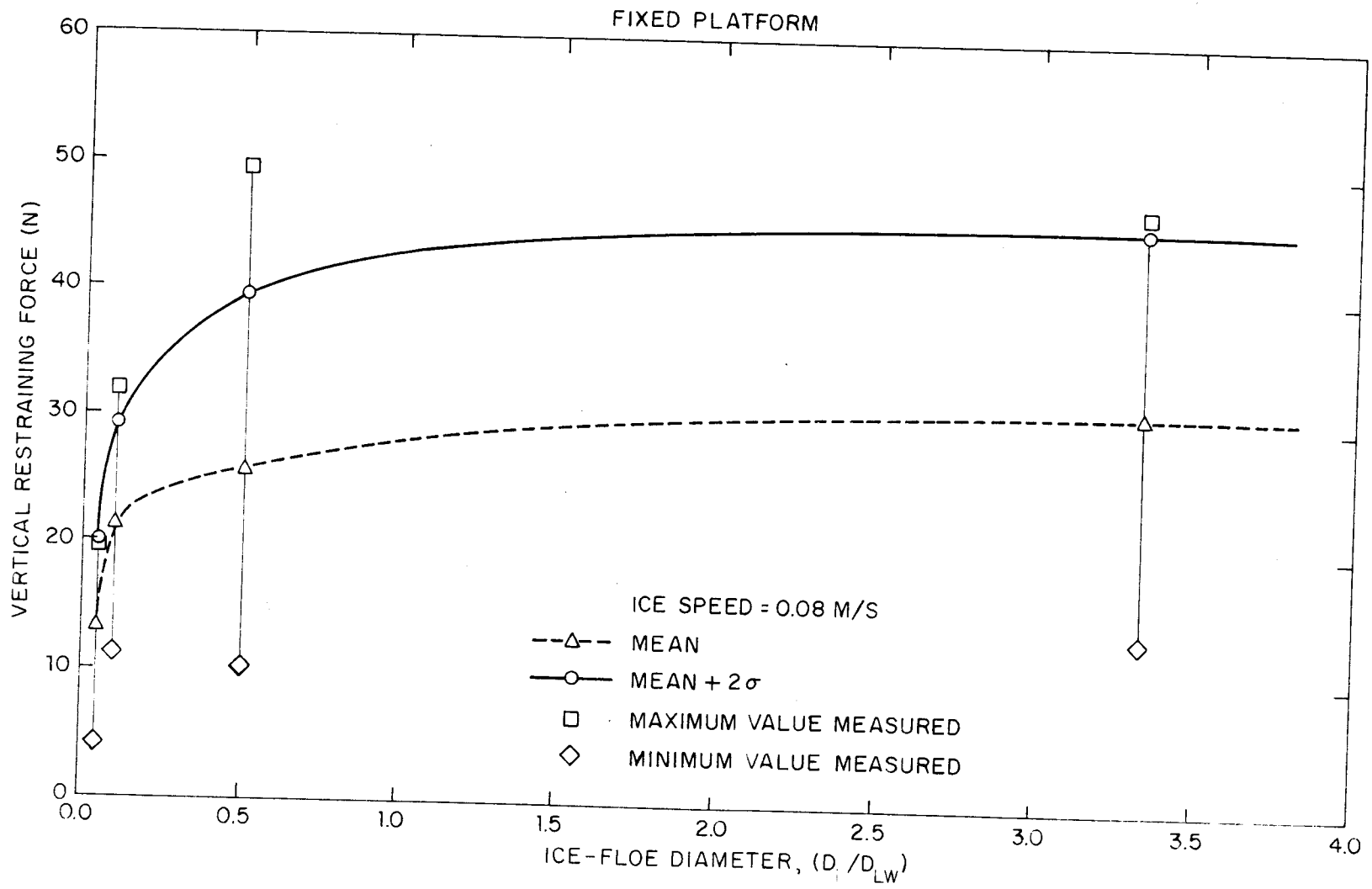

Figure 29. The effect of ice-floe diameter on vertical (heave) restraining forces.

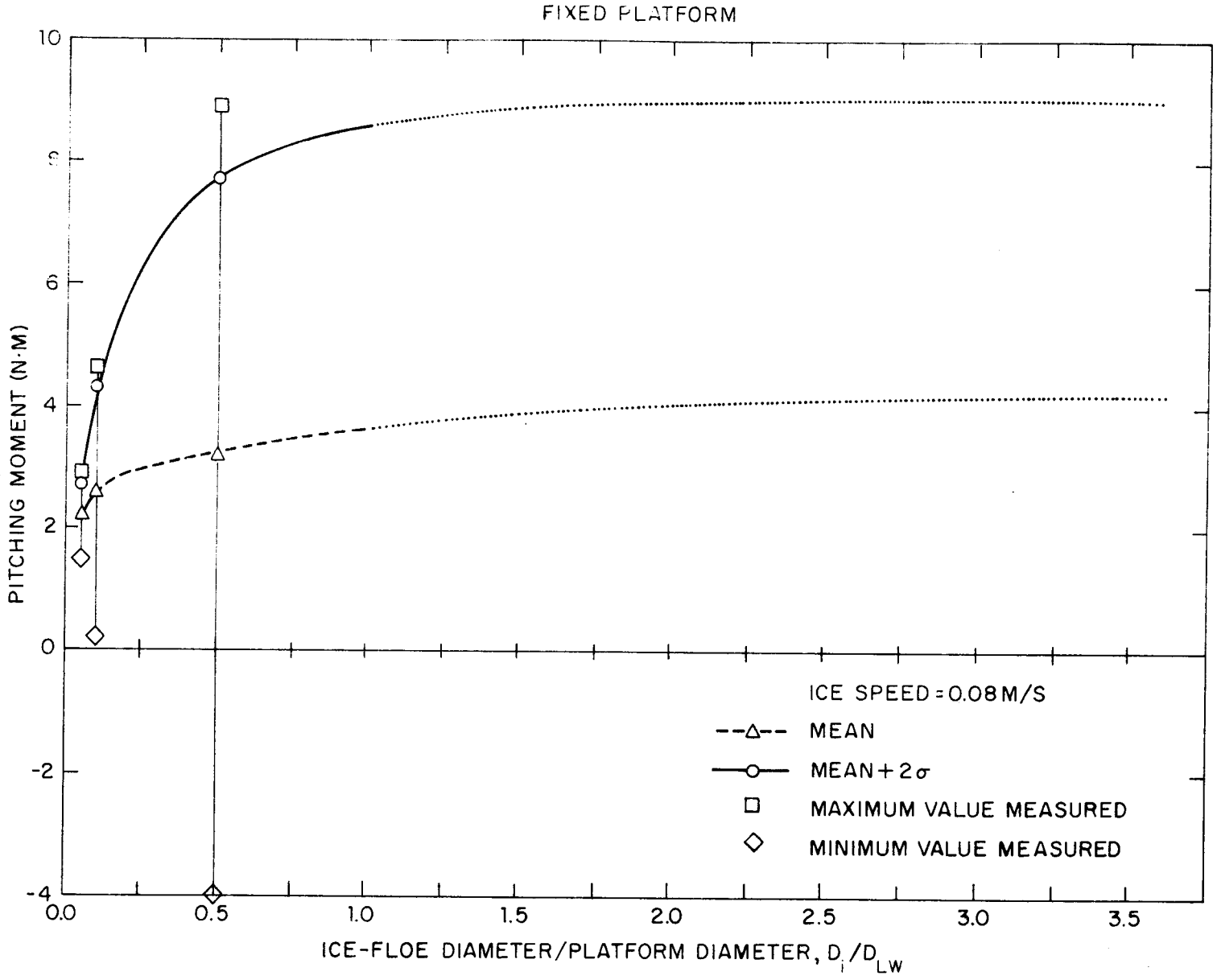

Figure 30. The effect of ice-floe diameter on pitching restraining moment.

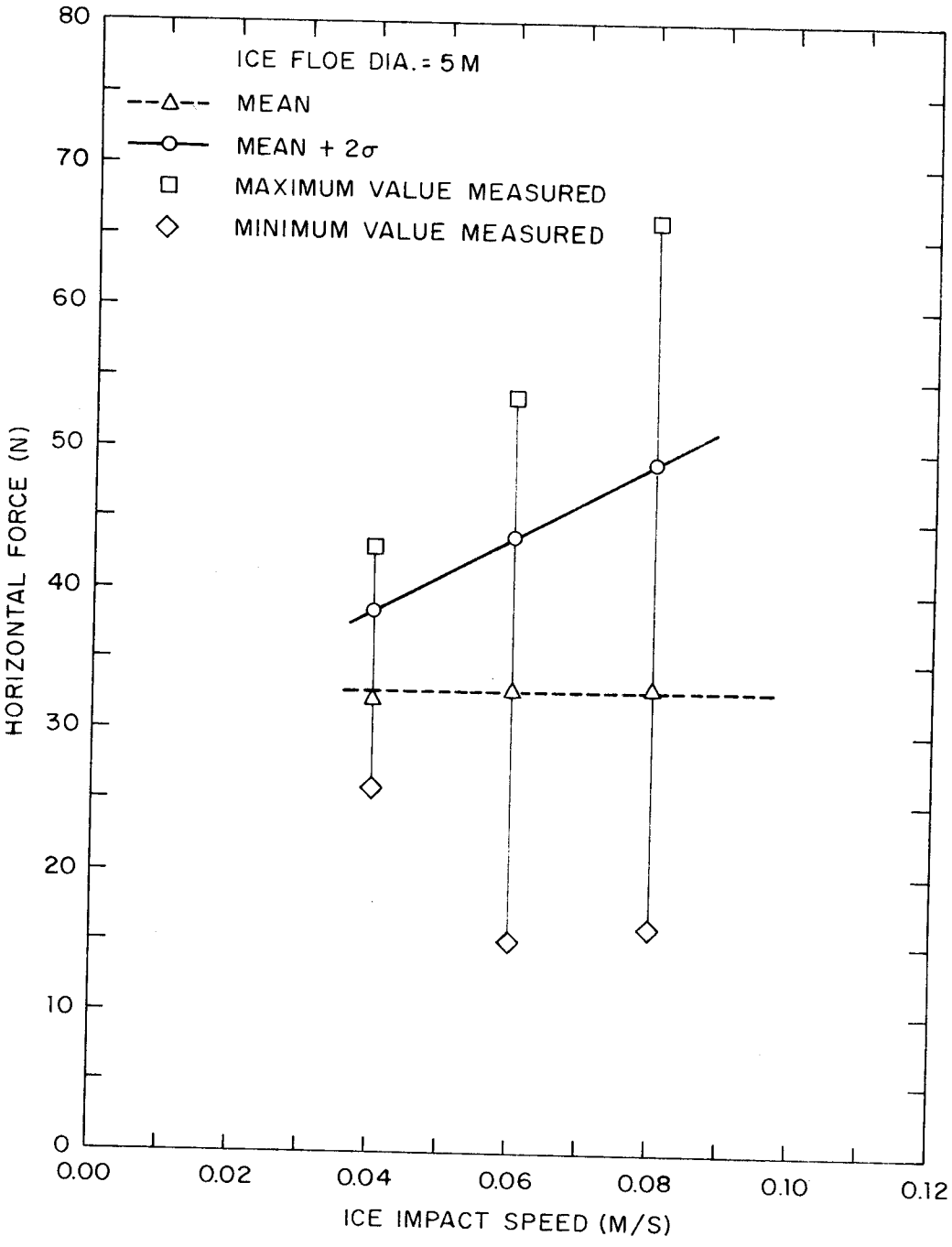

Figure 31. The effect of ice speed on horizontal (surge) restraining force.

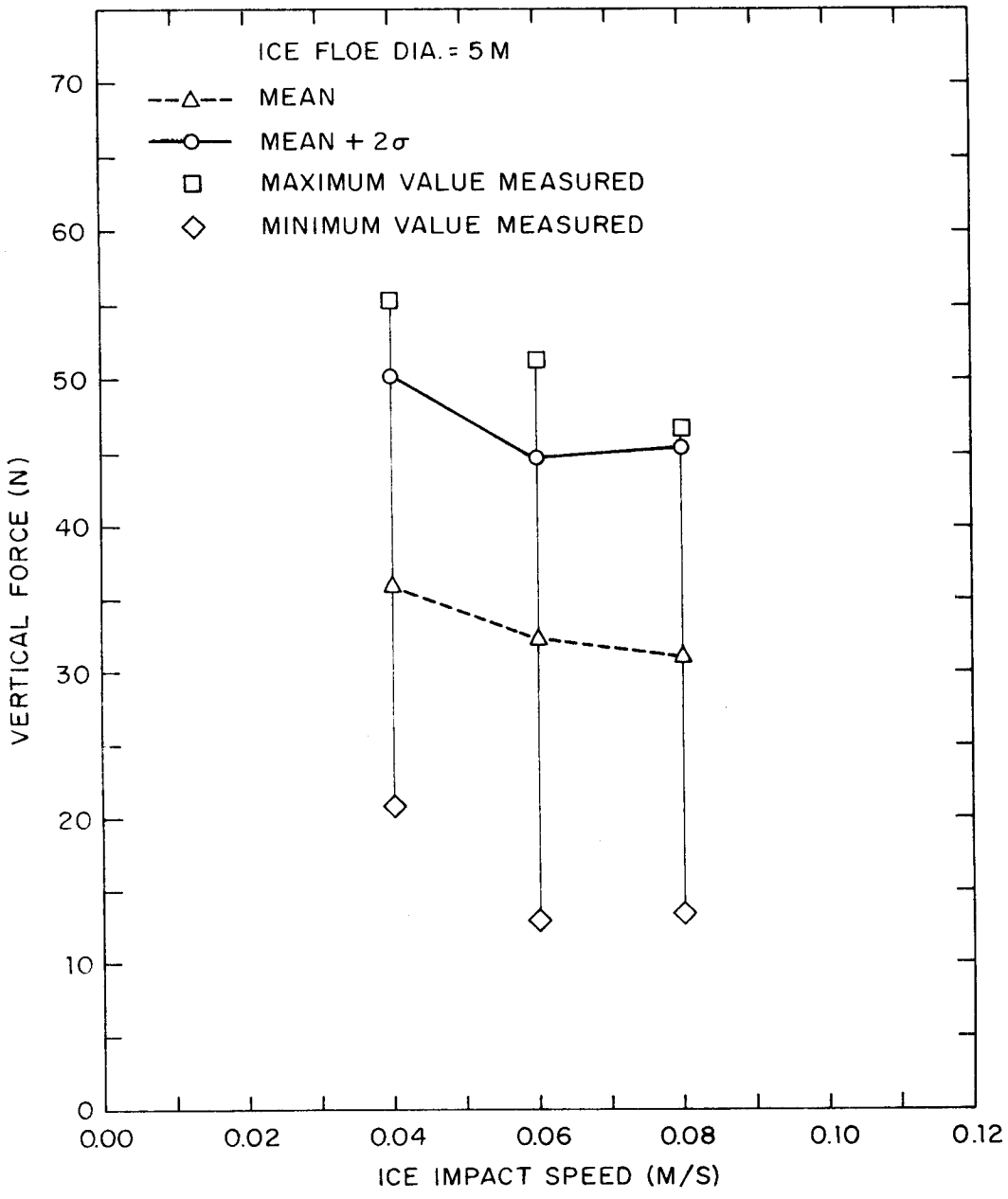

Figure 32. The effect of ice speed on vertical (heave) restraining force.

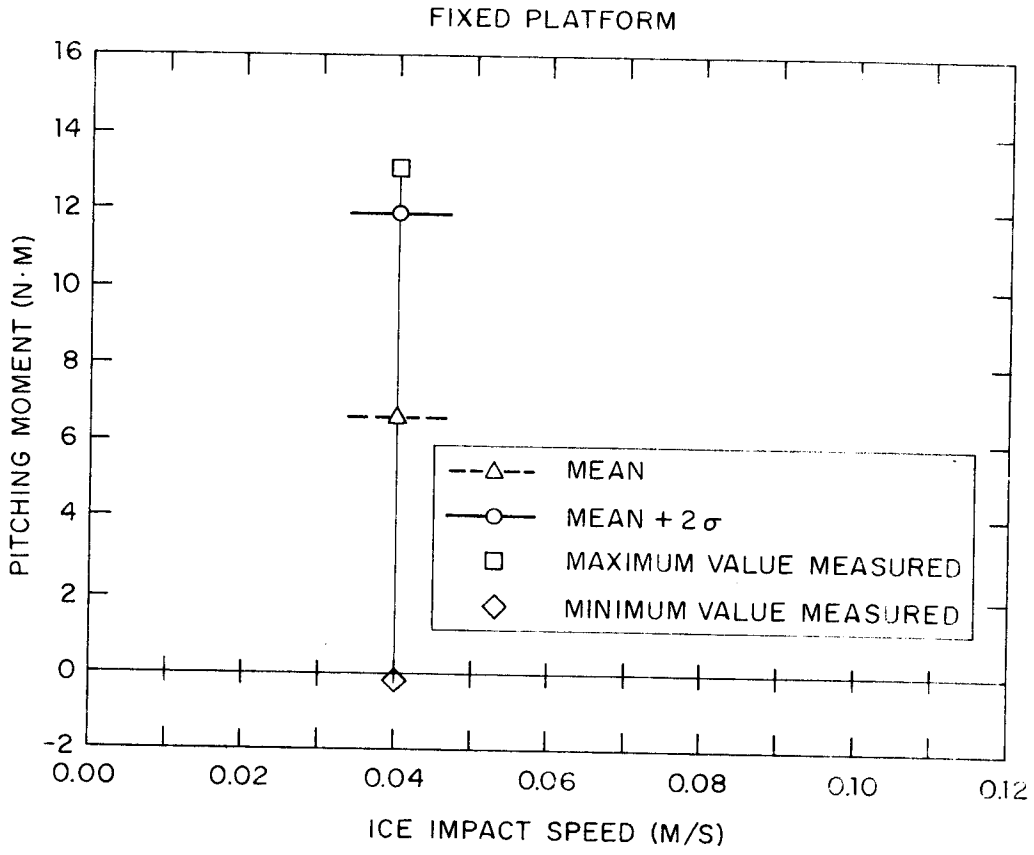

Figure 33. The effect of ice speed on pitch restraining moment.

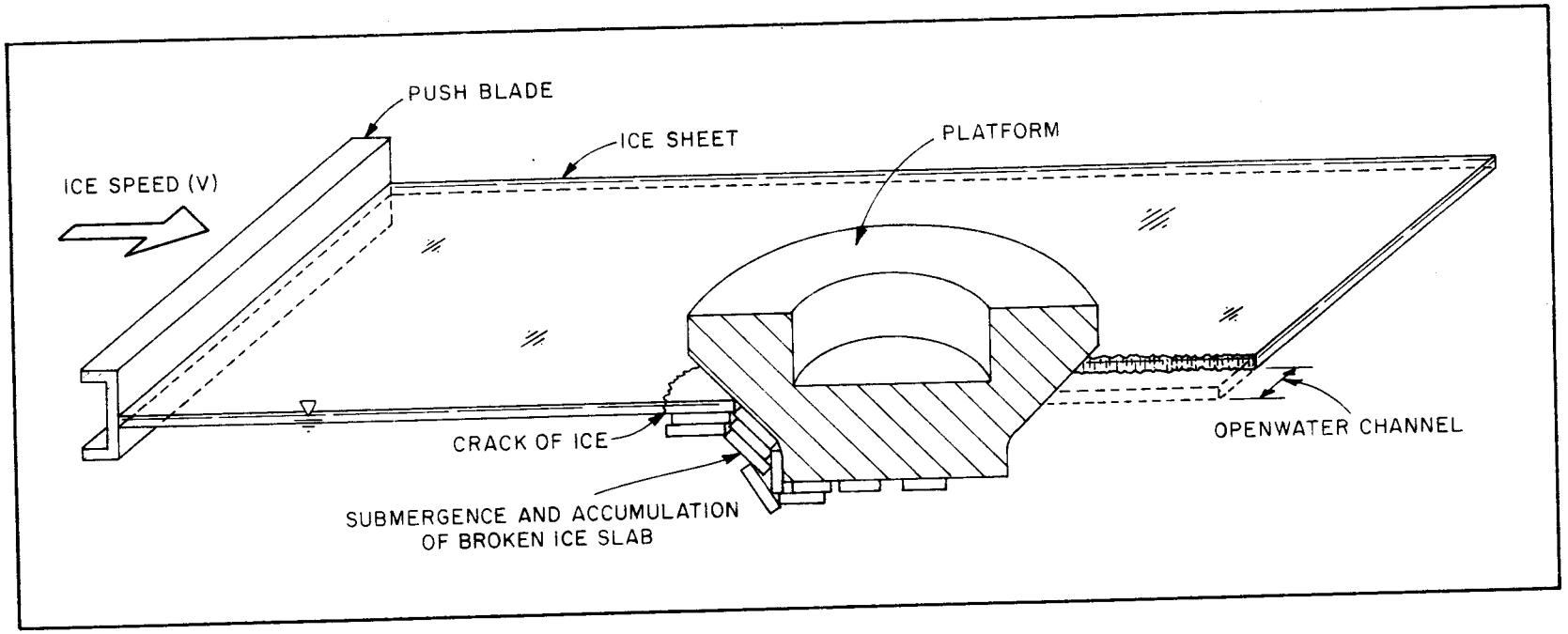

Figure 34. Ice-platform interaction mechanism.

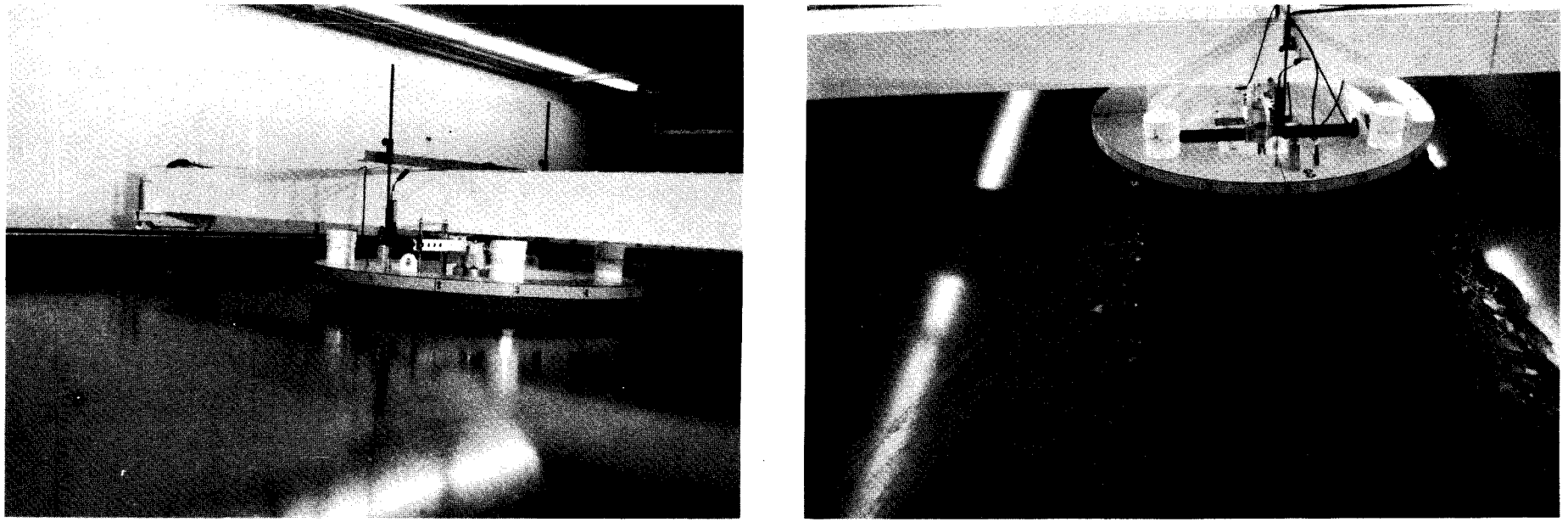

(a) Ice floe diameter = 5 m

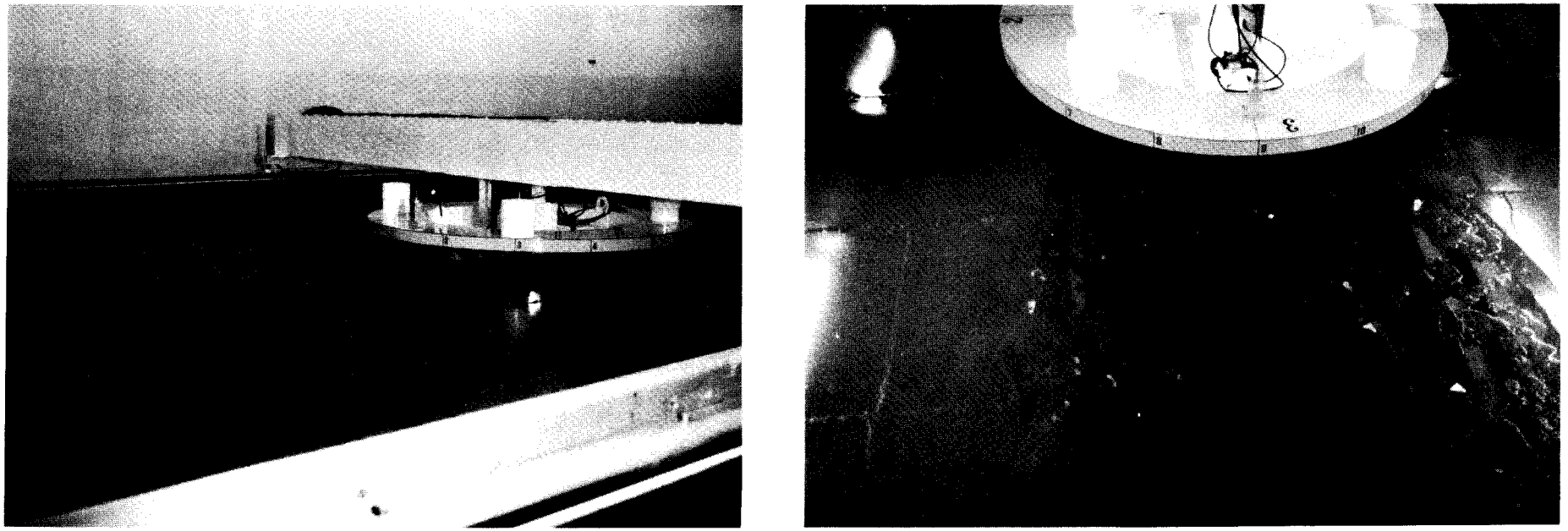

(b) Ice floe diameter = 0.75 m

Figure 35. Views of ice-floe impact with the test platform.

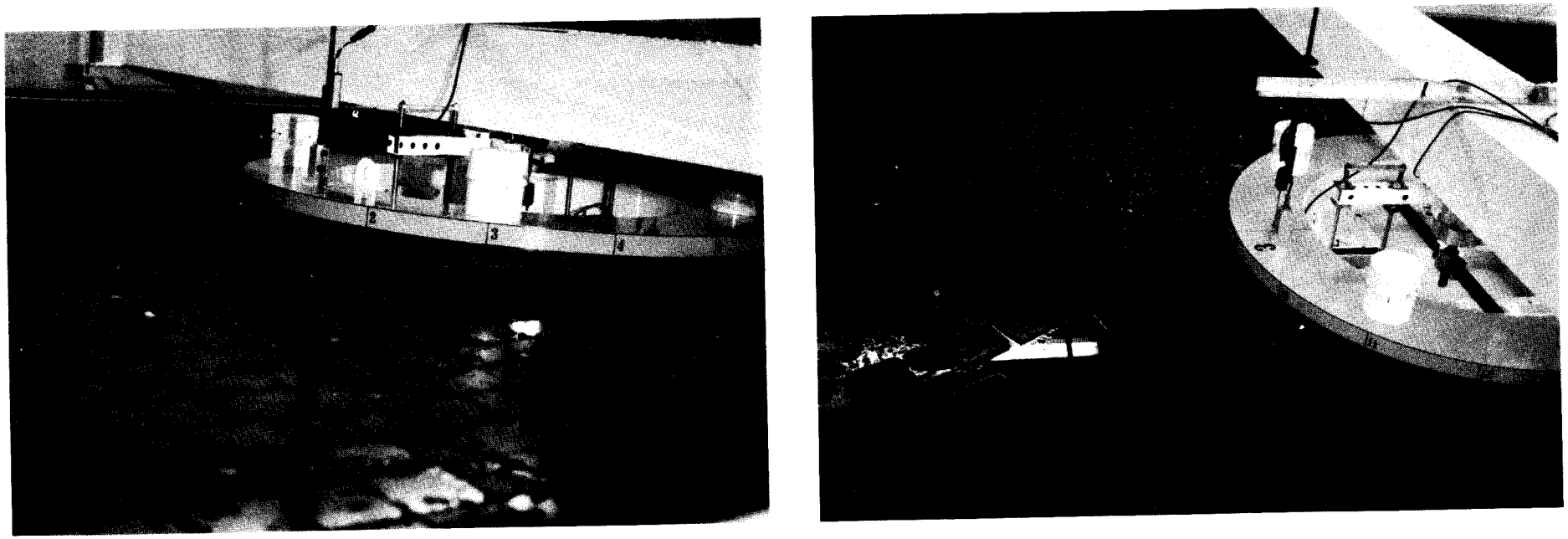

(c) Ice floe diameter = 0.15 m

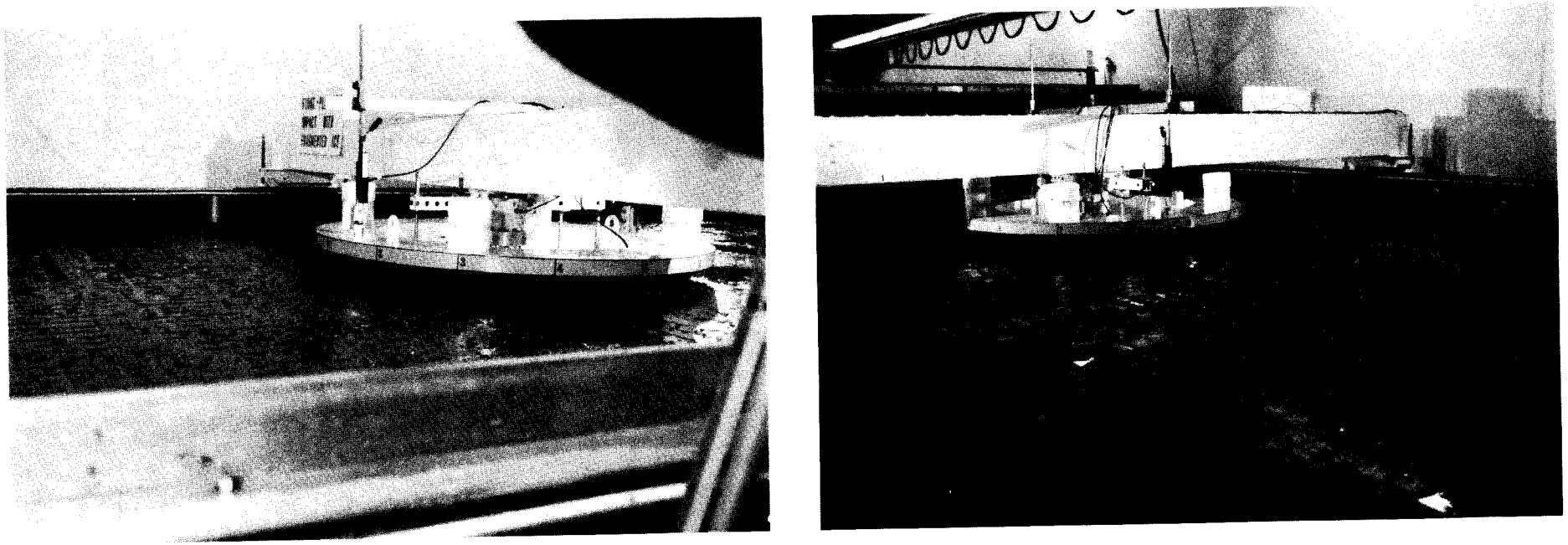

(d) Ice floe diameter = 0.075 m

Figure 35. Continued.

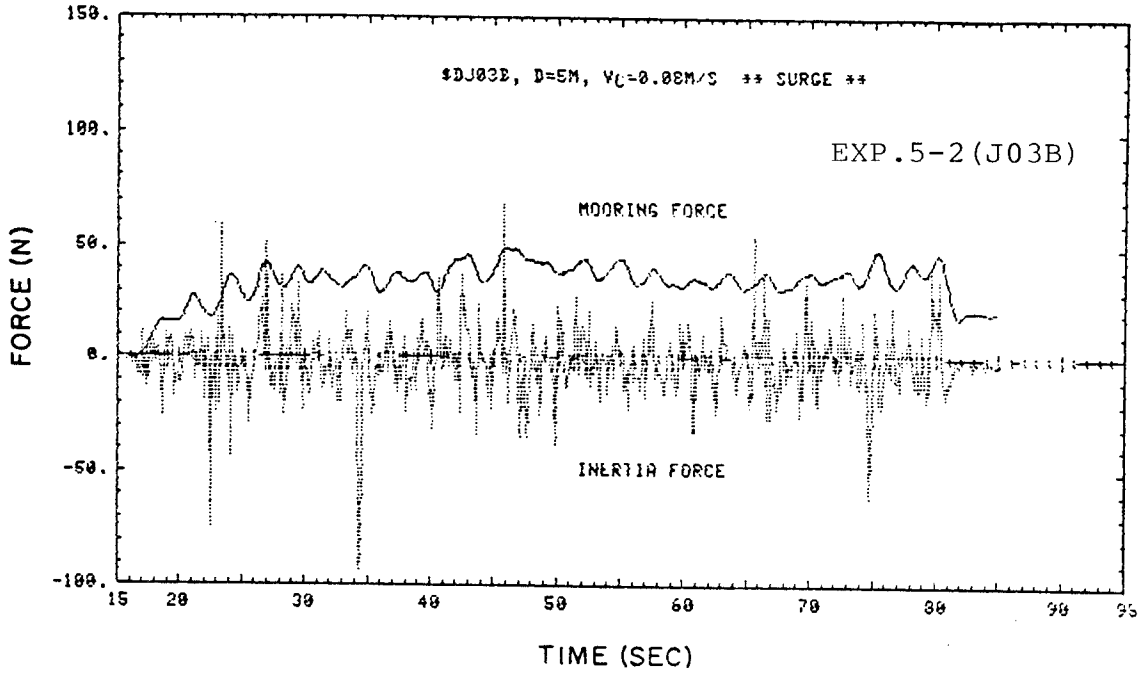

(a) surge(1)

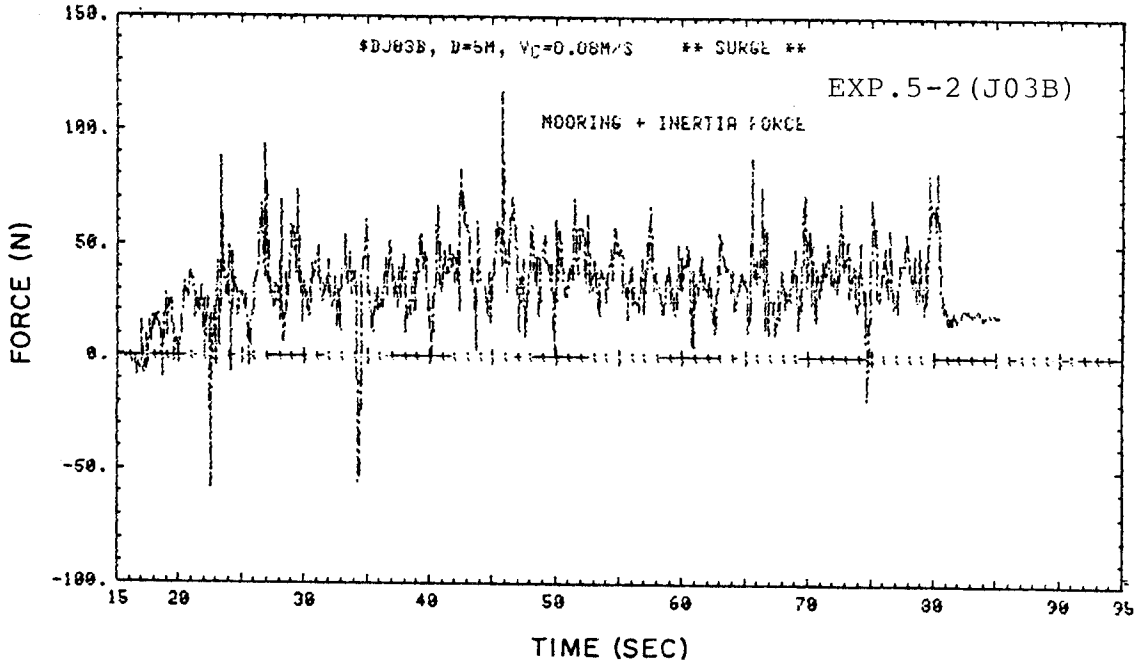

(b) surge(2)

Figure 36. Time histories of force components.

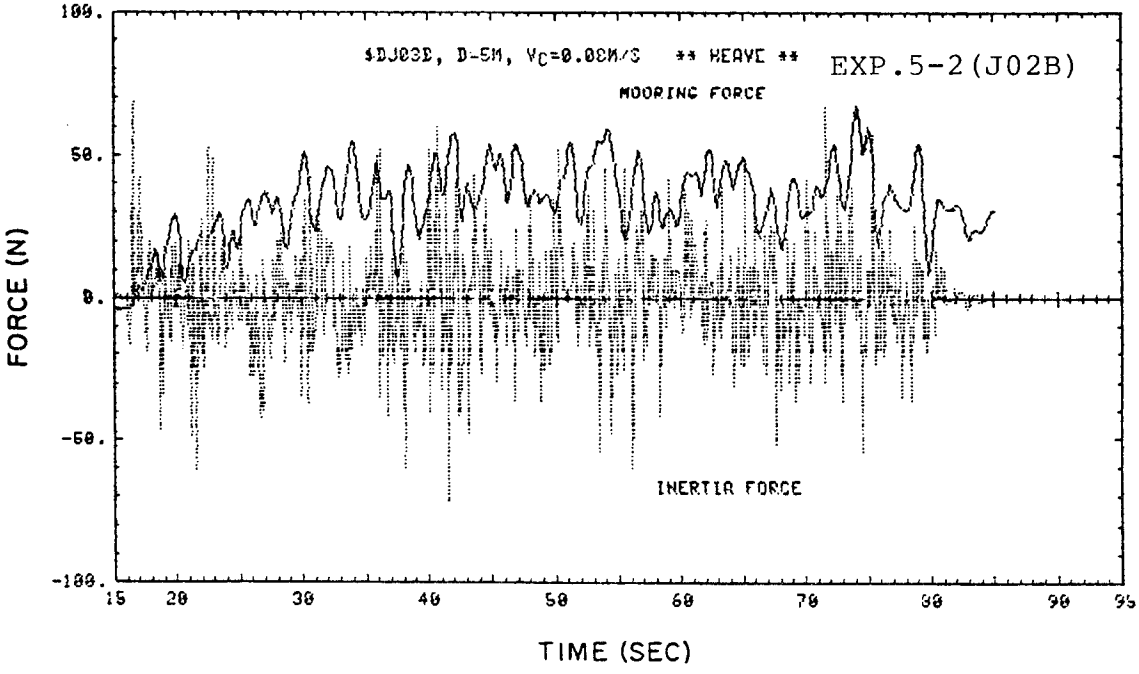

(c) heave(1)

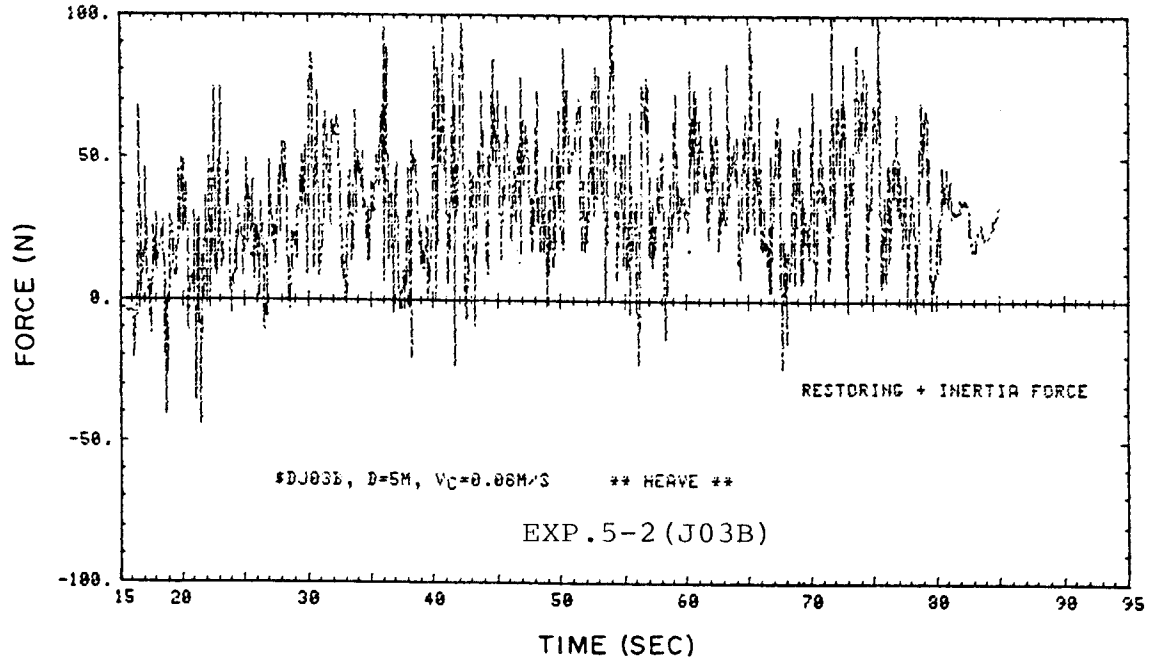

(d) heave(2)

Figure 36. Continued.

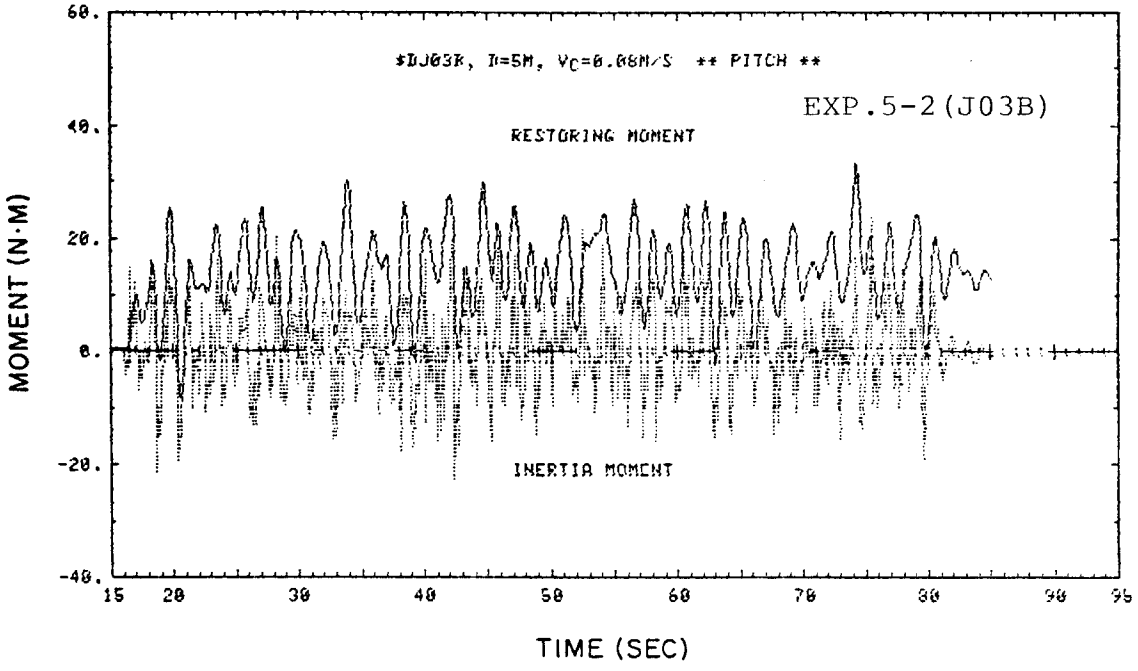

(e) pitch(1)

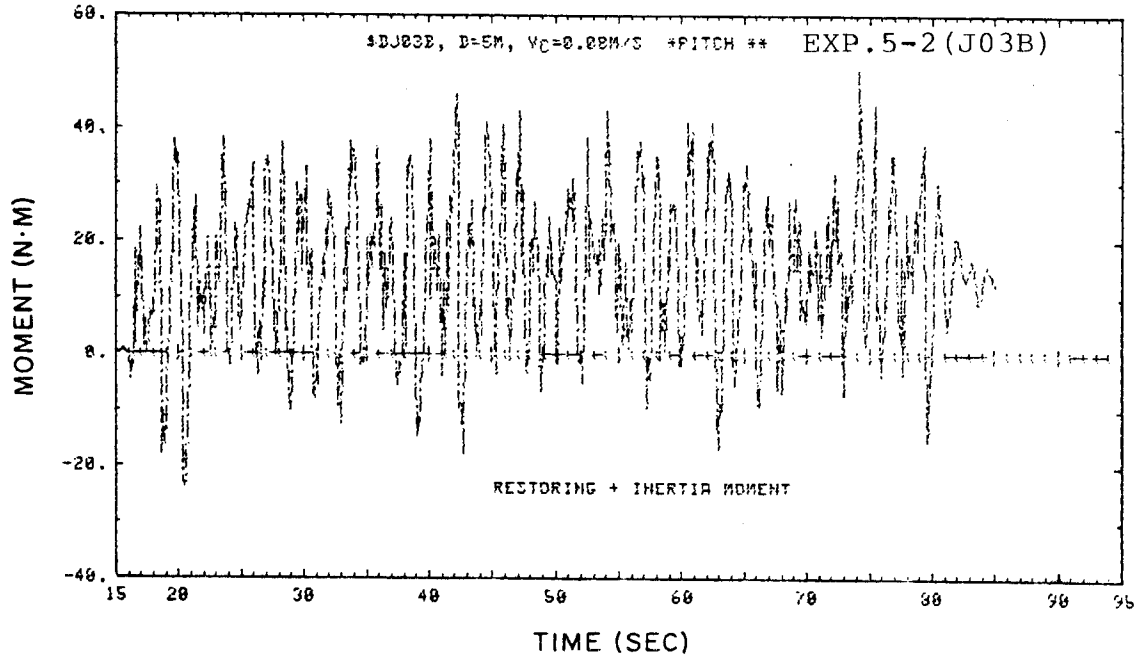

(f) pitch(2)

Figure 36. Continued.

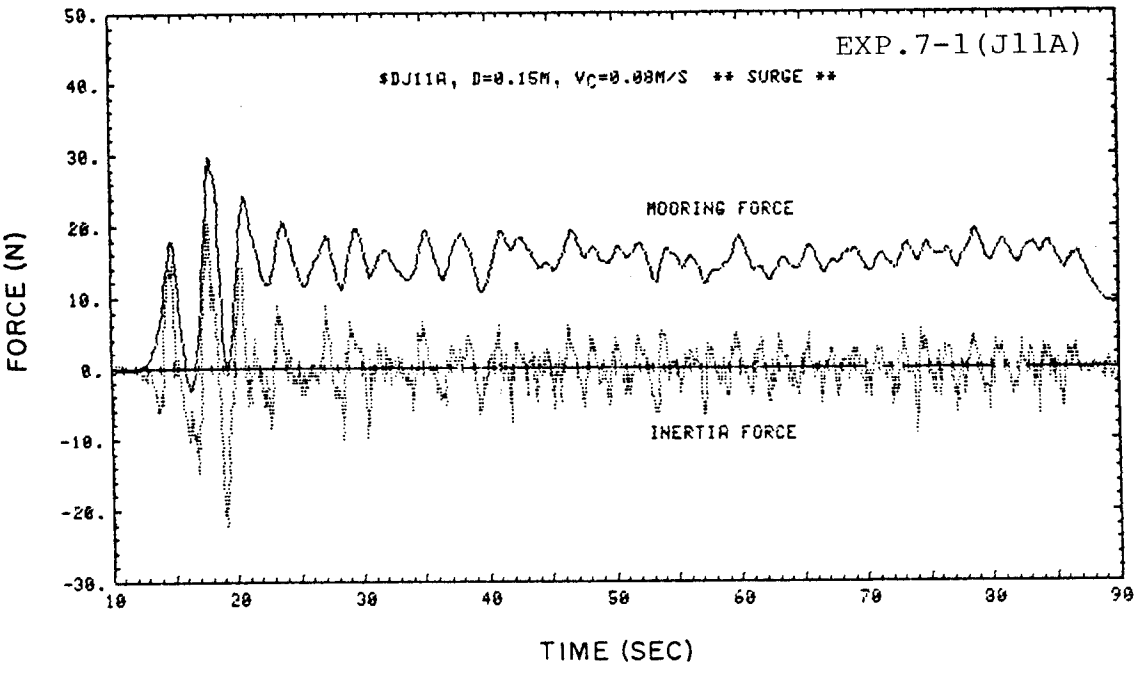

(a) surge(1)

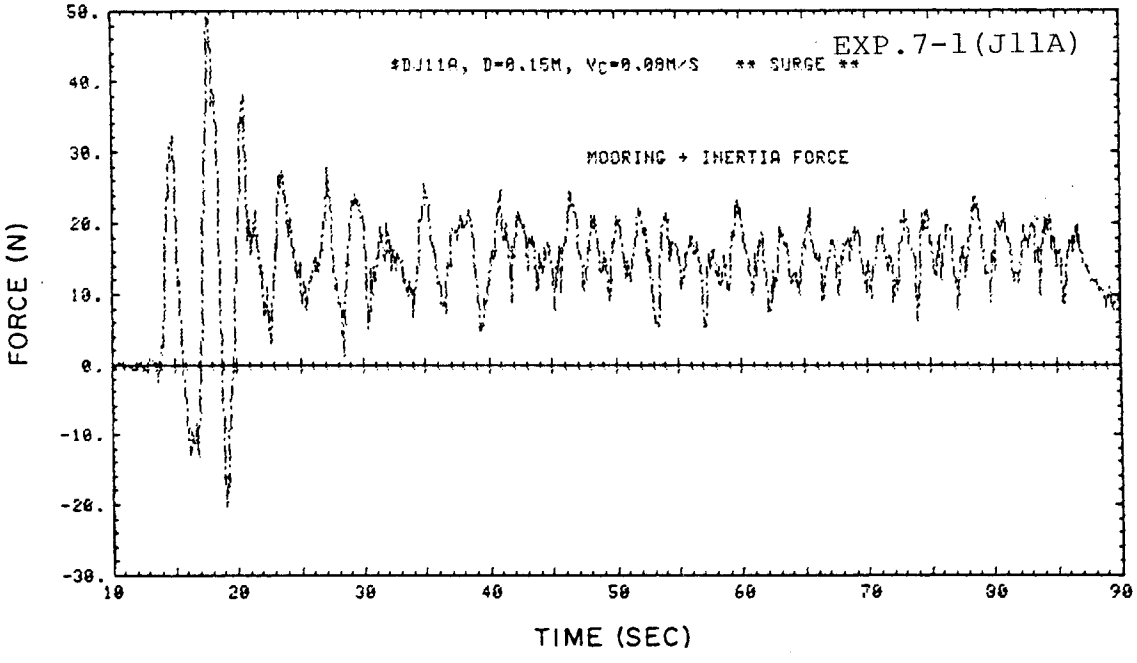

(b) surge(2)

Figure 37. Time histories of force components.

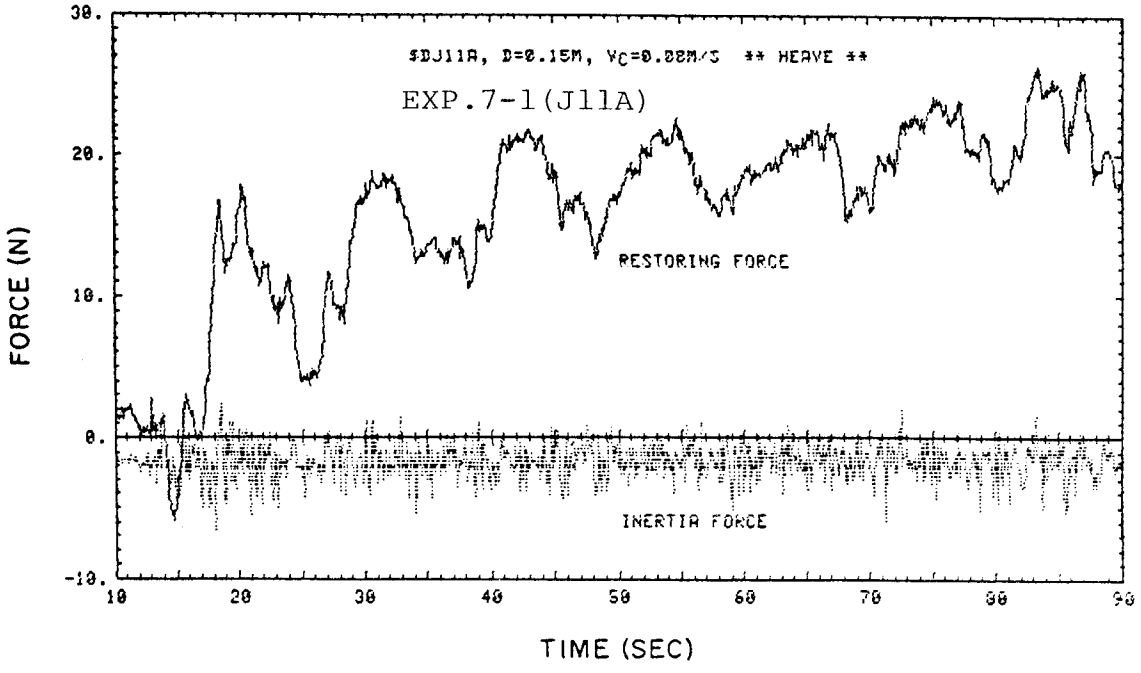

(c) heave(1)

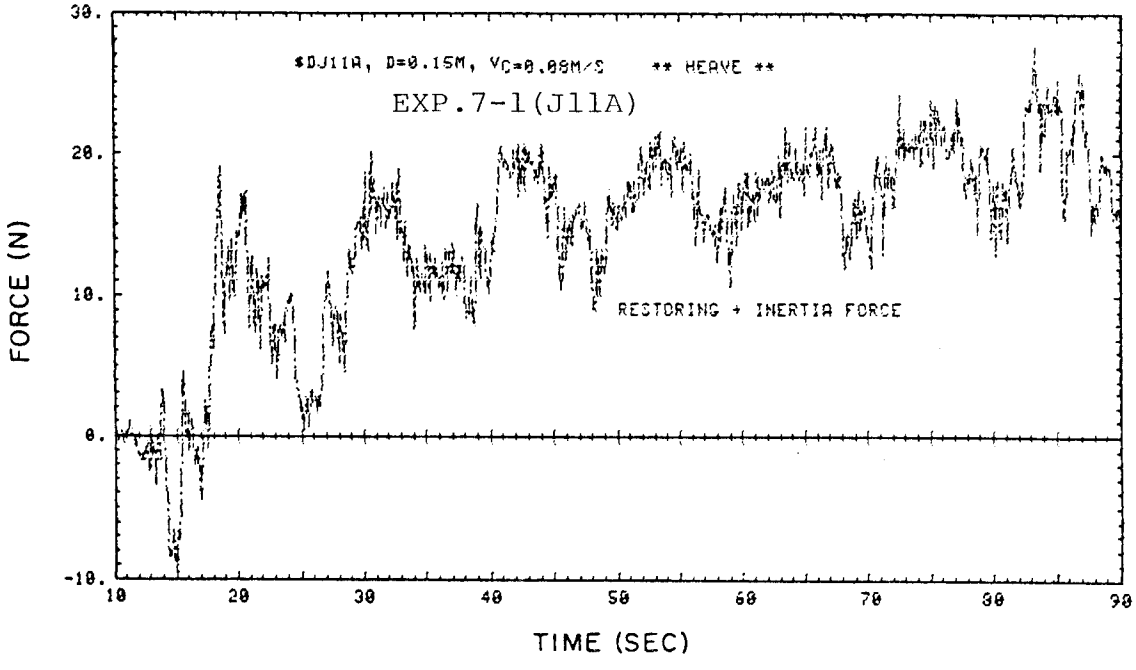

(d) heave(2)

Figure 37. Continued.

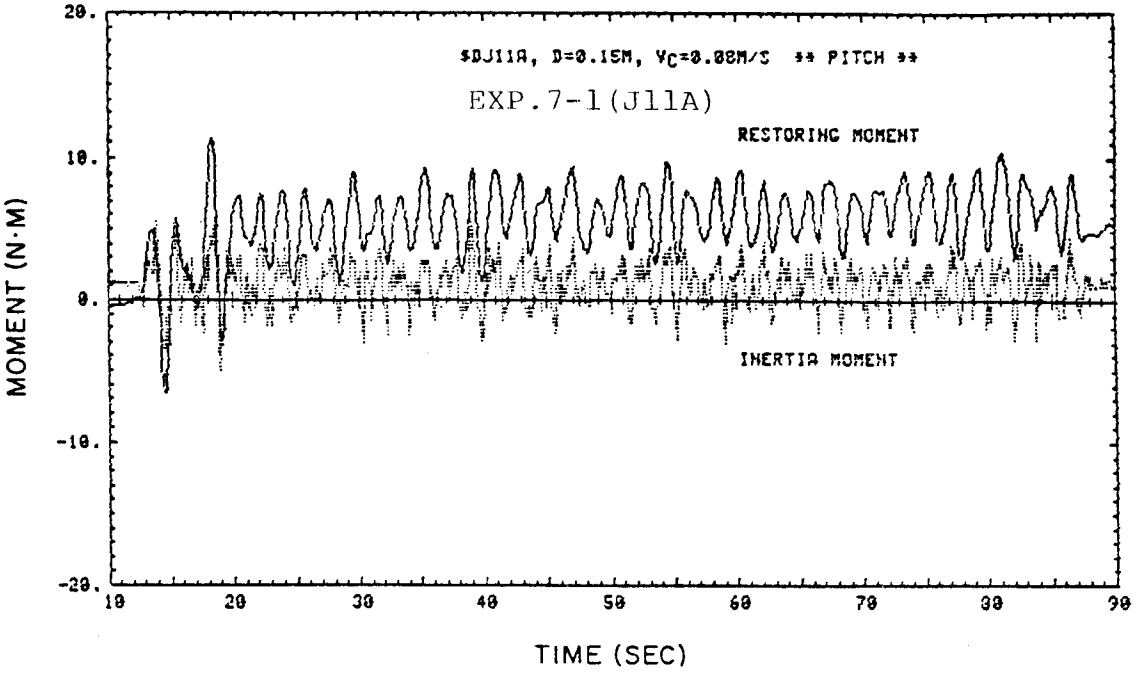

(e) pitch(1)

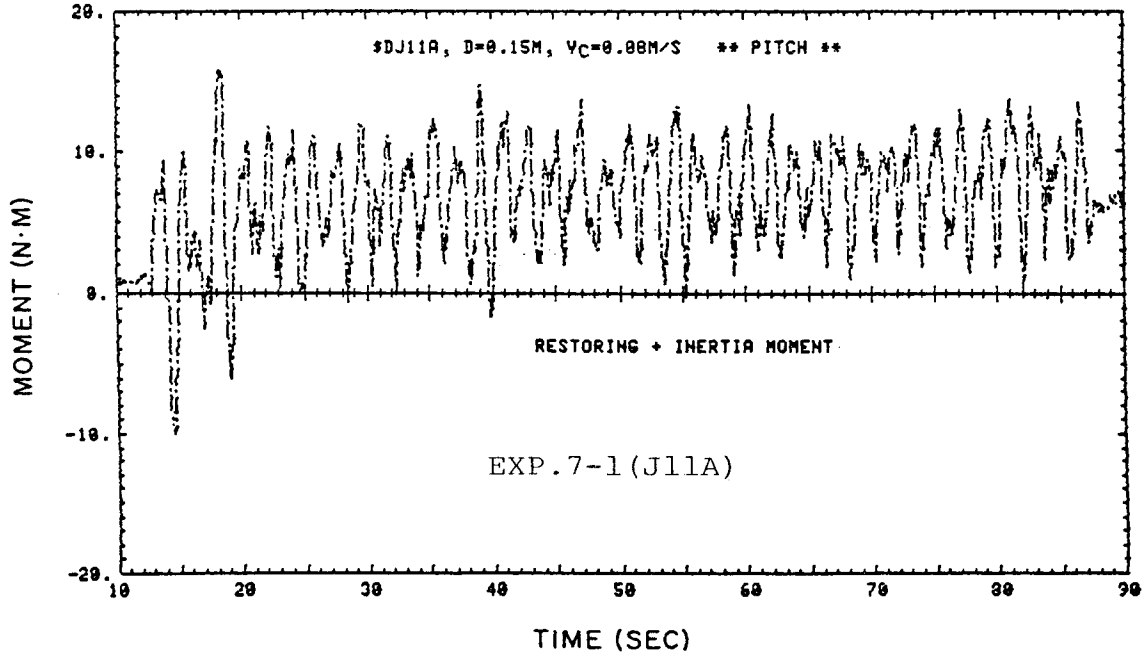

(f) pitch(2)

Figure 37. Continued.

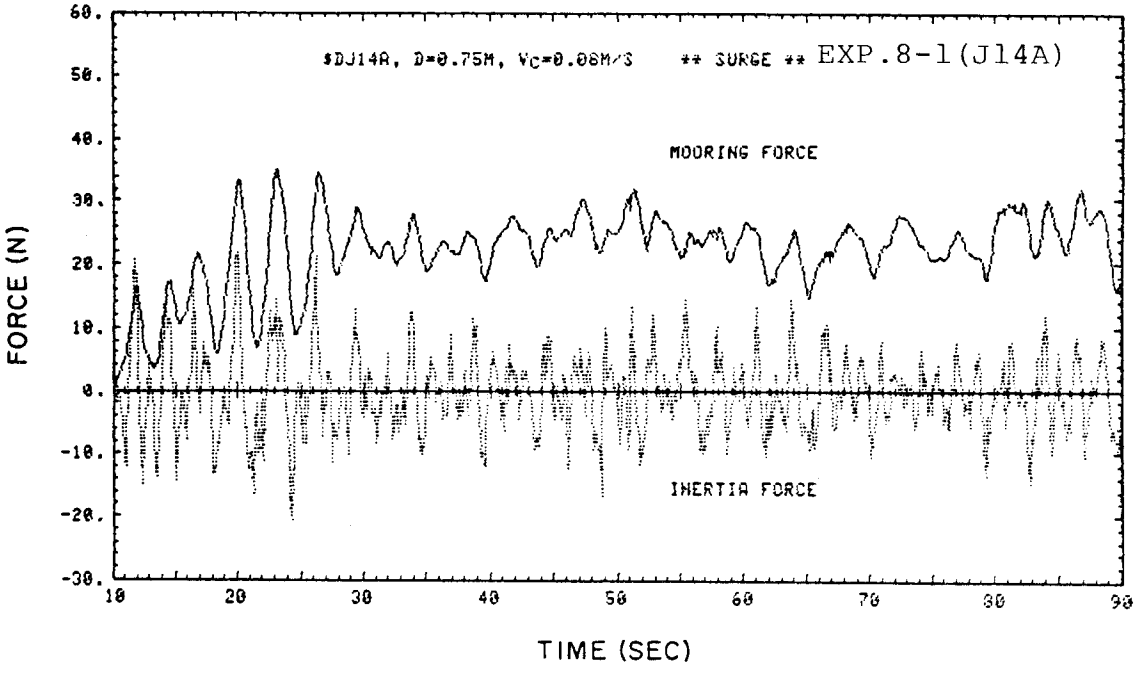

(a) surge(1)

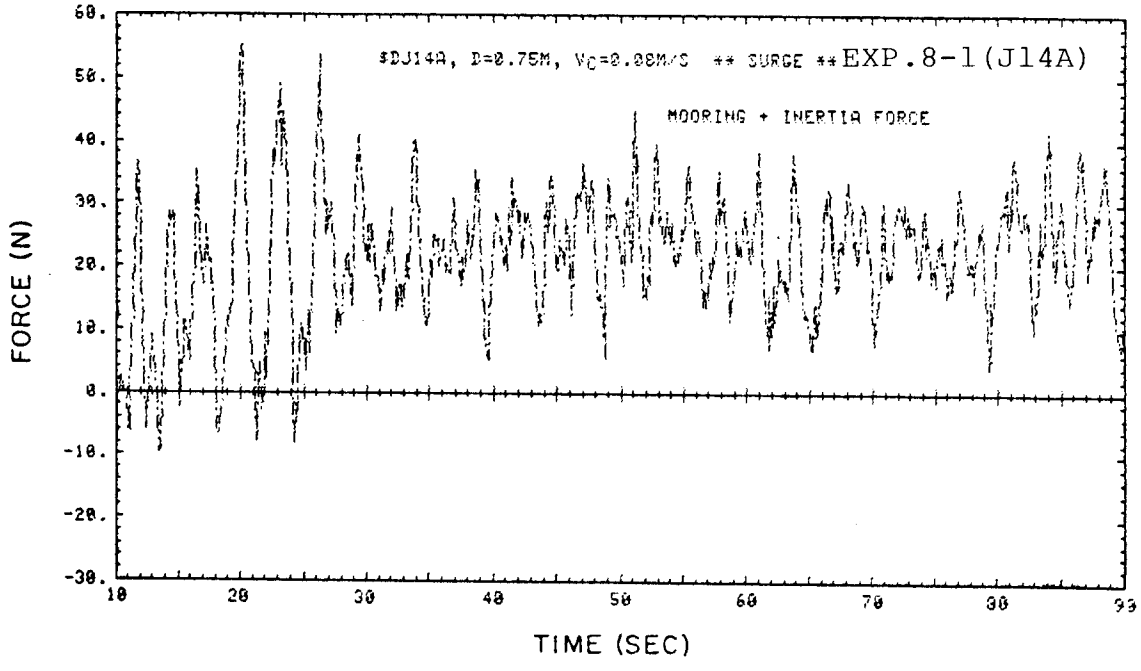

(b) surge(2)

Figure 38. Time histories of force components.

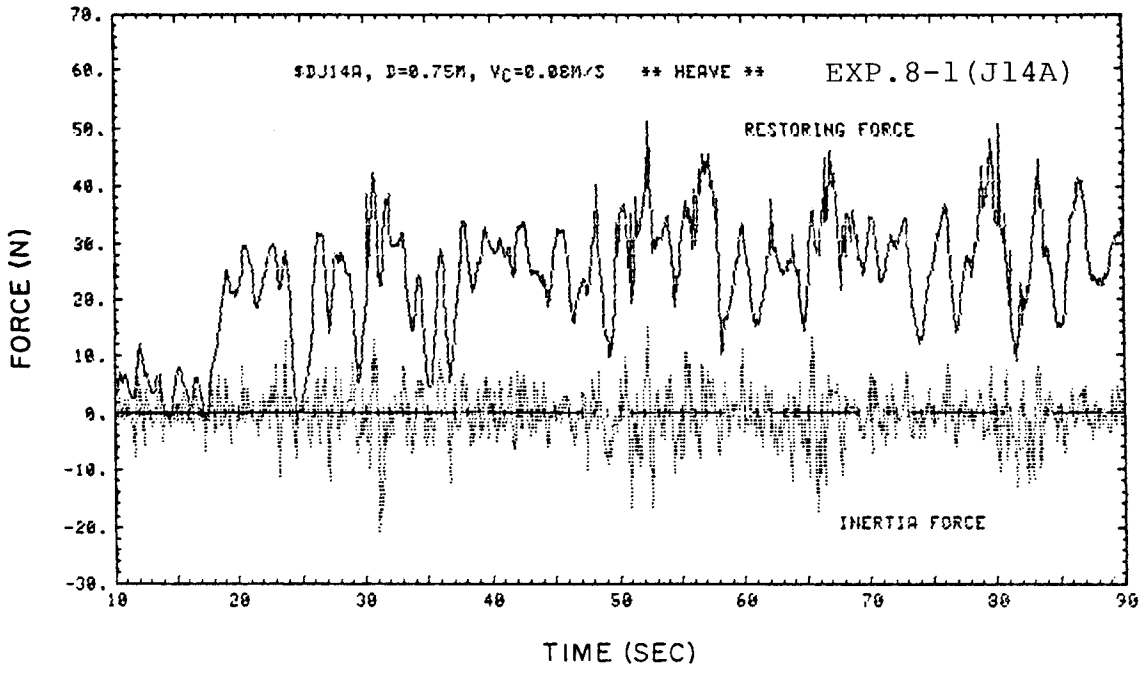

(c) heave(1)

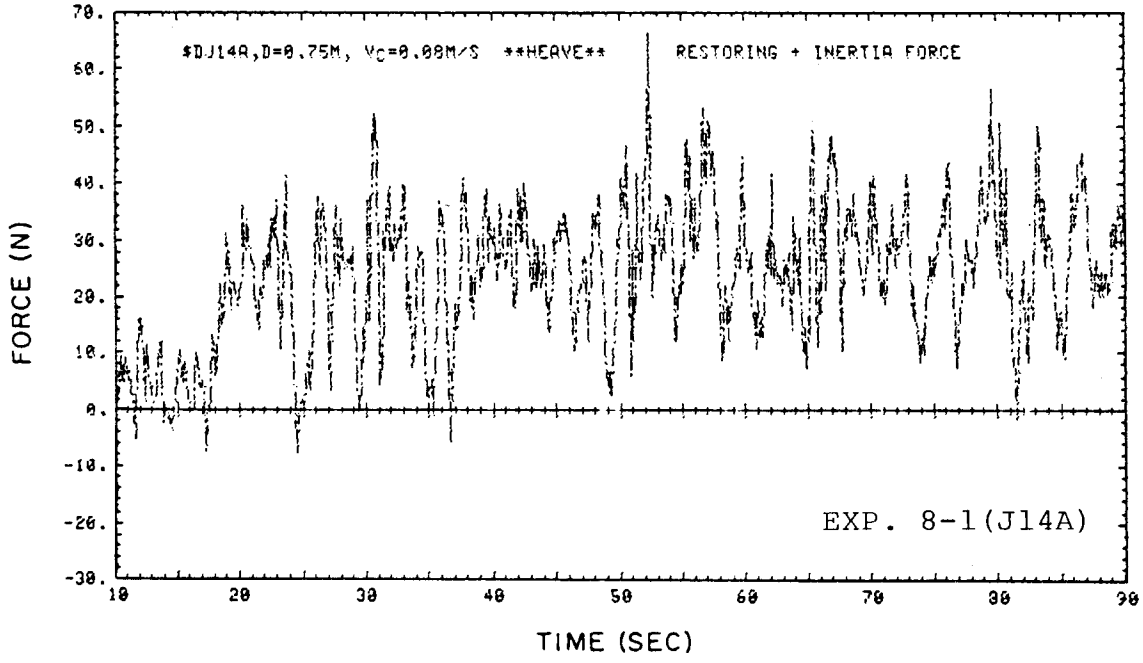

(d) heave(2)

Figure 38. Continued.

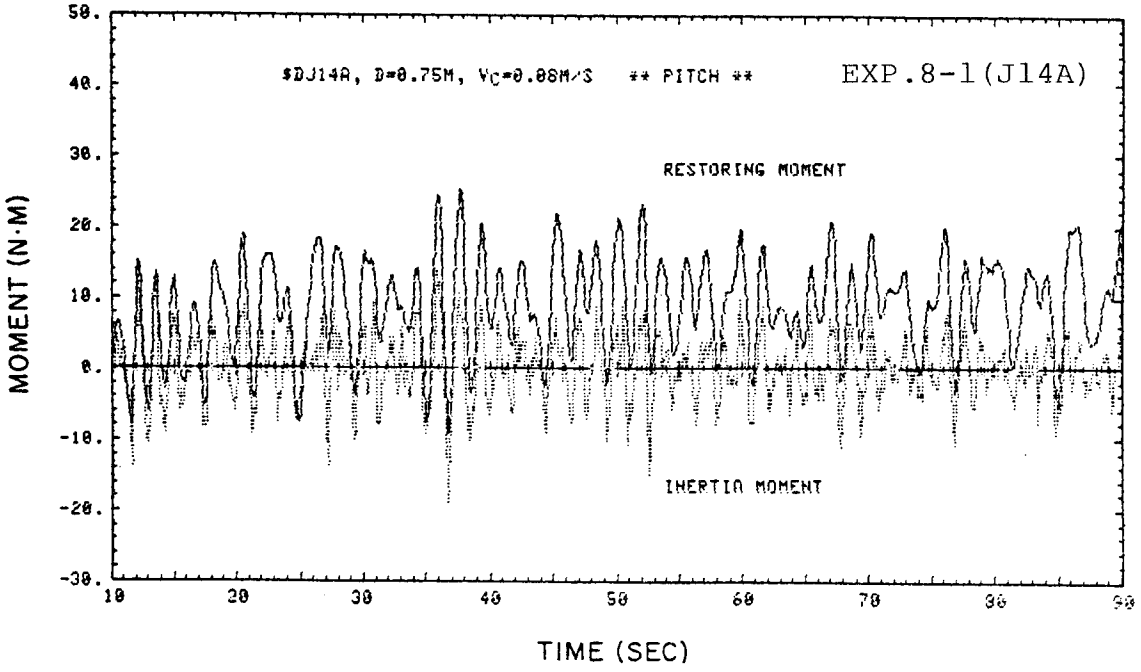

(e) pitch(1)

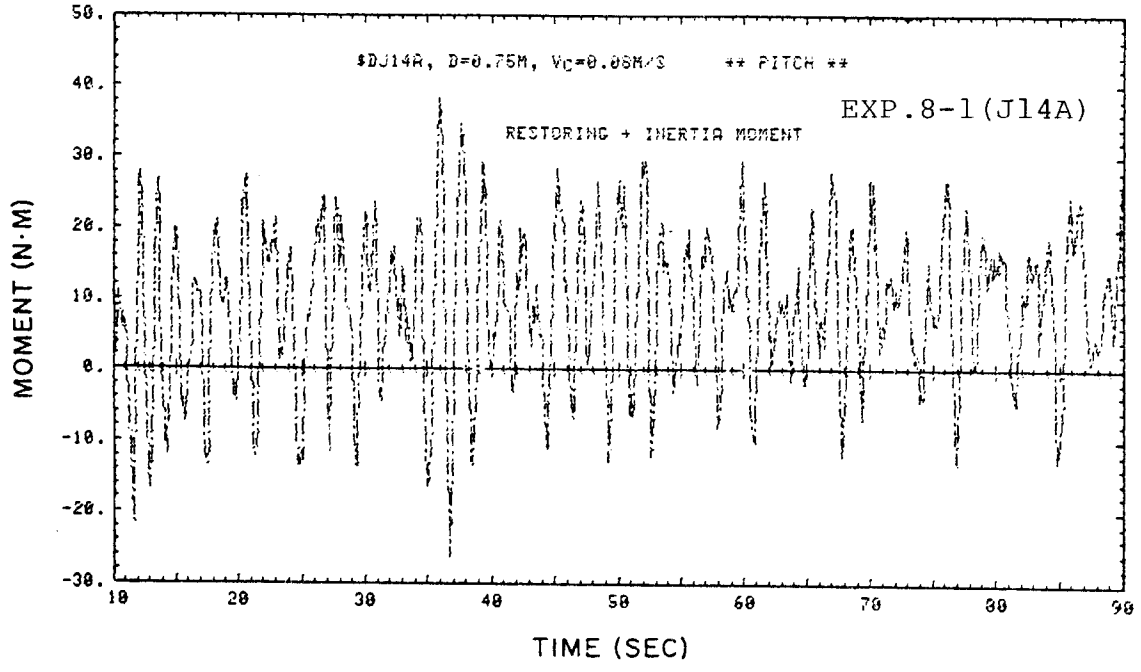

(f) pitch(2)

Figure 38. Continued.

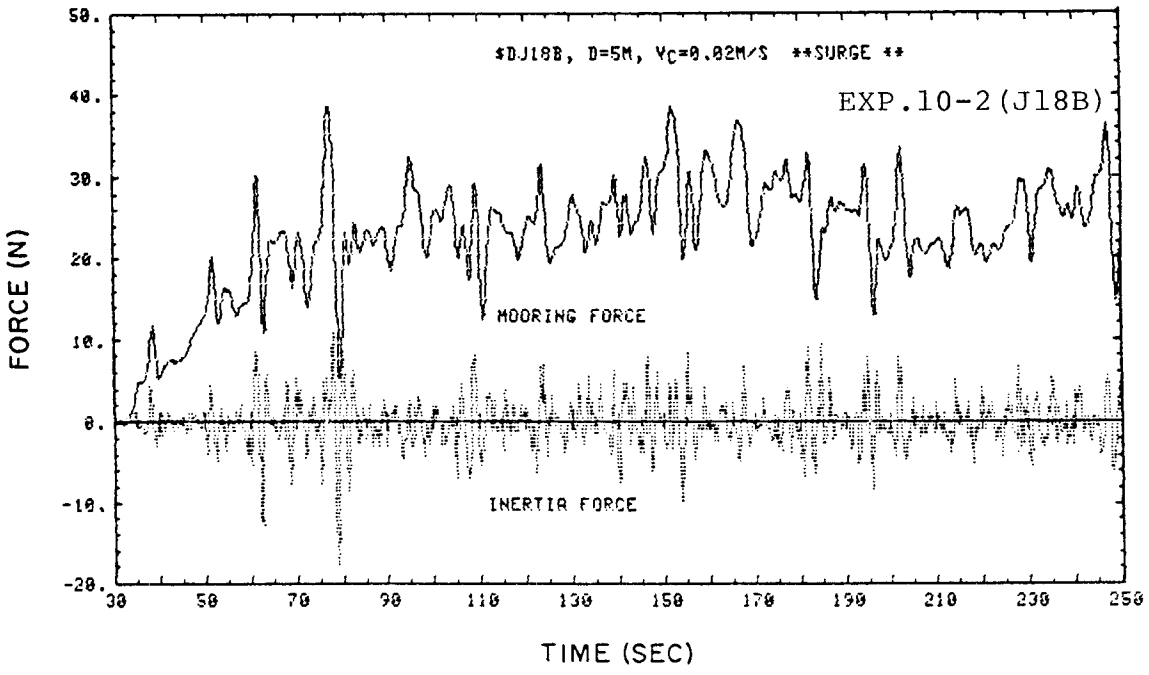

(a) surge(1)

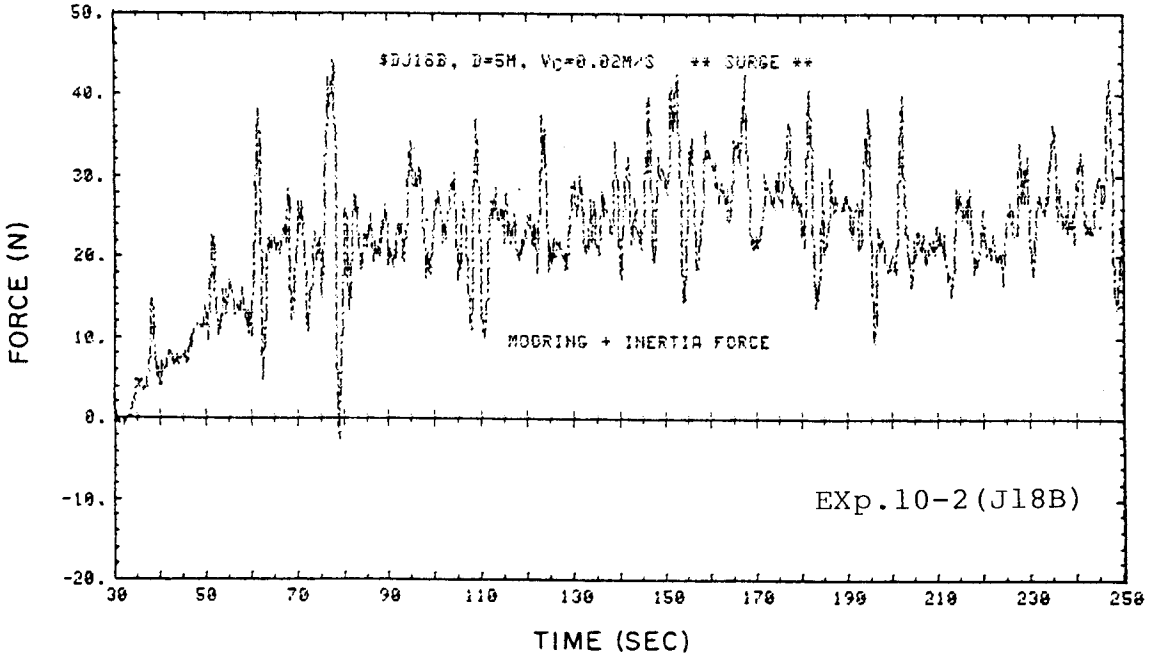

(b) surge(2)

Figure 39. Time histories of force components.

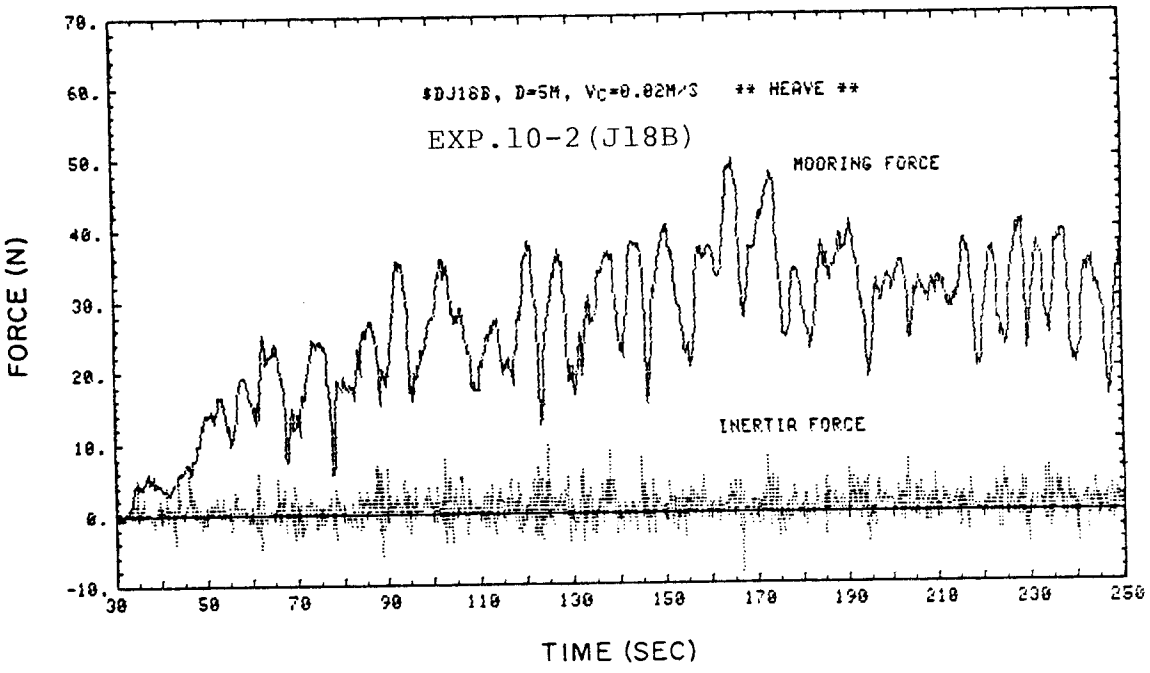

(c) heave(1)

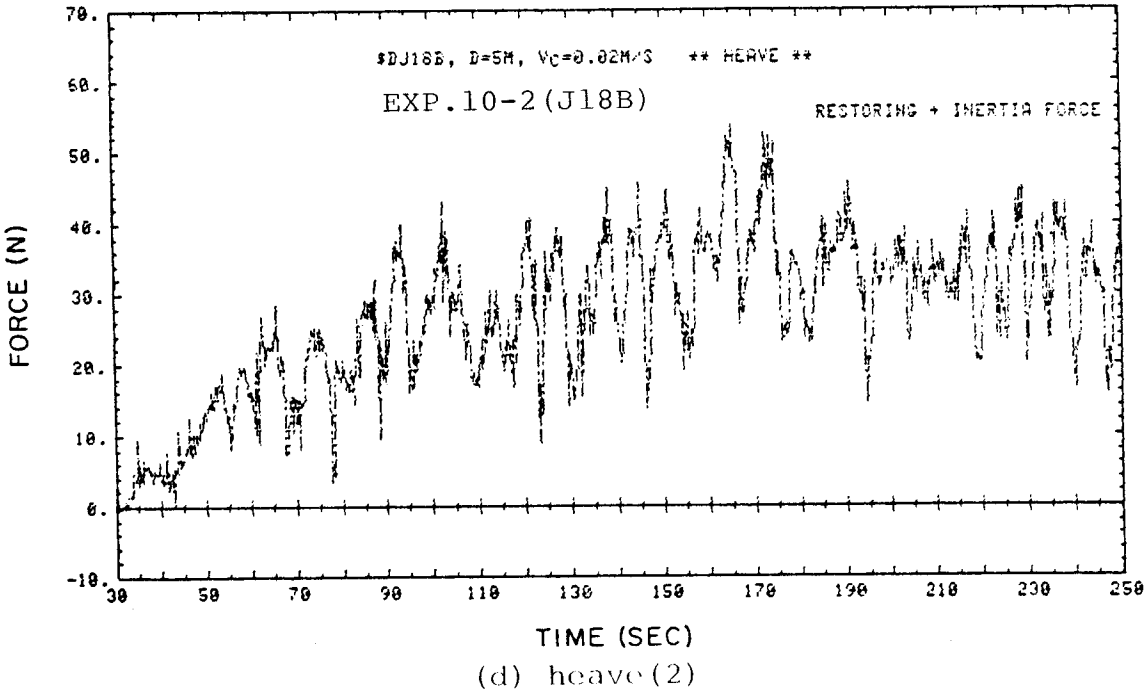

(d) heave(2)

Figure 39. Continued.

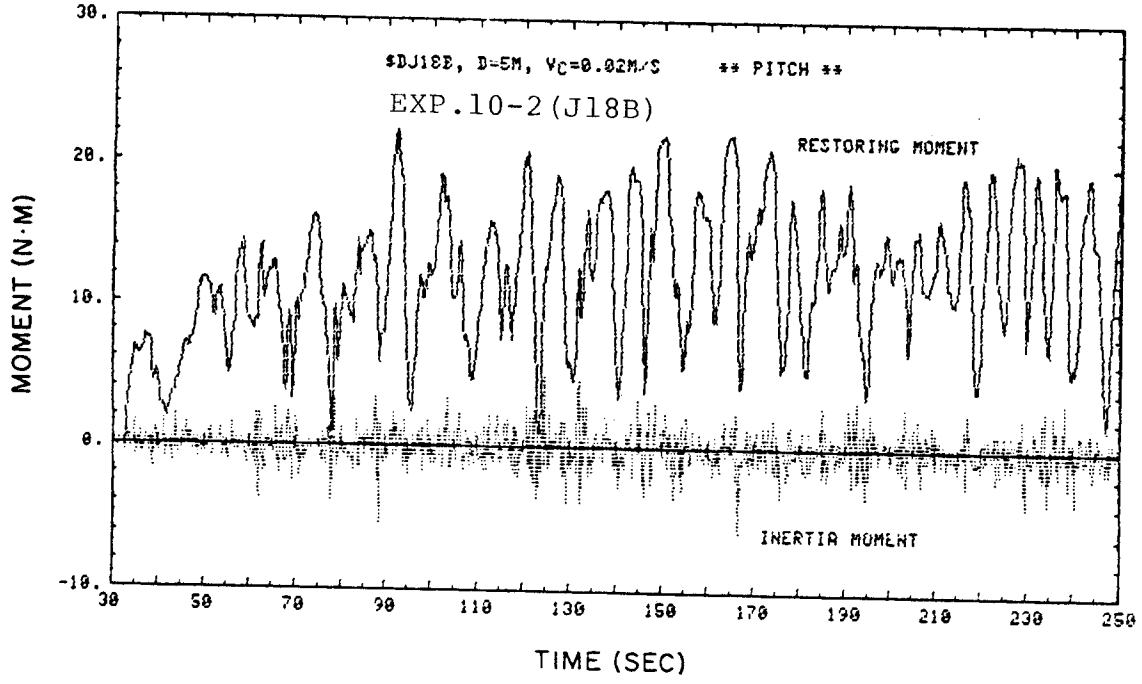

(e) pitch(1)

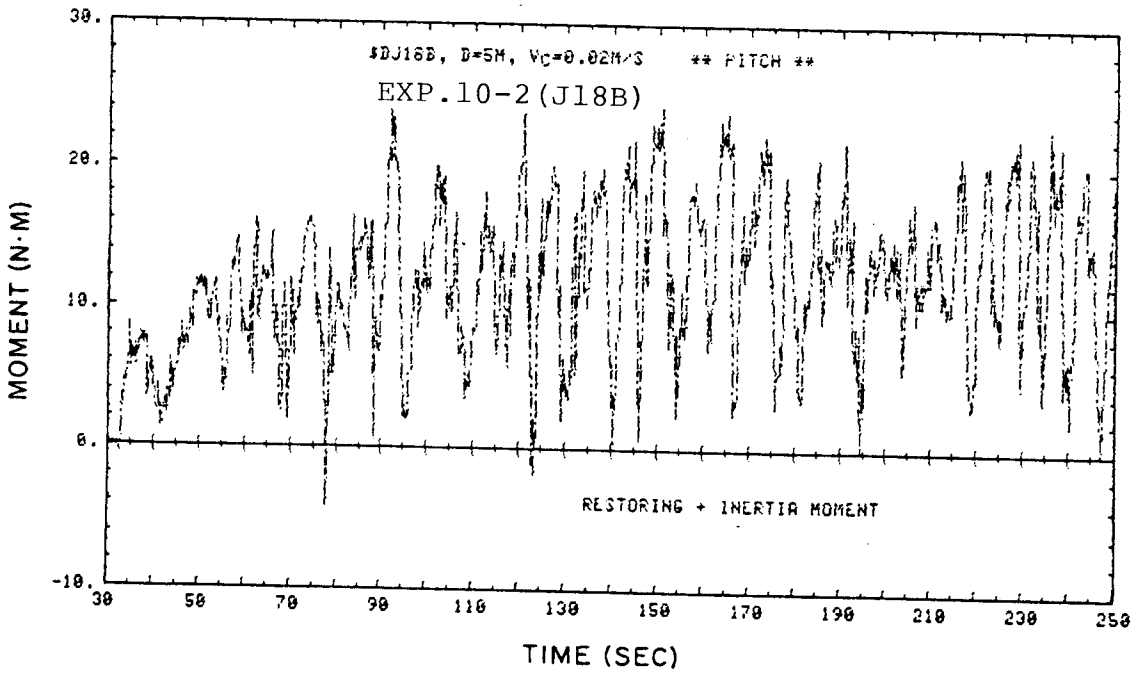

(f) pitch(2)

Figure 39. Continued.

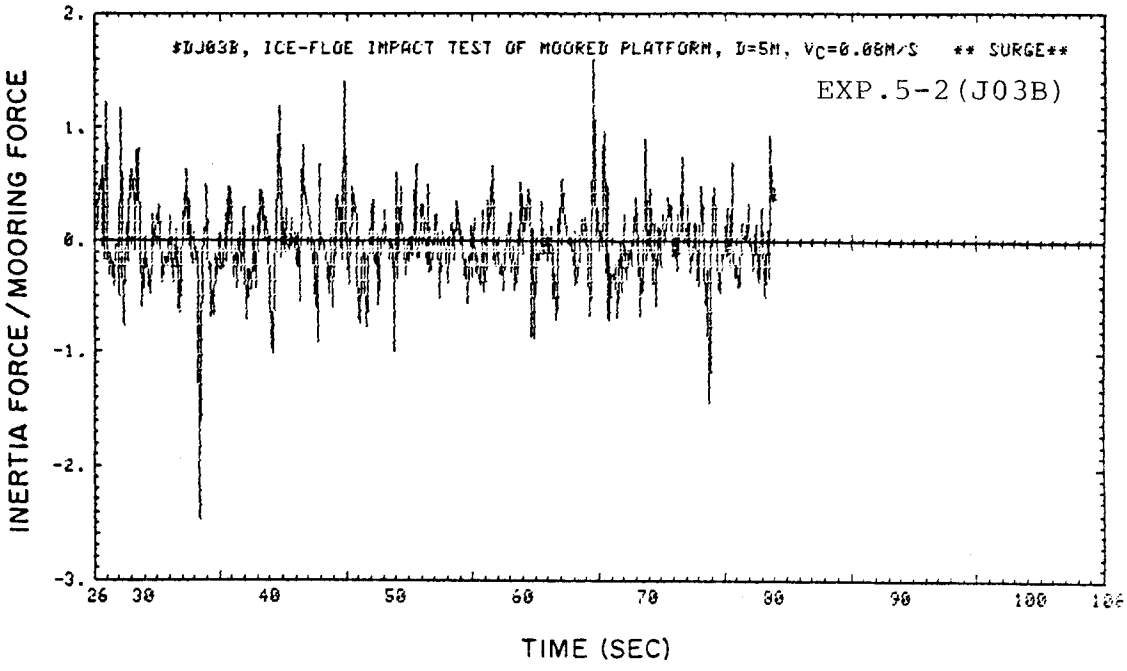

(a) surge

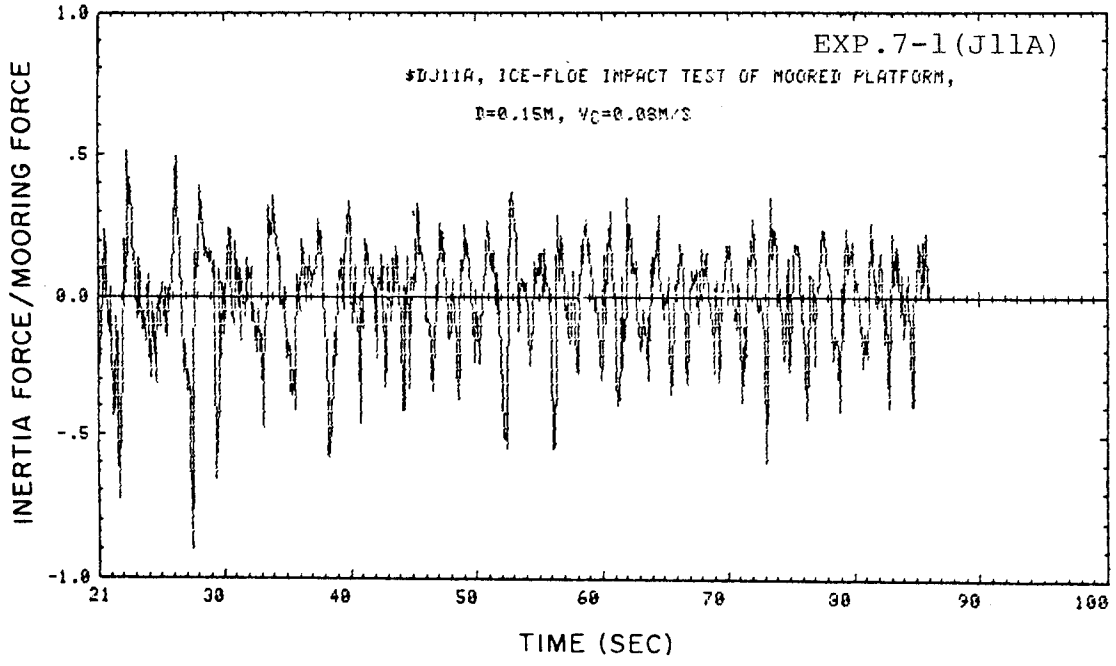

(b) surge

Figure 40. Time histories of force components.

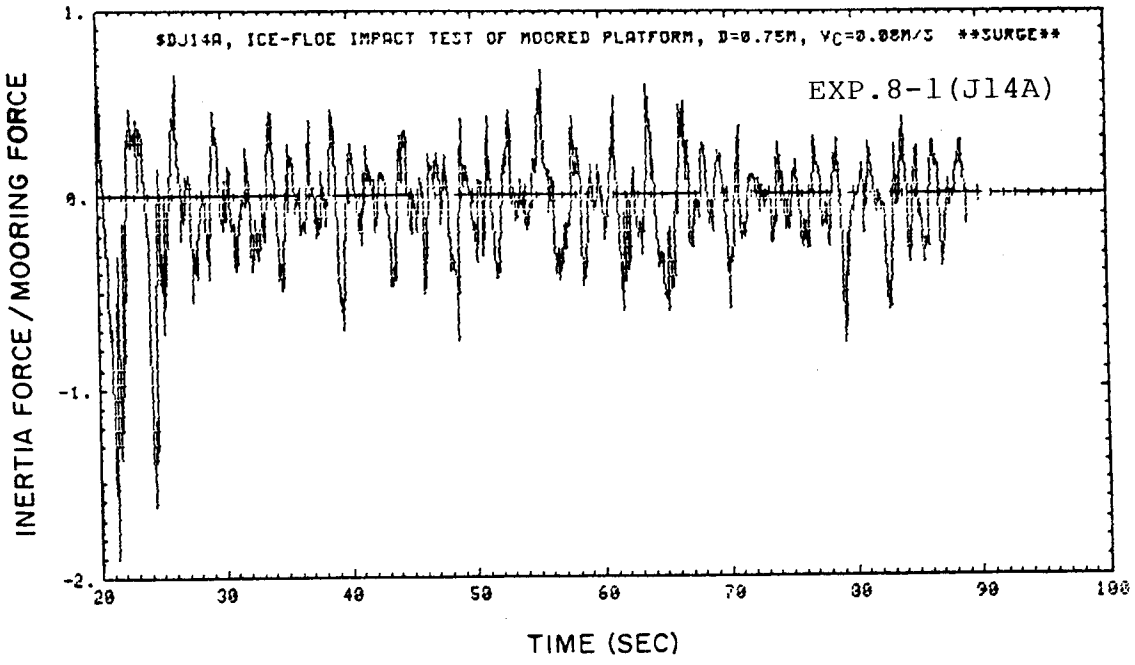

(c) surge

Figure 40. Continued.

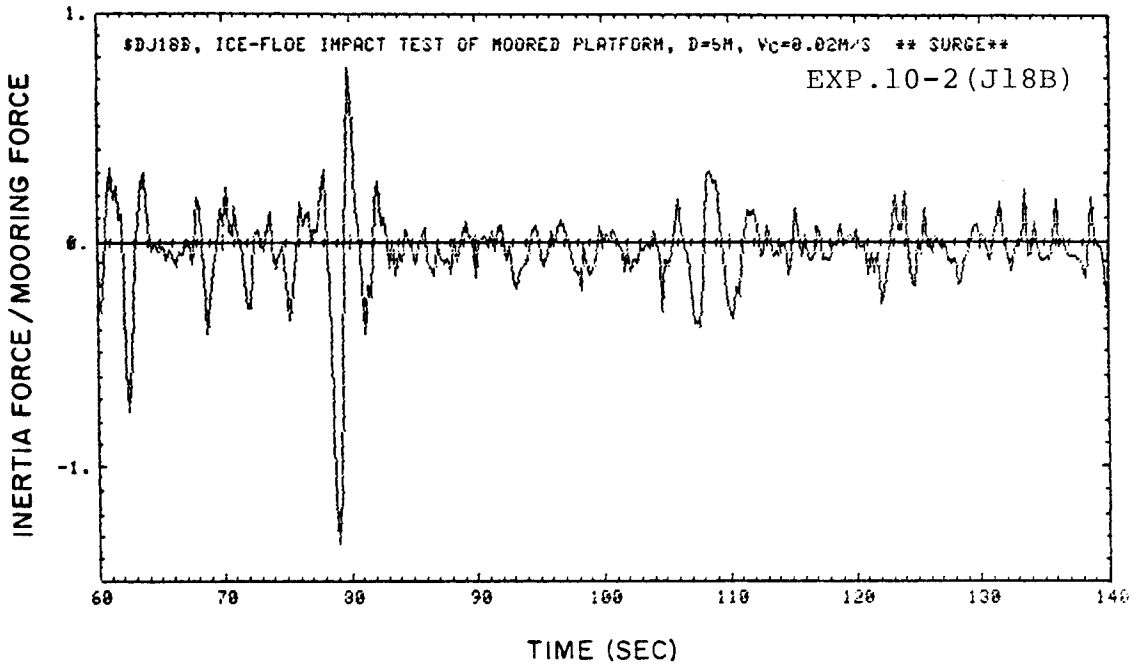

(d) surge(1)

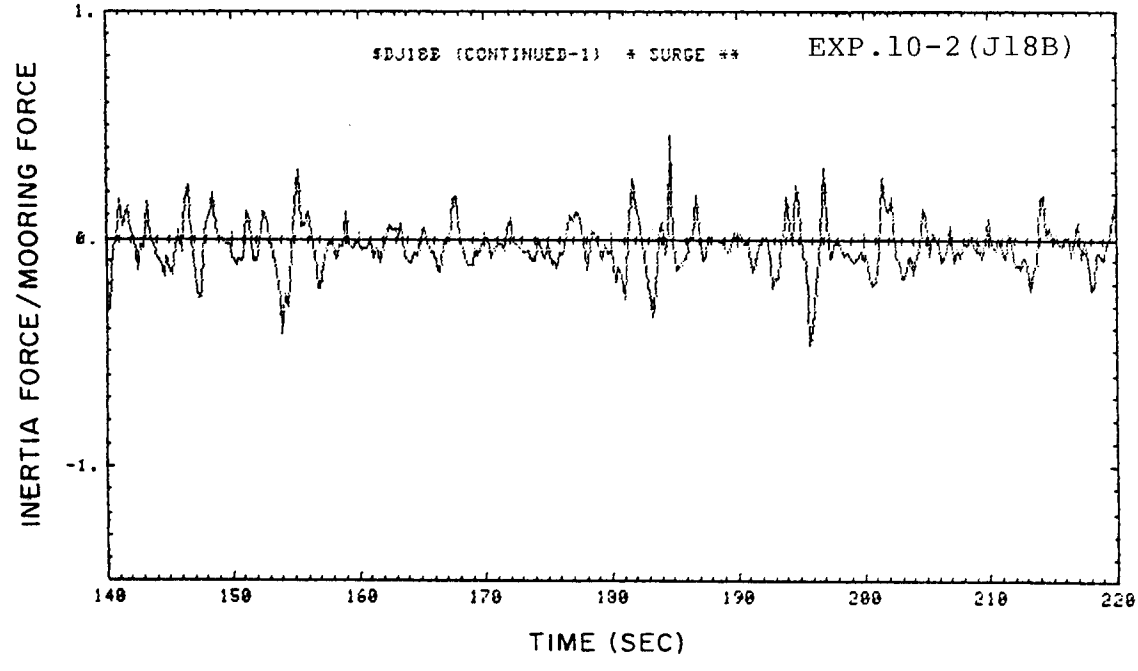

(e) surge(2)

Figure 40. Continued.

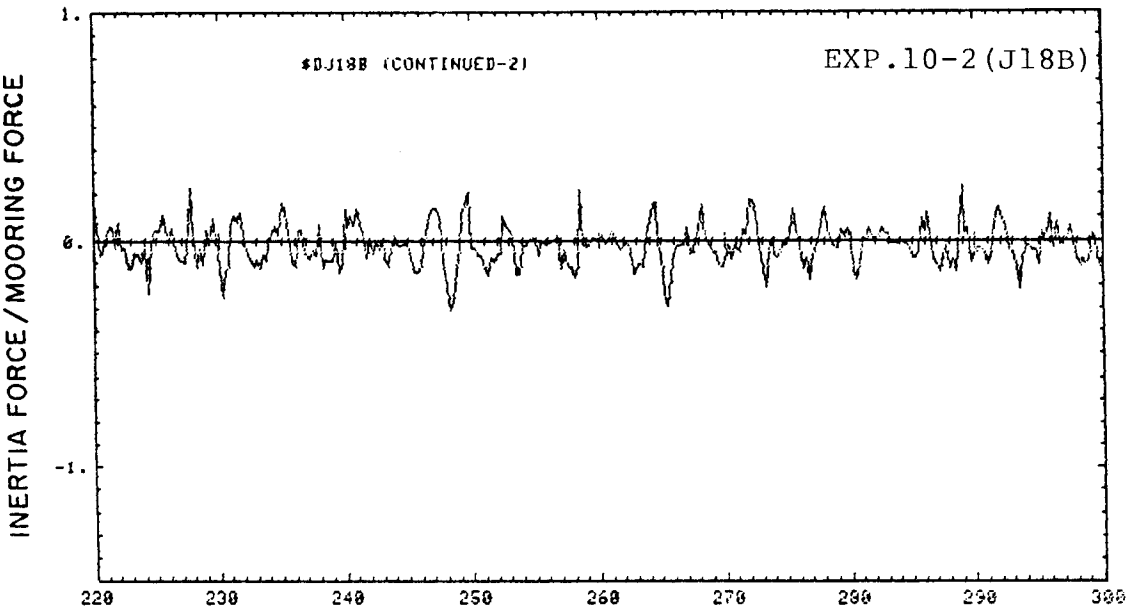

(f) surge(3)

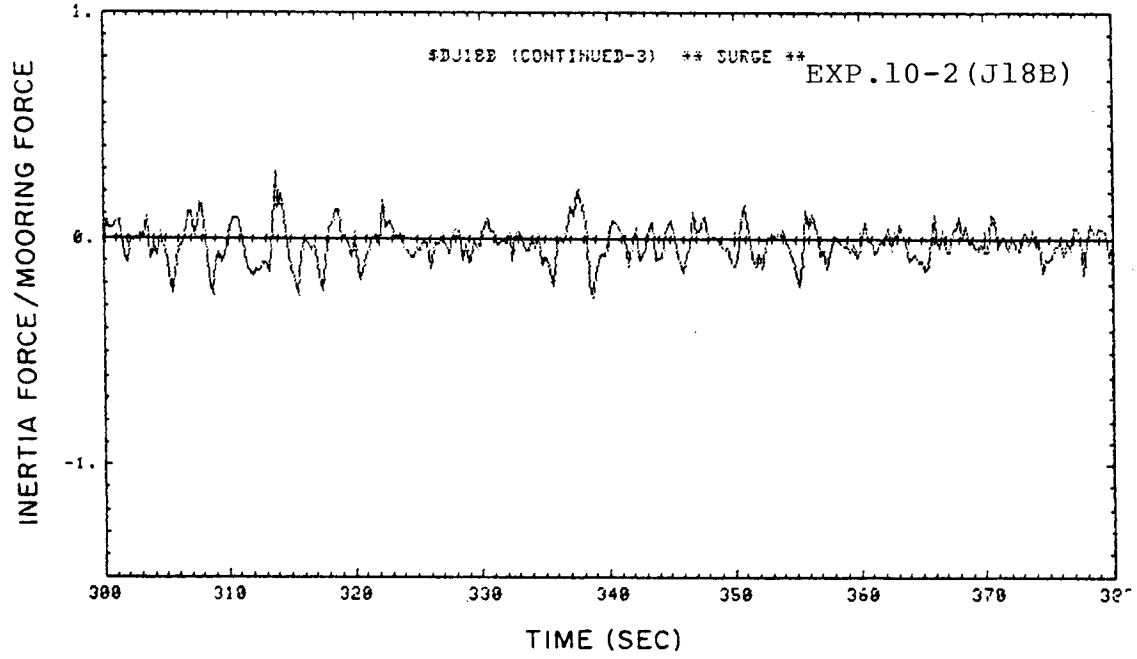

(g) surge(4)

Figure 40. Continued.

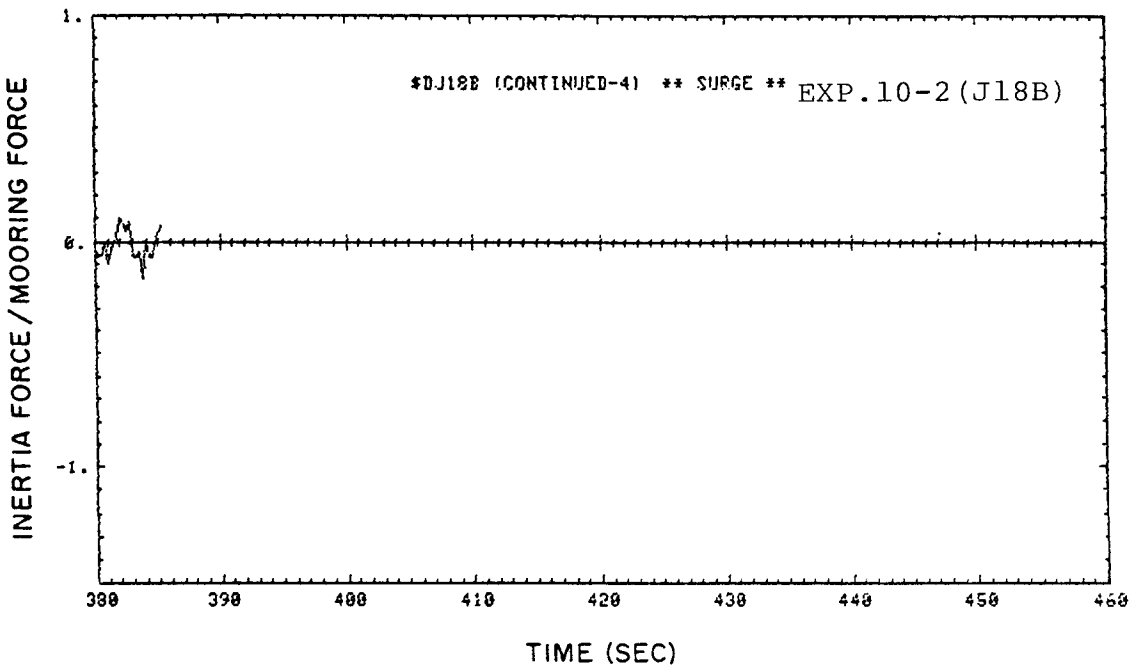

(h) surge(5)

Figure 40. Continued.

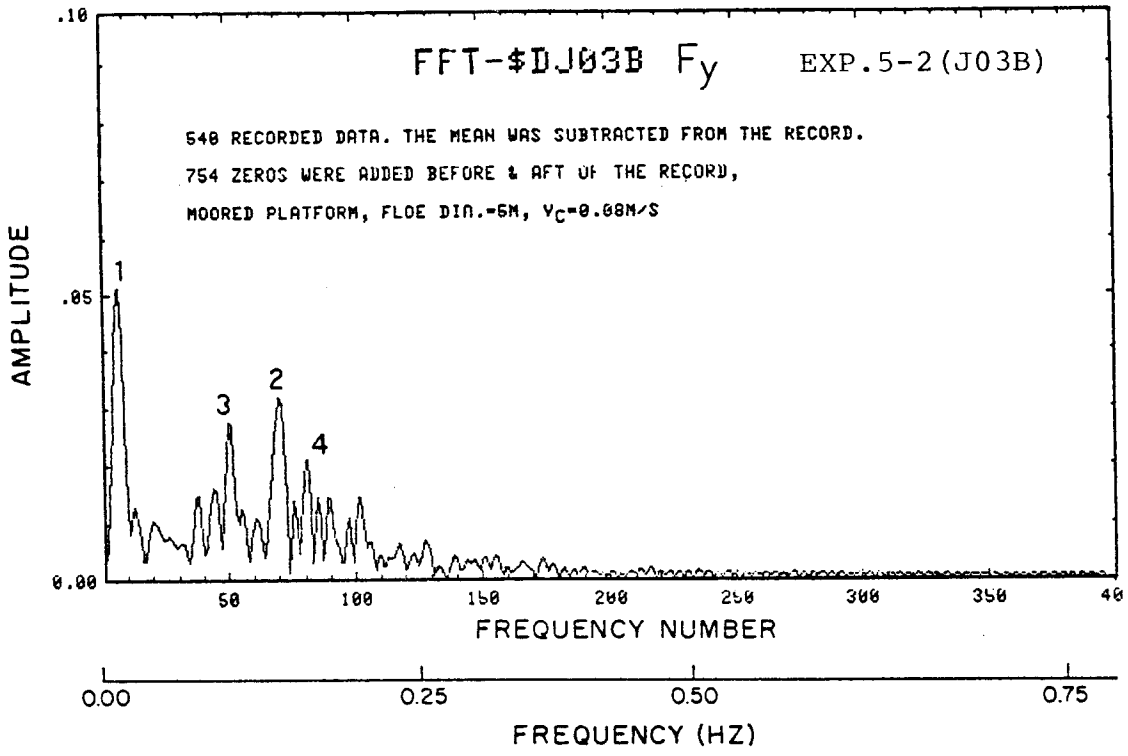

(a) surge(mooring force)

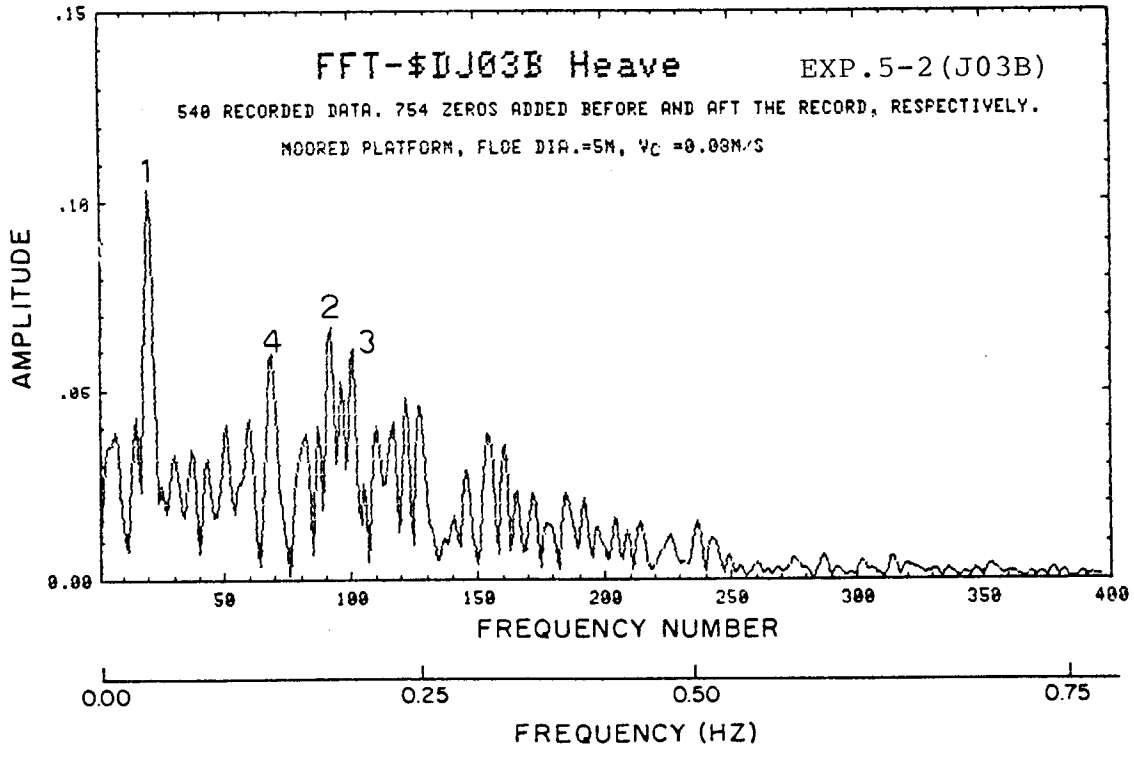

(b) heave motion

Figure 41. Spectral density (D=5m, V=0.08m/s).

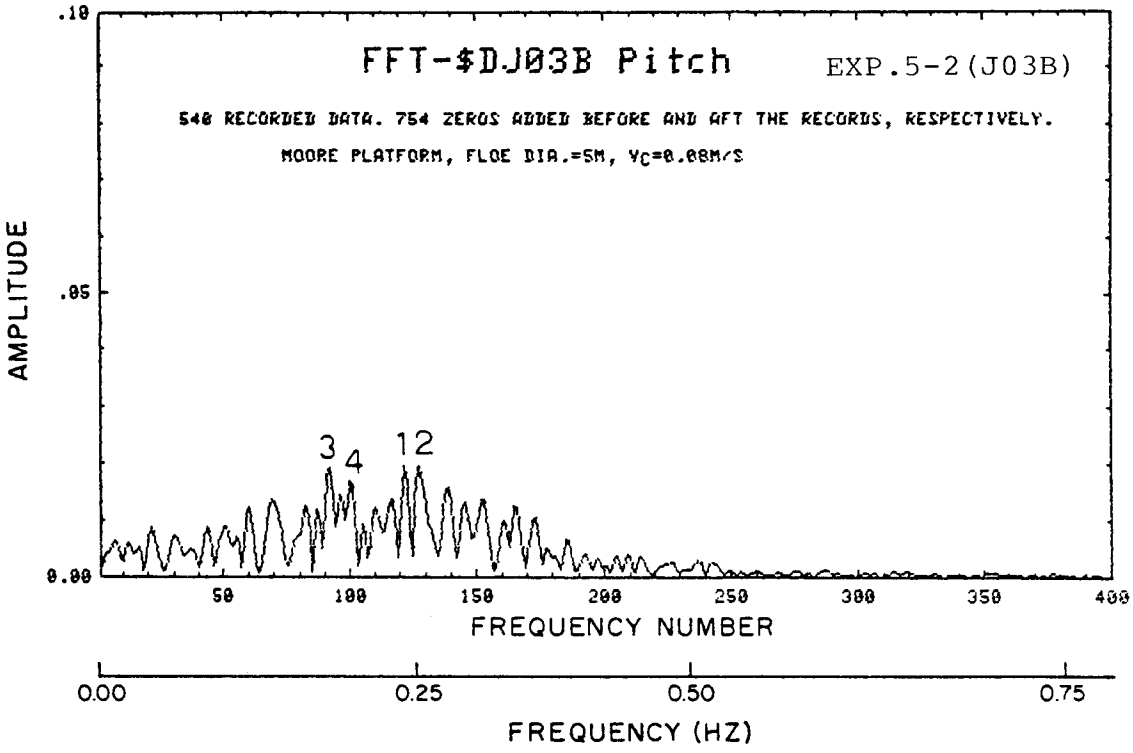

(c) pitch angle

Figure 41. Continued.

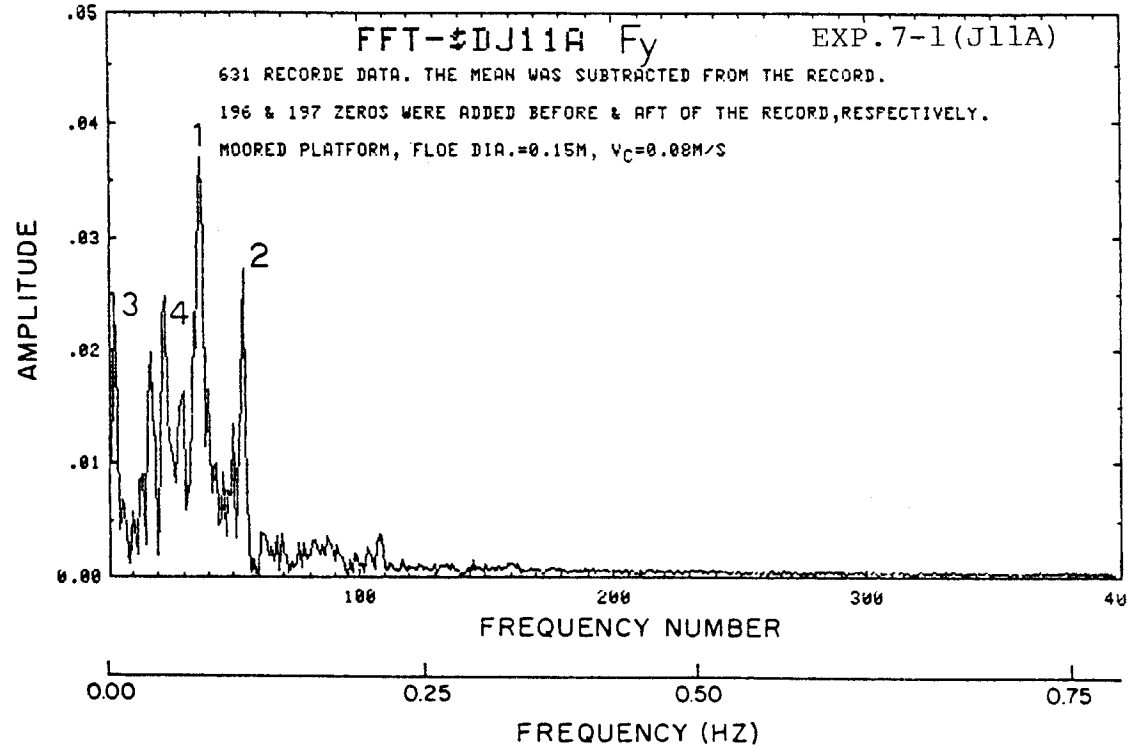

(a) surge

Figure 42. Spectral density (D=0.15m, V=0.08m/s).

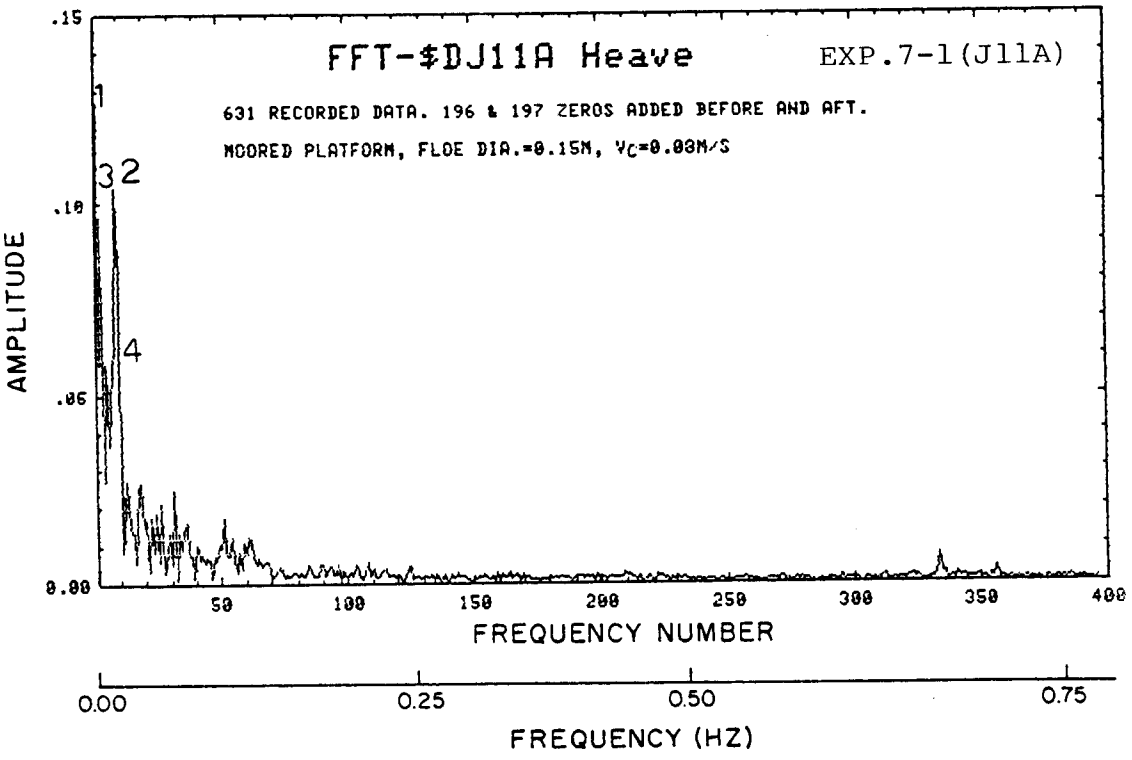

(b) heave

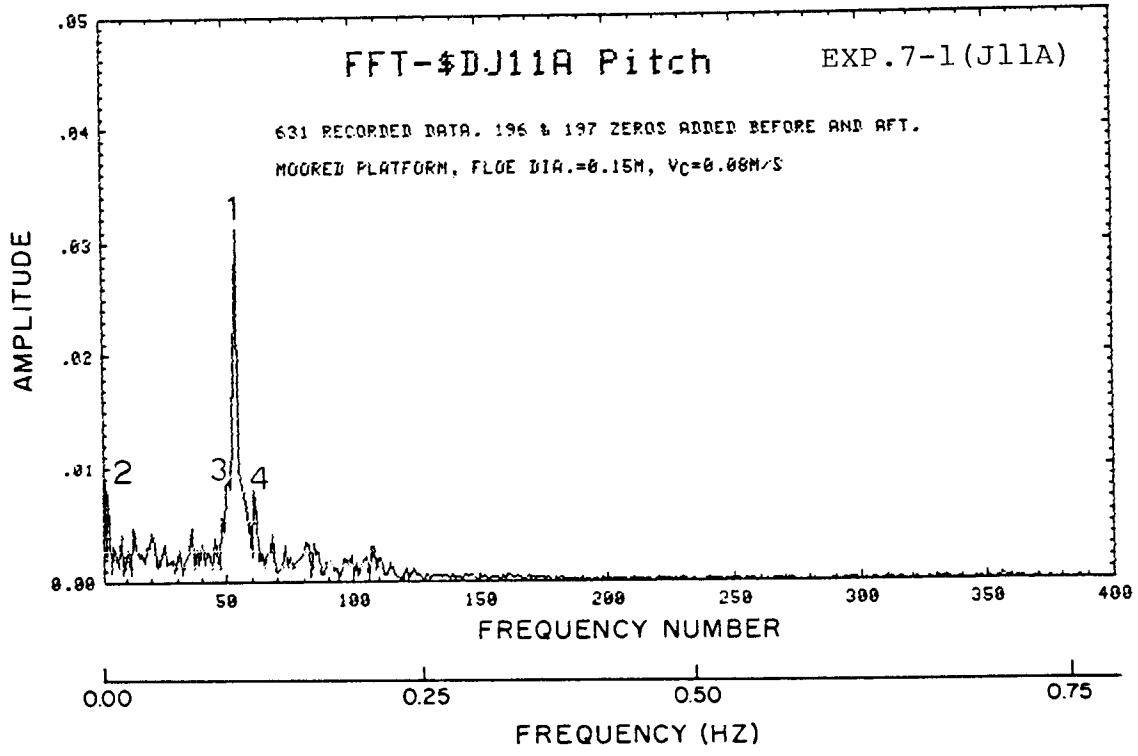

(c)pitch

Figure 42. Continued.

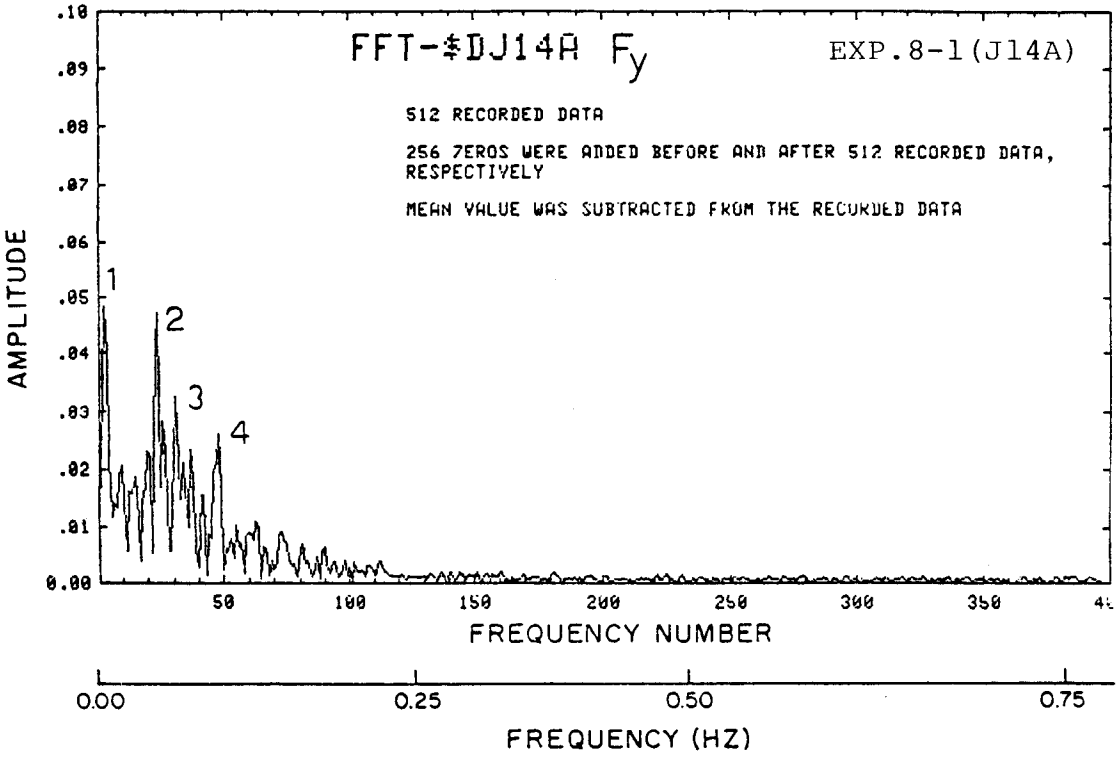

(a) heave

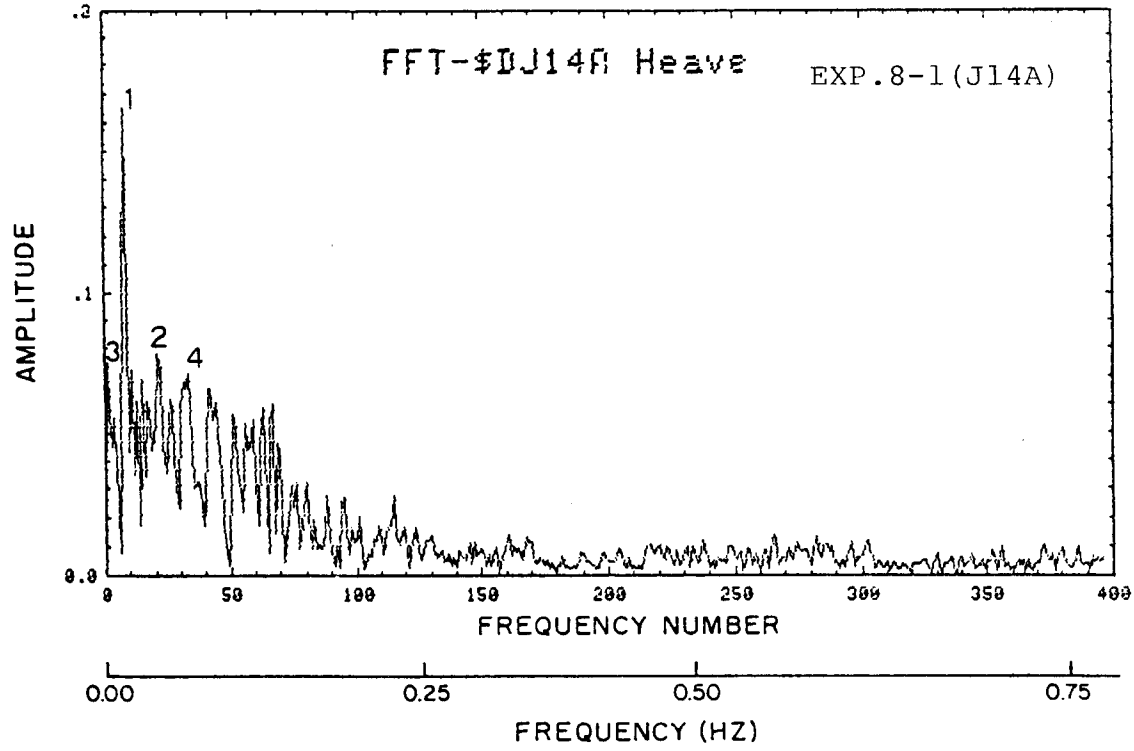

(b) heave

Figure 43. Spectral density (D=0.75m, V=0.08m/s).

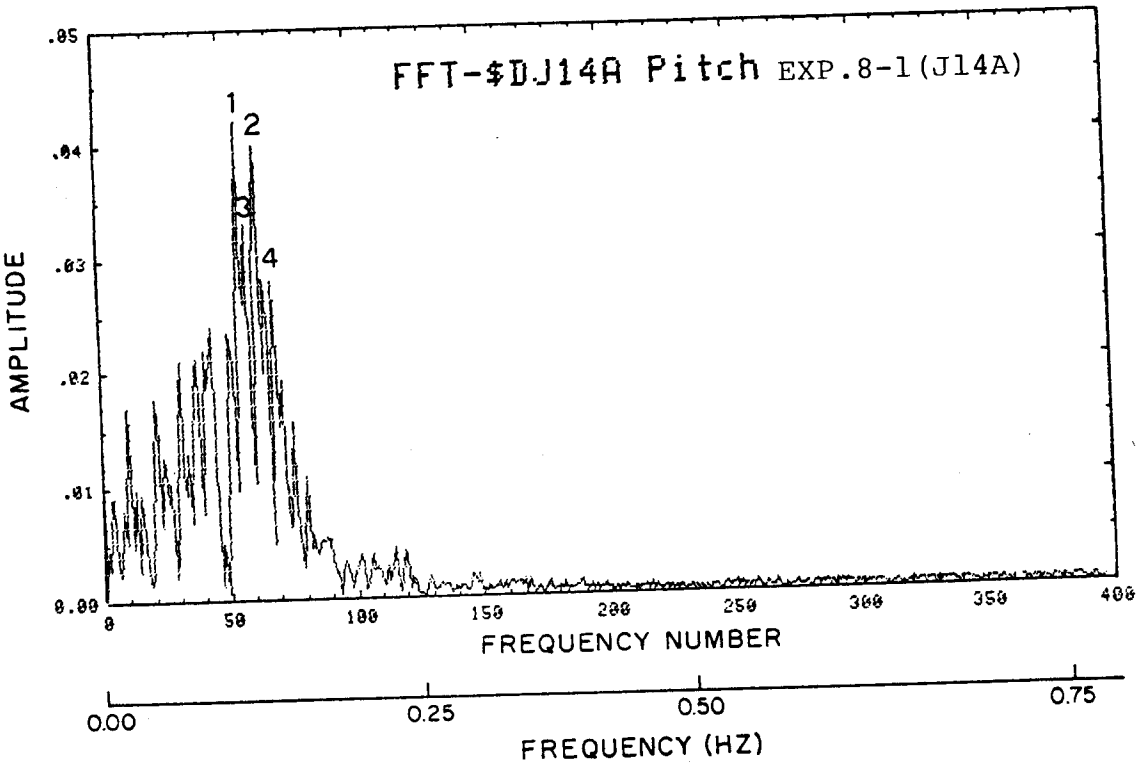

(c) pitch

Figure 43. Continued.

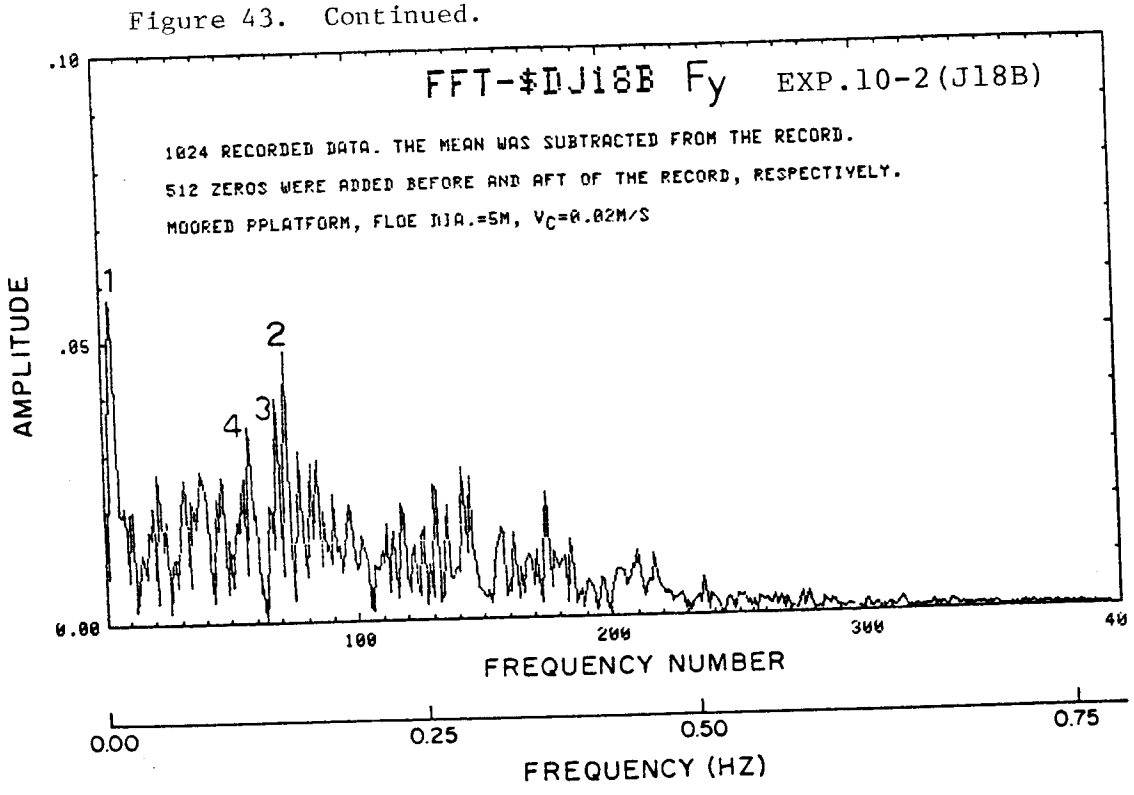

(a) surge

Figure 44. Spectral density (D=5m, V=0.02m/s)

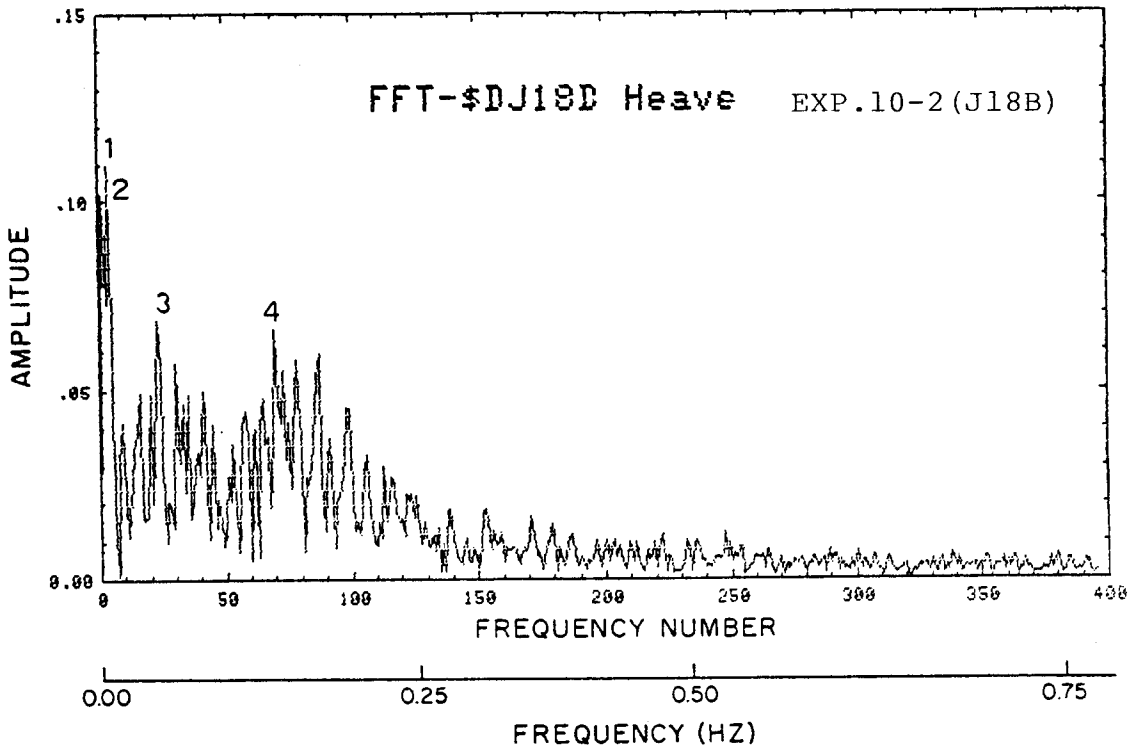

(b) heave

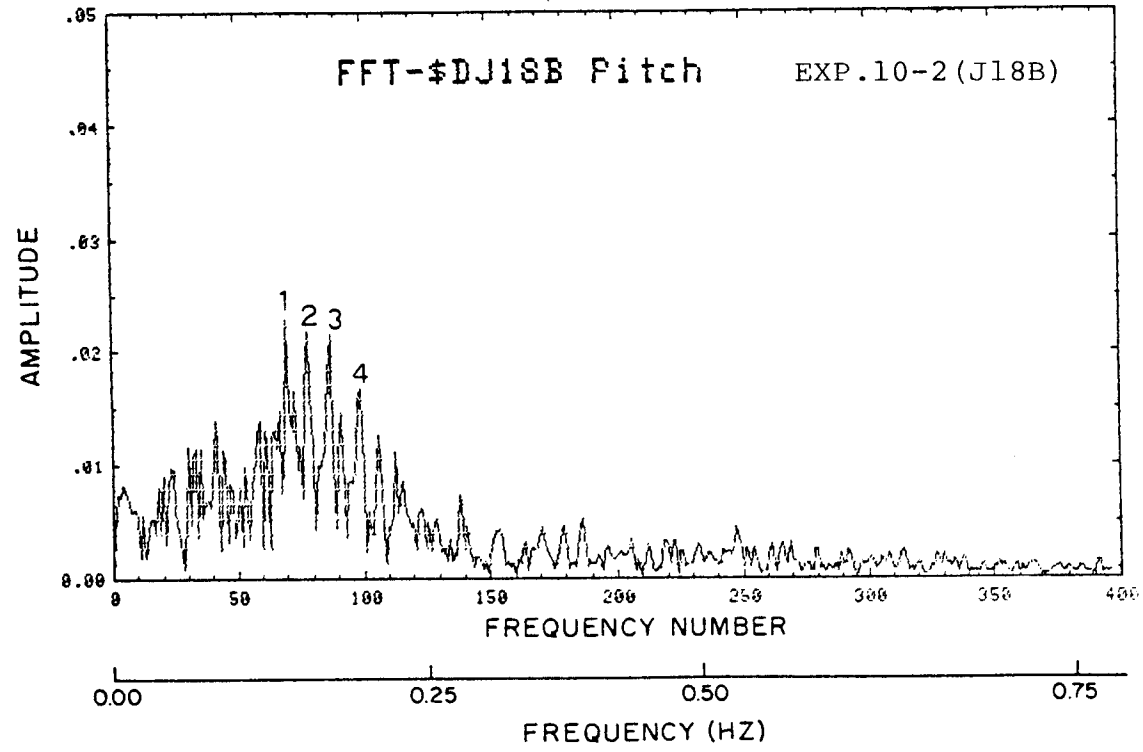

(c) pitch

Figure 44. Continued.

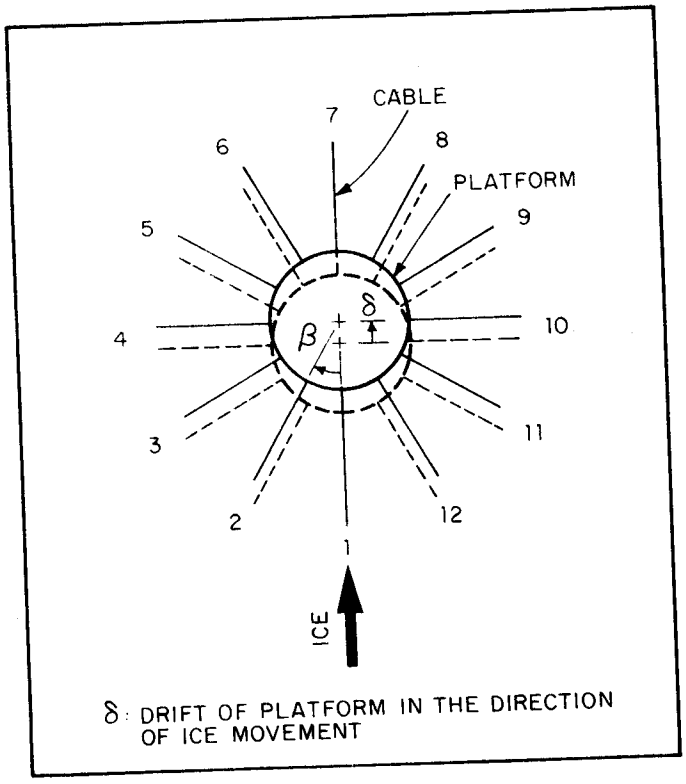

Figure 45. Arrangement of cables.

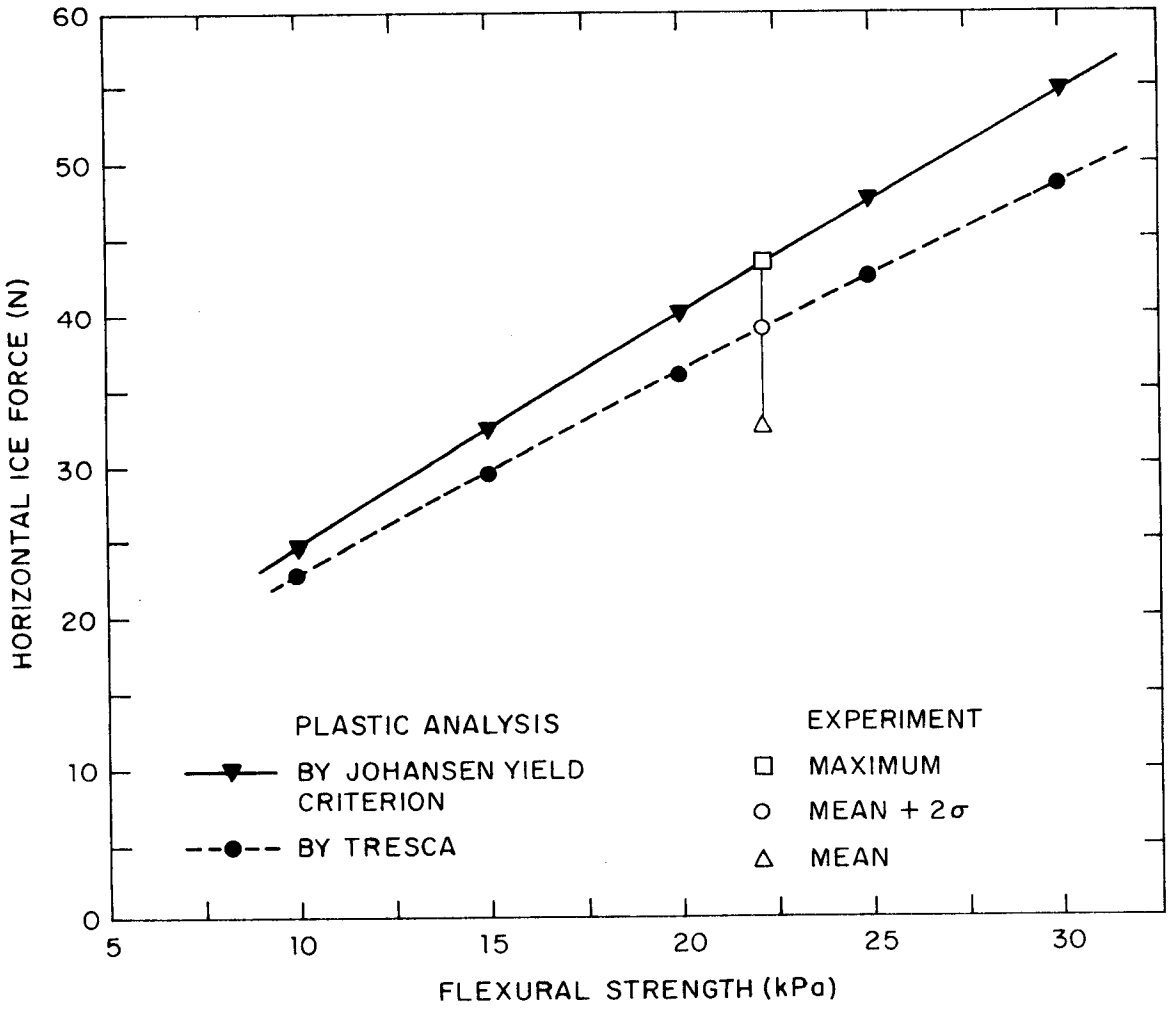

Figure 46. Comparison of horizontal ice forces.

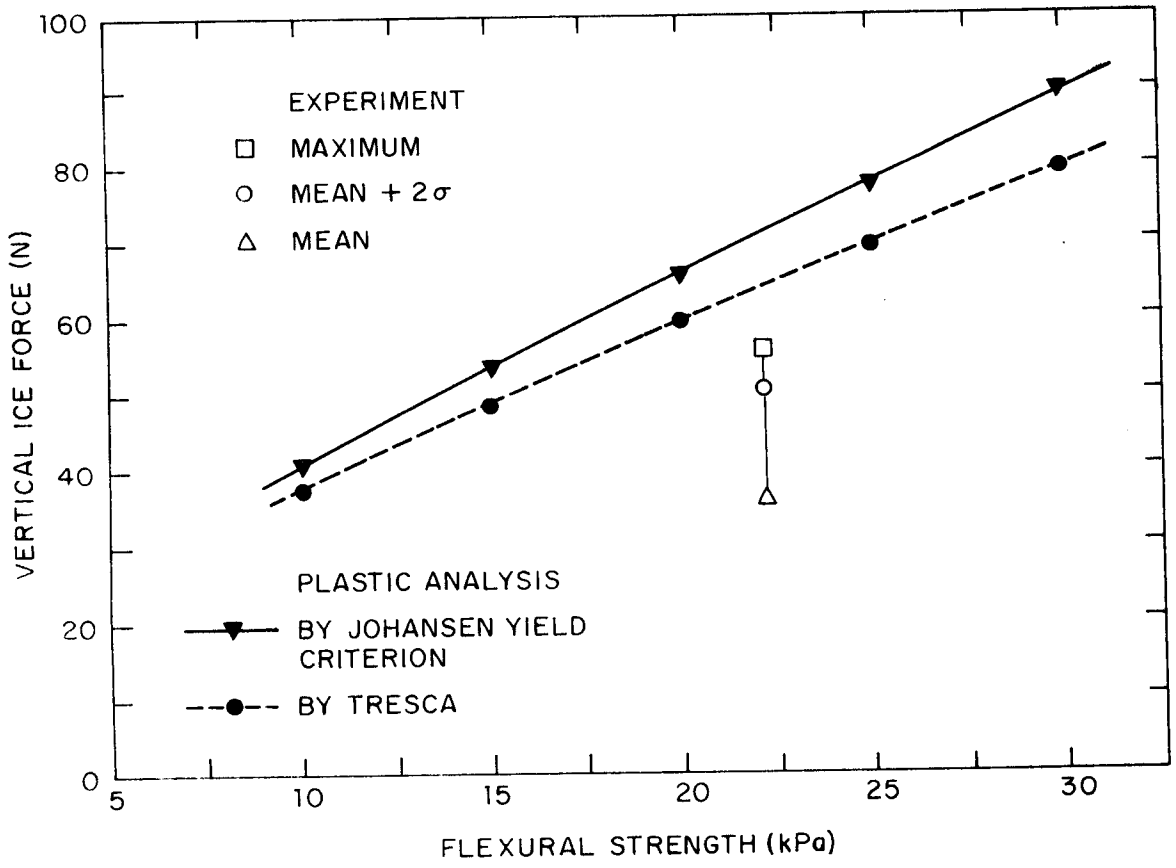

Figure 47. Comparison of vertical ice forces.

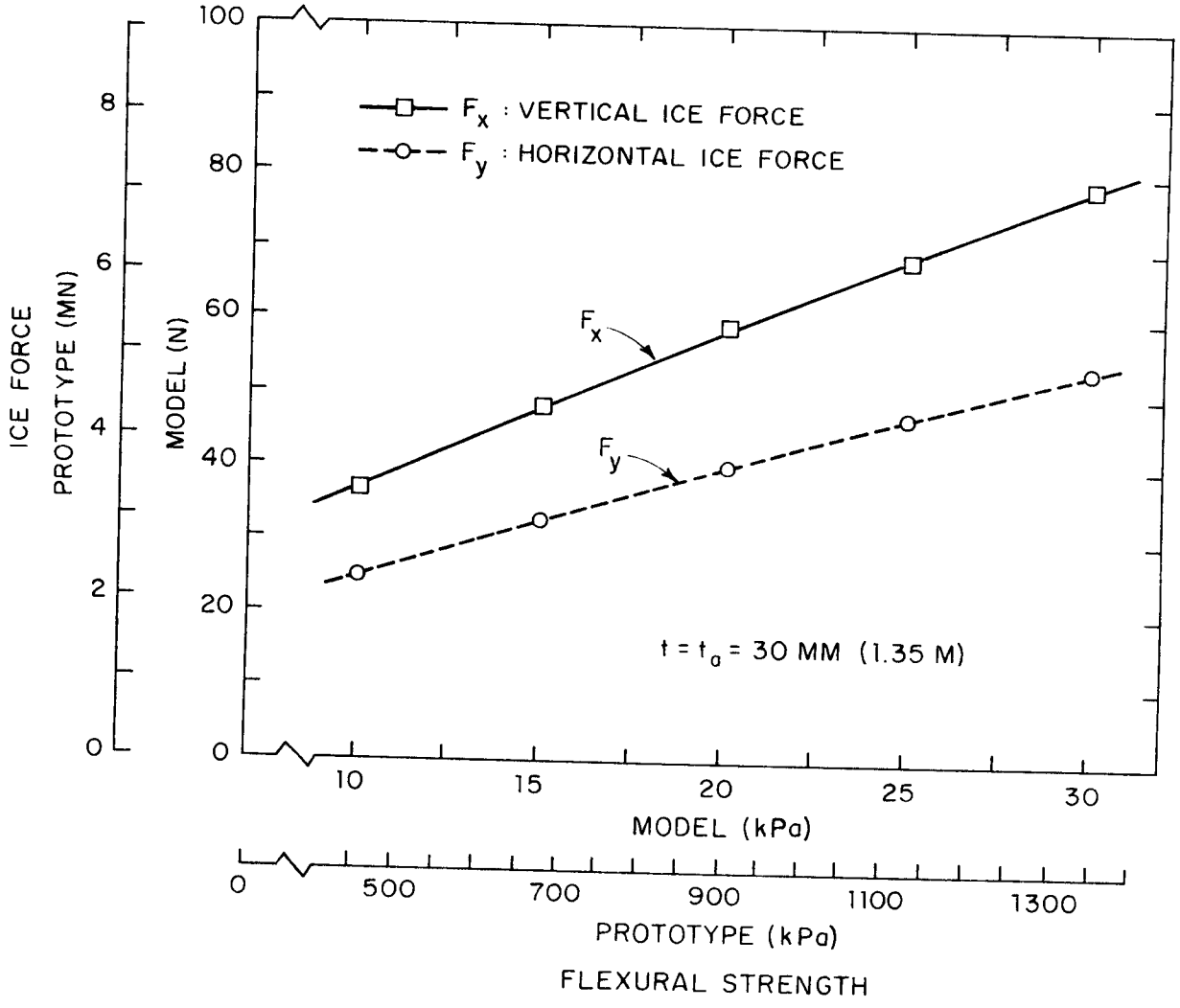

Figure 48. The effect of flexural strength on ice force.

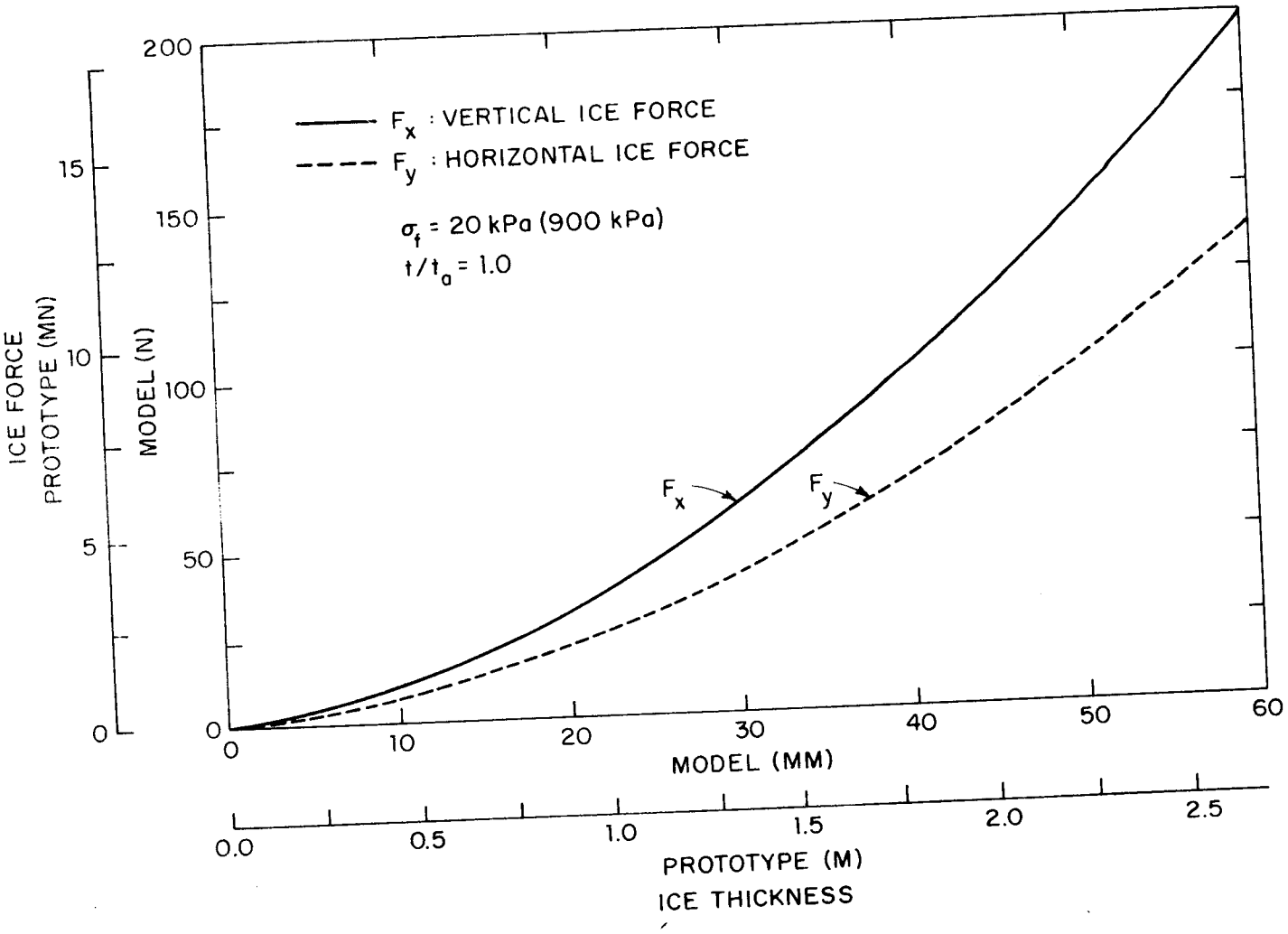

Figure 49. The effect of ice thickness on ice force.

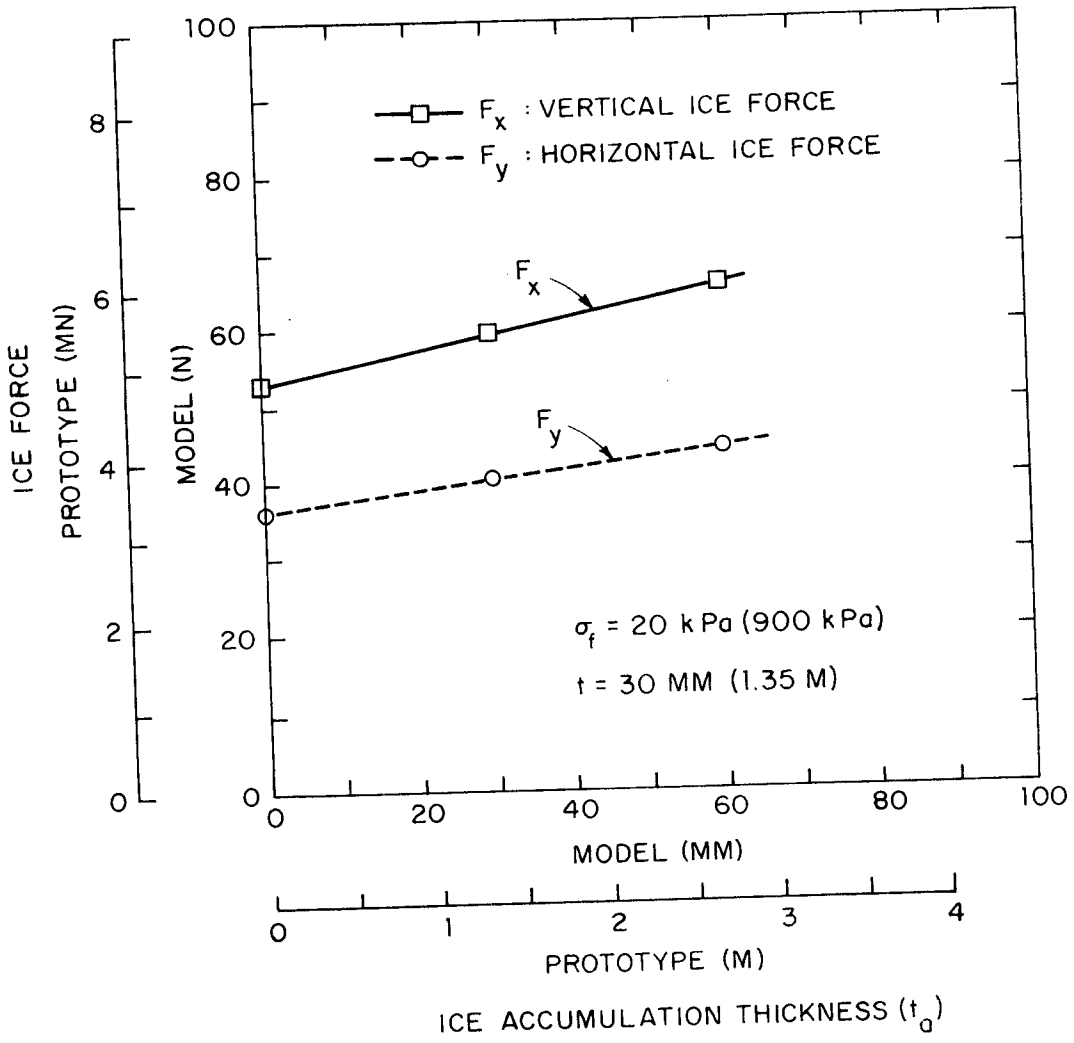

Figure 50. The effect of ice accumulation thickness on ice force.

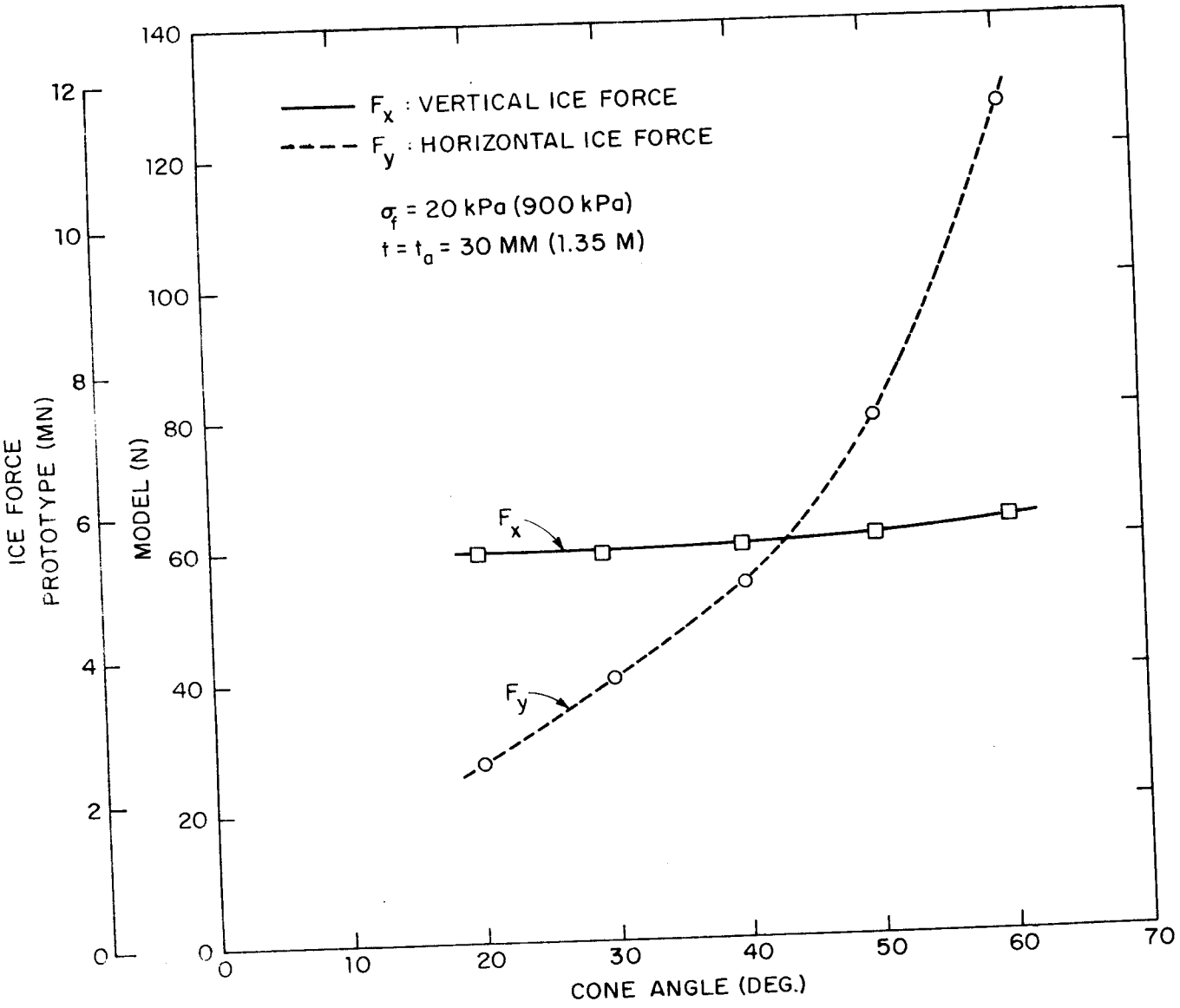

Figure 51. The effect of cone angle on ice force.

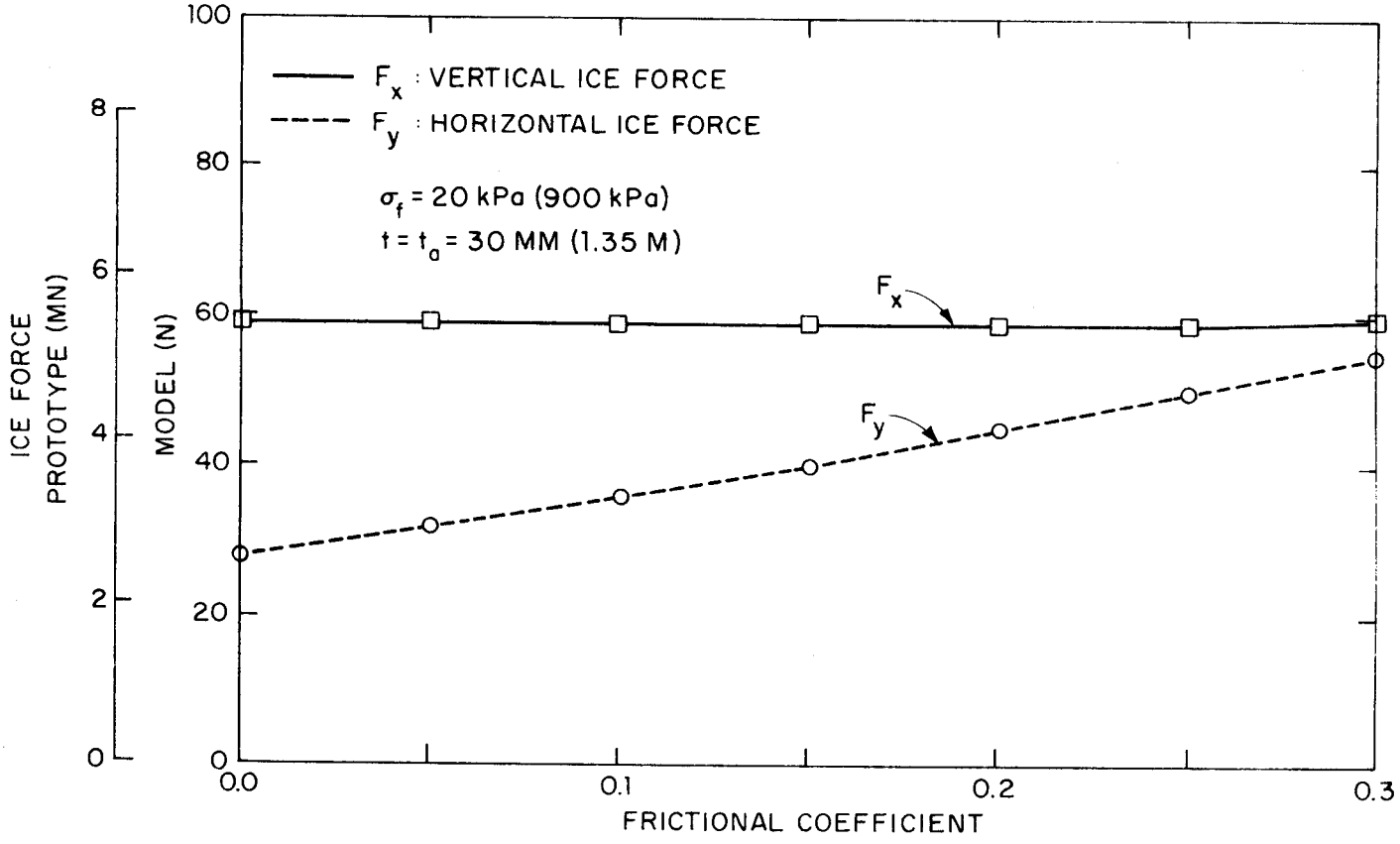

Figure 52. The effect of ice-structure friction coefficient on ice force.

Table 1. Principal Dimensions of the Test Platform and "Kulluk."

		Test Platform (1/45 scale)	"Kulluk"
Diameter at deck level, D_D	(m)	1.8	81.0
Diameter at load waterline, D_{LW}	(m)	1.5	67.5
Diameter at base line, D_B	(m)	1.334	60.0
Depth, D	(m)	0.334	15.5
Draft, d	(m)	0.187	8.4
Displacement, ∇	(m^3)	0.271	24700
Cone angle, α	(degree)	31.4	31.4

Table 2. Ice-sheet data

Thickness, t(m)	0.029-0.032
Flexural strength, σ_f (kPa)	16.6 - 24.4
Elastic modulus, E(MPa)	8.2 - 14.8

Table 3. Properties of Ice Sheets

Ice Sheet No	File No	Exp No	Date	Mean Thickness (mm)	Mean Flex Strength (kPa)	Mean Young's Modulus (MPa)
1	D17A I	1-1, 9	12-17-84	29.0	21.9	10.7
2	D21A F	2-1, 6	12-21-84	29.3	23.0	9.4
3	D27A N	3-1, 14	12-27-84	30.0	18.2	12.7
4	D29A E	4-1, 5	12-29-84	30.0	22.2	14.8
5	J03A I	5-1, 9	01-03-85	31.7	16.6	19.1
6	J07A	6-1	01-07-85	30.0	22.2	8.6
7	J11A H	7-1, 8	01-11-85	31.0	18.5	14.5
8	J14A F	8-1, 6	01-14-85	30.0	19.0	13.0
9	J16A G	9-1, 7	01-16-85	31.7	24.4	12.2
10	J18A E	10-1, 5	01-18-85	30.0	22.0	8.2
11	J21A H	11-1, 8	01-21-85	30.0	21.9	12.7

Table 4. Natural periods and logarithmic decrements of the test platform when moored

	SURGE	HEAVE	PITCH
Natural Period, T (seconds)	3.00	1.41	1.17
Logarithmic Decrement δ	0.29	--	0.55

Table 5. Summary of moored platform

Exp. No.	D (m)	V (ms/)	Mooring Force (N) $\bar{x}$	Mooring Force (N) $\bar{x}+2\sigma$	Mooring Force (N) Max.	Mooring Force (N) Min.	Heave (mm) $\bar{x}$	Heave (mm) $\bar{x}+2\sigma$	Heave (mm) Max.	Heave (mm) Min.	Pitch (deg) $\bar{x}$	Pitch (deg) $\bar{x}+2\sigma$	Pitch (deg) Max.	Pitch (deg) Min.
8-2	5.0	0.01	24.1	33.9	43.7	632	initial values not measured							
10-2	5.0	0.02	25.7	35.0	41.0	5.4	1.79	2.714	3.611	0.323	0.308	0.524	0.540	-0.013
9-4	5.0	0.04	30.3	36.9	41.1	18.8	1.986	2.802	2.852	0.88	0.283	0.531	0.535	-0.063
5-2	5.0	0.08	37.7	46.6	48.9	29.3	2.285	3.467	3.958	0.383	0.346	0.676	0.781	-0.063
11-2	5.0	0.12	46.8	50.9	56.0	36.0	2.37	3.636	4.316	0.445	0.393	0.749	0.857	-0.167
9-3	0.075	0.08	15.7	17.1	16.7	14.1	initial values not measured							
7-1	0.15	0.08	15-6	19.5	20.8	10.7	1.008	1.468	1.496	0.199	0.146	0.238	0.251	0.025
8-1	0.75	0.08	23.6	32.4	34.8	6.7	1.521	2.489	2.959	-0.121	0.222	0.532	0.594	-0.218

$\bar{x}$ = mean; $\bar{x}+2\sigma$ = 97.7% confidence limit

Max. = measured maximum, Min. = measured minimum

Table 6. Summary of fixed platform

Exp. No.	D (m)	V (m/s)	Hor. Force (N) $\bar{x}$	Hor. Force (N) $\bar{x}+2\sigma$	Hor. Force (N) Max.	Hor. Force (N) Min.	Vertical force (N) $\bar{x}$	Vertical force (N) $\bar{x}+2\sigma$	Vertical force (N) Max.	Vertical force (N) Min.	Pitch moment (N·m) $\bar{x}$	Pitch moment (N·m) $\bar{x}+2\sigma$	Pitch moment (N·m) Max.	Pitch moment (N·m) Min.
4-2	5.0	0.04	32.3	38.8	43.1	25.8	36.0	50.2	55.3	20.9	6.6	11.9	13.1	0.2
1-2	5.0	0.06	32.6	43.7	53.8	15.0	32.4	45.4	51.3	13.0	not measured			
1-3	5.0	0.08	33.1	49.5	66.1	15.9	30.9	45.3	46.6	13.4	initial zero not adjusted			
4-4	5.0	0.12	32.5	44.5	45.4	20.5	26.4	36.4	36.5	12.9	4.3	7.7	9.1	-0.5
4-1	0.075	0.08	13.3	16.9	16.5	9.5	13.3	20.1	19.5	4.1	2.2	2.7	2.9	1.5
2-1	0.15	0.08	16.7	21.9	25.4	11.7	21.2	29.2	31.9	11.2	2.6	4.3	4.6	0.2
3-1	0.75	0.08	31.1	38.6	42.9	22.8	25.9	39.2	49.2	10.4	3.2	7.7	8.9	-4.0

Table 7. Ratio of inertia force to mooring force (the mean force plus two times the standard deviation)

Exp. No.	Ice-Floe Dia. (m)	Ice Speed (m/s)	Inertia Force F_I (N)	Mooring Force F_M (N)	F_I/F_M
5-2	5	0.08	27.5	48.9	0.56
7-1	0.15	0.08	5.8	19.5	0.30
8-1	0.75	0.08	11.1	32.4	0.34
10-2	5	0.02	4.9	35.0	0.14

Table 8. Dominating Periods Corresponding Peaks in Spectrum

Exp. No.	Floe Dia. (m)	Ice Speed (m/s)	Dominating Peaks (s) Surge		Heave		Pitch	
5-2	5	0.08	1) 31.5	3) 4.1	1)10.2	3) 2.0	1) 1.7	3) 2.2
			2) 2.9	4) 2.5	2) 2.2	4) 3.0	2) 1.6	4) 2.0
7-1	0.15	0.08	1) 2.8	3)34.1	1)102	3)34.1	1) 1.9	3) 2.0
			2) 1.9	4) 4.6	2)11.4	4)20.5	2)102	4) 1.7
8-1	0.75	0.08	1) 34.1	3) 3.3	1)12.8	3)102	1) 1.8	3) 1.7
			2) 4.4	4) 2.2	2) 4.9	4) 3.1	2) 1.6	4) 1.6
10-2	5	0.02	1) 113	3) 7.4	1)128	3)22.3	1) 8.5	3) 7.3
			2) 7.0	4) 8.8	2)513	4) 7.3	2) 8.1	4) 5.7

Table 9. Comparison of ice force component of moored and fixed platforms

D_i	V_c	Type of force	mooring force / restraining force		
			surge	heave	pitch
5	0.04	mean	1.06	1.05	0.55
		mean+2σ	1.05	1.04	0.53
0.75	0.08	mean	1.32	0.98	0.34
		mean+2σ	1.19	0.91	0.34

APPENDIX 1: Time Histories of Measured Quantities

Note:

1) Ordinate is in voltage.

2) Calibration coefficient for ice-flow speed, V, is (0.417 Volts-0.0025) m/s

Table A-1. Calibration Coefficients

Exp. No.	F_x (N/Volt)	F_y (N/Volt)	M_z (N-m/Volt)	X_1 (mm/Volt)	X_2 (mm/Volt)	A_1, A_2, A_3 (m/s^2/Volt)
1-1 1-9	21.4	21.4	21.4	13.03	12.92	-
2-1 2-6	9.8	9.8	9.8	13.03	12.92	-
3-1 3-14	19-6	19.6	19.6	13.03	12.92	-
4-1 4-5	19.6	19.6	19.6	13.03	12.92	-
5-1 5-9	19.6	19.6	19.6	13.03	12.92	0.490
6-1	19.6	19.6	19.6	13.03	12.92	0.196
7-1 7-8	19.6	19.6	19.6	13.03	12.92	0.196
8-1 8-6	19.6	19.6	19.6	13.03	12.92	0.196
9-1 9-7	19.6	19.6	19.6	13.03	12.92	0.196
10-1 10-5	19.6	19.6	19.6	13.03	12.92	0.196
11-1 11-8	19.6	19.6	19.6	13.03	12.92	0.196

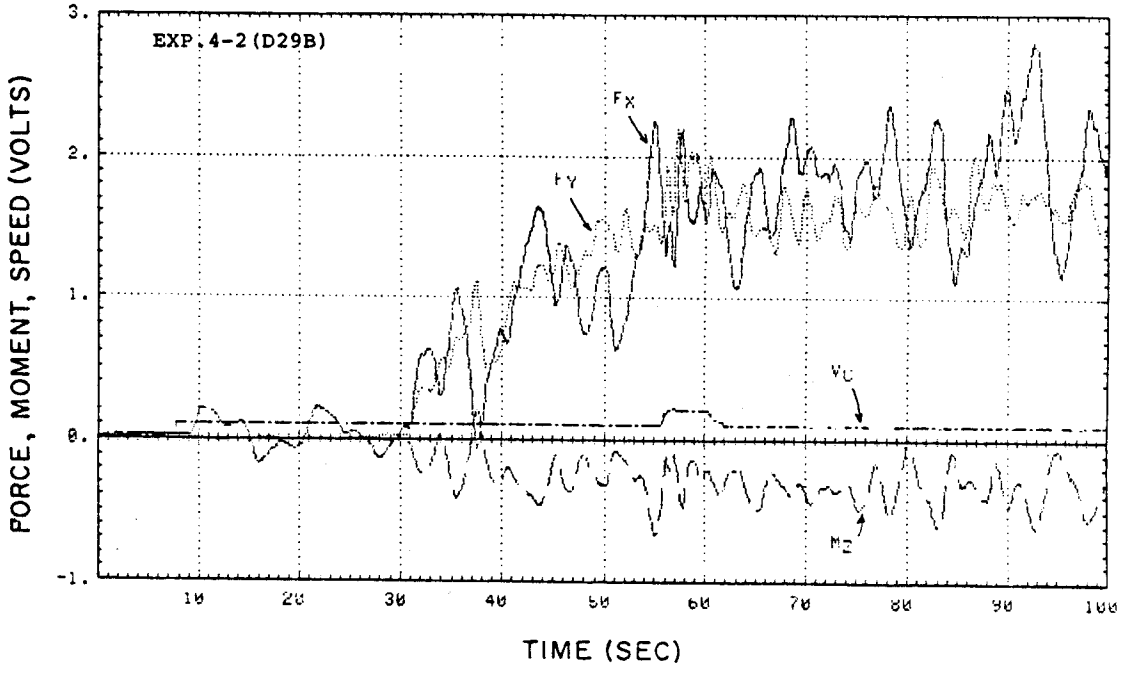
EXP.4-2(D29B)
FX
FY
VC
MZ
FORCE, MOMENT, SPEED (VOLTS)
TIME (SEC)
3.
2.
1.
0.
-1.
10
20
30
40
50
60
70
80
90
100

Fig. A-1

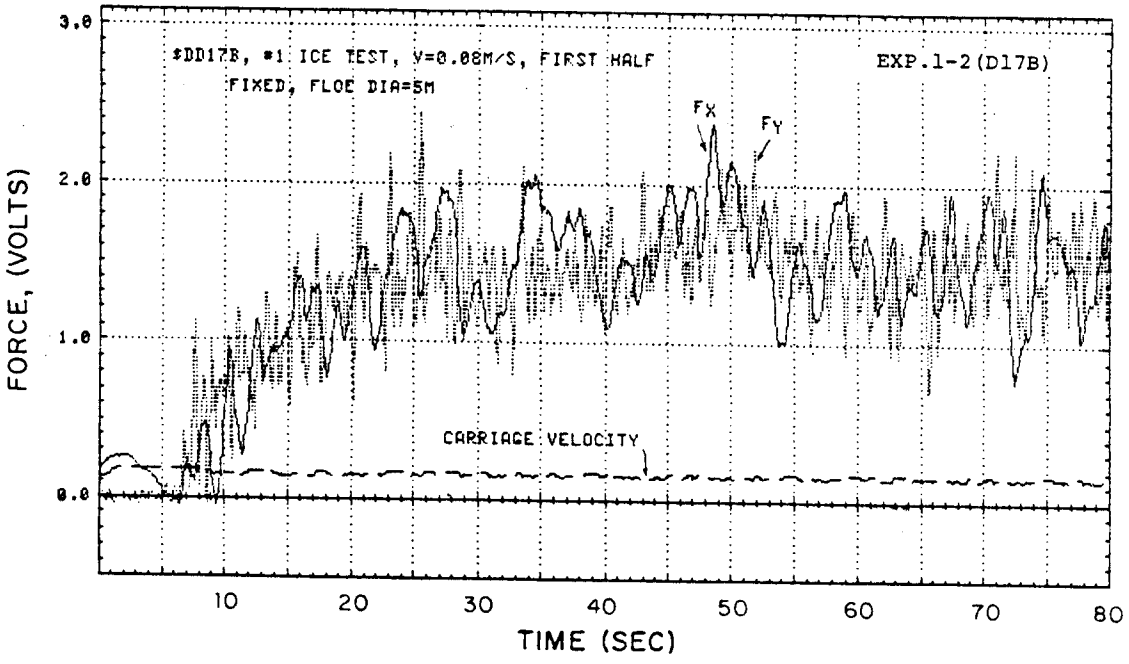
$DD17B, #1 ICE TEST, V=0.08M/S, FIRST HALF
FIXED, FLOE DIA=5M
EXP.1-2(D17B)
FX
FY
CARRIAGE VELOCITY
FORCE, (VOLTS)
TIME (SEC)
3.0
2.0
1.0
0.0
10
20
30
40
50
60
70
80

Fig. A-2

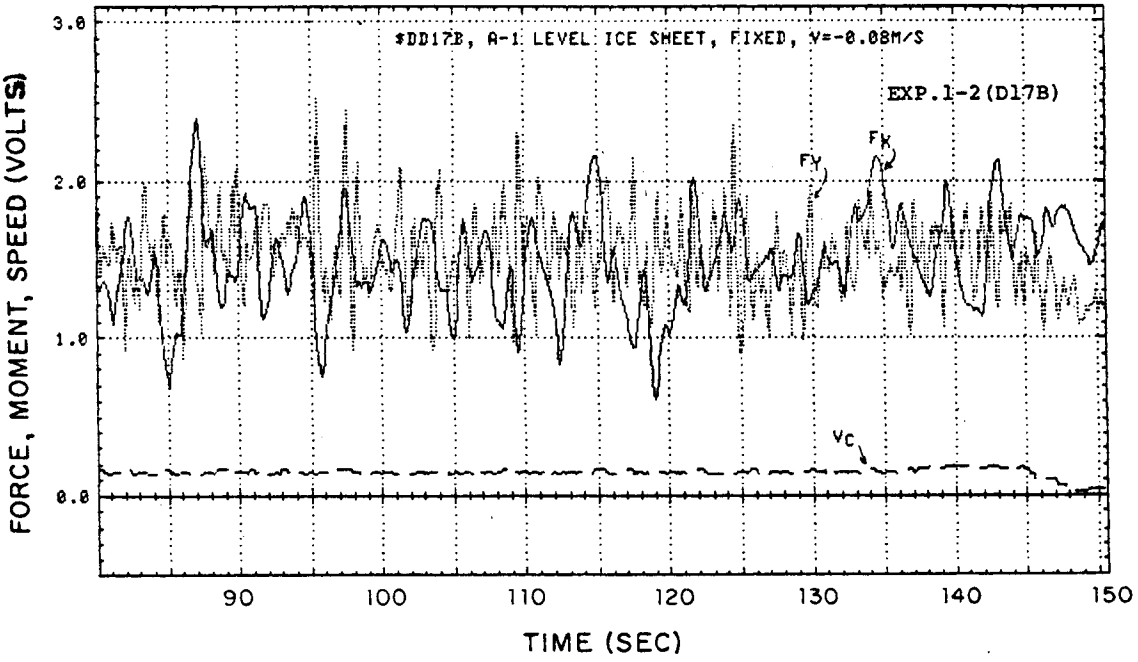
#DD17B, A-1 LEVEL ICE SHEET, FIXED, V=-0.08M/S
EXP.1-2(D17B)
FX
FY
VC
FORCE, MOMENT, SPEED (VOLTS)
3.0
2.0
1.0
0.0
90
100
110
120
130
140
150
TIME (SEC)

Fig. A-3

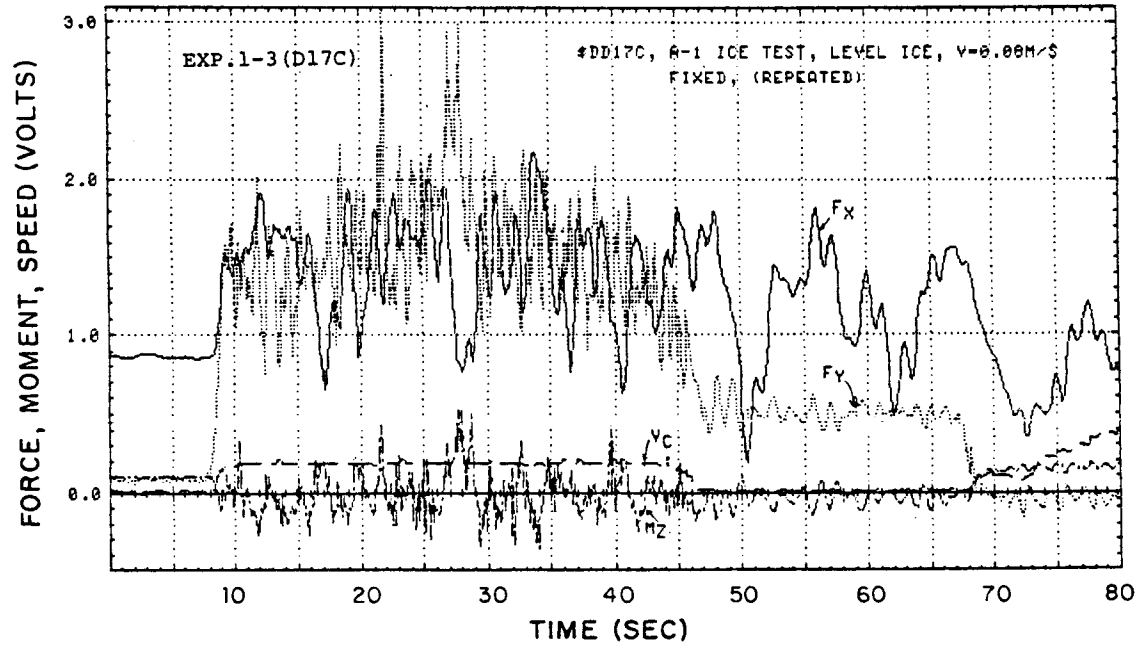
EXP.1-3(D17C)
#DD17C, A-1 ICE TEST, LEVEL ICE, V=0.08M/S
FIXED, (REPEATED)
FX
FY
VC
MZ
FORCE, MOMENT, SPEED (VOLTS)
3.0
2.0
1.0
0.0
10
20
30
40
50
60
70
80
TIME (SEC)

Fig. A-4

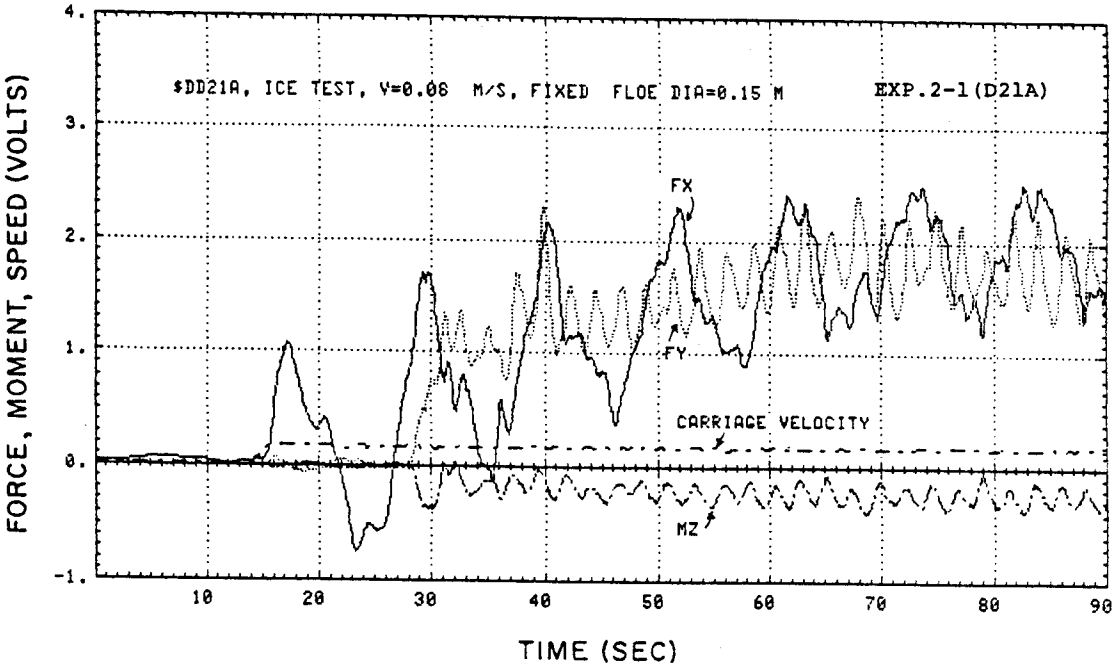
$DD21A, ICE TEST, V=0.08 M/S, FIXED FLOE DIA=0.15 M
EXP.2-1(D21A)
FX
FY
CARRIAGE VELOCITY
MZ
FORCE, MOMENT, SPEED (VOLTS)
TIME (SEC)

Fig. A-5

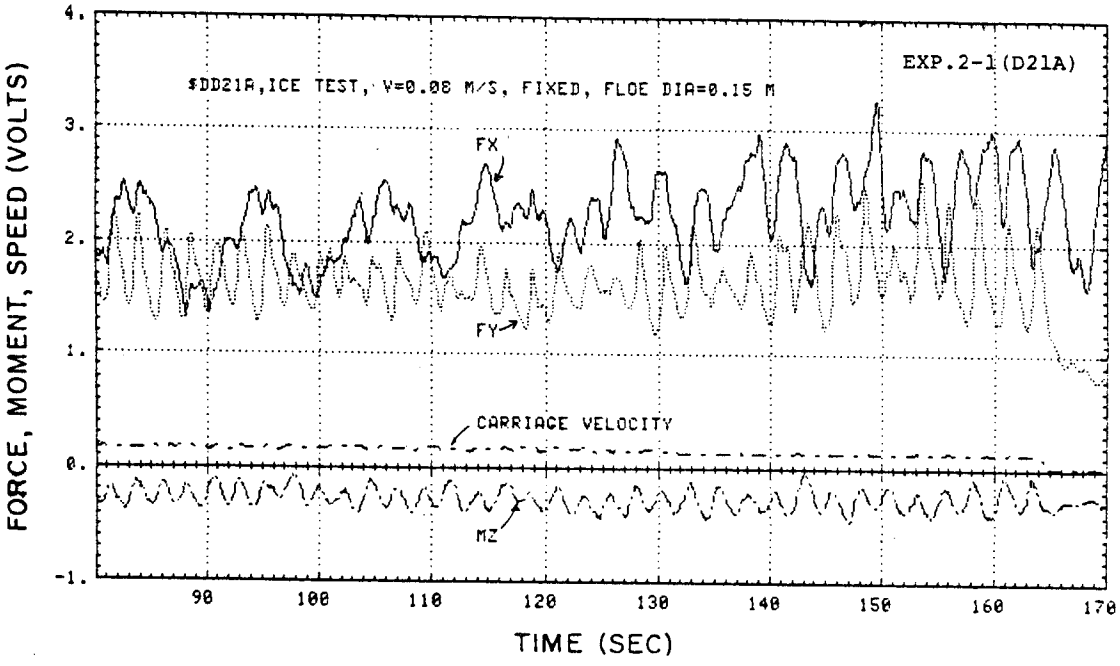
$DD21A,ICE TEST, V=0.08 M/S, FIXED, FLOE DIA=0.15 M
EXP.2-1(D21A)
FX
FY
CARRIAGE VELOCITY
MZ
FORCE, MOMENT, SPEED (VOLTS)
TIME (SEC)

Fig. A-6

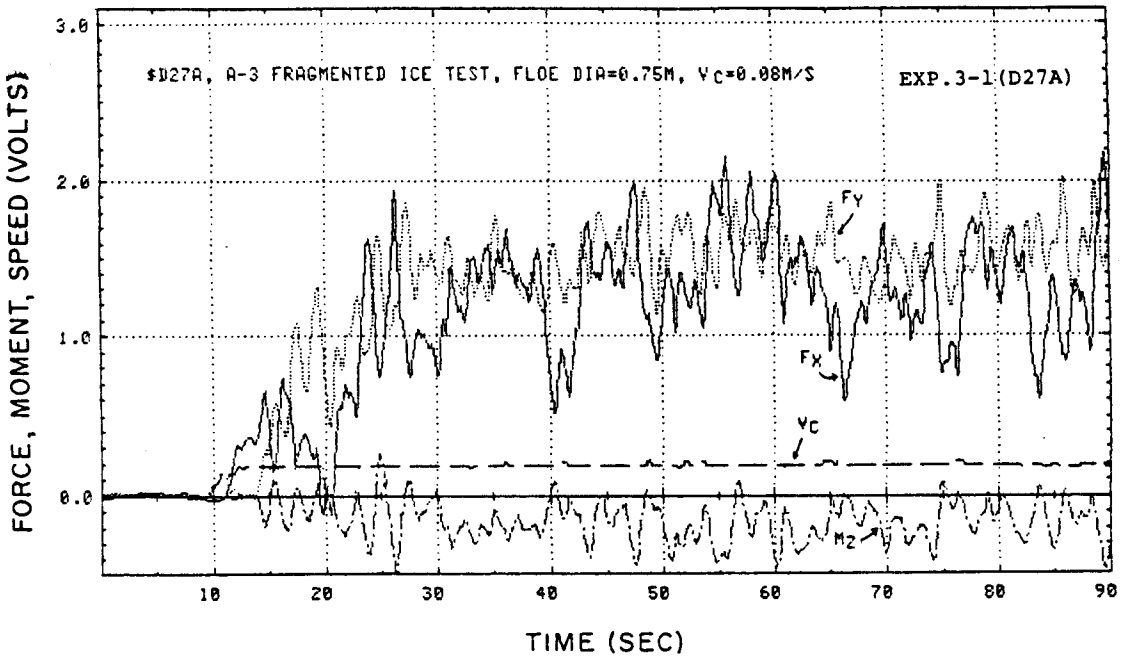
$D27A, A-3 FRAGMENTED ICE TEST, FLOE DIA=0.75M, Vc=0.08M/S
EXP.3-1(D27A)
FORCE, MOMENT, SPEED (VOLTS)
TIME (SEC)
Fy
Fx
Vc
Mz
3.0
2.0
1.0
0.0
10
20
30
40
50
60
70
80
90

Fig. A-7

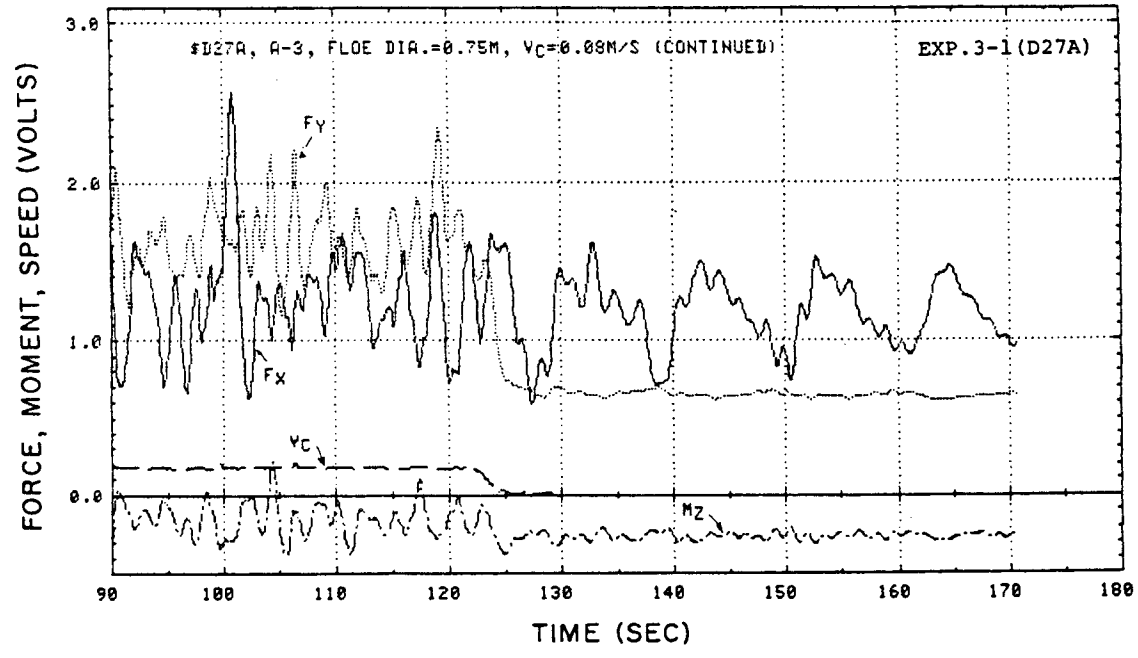
$D27A, A-3, FLOE DIA.=0.75M, Vc=0.08M/S (CONTINUED)
EXP.3-1(D27A)
FORCE, MOMENT, SPEED (VOLTS)
TIME (SEC)
Fy
Fx
Vc
Mz
3.0
2.0
1.0
0.0
90
100
110
120
130
140
150
160
170
180

Fig. A-8

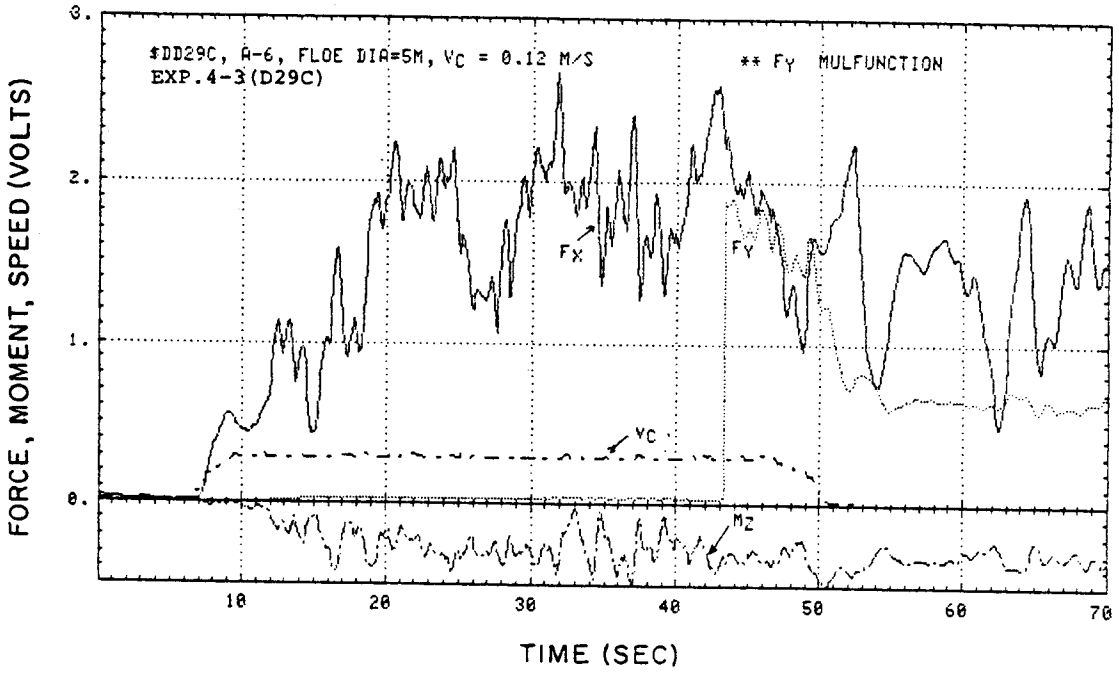

Fig. A-9

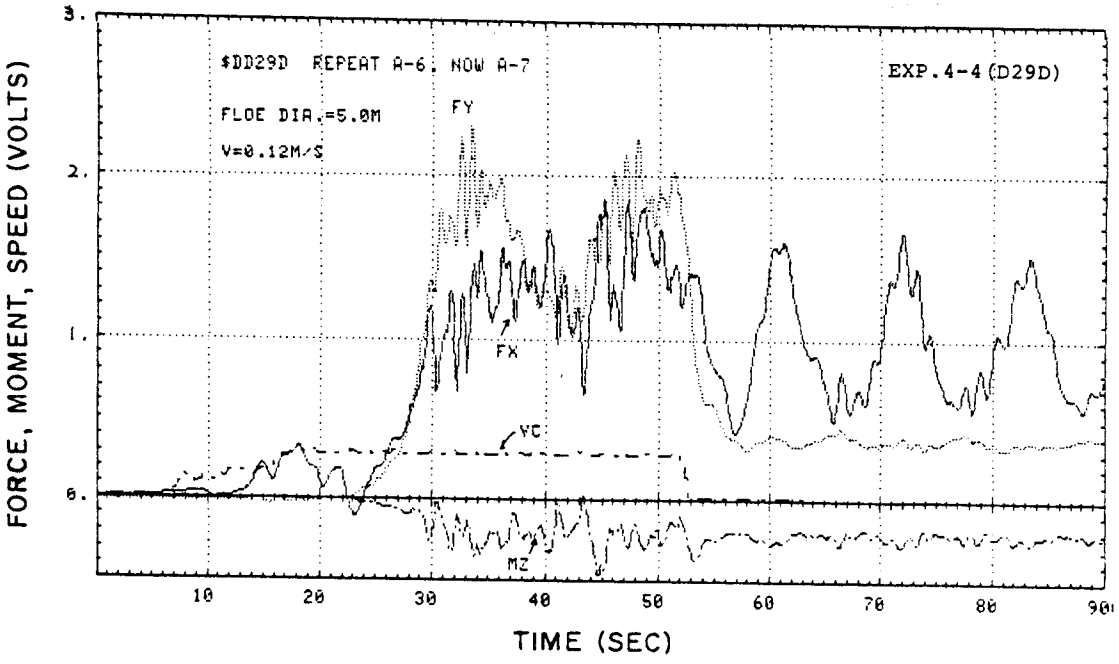

Fig. A-10

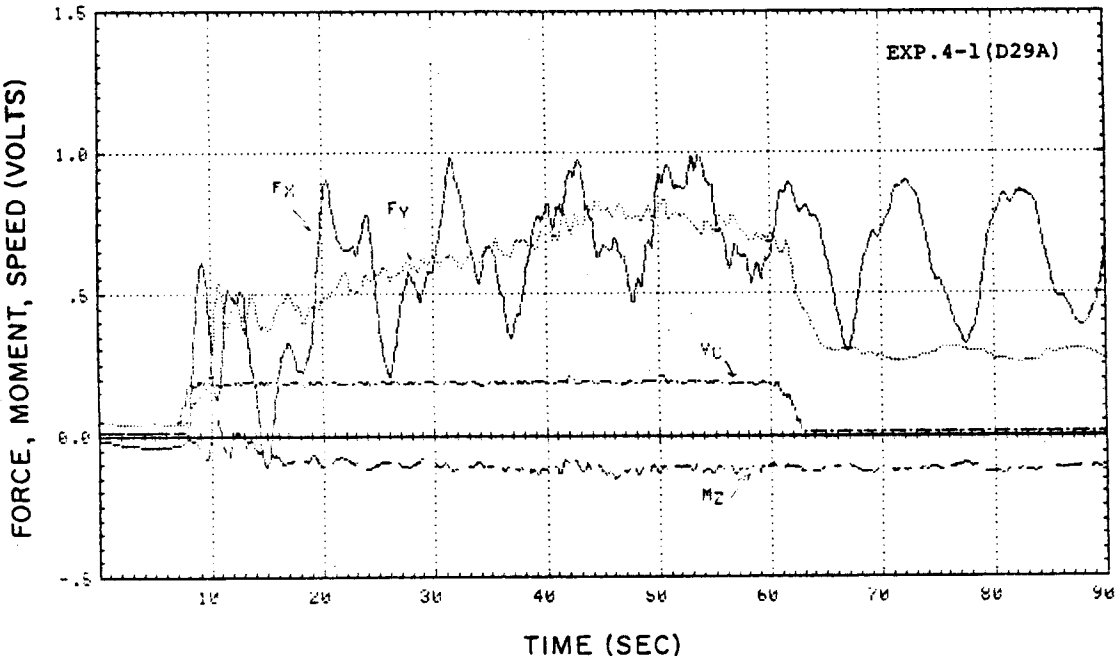

Fig. A-11

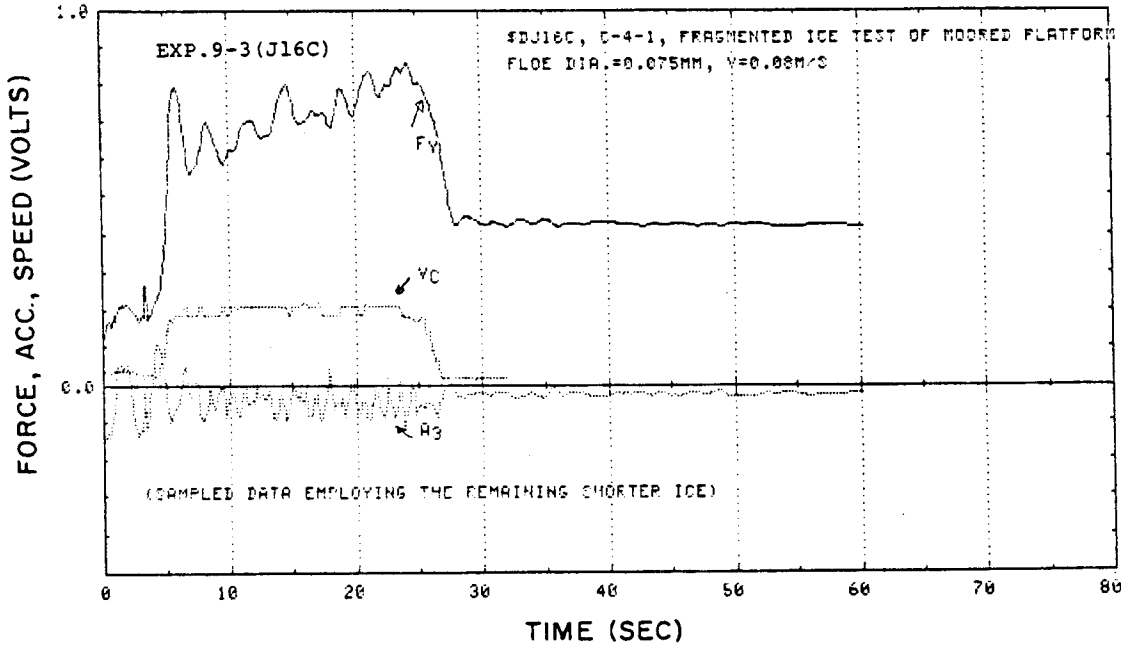

Fig. A-12

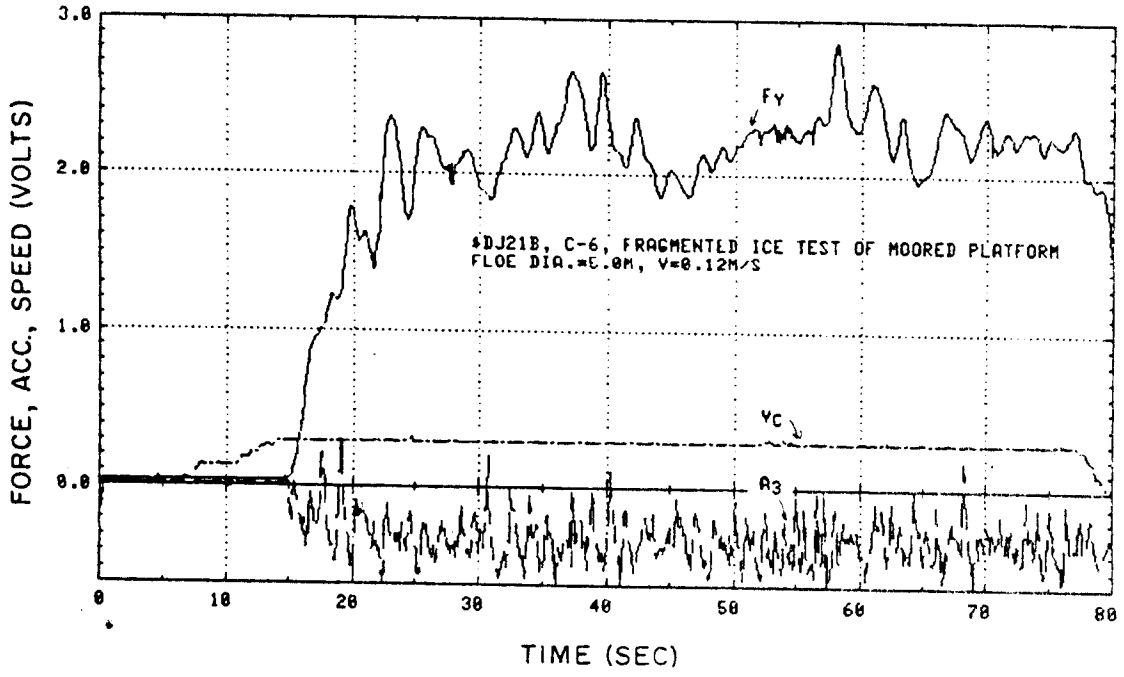

Fig. A-13

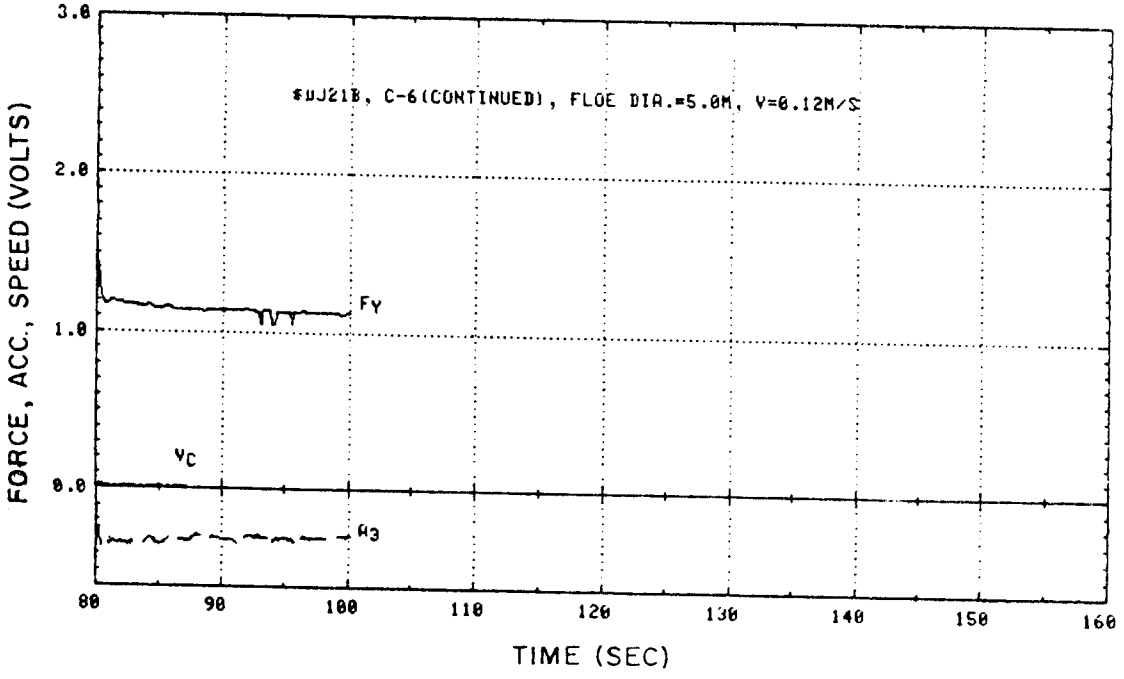

Fig. A-14

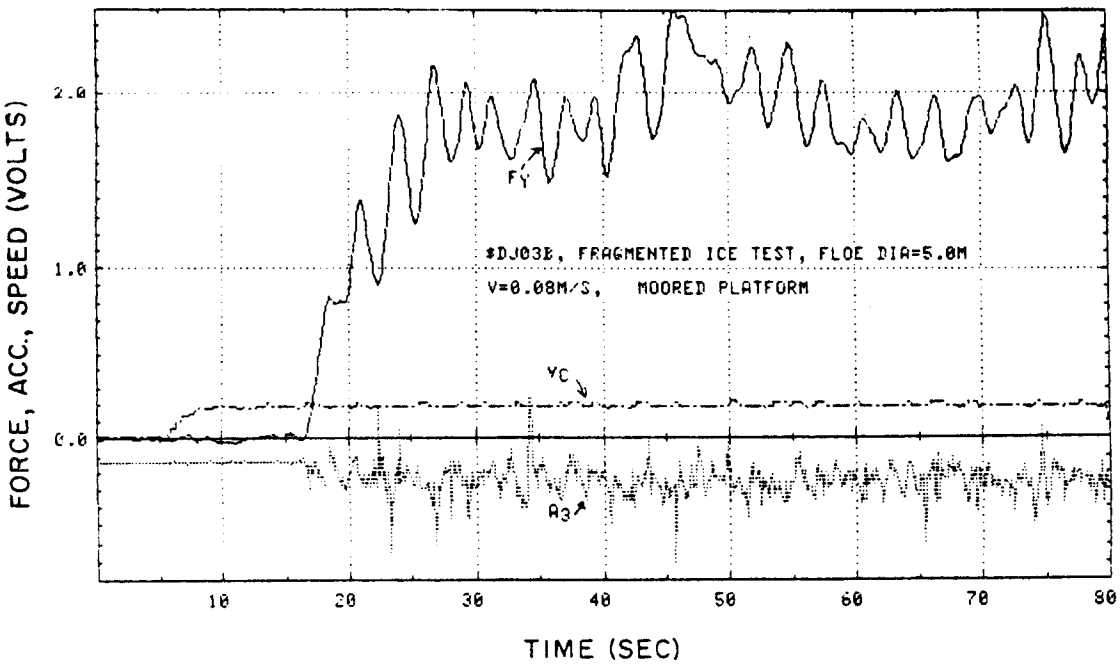

Fig. A-15

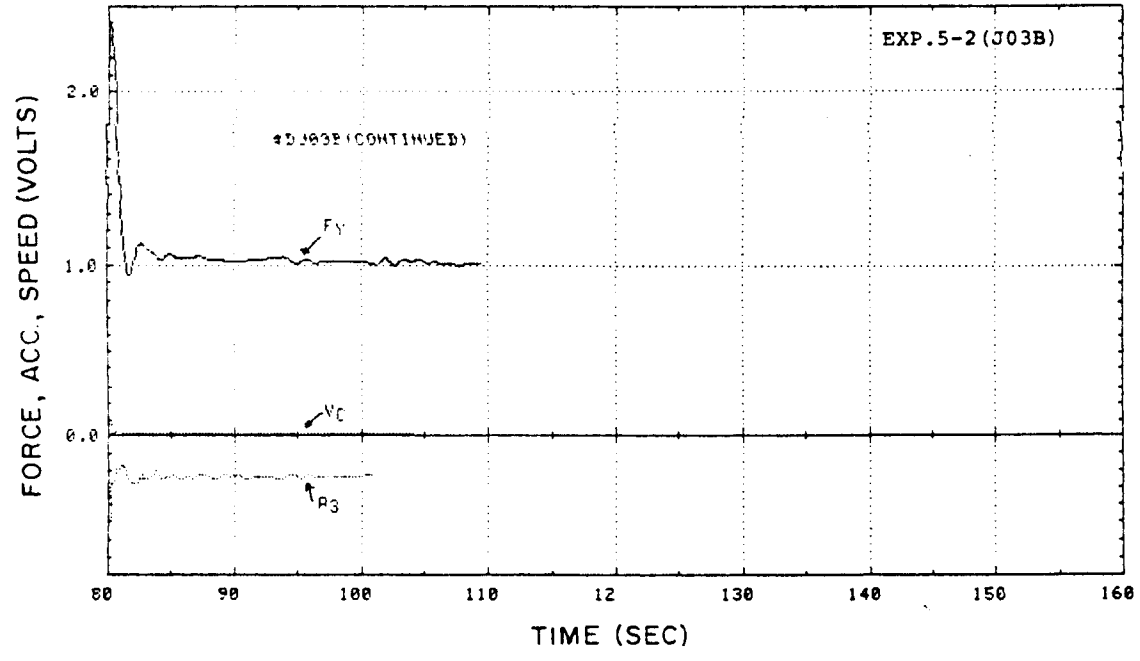

Fig. A-16

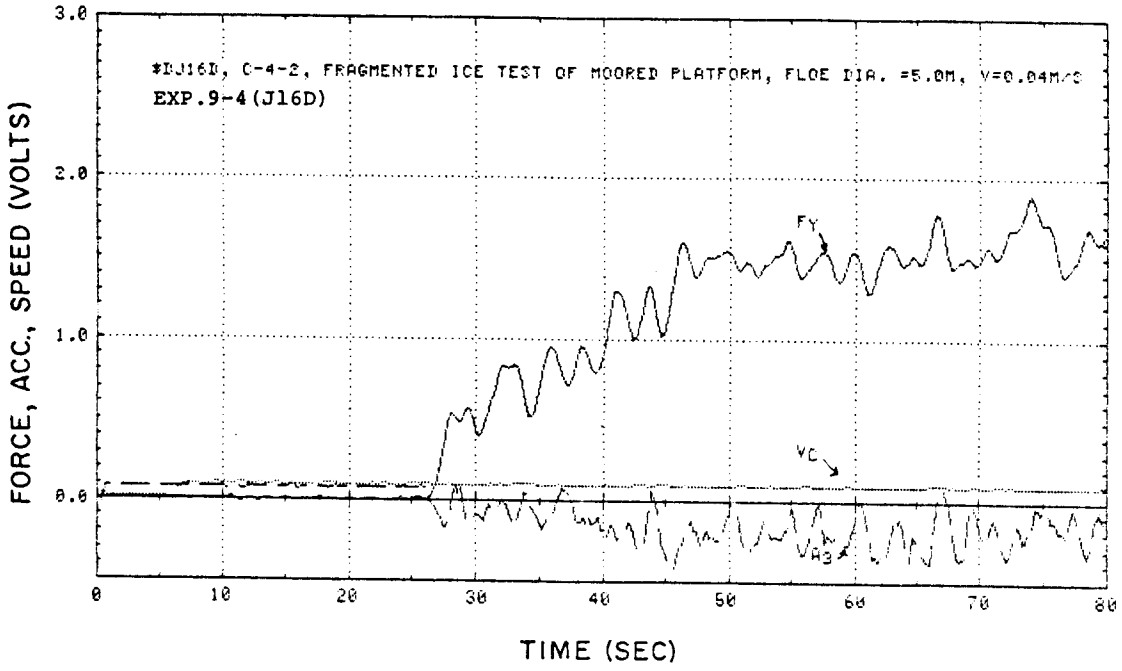

Fig. A-17

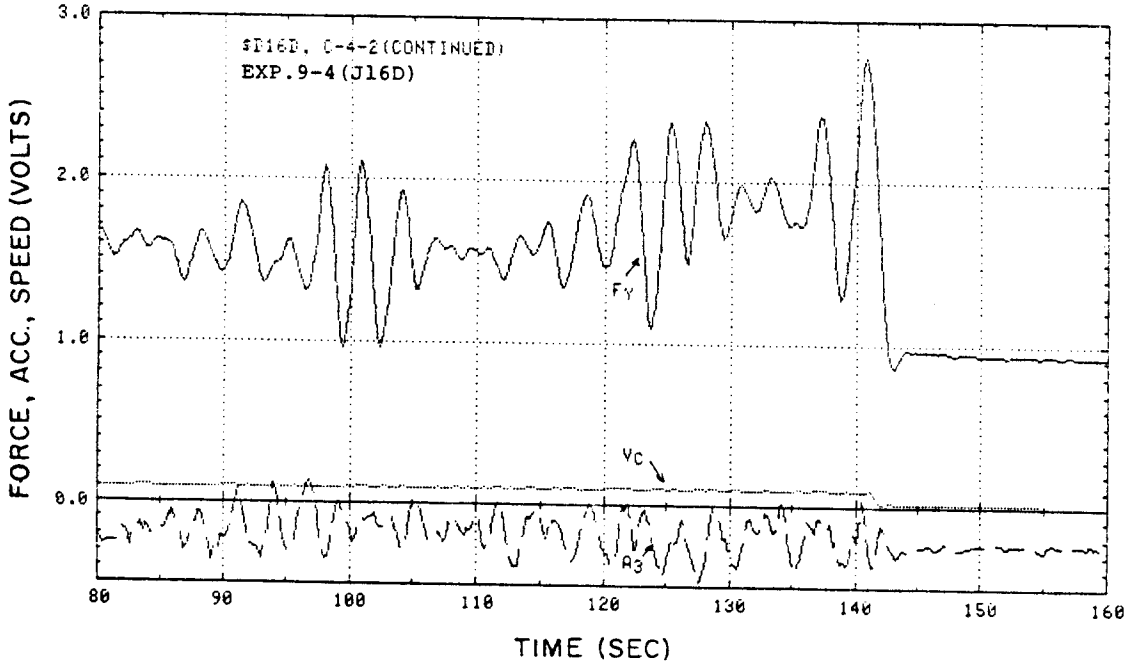

Fig. A-18

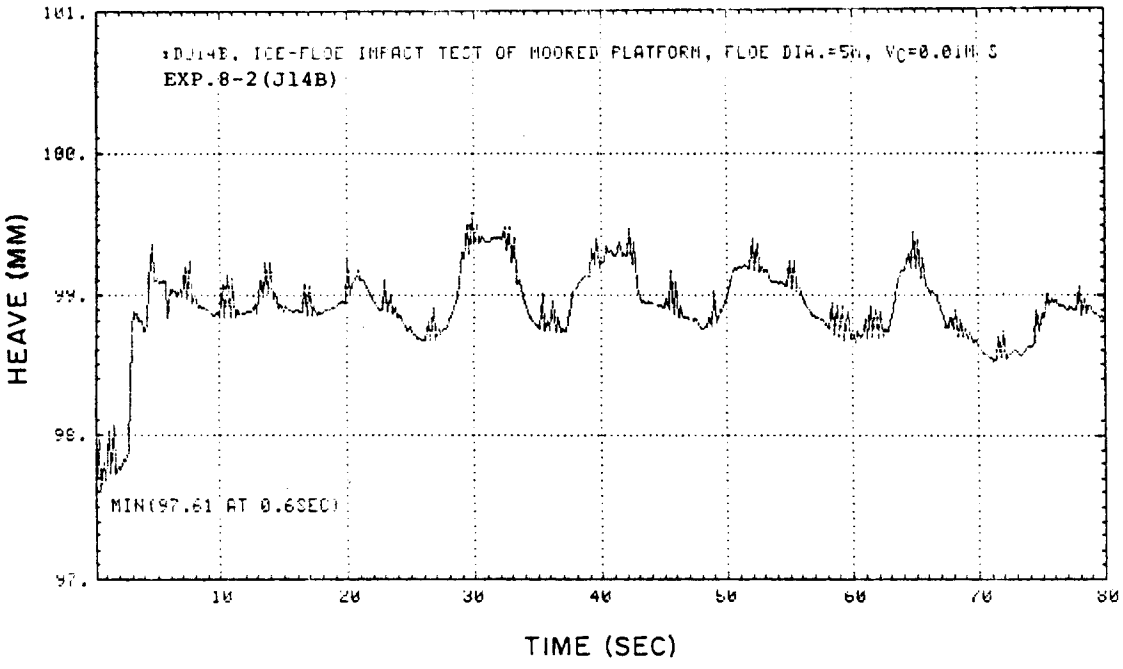

Fig. A-19

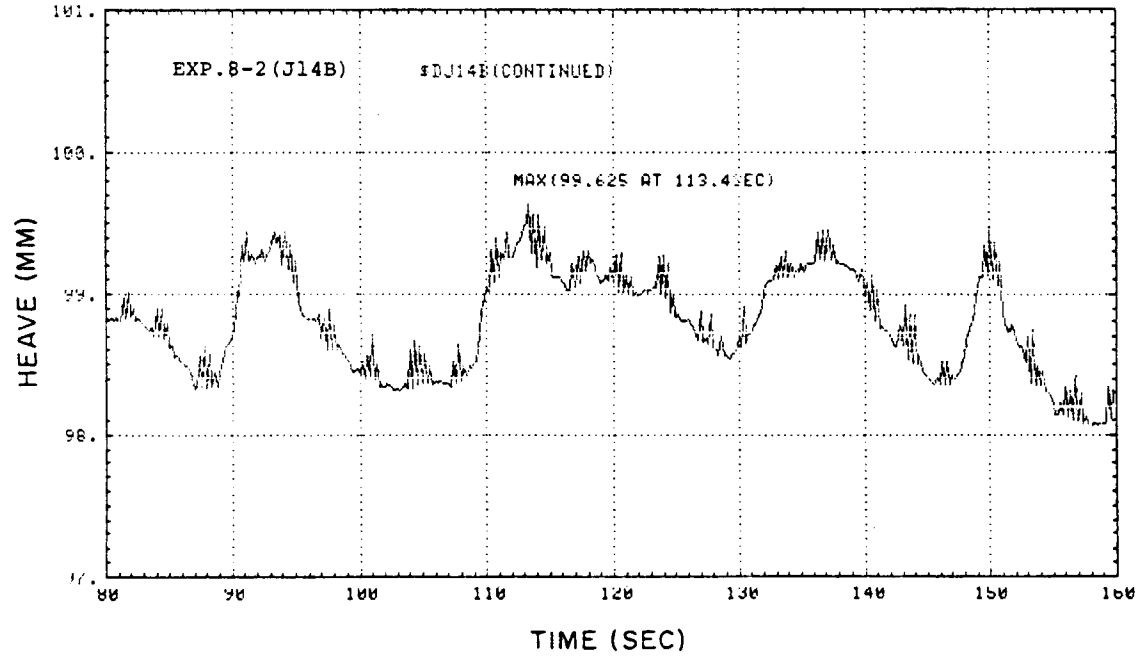

Fig. A-20

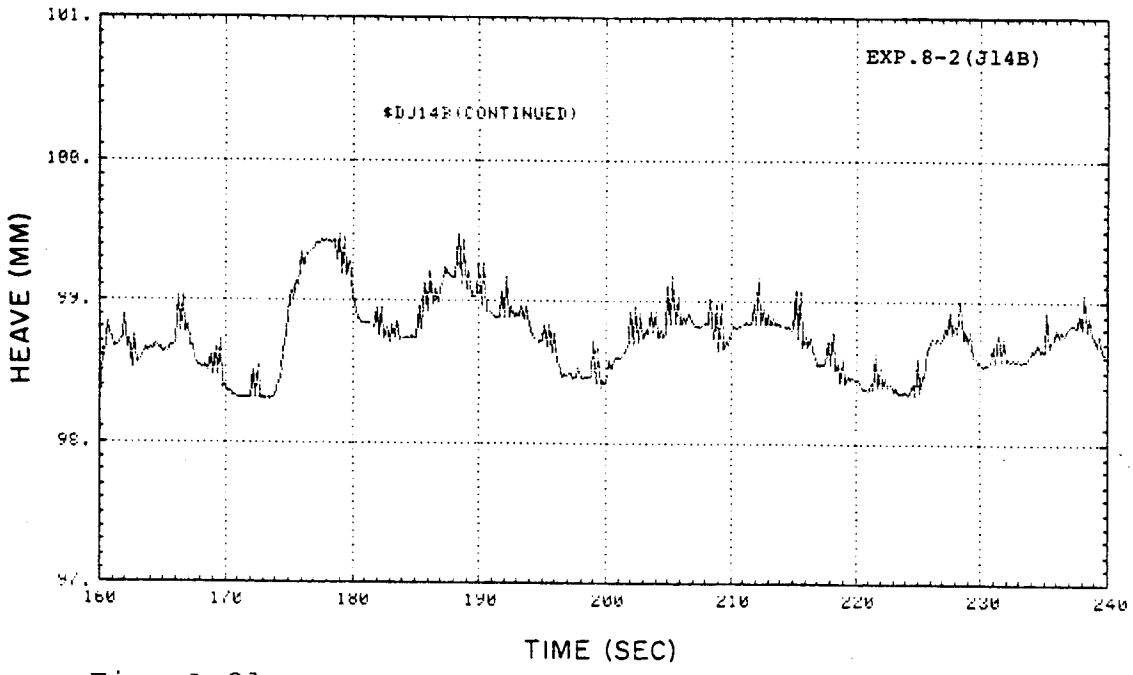

Fig. A-21

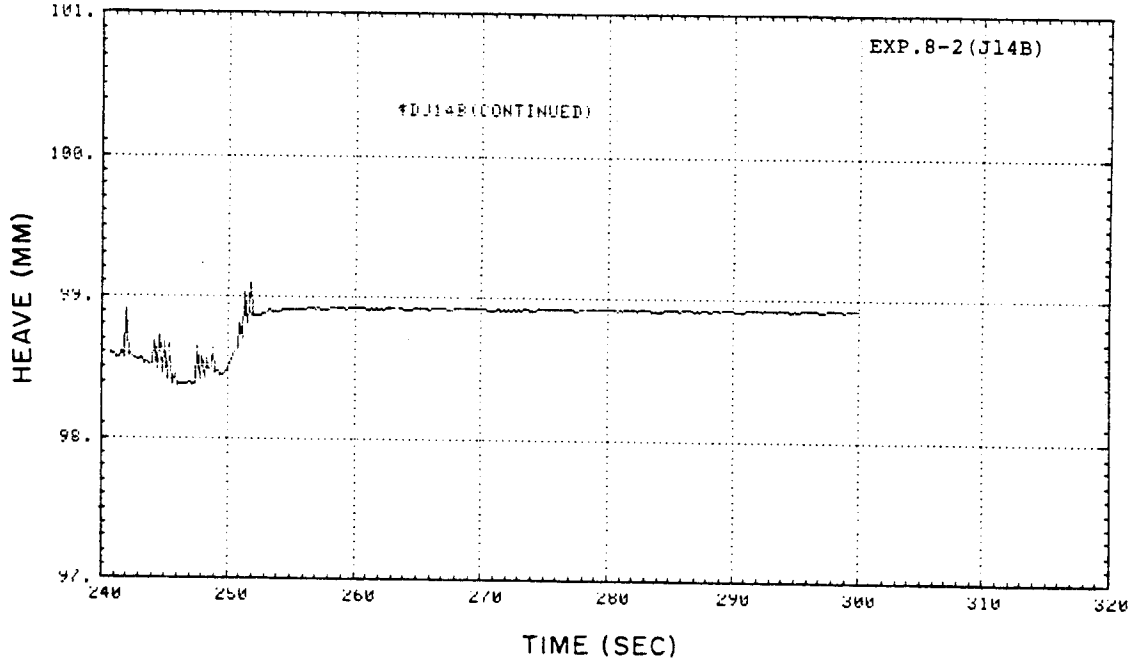

Fig. A-22

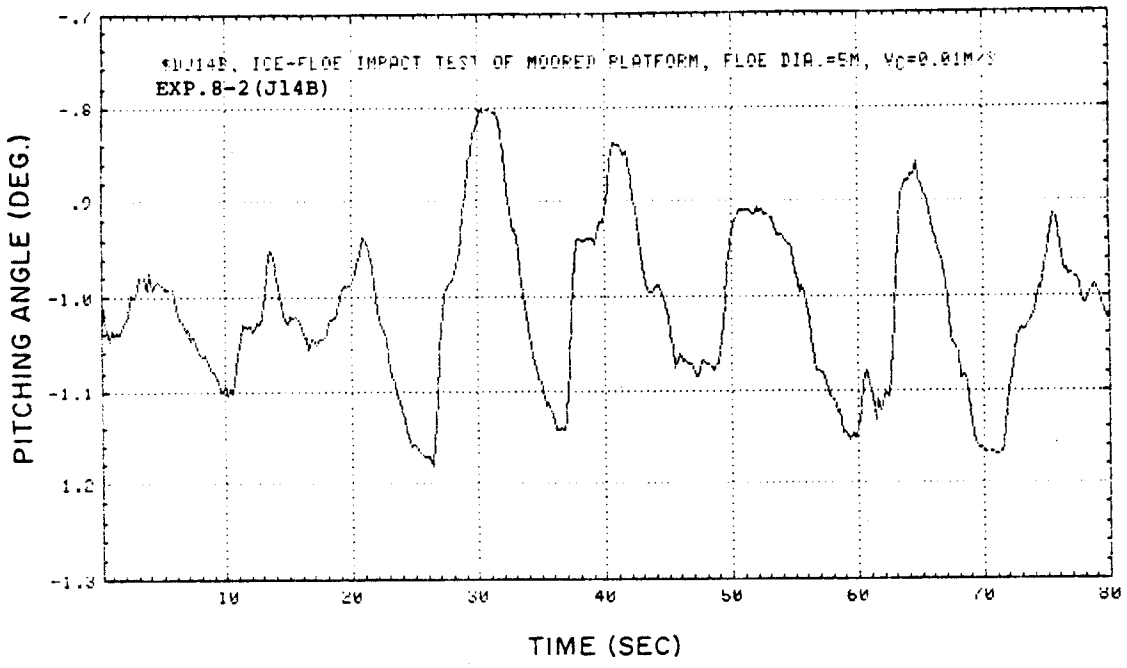

Fig. A-23

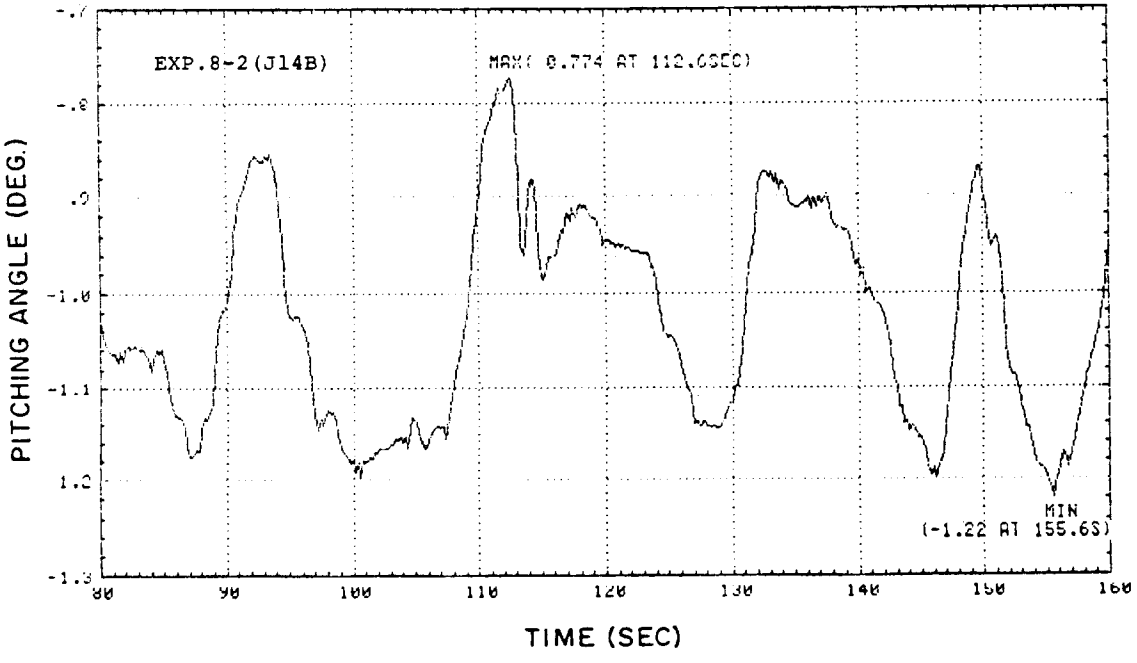

Fig. A-24

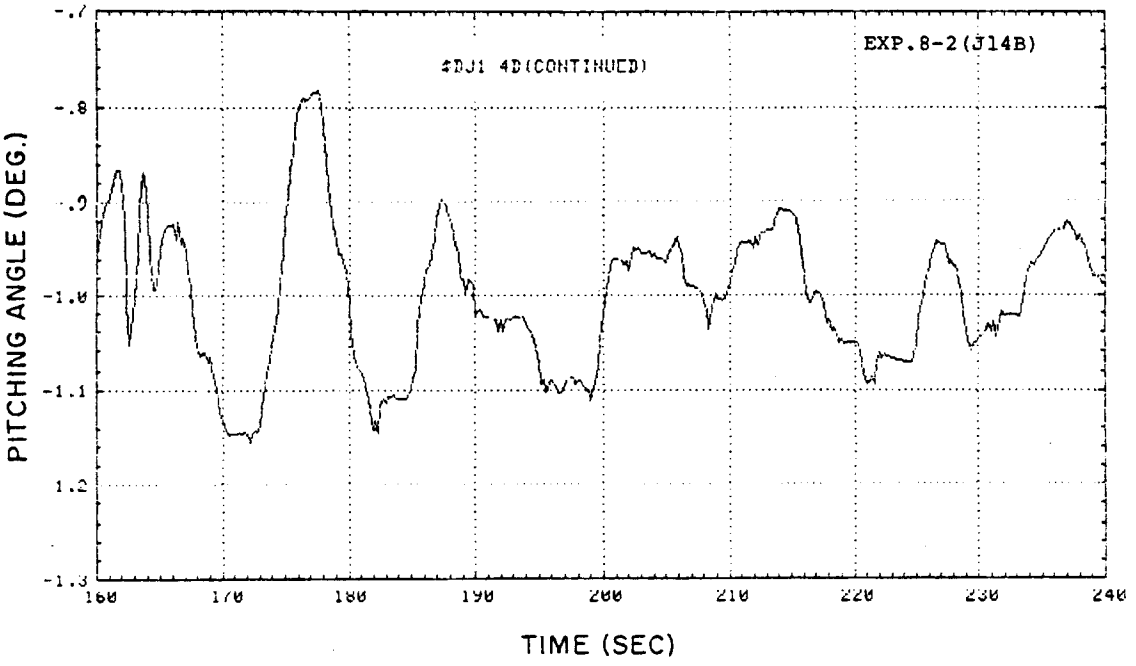

Fig. A-25

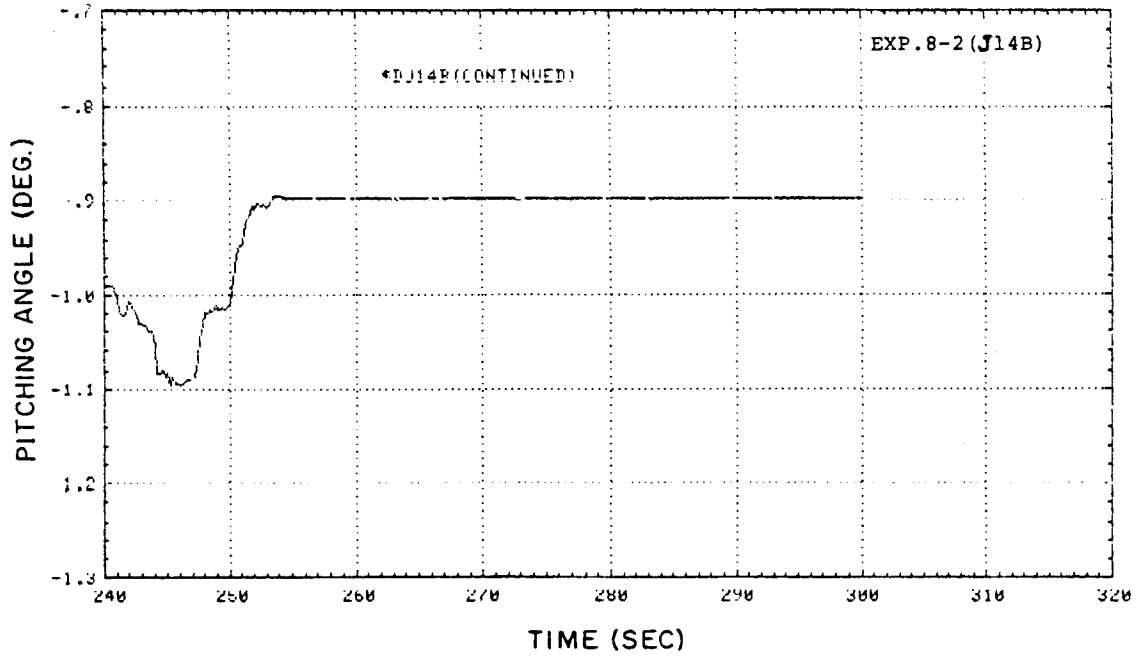

Fig. A-26

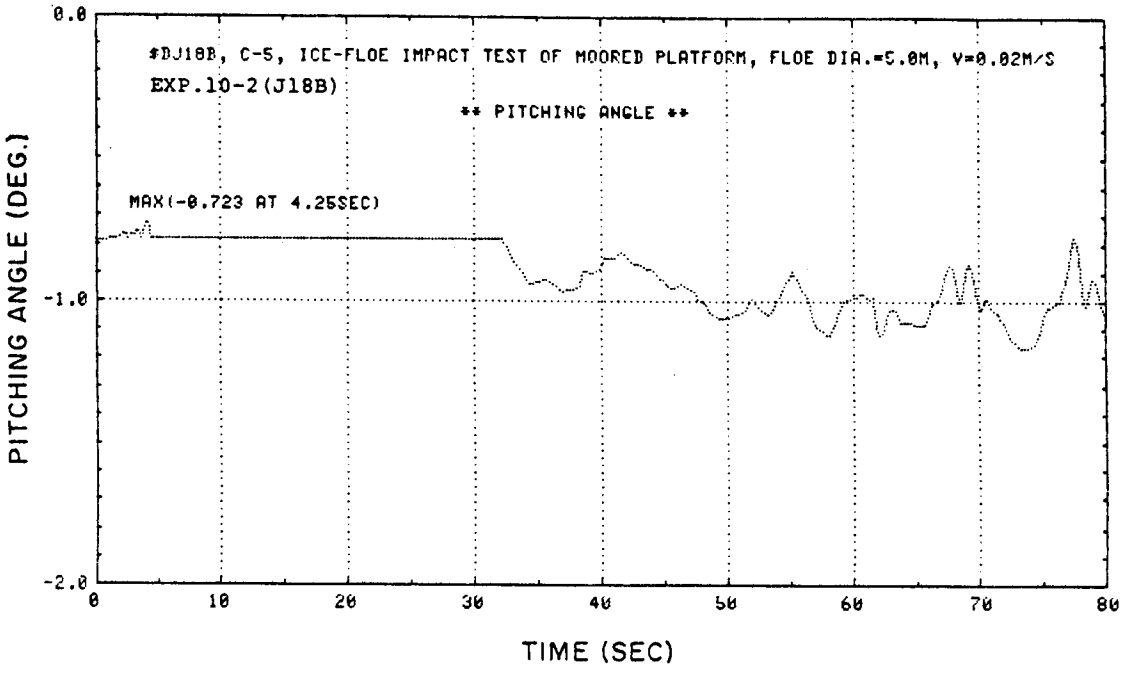

Fig. A-27

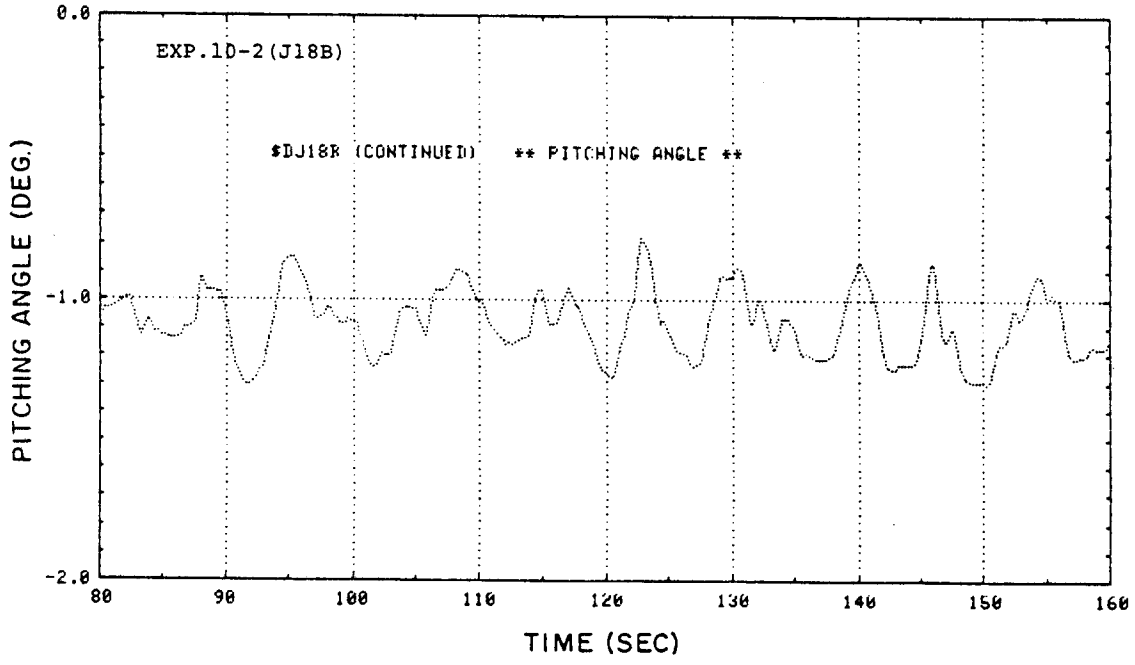

Fig. A-28

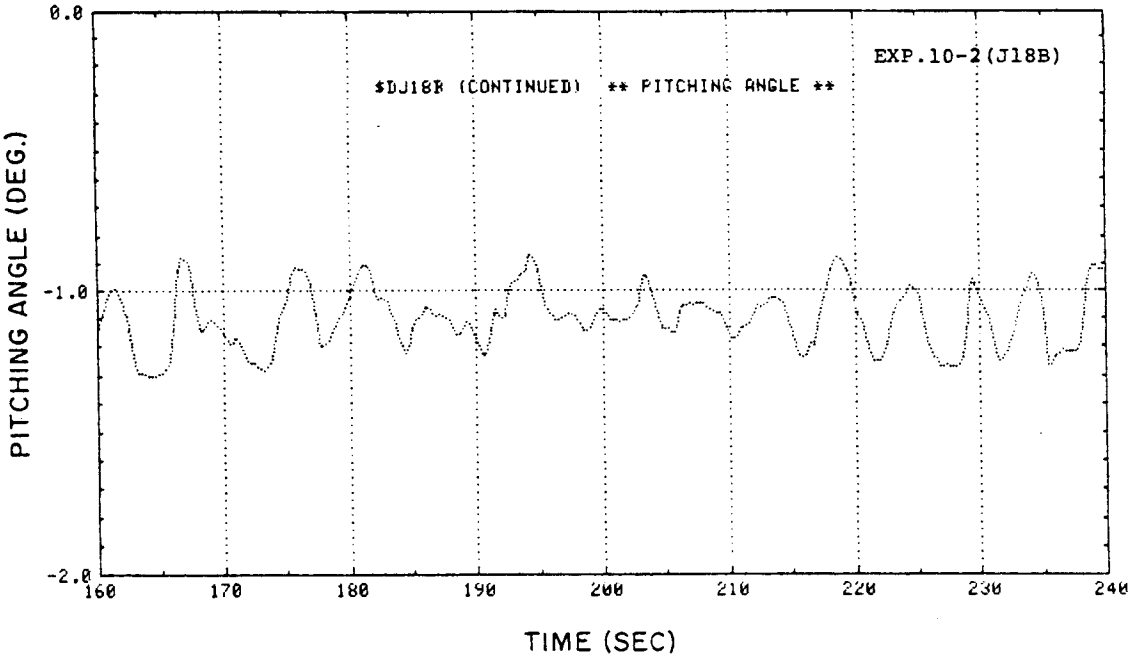

Fig. A-29

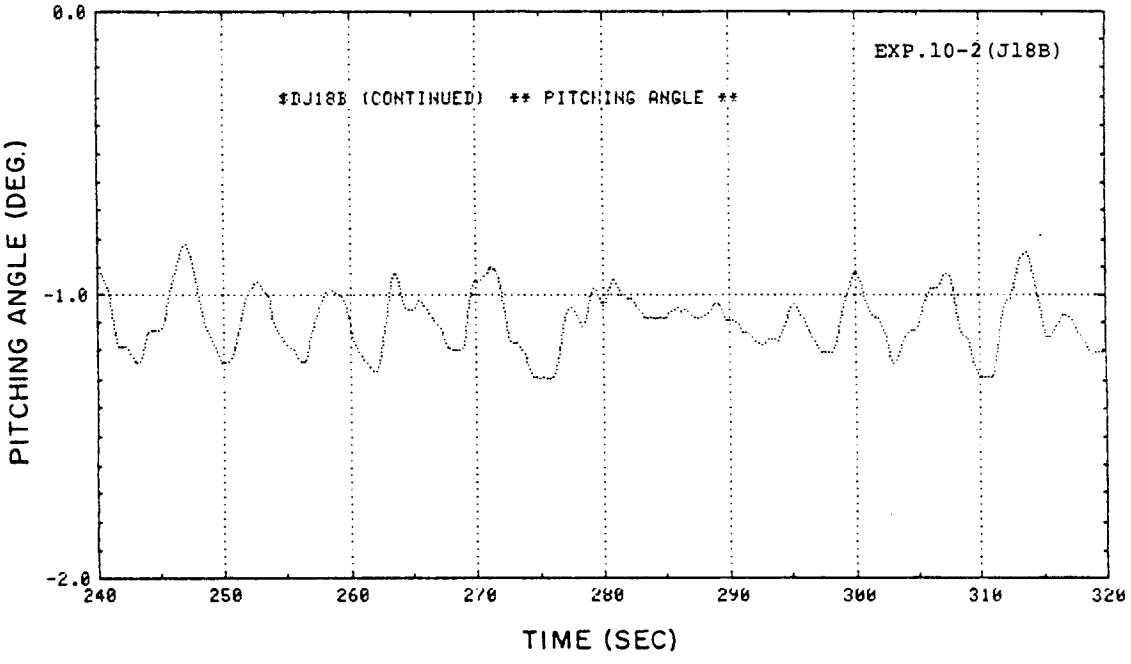

Fig. A-30

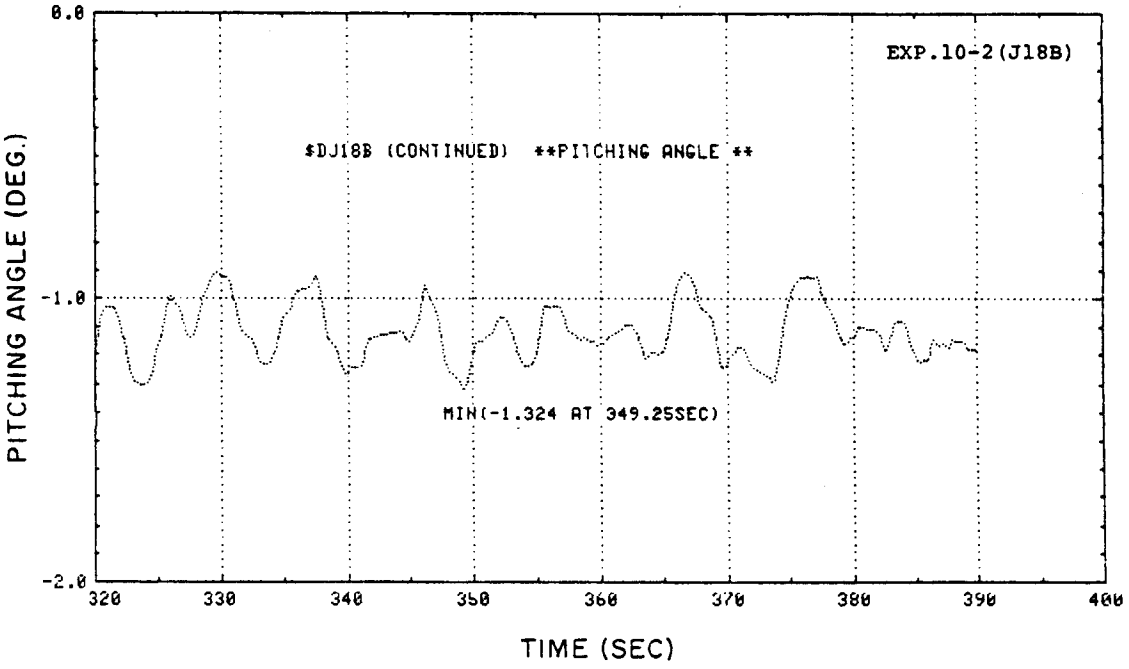

Fig. A-31

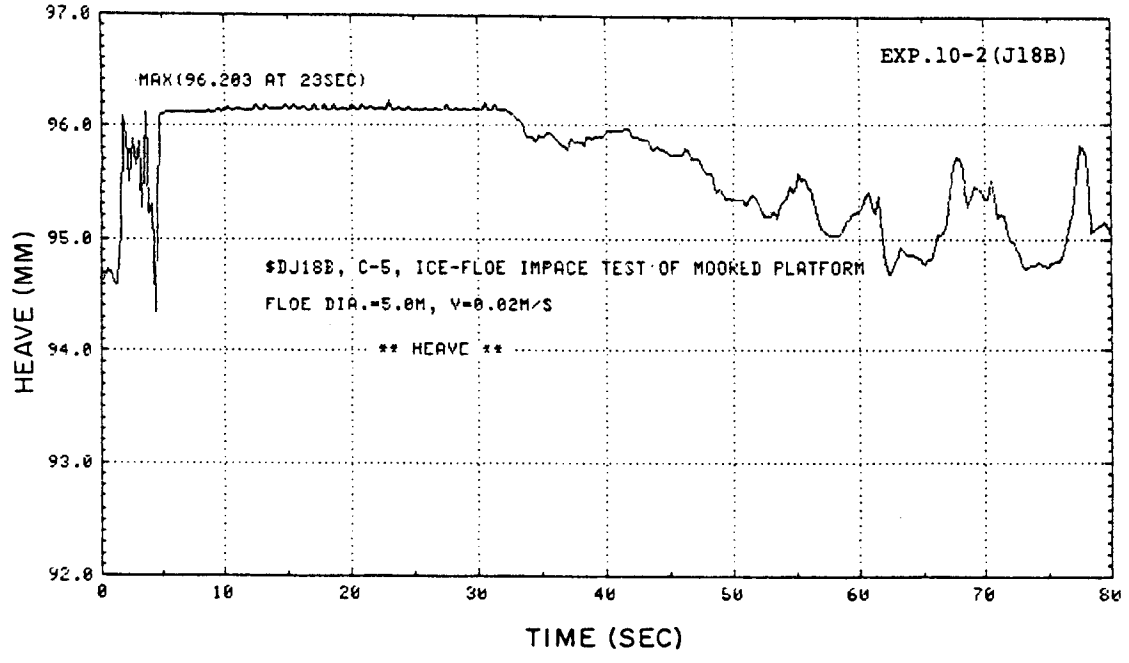

Fig. A-32

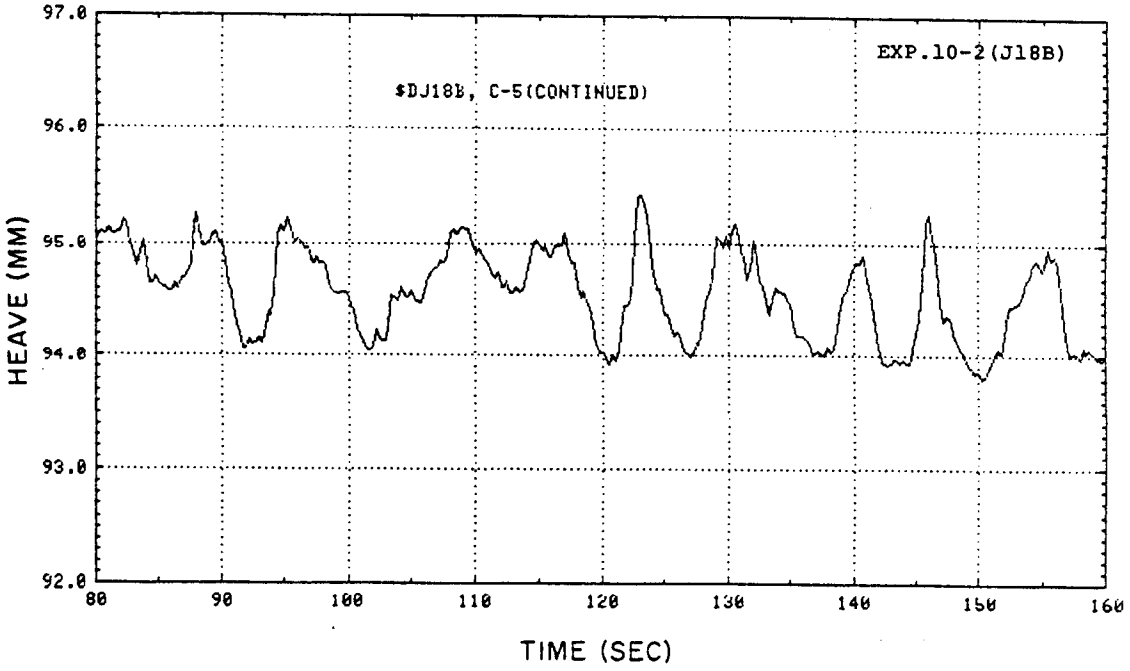

Fig. A-33

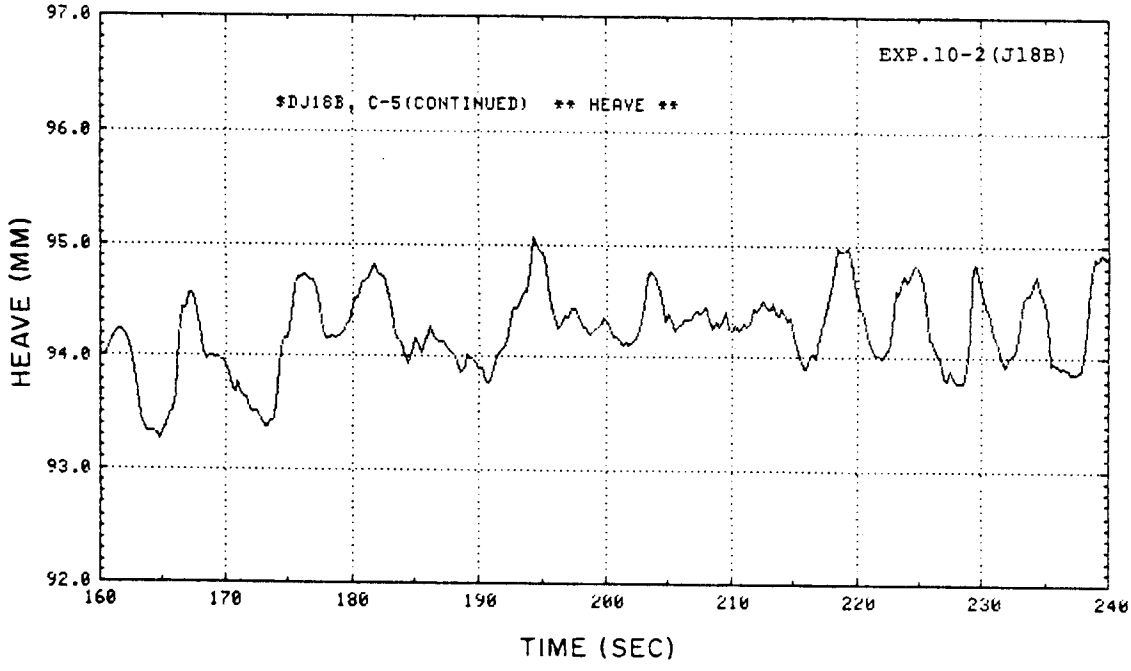

Fig. A-34

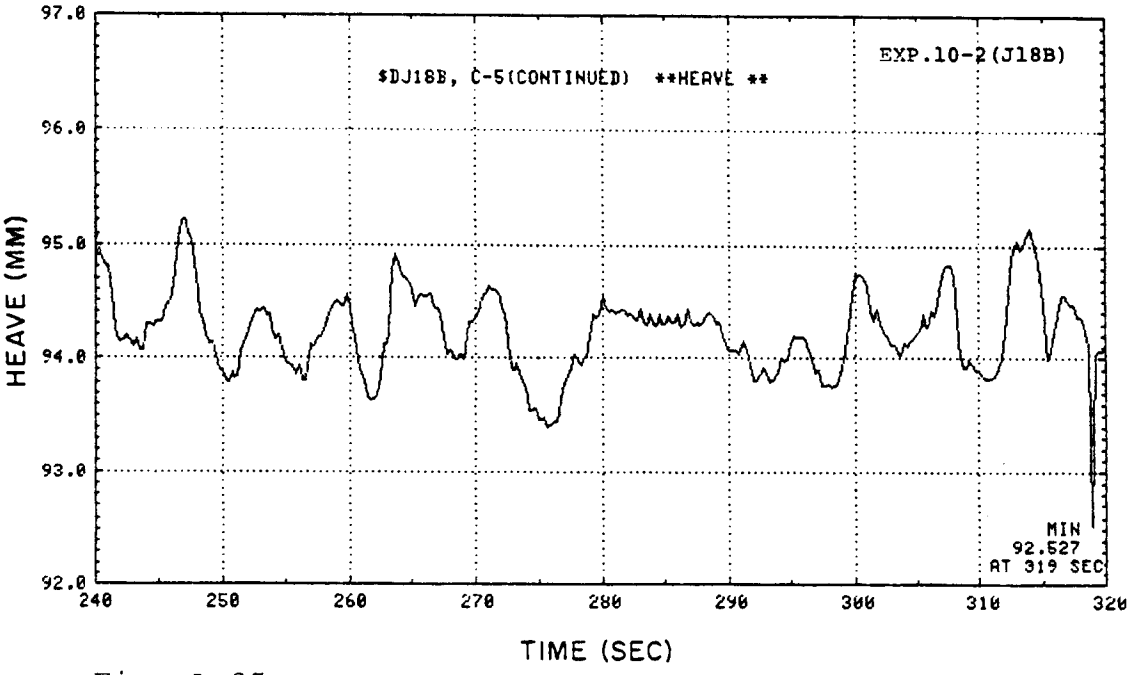

Fig. A-35

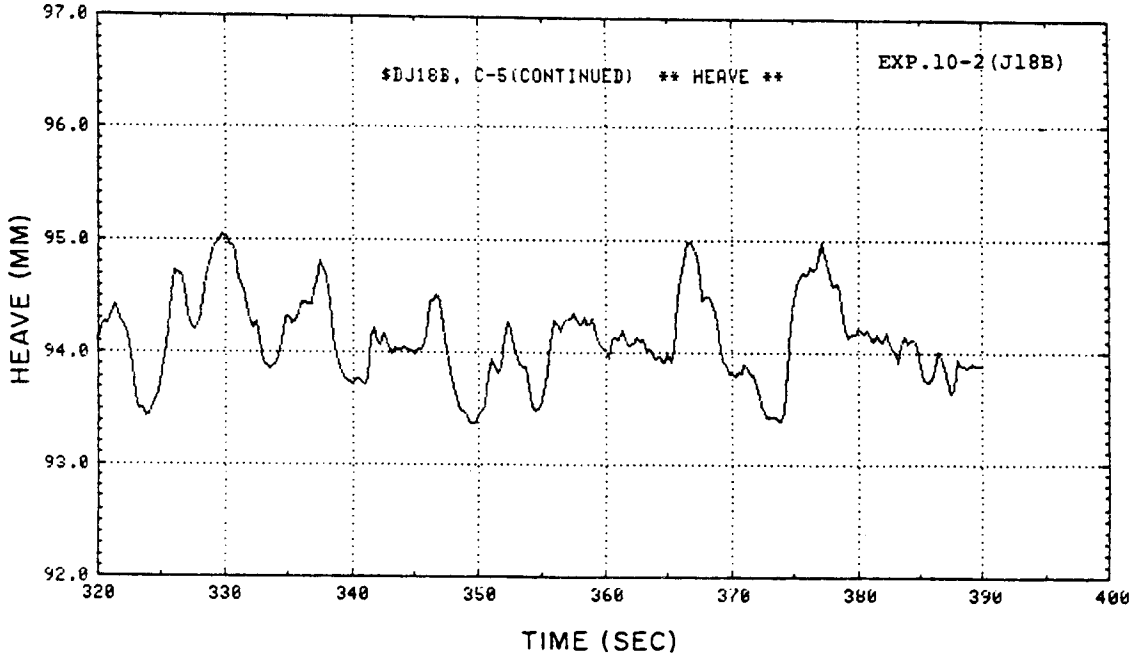

Fig. A-36

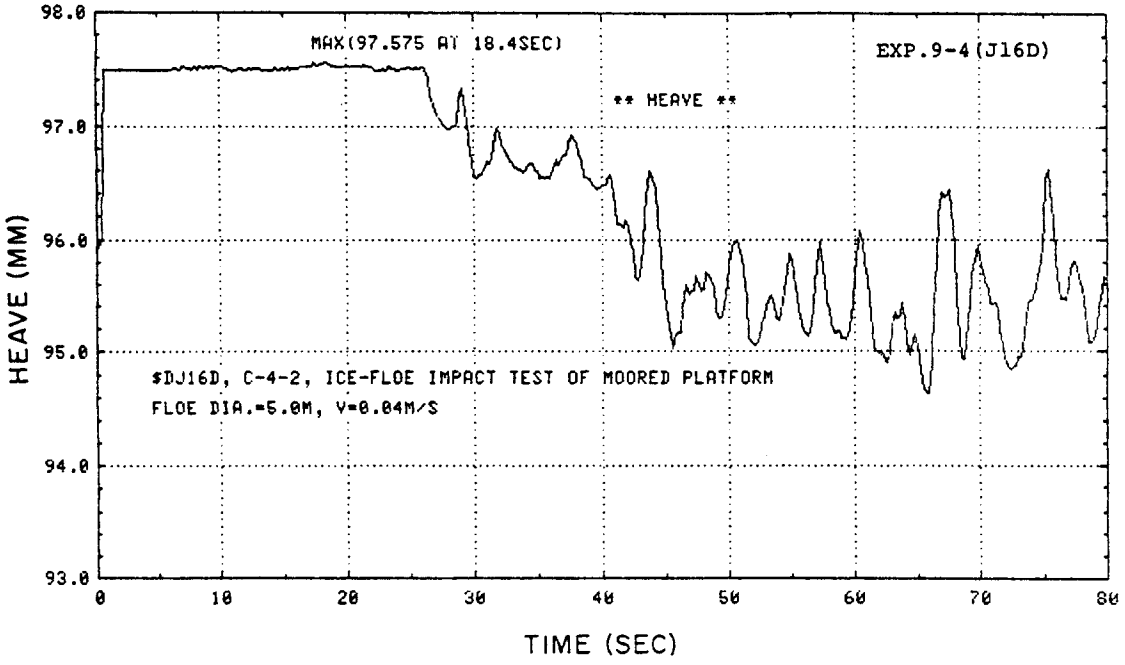

Fig. A-37

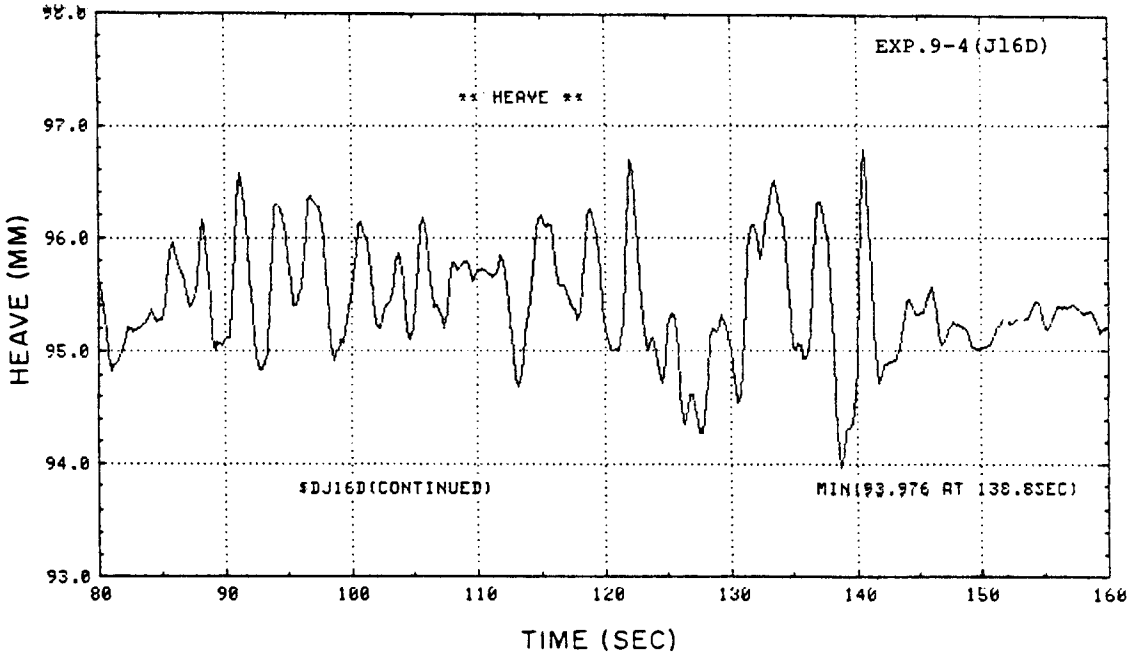

Fig. A-38

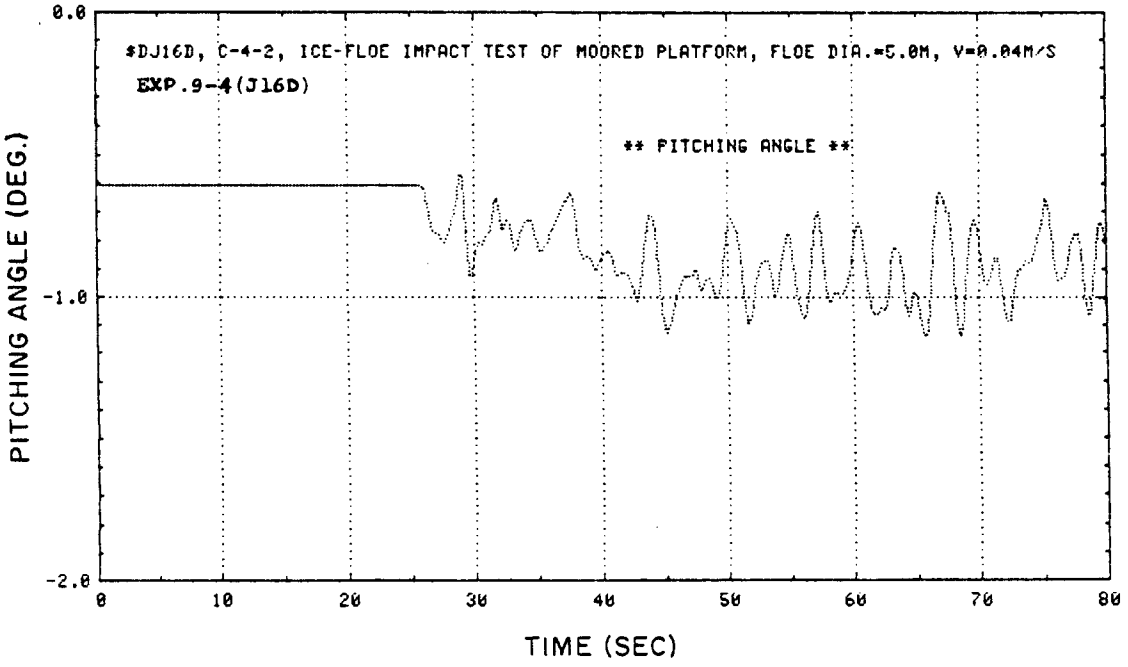

Fig. A-39

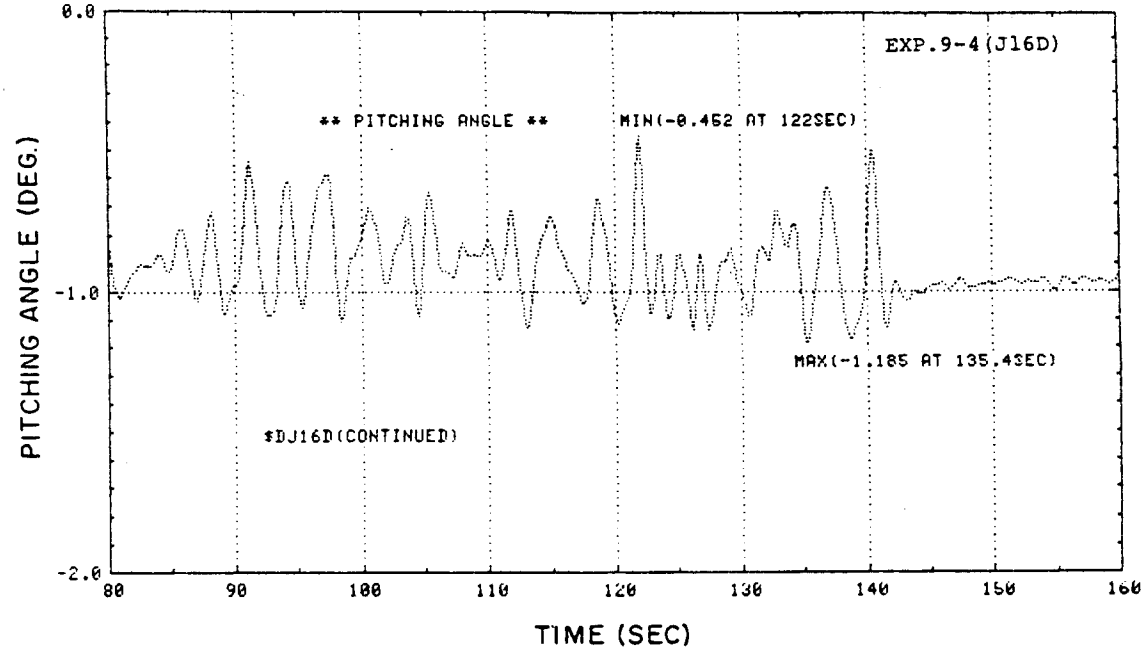

Fig. A-40

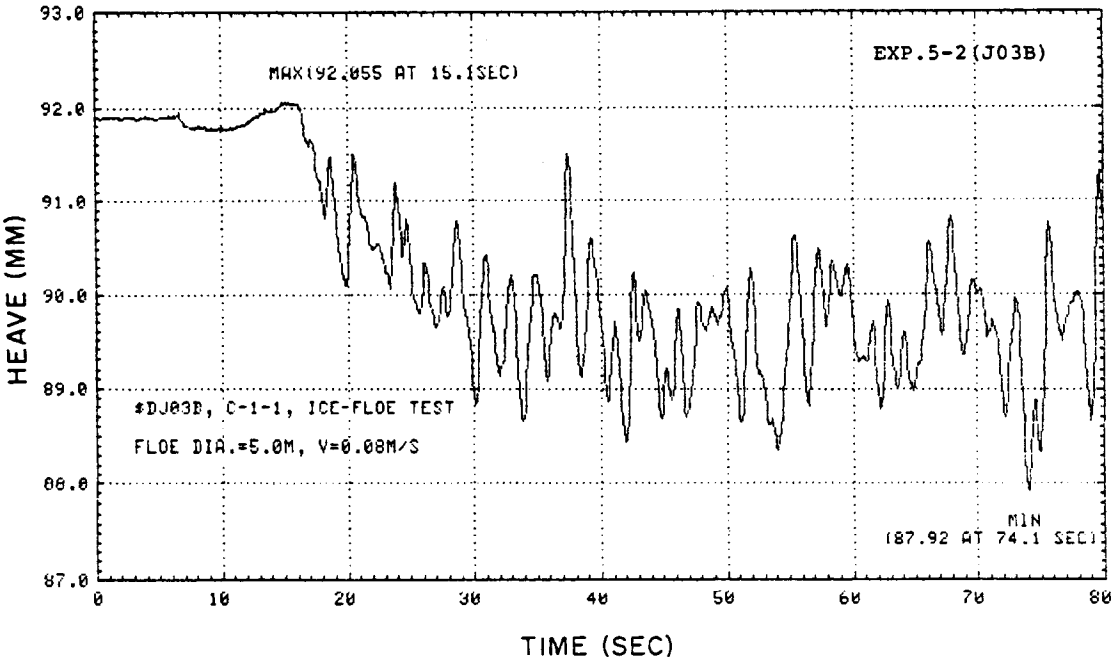

Fig. A-41

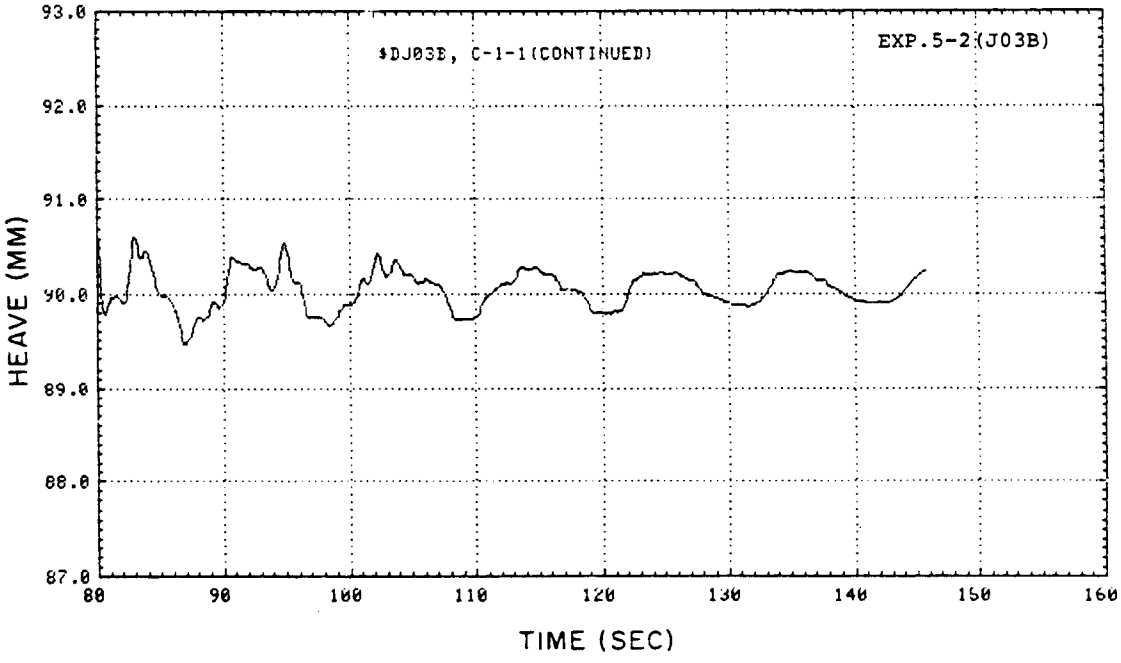

Fig. A-42

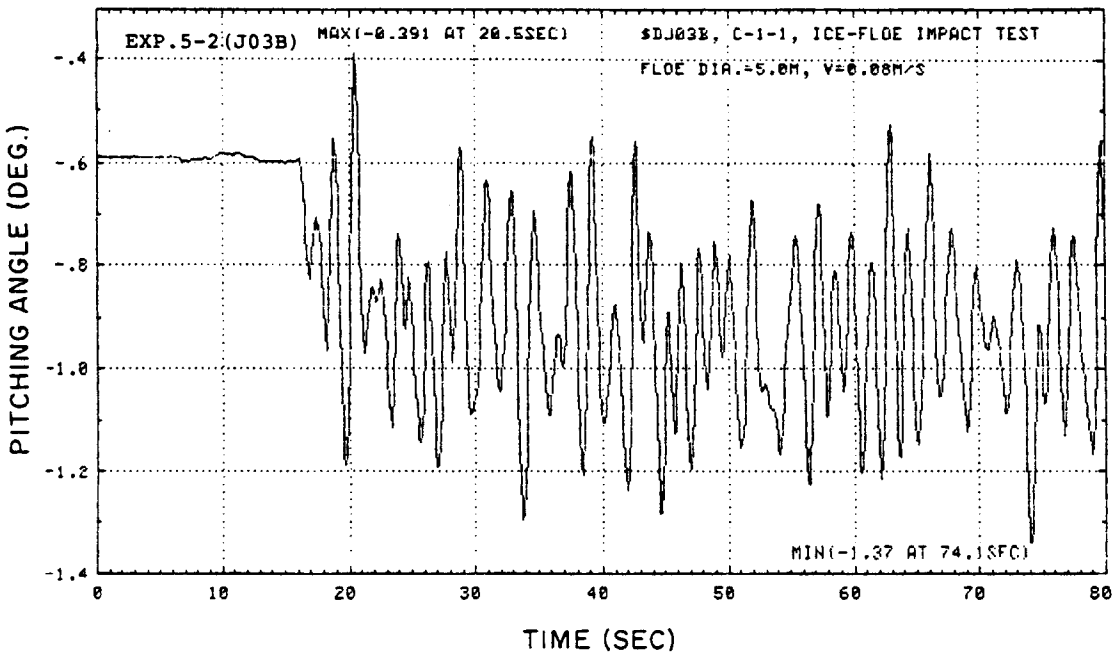

Fig. A-43

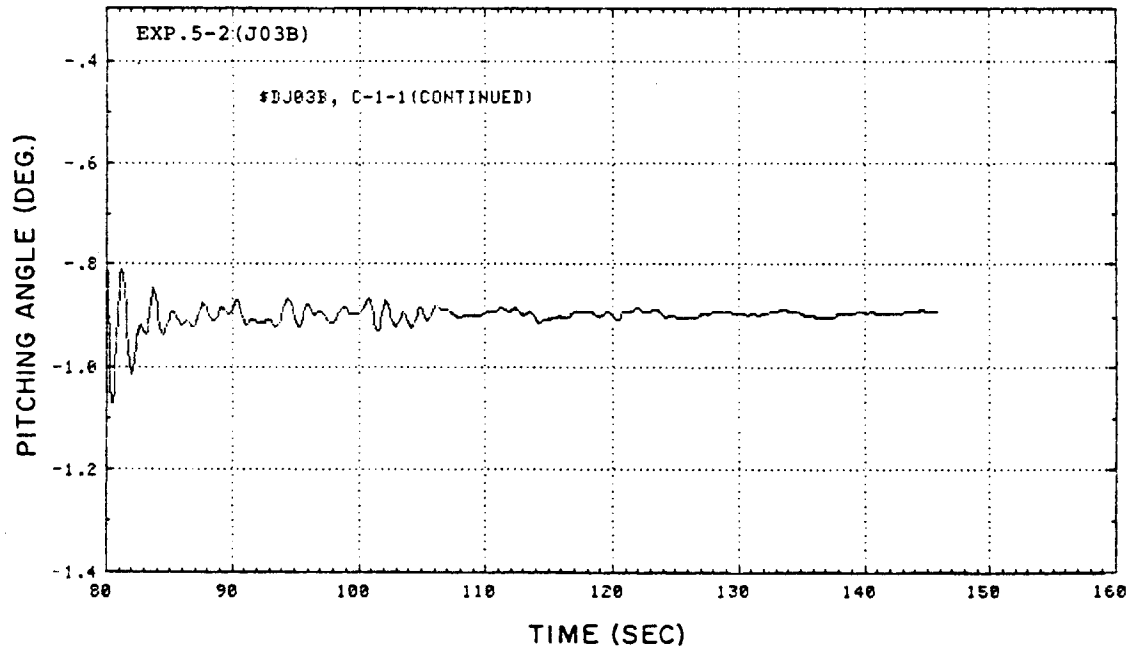

Fig. A-44

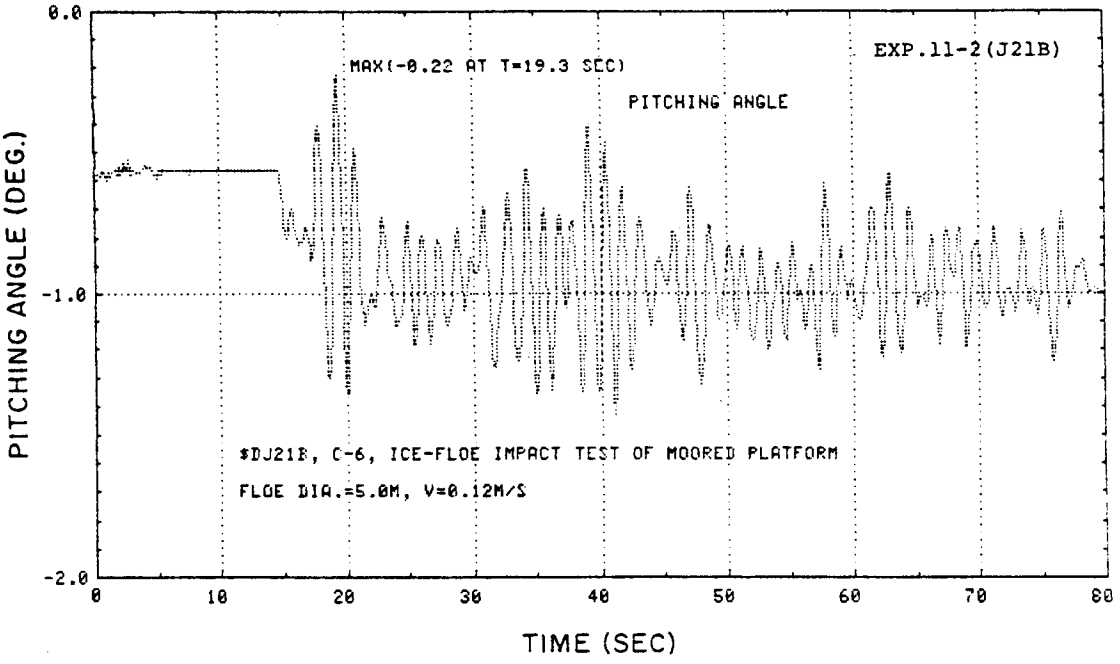

Fig. A-45

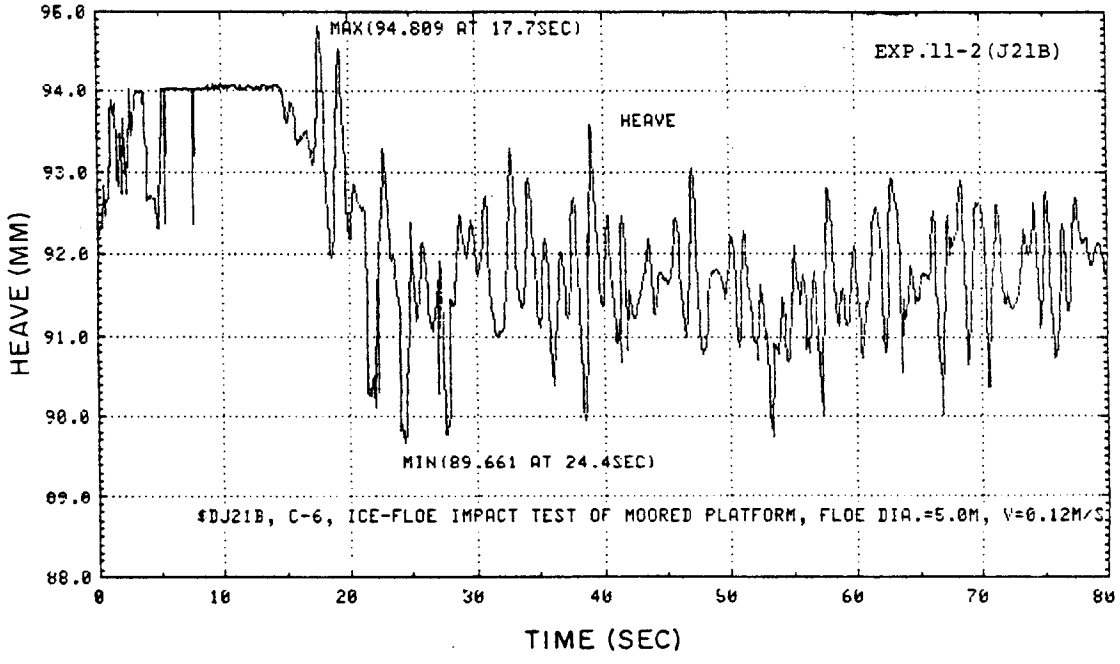

Fig. A-46

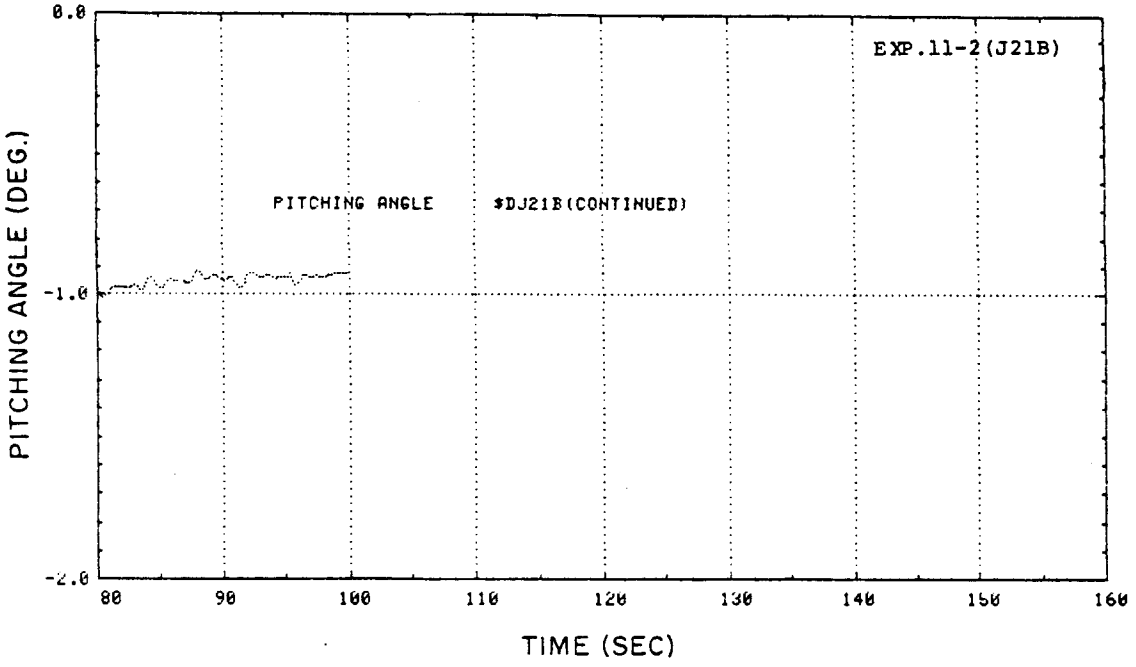

Fig. A-47

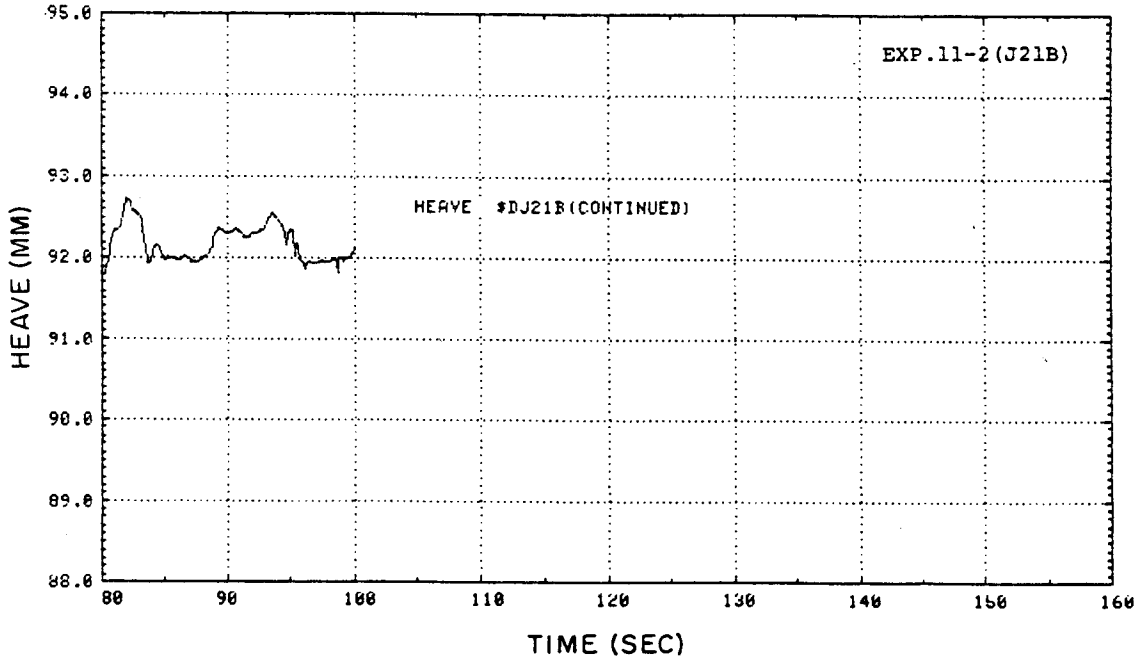

Fig. A-48

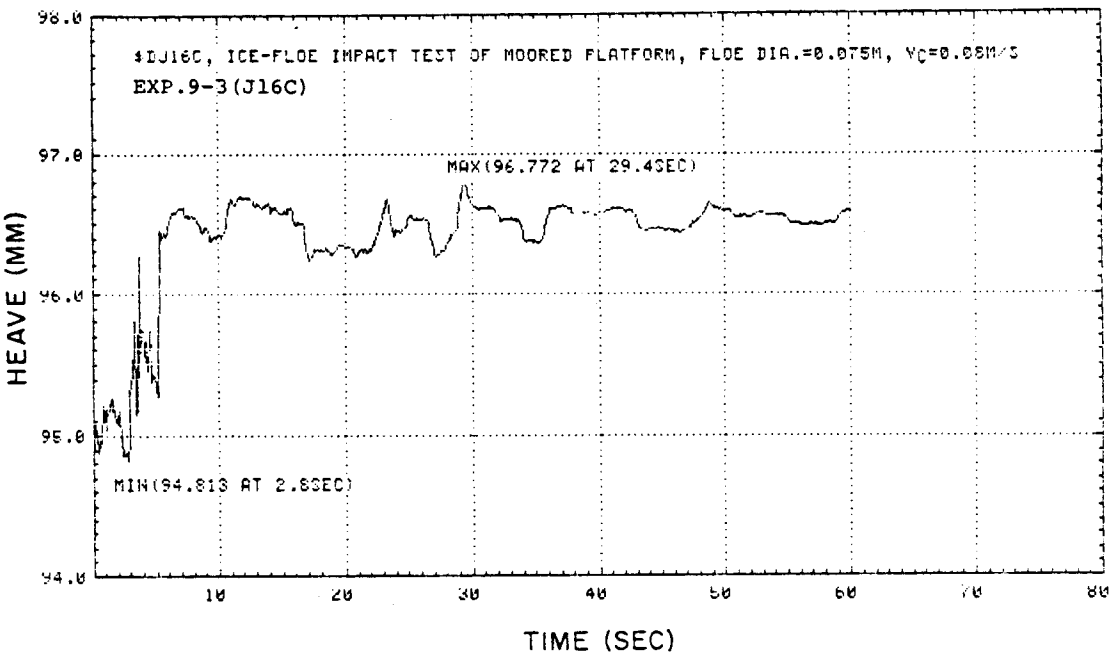

Fig. A-49

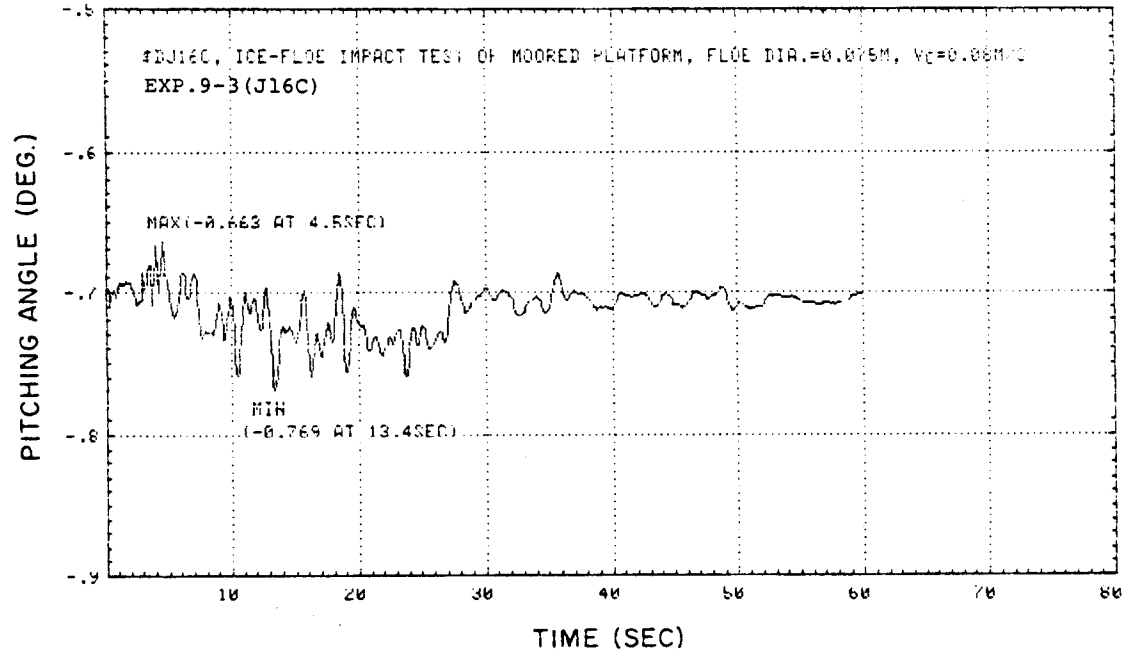

Fig. A-50

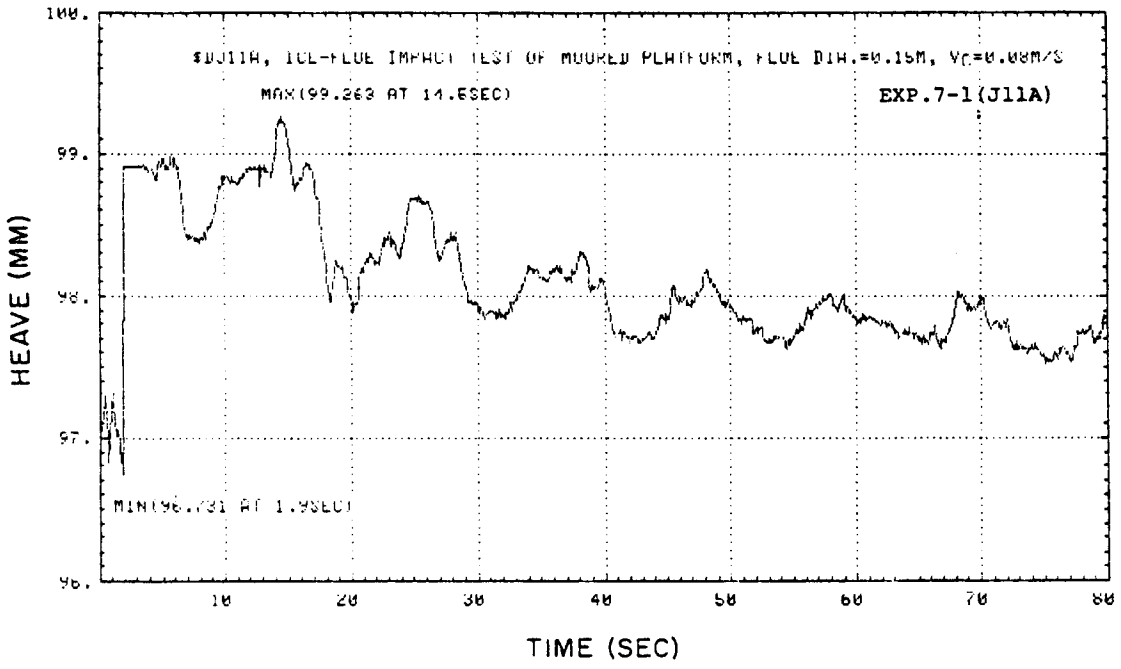

Fig. A-51

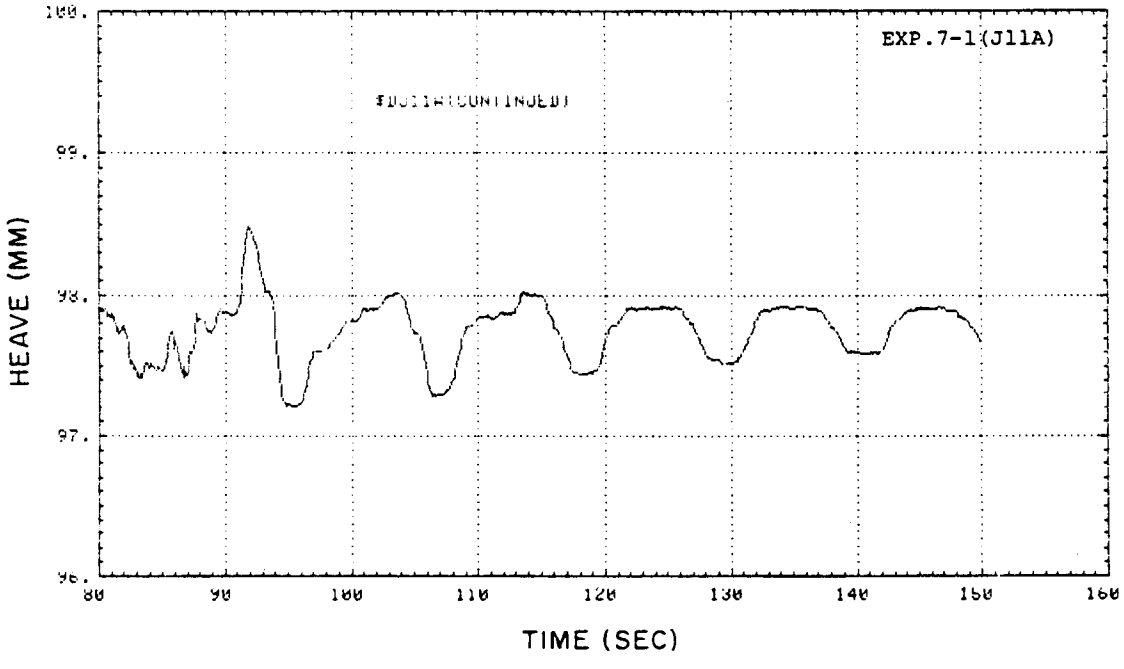

Fig. A-52

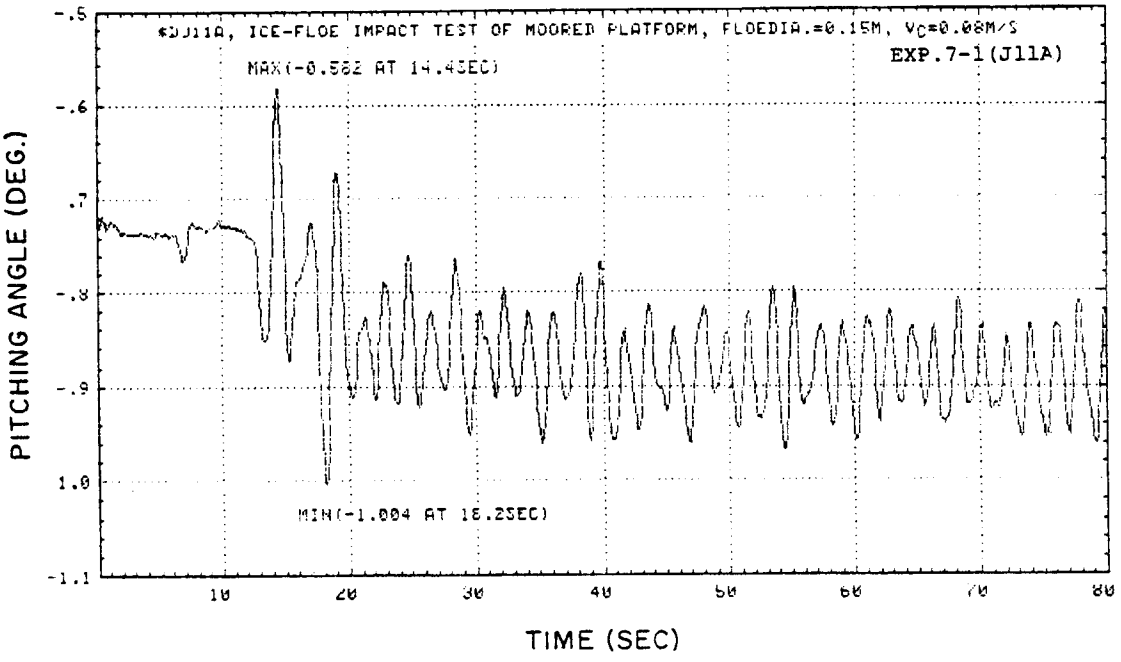

Fig. A-53

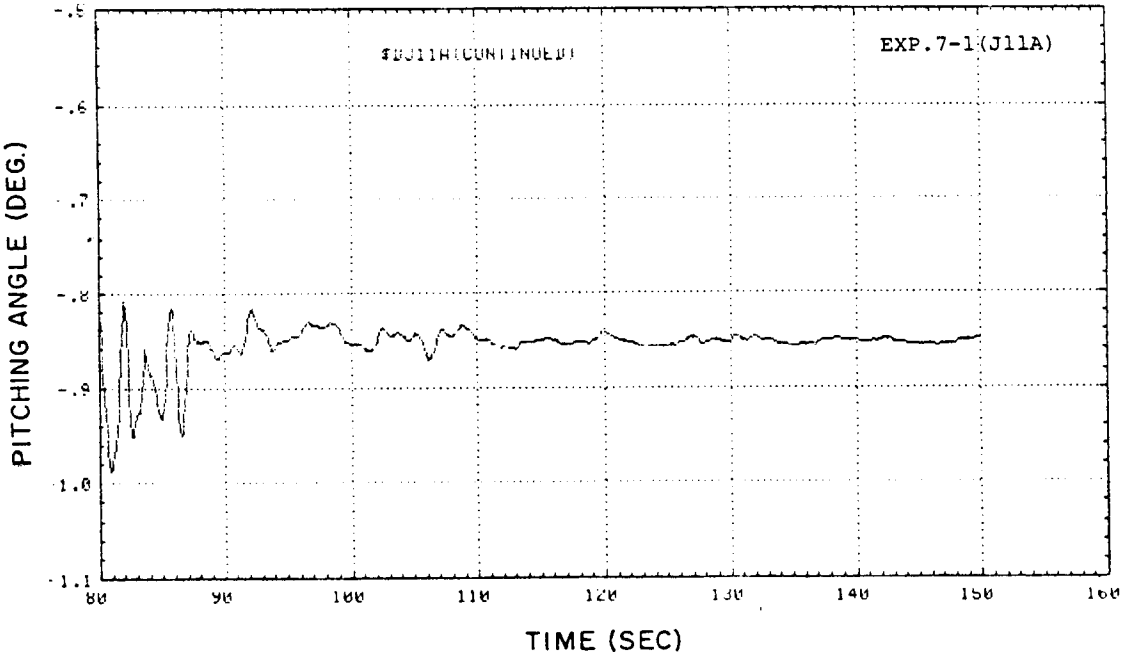

Fig. A-54

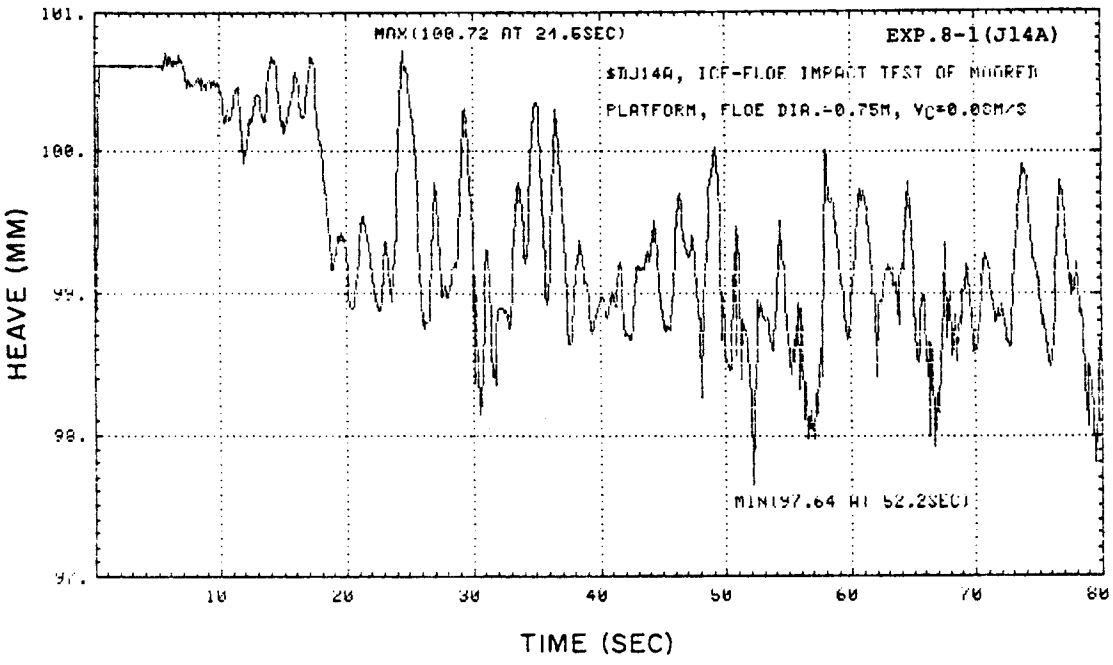

Fig. A-55

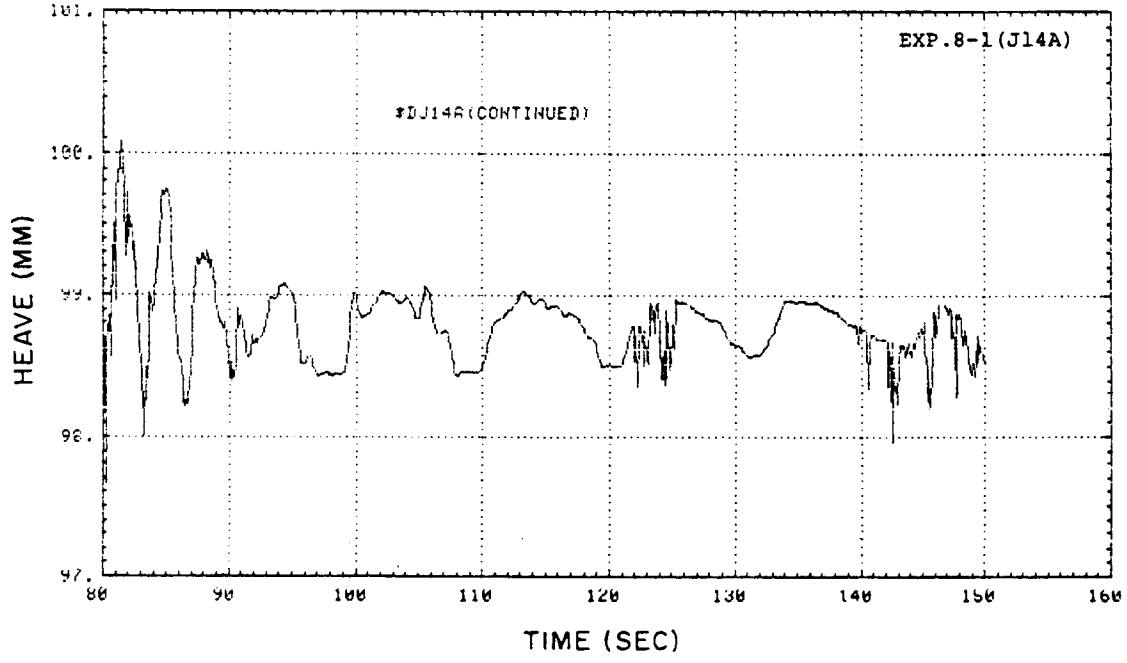

Fig. A-56

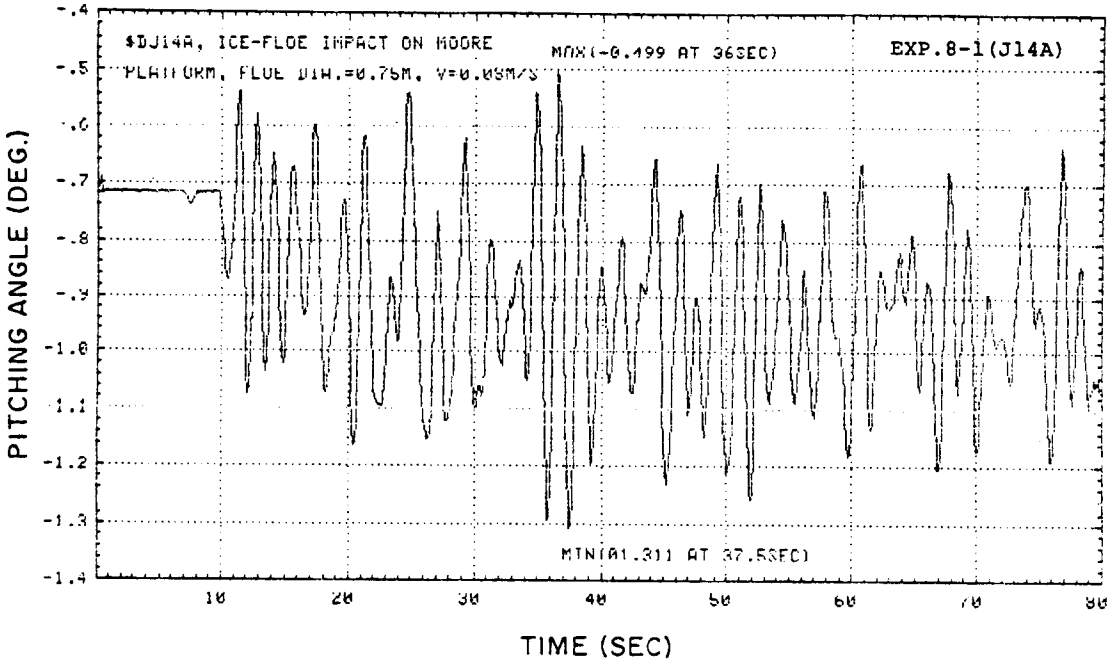

Fig. A-57

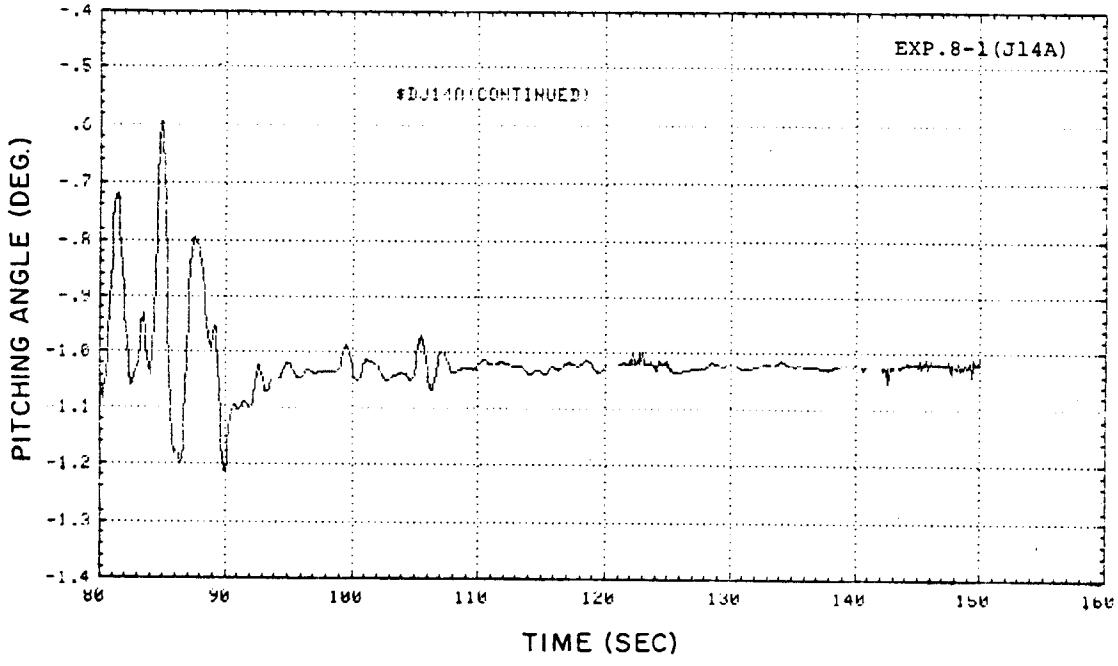

Fig. A-58

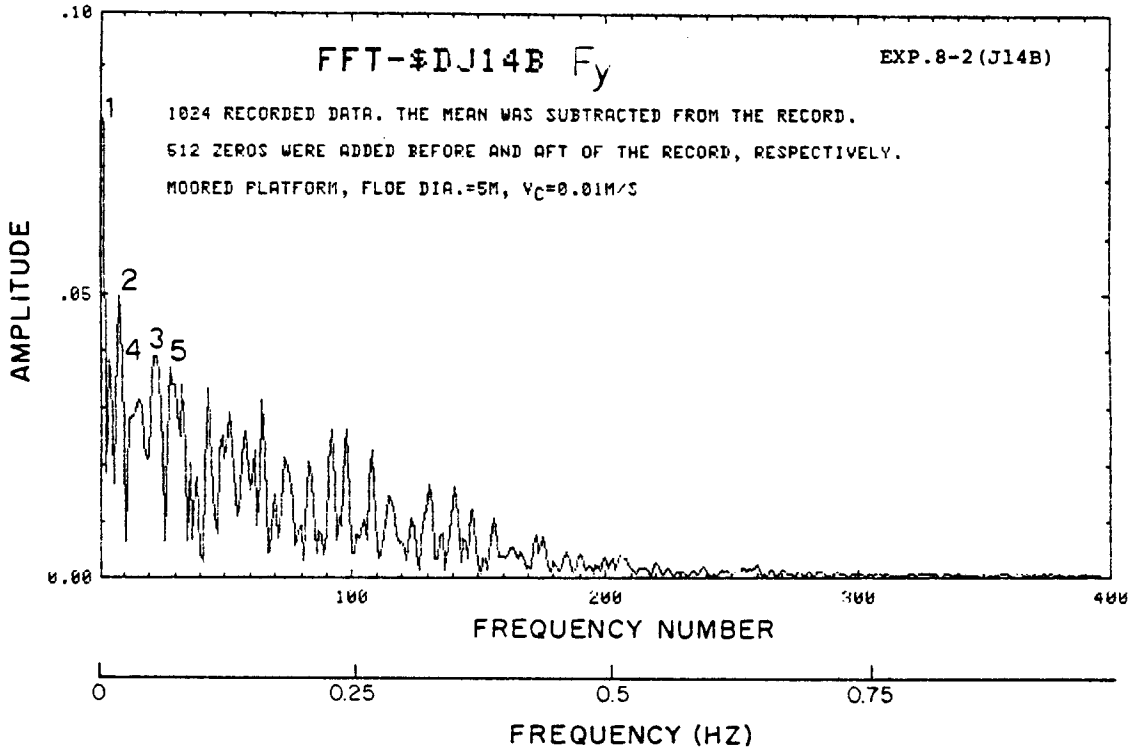

Fig. A-59

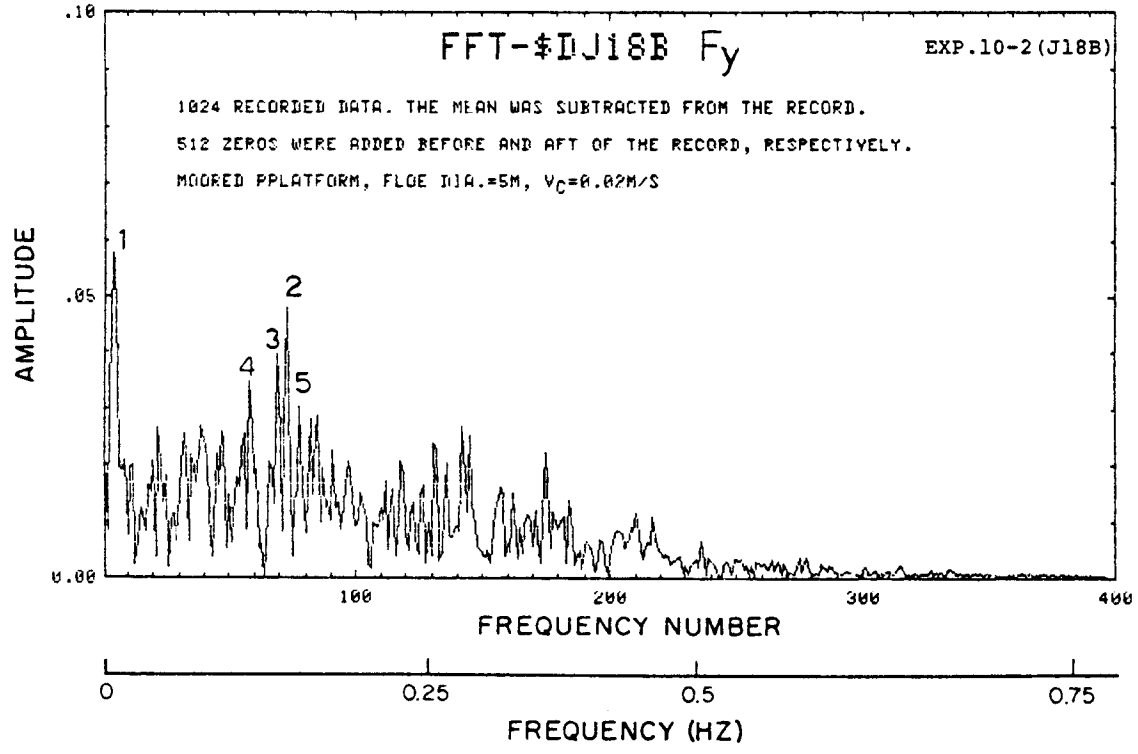

Fig. A-60

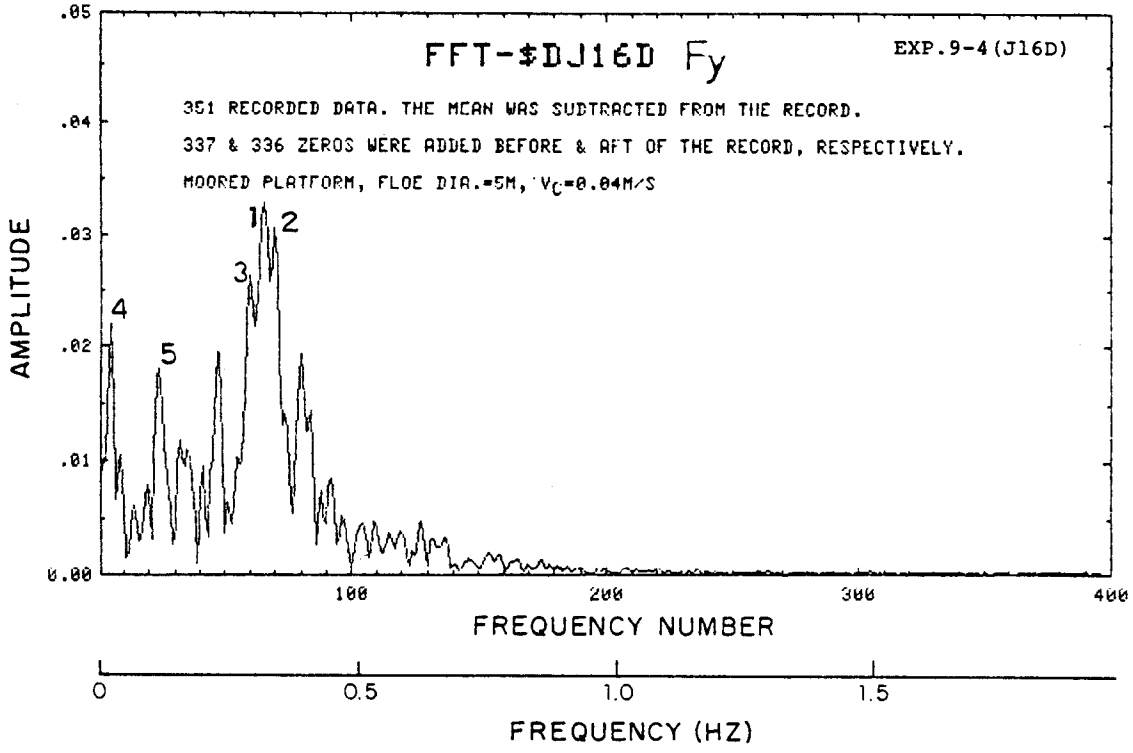

Fig. A-61

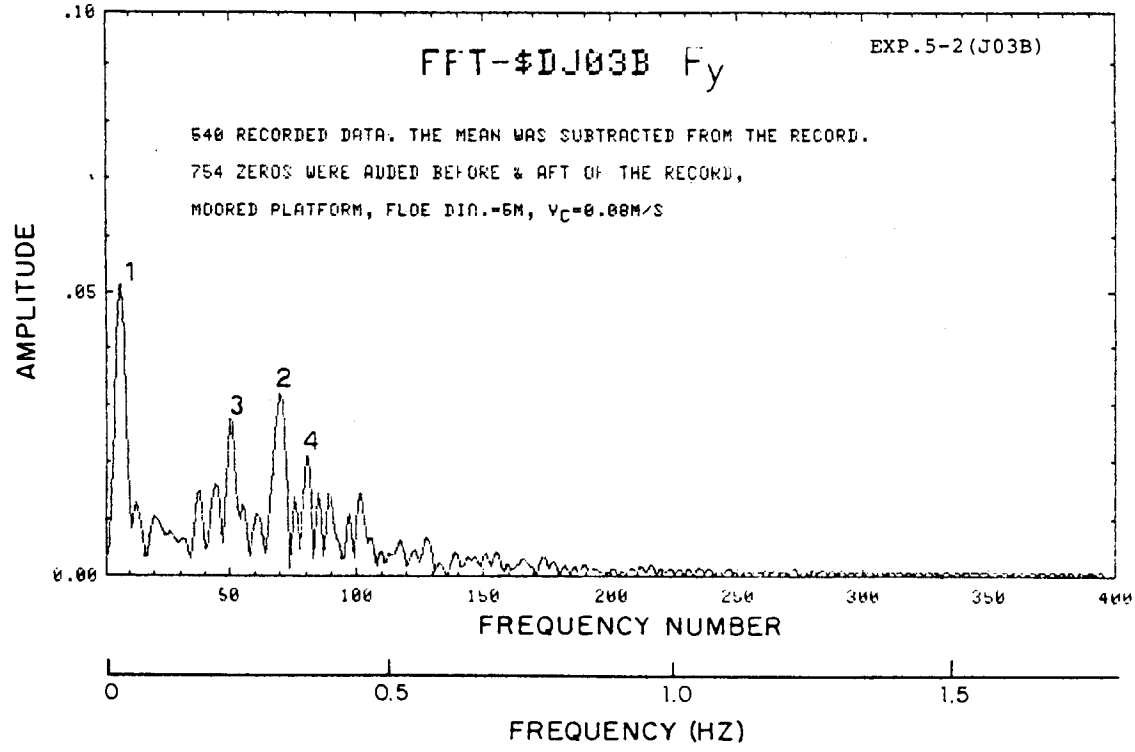

Fig. A-62

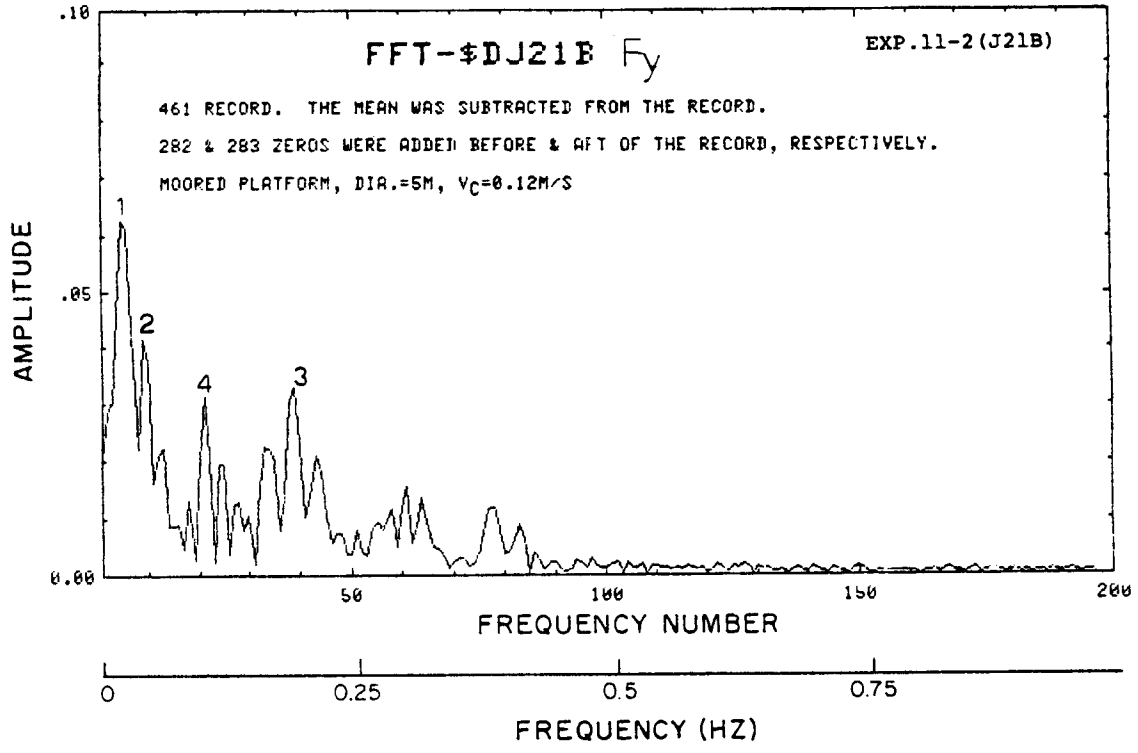

Fig. A-63

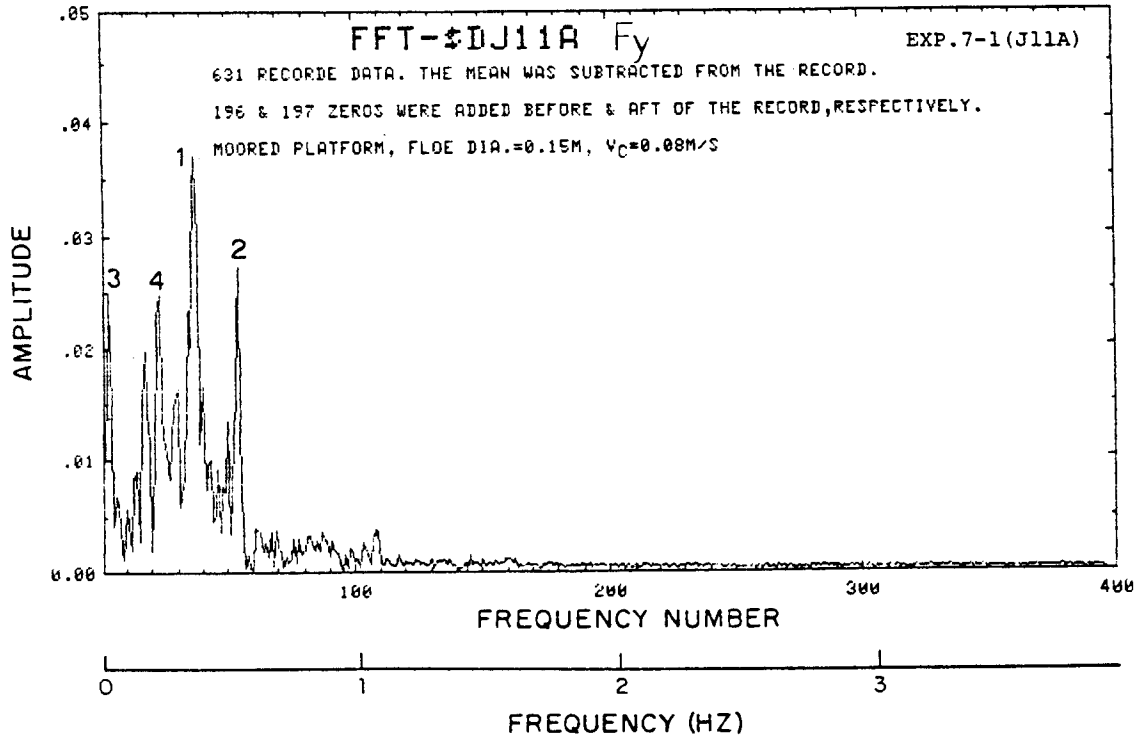

Fig. A-64

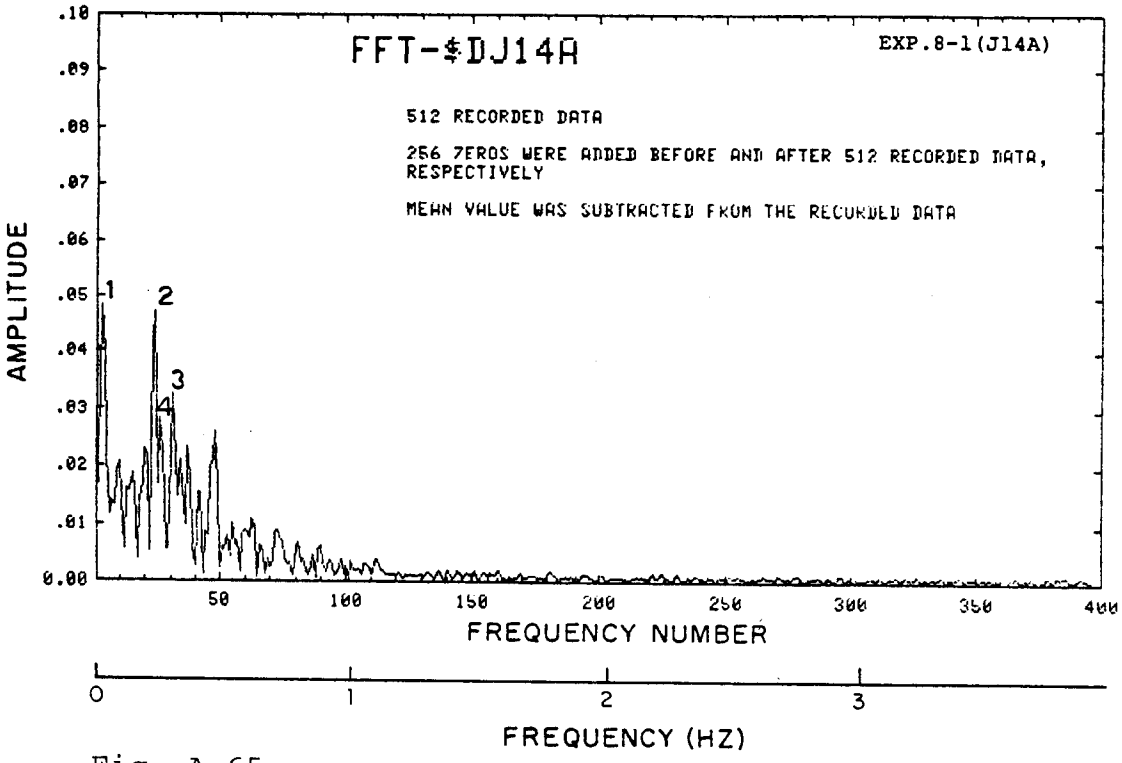

Fig. A-65

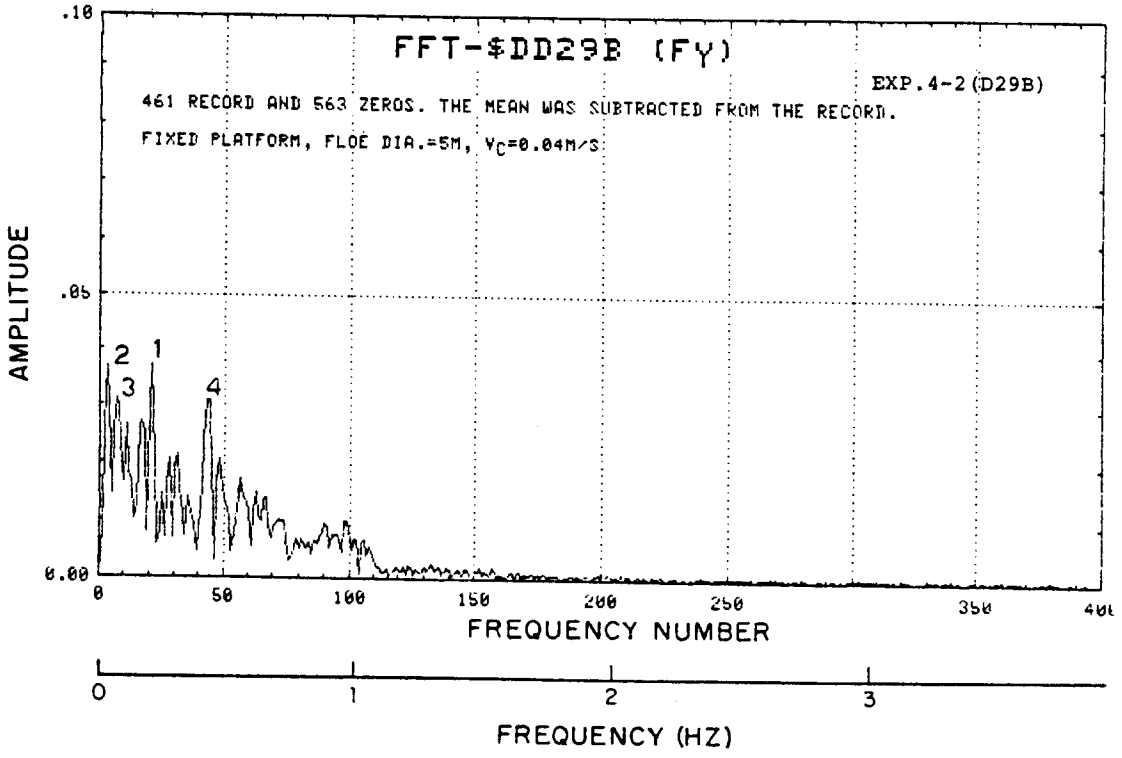

Fig. A-66

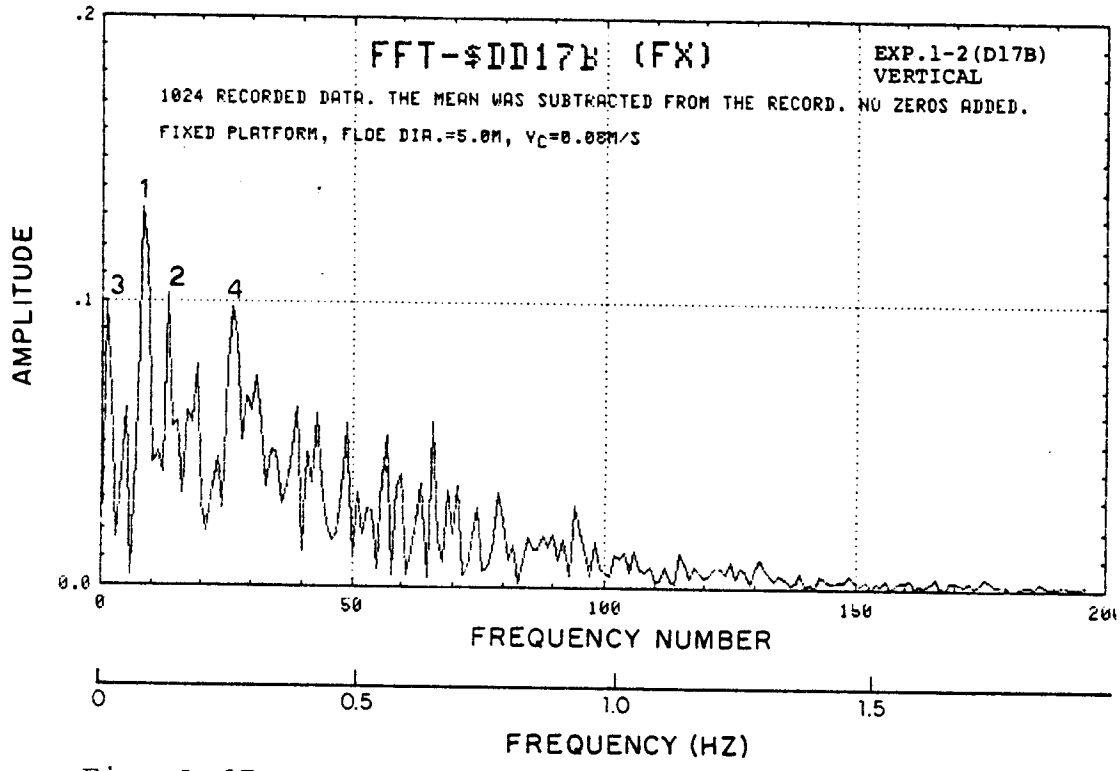

Fig. A-67

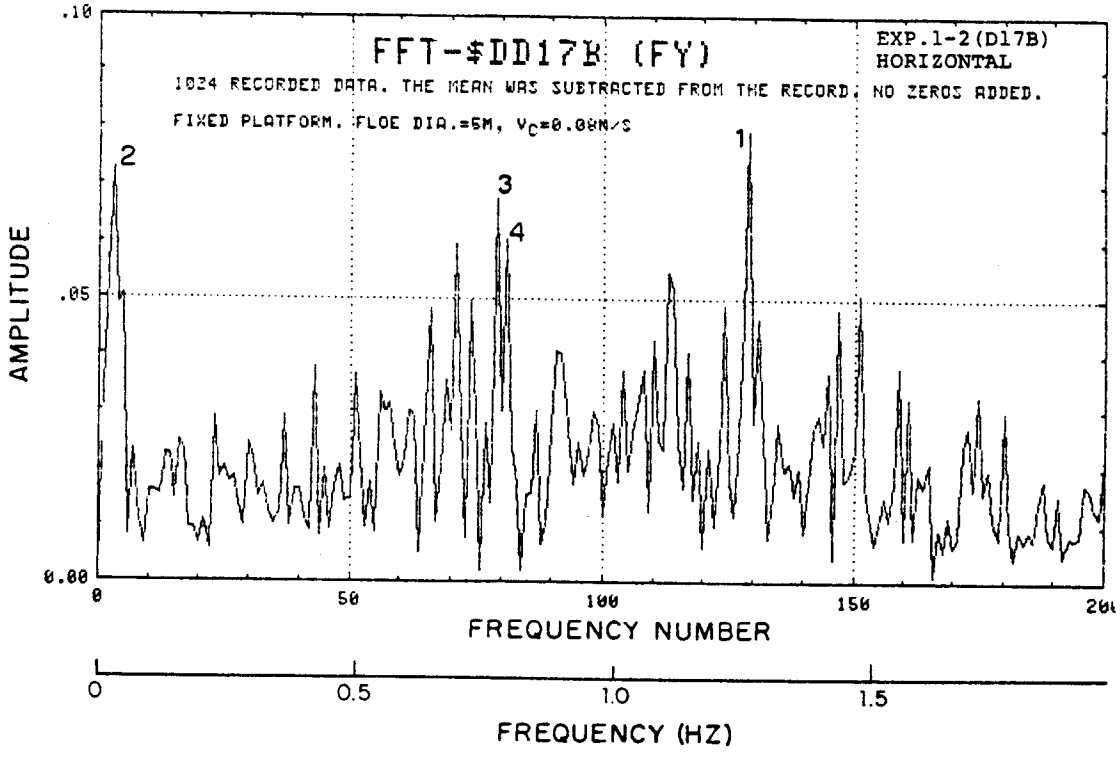

Fig. A-68

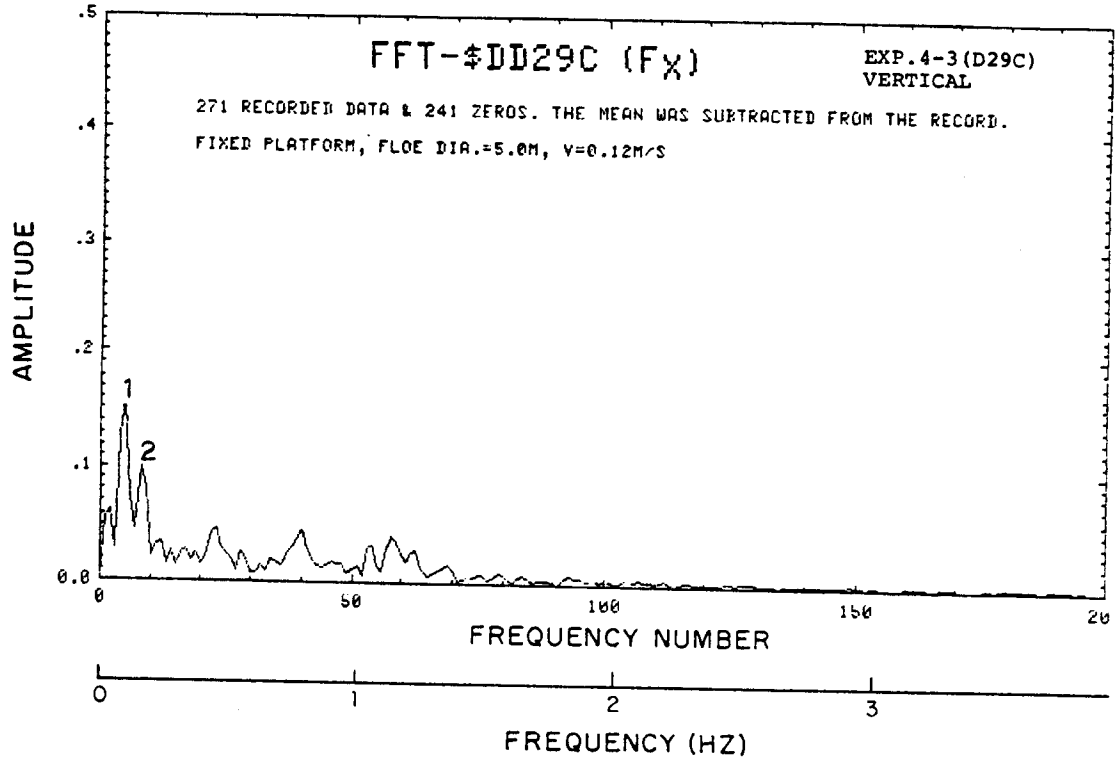

Fig. A-69

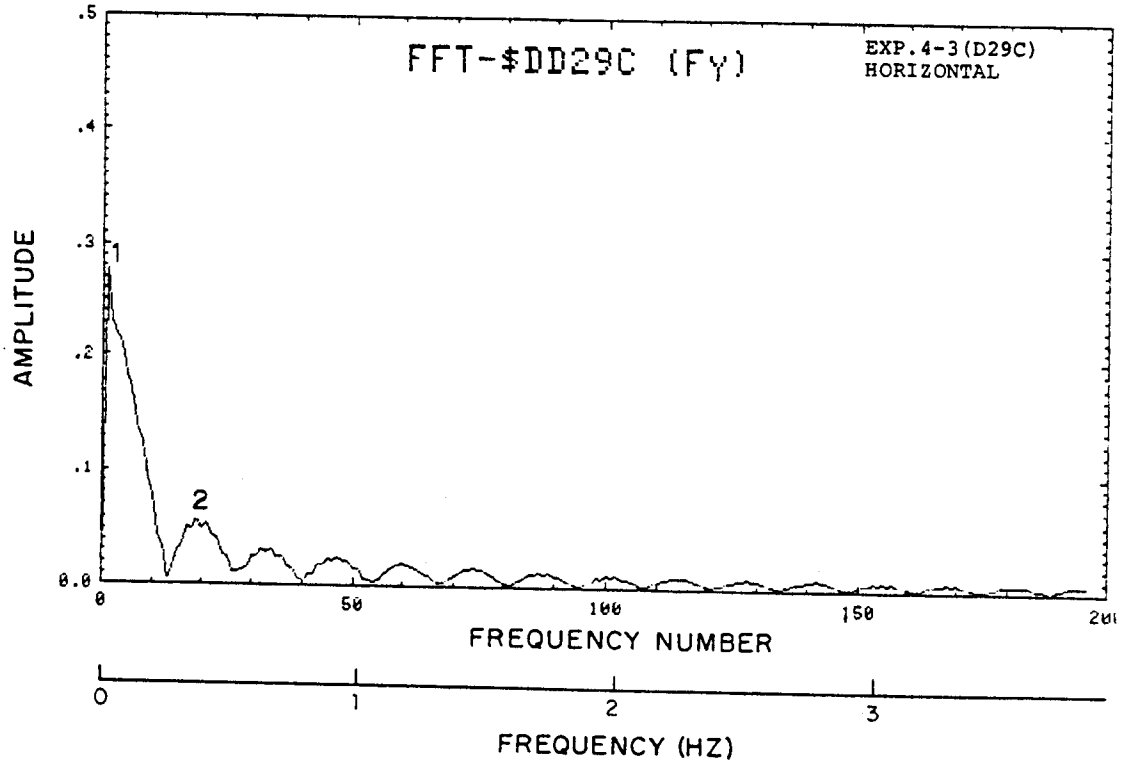

Fig. A-70

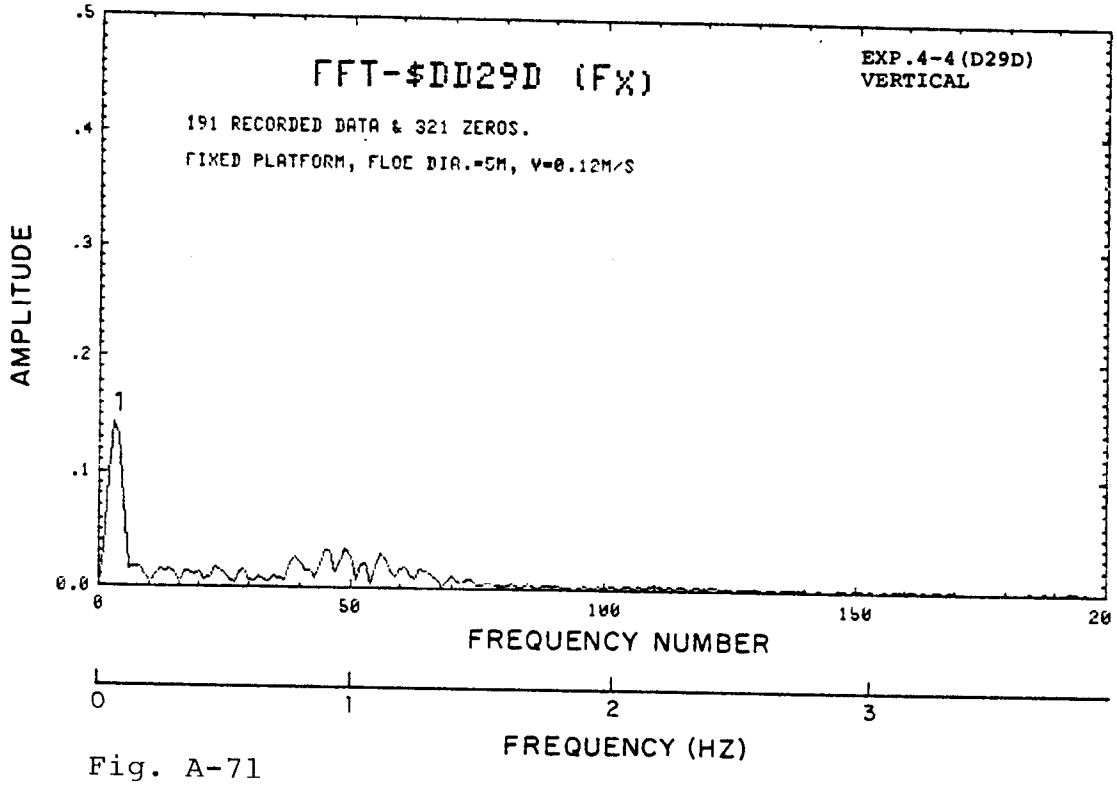

Fig. A-71

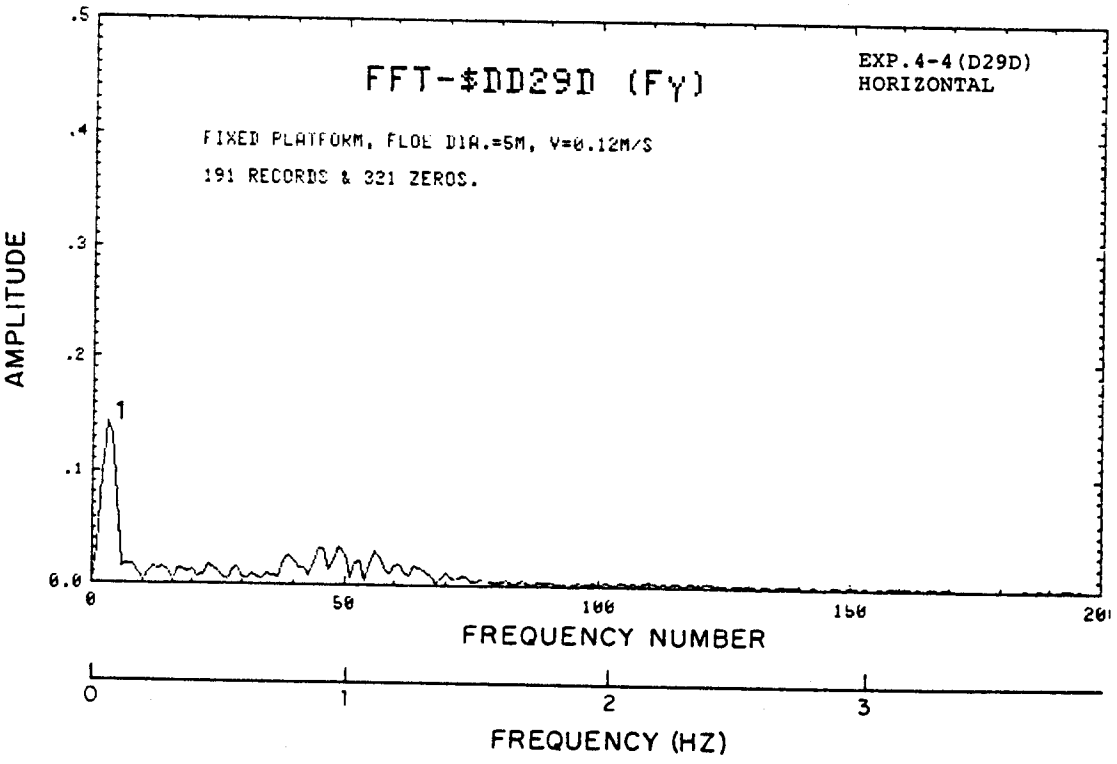

Fig. A-72

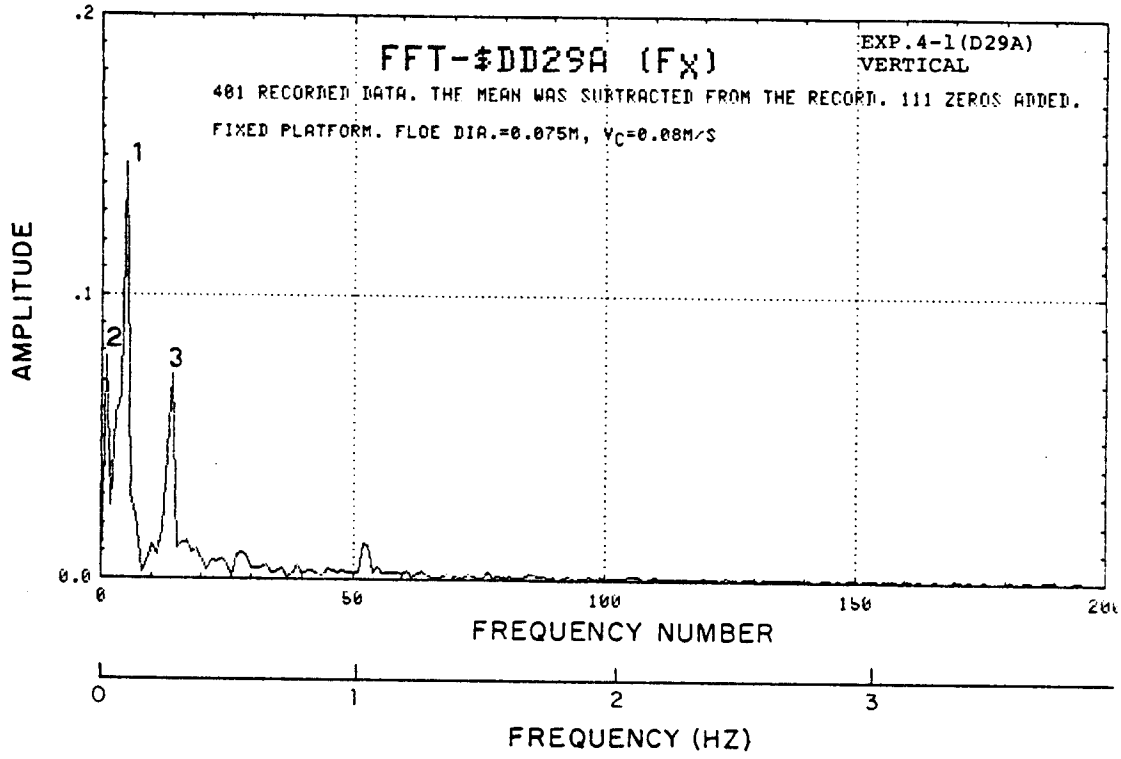

Fig. A-73

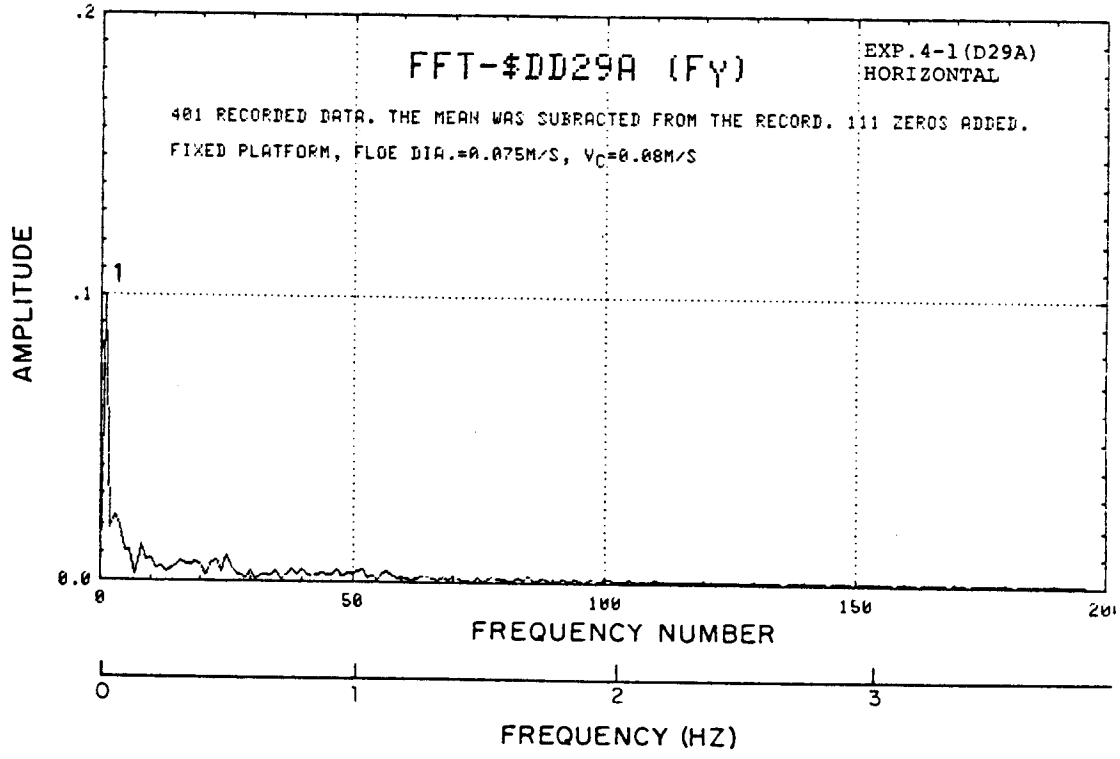

Fig. A-74

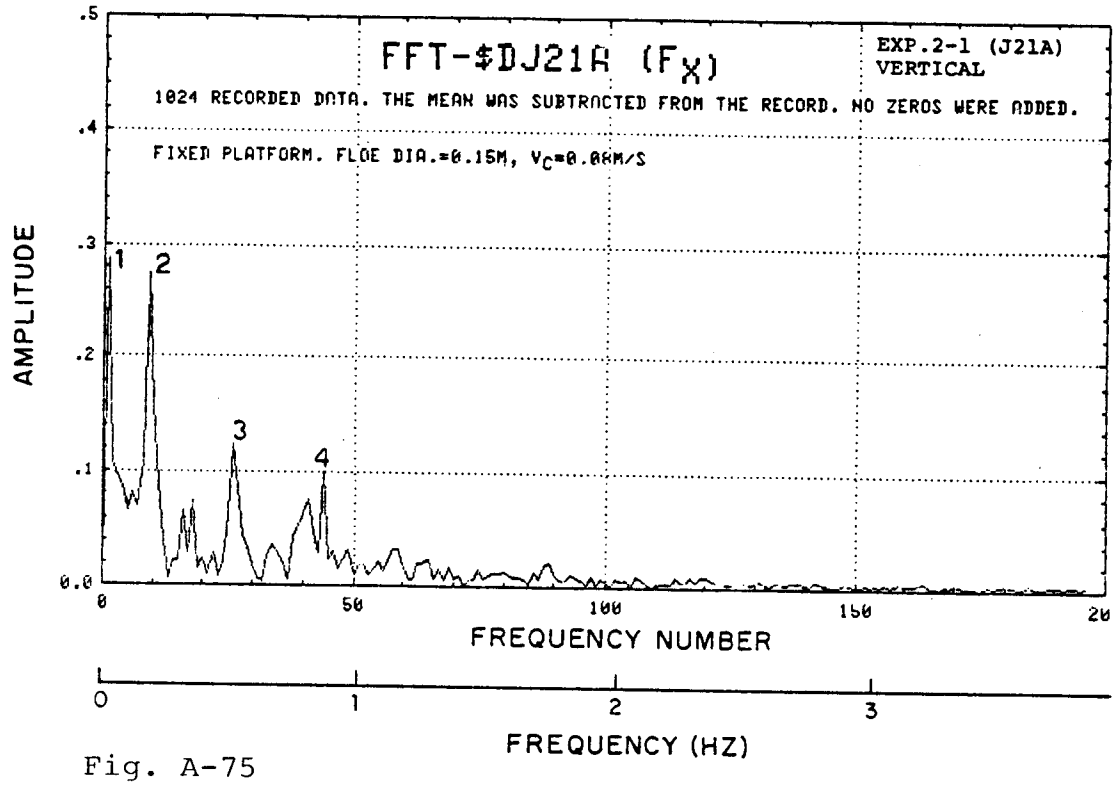

Fig. A-75

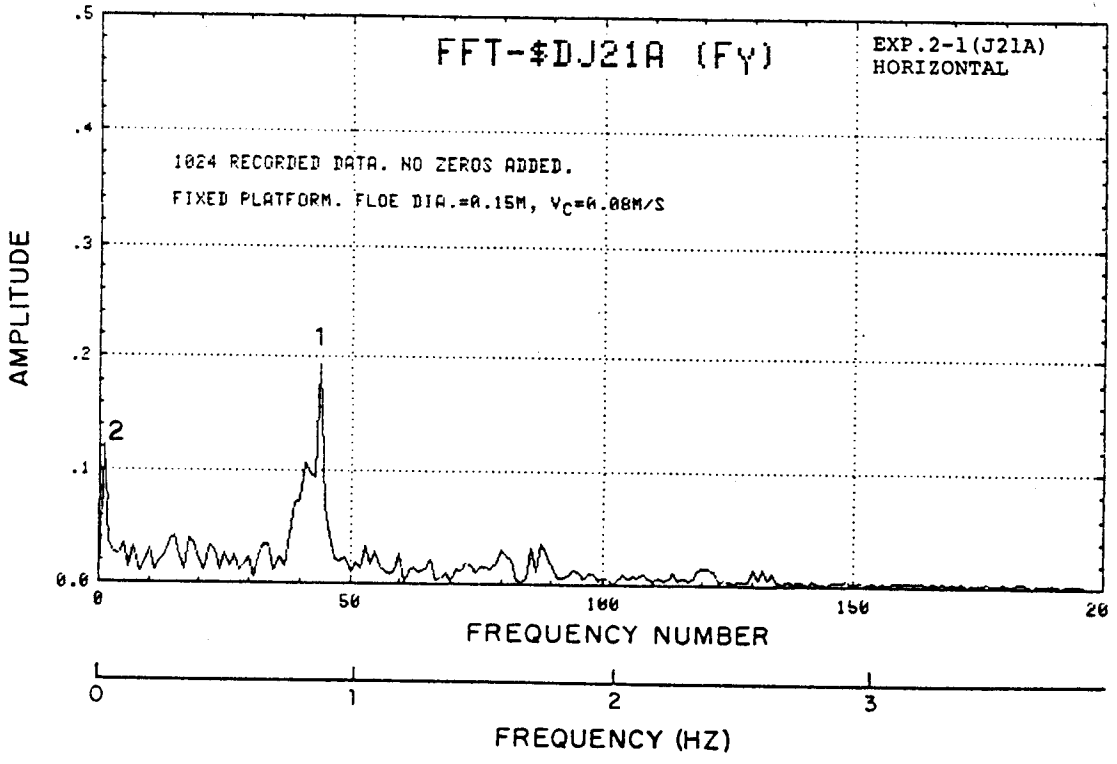

Fig. A-76

APPENDIX 2: Cable-Mooring Systems for Floating Platforms

Generally, the relationship between mooring force acting through a mooring cable and the displacement experienced by the cable is increasingly non-linear with decreasing depth of water in which a platform, or vessel, is moored. Typical relationships between mooring force and horizontal displacement of cable are shown in figure A-77.

For a platform which is moored by a system of cables, the relationship between total mooring force experienced by the system of cables and the horizontal displacement of the moored platform is influenced by the following: number of cables; arrangement of cables; and initial tensions applied to the cables. An example is shown in figure A-78 of the relationship between total mooring force, for a system of cables, and platform drift. Figure A-78 involves the following specifications:

* for each cable, the force-displacement relationship is as indicated in figure A-77.

* eight cables, each 76 mm in diameter, are used to moor the platform.

* the cables are arrayed symmetrically around the platform.

* initial tension is such so that the leading cable (e.g., cable 1 in figure 45, for a 12-cable array), which undergoes the maximum laoding during ice impact, becomes tensioned to one-third of its breaking strength when the platform drifts, or moves horizontally, 5% of the water depth upon which it is floating.

Although the precise characteristics of the mooring system for "Kulluk" are unavailable to the authors, it can be assumed, for the following reasons, that the mooring system can be treated as being linear:

a) the mooring system is stiffened by pre-tensioning of its cables, such that its response is along the near linear portion of the curve, shown in figure A-77, for a water depth fo 50 m; and

b) the allowable drift of the platform is less than 5% of water depth--i.e., less than about 2.5 m--in order to protect the drill string from excessive, dynamic, loadings. For this allowable drift the relationship between total mooring force and horizontal drift can be assumed to be linear.

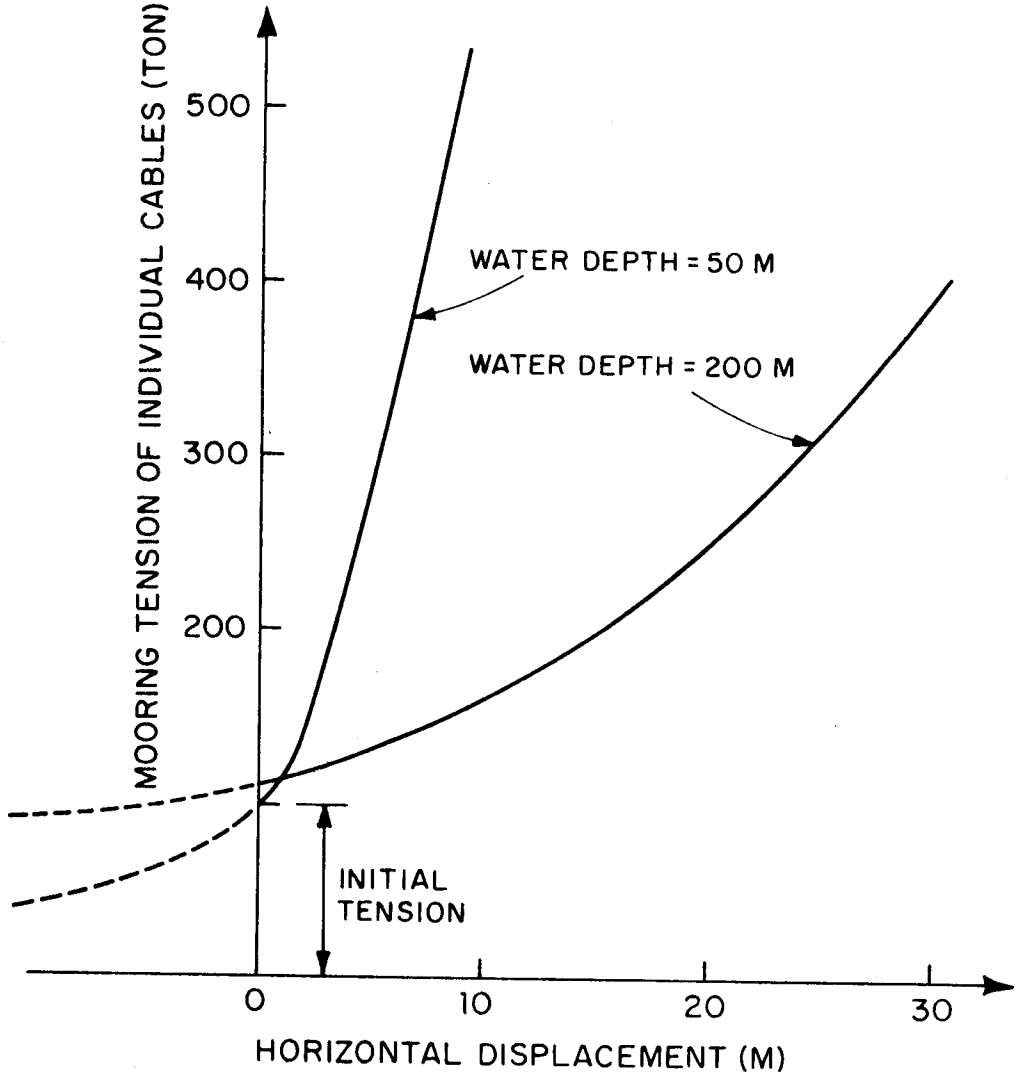

Figure A-77. Example of the relationship between mooring tension and horizontal displacement of a mooring cable. Note: (i) cable diameter is 76 mm; (ii) initial tension is prescribed such that the total tension reaches one-third of its breaking strength when a moored platform drifts horizontally 5% of water depth (Det Norske Veritas 1984).

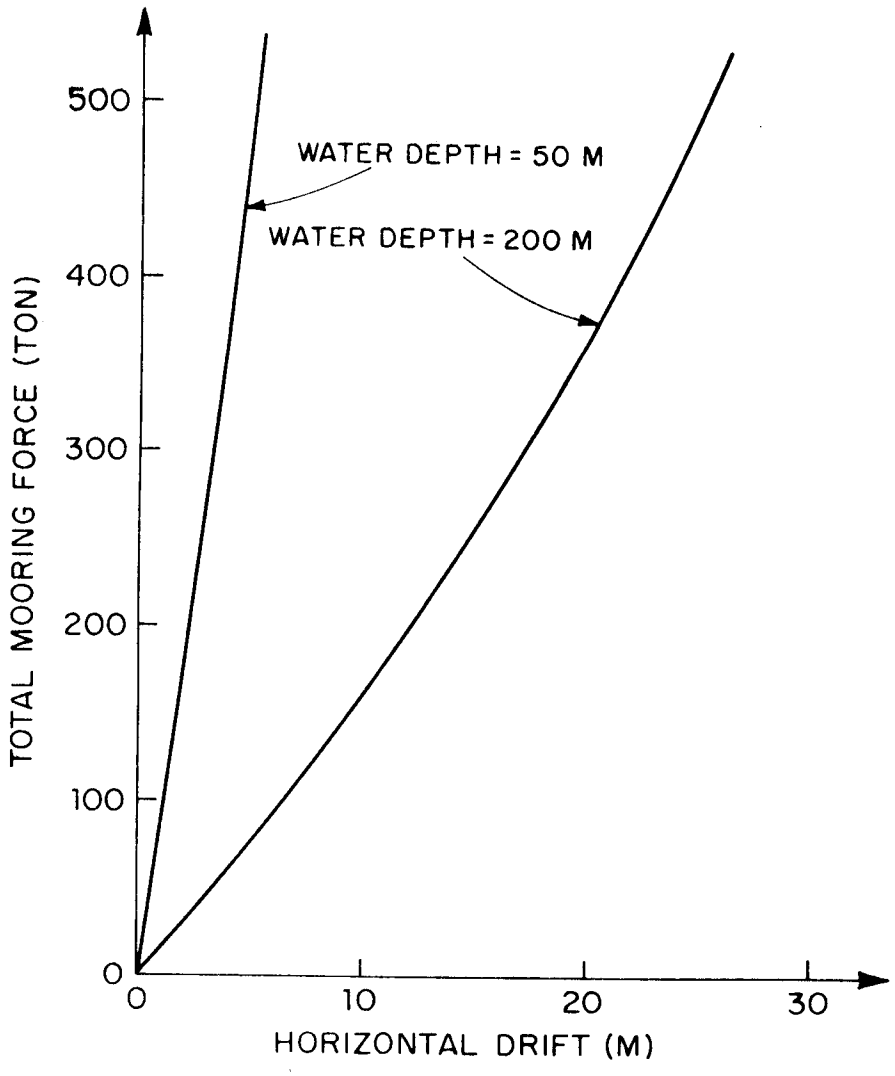

Figure A-78. Example of the relationship between total mooring force, for a system of eight cables, and horizontal drift.